

INVESTIGATION OF MOLECULAR SIGNALS REGULATING CELL  
PROLIFERATION AND NEUROGENESIS IN THE INTACT AND INJURED  
ZEBRAFISH (*DANIO RERIO*) OLFACTORY EPITHELIUM

by

Mehmet Can Demirler

B.S, Molecular Biology and Genetics, Boğaziçi University, 2014

Submitted to the Institute for Graduate Studies in  
Science and Engineering in partial fulfillment of  
the requirements for the degree of  
Doctor of Philosophy

Graduate Program in Molecular Biology and Genetics

Boğaziçi University

2021



## ACKNOWLEDGEMENTS

I have met many generations of people in this department, all of whom added another color to my life. That is why I would like to initially thank everybody in BOUN MBG, scientific personnel or otherwise, for their support. First, I would like to thank all my PhD Jury members for their contribution to my work. I am thankful to Vivarium people for their friendship and help in the FishRoom. I would like to specifically thank Ulduz Sobhiahshar, Tolga Aslan, Burçin Duan Şahbaz, Aybüke Alıcı Garipcan, Aysin Akpınar, Hatice Bahar Şahin, Neslihan Zöhrap not only for their mentorship but also for their wonderful friendship. I would like to thank Yiğit Kocagöz for his collaboration in the lab, critical contributions to my work and especially for his friendship. I thank all my current lab mates Aysu, Zeynep, Şiran, Sinay, also sister-lab mates Barış, Ayşe, and all previous lab mates especially Selif, Uğurcan, Metin, Emir, Xalid, Büşra, Burak, Çağrı and Gizem. I would like to thank all the faculty members, but specially Kuyaş Buğra for when she directed me to Stefan Fuss, when I told her what I was interested in for my future. I cannot thank enough to Stefan Fuss for all the opportunities he provided me with. I am grateful for his excellent mentorship that made me who I am today. His attitude towards science, his work and his patience towards me are, and will always be, golden examples for me to look up to. I will be forever proud of working in his lab and learning from him. Because of him, my PhD life is a story that I will always be happy to tell.

I would also like to thank my whole family (including in-laws) for their support and unprecedented understanding during my PhD life. Lastly, I am exceedingly thankful to my wife Hilal Serin Demirler. Without her friendship, understanding and especially her support, life would be much harder for me. Her understanding and appreciation towards my work encouraged me and helped me to boldly pursue a scientific career. Her presence raises my spirit, willingness, and gives me joy which helped me immensely during my studies.

Work on this thesis was supported by the Scientific and Technological Research Council of Turkey (TÜBİTAK) through Grant No:113T038 to SHF.

## ABSTRACT

### **INVESTIGATION OF MOLECULAR SIGNALS REGULATING CELL PROLIFERATION AND NEUROGENESIS IN THE INTACT AND INJURED ZEBRAFISH (*DANIO RERIO*) OLFACTORY EPITHELIUM**

The zebrafish olfactory epithelium (OE) can recover from the near total loss of olfactory sensory neurons (OSNs) within only a week when the OE is damaged by external causes. This remarkable neurogenic activity depends on the differential activation of horizontal basal cell (HBC) progenitors, which are quiescent in the intact tissue. Under physiological conditions, an independent pool of mitotically active progenitors, the globose basal cells (GBCs), constitutively generate new neurons to replace OSNs that reach the end of their natural life span. Unique to the zebrafish OE, the two progenitor types are spatially segregated, and HBC and GBC activity can easily be discriminated by analyzing the epithelial position of mitotic activity under different tissue conditions. However, detailed knowledge about the diversity of non-neuronal cells and the molecular cues that regulate the rate of maintenance neurogenesis or trigger OE regeneration, is largely missing. This study shows that HBCs, GBCs and sustentacular glial cells (SCs) express Sox2, that they segregate within distinct layers of the basal OE, and that they are selectively sensitive to purine compounds. HBCs occupy the basal OE and respond strongly to ATP and 2-MeSATP, while GBCs and SCs occupy suprabasal strata and show high and low ATP sensitivity, respectively. ATP stimulates GBC activity but does not affect HBC proliferation, indicating that purinergic signaling has a selective function in regulating maintenance neurogenesis. In contrast, exposure to the cytokine IL-6 results in HBC expansion and subsequent OSN generation. Detailed analysis of the tissue dynamics in the intact OE revealed that HBCs are more active than anticipated but only rarely, if at all, contribute to OSN or SC neurogenesis. A preliminary model of maintenance neurogenesis could be developed, which suggests the existence of a novel SC progenitor within the neurogenic niche of the intact OE.

## ÖZET

### SAĞLAM VE HASARLI ZEBRABALIĞI OLFAKTÖR EPİTELİNDEKİ HÜCRE BÖLÜNMESİ VE NÖROJENEZİ DÜZENLEYEN MOLEKÜLER SİNYALLERİN ARAŞTIRILMASI

Zebrabalığı olfaktör epiteli (OE) çevresel sebeplerden ötürü tüm olfaktör duyu nöronlarının (OSN) kaybından dahi bir hafta içerisinde tamamen iyileşebilir. Bu olağanüstü nörojenik aktivite, sağlam dokuda durgun olan yatay bazal hücre (HBC) progenitörlerinin farklı aktivasyonuna bağlıdır. Fizyolojik şartlarda, mitotik olarak aktif, bağımsız bir kök hücre havuzu olan küresel bazal hücreler (GBC) durmadan doğal yaşam süresini doldurmuş olan OSN yerine yeni nöronlar üretir. Zebrabalığı OE'ne özgün olarak, bu iki kök hücre grubu uzaysal olarak birbirinden ayrılmıştır ve farklı doku şartlarında epiteldeki mitotik aktivitenin analiziyle, HBC ve GBC aktivitesi birbirinden rahatlıkla ayrıştırılabilir. Ancak, sinir hücresi olmayan hücrelerin farklılıkları ya da onarım nörogenezi hızını kontrol eden veya OE rejenerasyonunu tetikleyen moleküler belirteçler hakkındaki bilgiler oldukça dar. Bu çalışma, HBC, GBC ve destekleyici hücrelerin (SC) Sox2 ifade ettiğini, bazal OE üzerinde farklı katmanlarda bulduklarını ve purin bileşenlerine farklı tepkiler verdiğini göstermektedir. OE'de HBC'ler bazal katmanı işgal eder ve ATP ve 2-MeSATP'ye yüksek tepki verirken GBC ve SCler üstbazal katmanlarda bulunur ve ATP'ye sırayla yüksek ve düşük tepki verirler. ATP, GBC aktivitesini tetikleyebilirken, HBC bölünmesine etkilememektedir ve bu da purin sinyallerinin onarım nörogenezini kontrolüne özgün fonksiyonlarına işaret etmektedir. Öte yandan, sitokin IL-6'ya maruz kalmak HBC havuzunun genişlemesine ve buna bağlı OSN üretimine sebep olmaktadır. Sağlam haldeki OE'nin doku dinamiklerinin detaylı analizi HBC'lerin beklenilenden çok daha aktif olduğunu ancak eğer bulunuyorsa bile, nadiren OSN veya SC üretimine katkıda bulunduğunu gösterdi. Buradaki bulgularla öncül bir onarım nörogenezi modeli geliştirilebilir. Bu öncül model, SC üreten yeni ve özgün bir kök hücre türünün sağlam OE dokusundaki nörojenik nişteki varlığını öngörmektedir.

## TABLE OF CONTENTS

ACKNOWLEDGEMENTS.....	iii
ABSTRACT.....	iv
ÖZET.....	v
LIST OF FIGURES .....	x
LIST OF TABLES.....	xiv
LIST OF SYMBOLS .....	xvi
LIST OF ACRONYMS / ABBREVIATIONS.....	xvii
1. INTRODUCTION .....	1
1.1. Adult Neurogenesis .....	1
1.2. Olfactory system.....	5
1.3. Organization of the Vertebrate OE and OSN Neurogenesis .....	7
1.4. Organization of the Zebrafish OE and OSN Neurogenesis .....	12
1.5. Molecular Regulation of Neurogenesis .....	19
2. PURPOSE.....	22
3. MATERIALS AND METHODS.....	25
3.1. Materials .....	25
3.1.1. Animals.....	25
3.1.2. Equipment and Supplies .....	25
3.1.3. Buffers and Solutions .....	25
3.2. Methods .....	26
3.2.1. Zebrafish Maintenance .....	26
3.2.2. Dissection of Zebrafish Olfactory Organ .....	26
3.2.3. Cryosectioning of the OE .....	27
3.2.4. Labeling of Dividing Cells by Thymidine Analogue Incorporation .....	27

3.2.5. Tissue Dissociation Assay .....	28
3.2.6. Immunohistochemistry .....	29
3.2.7. Chemical Lesion of the OE using Triton X-100.....	31
3.2.8. Functional Ca <sup>2+</sup> Imaging and Analysis.....	31
3.2.9. Staining with CellTrace™ .....	32
3.2.10. Confocal Microscopy and Positional Quantification.....	32
3.2.11. Statistical Analysis and Graphing.....	33
3.2.13. Transcriptome Analysis .....	34
3.2.14. Systemic ATP Administration.....	35
3.2.15. IL-6 Administration to the OE.....	35
4. RESULTS.....	36
4.1. Identification of ATP-responding Non-neuronal Cells and the Effect of ATP in Zebrafish OE Neurogenesis.....	37
4.1.1. Purine-sensitive Cells are Predominantly Non-neuronal in the Zebrafish OE.....	38
4.1.2. The Sensory OE is Populated by OSNs and Sox2-positive Cells.....	40
4.1.3. ATP Responding Non-neuronal Cells are a Heterogenous Population .....	42
4.1.4. Spatially Restricted GBCs are Highly ATP Sensitive .....	46
4.1.5. Sox2-positive Non-neuronal Cells Constitute a Heterogenous Population ...	48
4.1.6. Sustentacular Cells Constitute the ATP-sensitive Suprabasal Sox2 Layer ...	50
4.1.7. HBCs Form the Basal Layer of Both Sox2-positive Cells and ATP-induced Transients .....	54
4.1.8. ATP Induces Spatially Restricted Proliferative Activity Through GBCs ..	55
4.1.9. ATP does not Activate HBC Proliferation in Intact Tissue.....	59
4.2. Characterization of Intact Tissue Dynamics of Sox2-positive Cells in the Zebrafish OE.....	62

4.2.1.	Proliferative Activities of Sox2-positive cells in the intact tissue .....	62
4.2.2.	Proliferative Activities of Sox2-positive Cells in Response to Damage ...	69
4.2.3.	HBCs Show Continuous Proliferative Activity with Varied Frequencies Along Radial Positions .....	74
4.2.4.	HBC Activity Cannot be Detected Three Months After Labeling .....	78
4.2.5.	BrdU-labelling Could Indicate Relative Proliferative Activity of Non- neuronal Cells .....	80
4.2.6.	SCs are BrdU-positive Mainly in Mid-sensory Regions After Three Months Following BrdU labeling .....	84
4.2.7.	HBCs are Almost Completely Renewed within Two Weeks with Rare Neurogenic Activity .....	86
4.2.8.	SCs Originate from ILC and SNS in the Intact OE and Displace with OSNs .....	90
4.2.9.	Lineage Tracing with EdU and Two-week Continuously BrdU Labeled Intact Tissue .....	96
4.2.10.	Clonal BrdU-positive Cells can Help Uncover OSN Cell Lineage Dynamics in Zebrafish OE .....	99
4.3.	Transcriptome Profiling of the Regenerating Zebrafish OE .....	102
4.3.1.	Quality Control and Genomic Alignment Rates .....	103
4.3.2.	PCA and Hierarchical Clustering of Gene Expression Reveal Distinct Phases of Regeneration .....	105
4.3.3.	k-means Clustering Revealed Early and Late Enriched Genes in the Regenerating OE .....	107
4.3.4.	Differentially Expressed Cytokines Could Have a Signaling Role in Regenerative Neurogenesis .....	111
4.3.5.	Il6 Promotes Cell Proliferation in the Intact OE .....	114
4.3.6.	IL-6 Induces Neurogenesis Through HBC Proliferation .....	117
5.	DISCUSSION .....	122
5.1.	Purine-Sensitive Non-Neuronal Cells in the Zebrafish OE .....	123

5.2. ATP Selectively Modulates Maintenance Neurogenesis.....	128
5.3. HBC Dynamics Under Physiological Conditions .....	130
5.4. HBC-derived Cell Clones Provides Insights into the OSN Lineage under Physiological Conditions .....	132
5.5. SC Dynamics Under Physiological Conditions.....	134
5.6. A Proposed Maintenance Neurogenesis Model for the Zebrafish OE .....	138
5.7. Transcriptome of the Lesioned OE Describes Distinct Phases of Regeneration.	143
5.8. Regulatory Effect of IL-6 on the HBC Progenitor Pool.....	145
REFERENCES .....	149
APPENDIX A: Chemicals and Reagents .....	179
APPENDIX B: Disposable and Non-disposable Equipment.....	181
APPENDIX C: Transcriptome Sequencing Depth Before and After FastQC.....	182
APPENDIX D: Transcriptome KEGG Pathway GO term Analysis .....	183
APPENDIX E: Transcriptome Biological Process GO term Analysis.....	186
APPENDIX F: Transcriptome Molecular Function GO term Analysis .....	191

## LIST OF FIGURES

Figure 1.1. Structural overview of the zebrafish OE. ....	13
Figure 1.2. Cellular composition of the zebrafish OE. ....	14
Figure 4.1. Stimulation of the OE slices with ATP or KCl. ....	39
Figure 4.2. Cellular architecture of the sensory epithelium.....	41
Figure 4.3. 2-MeSATP responding cells show earlier response onsets to ATP. ....	43
Figure 4.4. Positional profile of ATP responding intermediate cells.....	45
Figure 4.5. GBCs correlate with radial and vertical positions of high ATP sensitive cells. ....	47
Figure 4.6. Sox2-positive cells with different morphologies define distinct epithelial strata.....	49
Figure 4.7. Suprabasal Sox2-positive cells are SCs.....	51
Figure 4.8. CKII exclusively label SCs in sensory region.....	52
Figure 4.9. Immunostaining on dissociated tissue chunks.....	53
Figure 4.10. Purine sensitive basal cells are HBCs.....	55
Figure 4.11. ATP-induced proliferative activity at 72hpi.....	57
Figure 4.12. ATP does not activate HBC proliferation at 72 hpi.....	58

Figure 4.13. Cumulative cell type specific effect of fish injected with PBS, ATP, or ATP and Suramin at 72 hpi .....	60
Figure 4.14. PCNA-immunoreactive cells are Sox2-positive in the sensory region. ....	63
Figure 4.15. 24h proliferative activity of HBCs and SCs in the intact tissue. ....	65
Figure 4.16. Transition of cell morphology at the SNS. ....	66
Figure 4.17. OE tissue stained against Krt5 and BrdU following a 24h BrdU pulse. ....	68
Figure 4.18. Chemically lesioned OE compared to intact tissue at 24hpl. ....	70
Figure 4.19. Lesion activated HBCs show changes in morphology and invade the tissue. ....	71
Figure 4.20. Sustentacular cells regenerate following a chemical lesion. ....	73
Figure 4.21. Radial distribution of Krt5/BrdU cells after a 24 and 168 h BrdU pulse. ....	75
Figure 4.22. Quantification of active HBCs and prediction of HBC cell cycle time. ....	77
Figure 4.23. 168 h BrdU pulse chased for 3 months in the intact OE. ....	79
Figure 4.24. BrdU-labeling shows variability after 3 months of BrdU staining (green). ....	81
Figure 4.25. BrdU-label intensities of BrdU+ only and double-labeled cells after 3 months. ....	82
Figure 4.26. Sustentacular cell activity in tissue labeled with BrdU for 168 h after 3 months. ....	85
Figure 4.27. HBC activity in OEs labeled with BrdU (green) for two weeks counterstained with Krt5 (red) and HuC/D (blue). ....	87

Figure 4.28. Positional quantification of BrdU+ cells continuously labeled for 2 weeks ..	88
Figure 4.29. SC activity on 2-week continuously BrdU labeled OE. ....	91
Figure 4.30. Sustentacular cells originate from the ILC and SNS. ....	93
Figure 4.31. Sustentacular cells originate from ILC and SNS. ....	95
Figure 4.32. Single pulse EdU on 2-week continuously BrdU incorporated tissue after 24h. ....	97
Figure 4.33. Asymmetric HBC division only forms GBCs in sensory region. ....	98
Figure 4.34. Normalized number of cell composition of clonal clusters. ....	100
Figure 4.35. Genomic alignment and transcriptome analysis pipeline. ....	104
Figure 4.36. Quality of RNA reads before and after FastQC cleaning. ....	104
Figure 4.37. PCA, correlation matrix and hierarchical clustering of gene expression. ....	105
Figure 4.38. k-means clustering of differentially expressed genes. ....	108
Figure 4.39. Cytokines are among the most upregulated genes in regenerating OE. ....	113
Figure 4.40. Effect of IL-6 on proliferation at 24 hpi. ....	115
Figure 4.41. Cell type specific immediate effect of IL-6 stimulation at 24 hpi. ....	116
Figure 4.42. Effect of IL-6 on cell proliferation at 72 hpi. ....	118
Figure 4.43. Quantitative analysis of the effect of IL-6 on proliferation at 72 hpi. ....	119

Figure 4.44. Statistical analysis of IL-6 effect on cell types in radial positions at 72 hpi. 121

Figure 5.1. Distinct proliferation events taking place in the SNS under physiological conditions..... 136

Figure 5.2. Lineage relation of different cell types in the zebrafish OE..... 139

## LIST OF TABLES

Table 3.1.	List of primary antibodies .....	29
Table 3.2.	List of secondary antibodies and nuclear markers.....	30
Table 4.1.	KEGG pathway GO-terms of k-means clusters. ....	110
Table 4.2.	GO-term analysis summary of interesting KEGG pathways significantly regulated at 4, 12 and 24 hpl.....	112
Table A.1.	List of chemicals and reagents used in this study.....	179
Table A.2.	List of chemicals and reagents used in this study (cont.).....	180
Table B.1.	List of disposable and non-disposable equipment.....	181
Table C.1.	Read numbers before and after rRNA sorting and adapter trimming. ....	182
Table D.1.	List of KEGG pathway GO terms significantly regulated at 4h post lesion.	183
Table D.2.	List of KEGG pathway GO terms significantly regulated at 12h post lesion.....	184
Table D.3.	List of KEGG pathway GO terms significantly regulated at 24h post lesion.....	185

Table E.1.	List of biological process GO terms significantly regulated at 4 h post lesion.....	186
Table E.2.	List of biological process GO terms significantly regulated at 4h post lesion (cont.). .....	187
Table E.3.	List of biological process GO terms significantly regulated at 12h post lesion.....	188
Table E.4.	List of biological process GO terms significantly regulated at 12h post lesion (cont.). .....	189
Table E.5.	List of biological process GO terms significantly regulated at 24h post lesion.....	190
Table F.1.	List of molecular function GO terms significantly regulated at 4h post lesion.....	191
Table F.2.	List of molecular function GO terms significantly regulated at 4h post lesion (cont.). .....	192
Table F.3.	List of molecular function GO terms significantly regulated at 12h post lesion.....	193
Table F.4.	List of molecular function GO terms significantly regulated at 12h post lesion (cont.). .....	194
Table F.5.	List of molecular function GO terms significantly regulated at 24h post lesion.....	195

**LIST OF SYMBOLS**

F	Fluorescence
G	Gauge
H	Hour
hpi	Hour post injection
hpl	Hour post lesion
l	Liter
mg	Milligram
mm	Millimeter
mM	Millimolar
n	Number of samples
ng	Nanogram
$\mu$ l	Microliter
$\mu$ g	Microgram
$^{\circ}$ C	Degree Celcius
$\mu$ m	Micrometer
$\pm$	Plus or minus
$\Delta$ F	Change in fluorescence
$\Delta$ F/F	Fold change in fluorescence

## LIST OF ACRONYMS / ABBREVIATIONS

2-MeSATP	2-methylthio-adenosine-5'-triphosphate
ACSF	Artificial Cerebrospinal Fluid
Adj.Pval	Adjusted P value
ANOVA	Analysis of Variance
AOB	Accessory Olfactory Bulb
Ascl1	Achaete Scute Homolog – 1
ATP	Adenosine Triphosphate
BrdU	Bromodeoxyuridine
CKII	Cytokeratin Type-2
DEG	Differentially Expressed Gene
IL-6	Interleukin 6
DG	Dentate Gyrus
EdU	5-ethynyl-2'-deoxyuridine
EF	Epithelial Fold
GAGE	Generally Applicable Gene Set Enrichment
Ctrl	Control Condition
GBC	Globose Basal Cell
GBC <sub>INP</sub>	Immediate Neuronal Precursor Globose Basal Cell
GBC <sub>MPP</sub>	Multipotent Progenitor Globose Basal Cell
OPP/GBC	Olfactory Placodal Progenitor Globose Basal Cell
GBC <sub>TA</sub>	Transiently Amplifying Globose Basal Cell
GBC <sub>SC</sub>	Sustentacular Cell precursor Globose Basal Cell
GO	Gene Ontology
HBC	Horizontal Basal Cell
high K	High Concentration of Potassium
HuC/D	Hu Protein C / D
Idep	Integrated Differential Expression and Pathway Analysis

ILC	Inter Lamellar Curve
Krt5	Keratin 5
MS222	Tricaine Methanosulfonate
MVG	Most Varied Genes
Ns	Non-sensory
OB	Olfactory Bulb
OE	Olfactory Epithelium
OMP	Olfactory Marker Protein
OSN	Olfactory Sensory Neuron
p63	Tumor Protein 63
PBS	Phosphate Buffered Saline
PBST	Phosphate Buffered Saline with Tween 20
PCA	Principal Component Analysis
KEGG	Kyoto Encyclopedia of Genes and Genomes
PCNA	Proliferating Cell Nuclear Antigen
PFA	Para Formaldehyde
pH	Potential / Power of Hydrogen
RNA	Ribonucleic Acid
RNA-seq	RNA-sequencing
SC	Sustentacular Cell
SEM	Standard Error of Means
SGZ	Subgranular Zone
SNS	Sensory / Non-sensory Border
Sox2	Sex Determining Region Y-box 2
TrX	1% Triton X-100
VNO	Vomeronasal Organ
V-SVZ	Ventricular-Subventricular Zone

# 1. INTRODUCTION

## 1.1. Adult Neurogenesis

Santiago Ramon y Cajal's observations of the structure and connections of neurons and extremely detailed illustrations of the central nervous system (CNS) provided the scientific community with the first look into the brain in a way that was never seen before (Cajal, 1913). However, the sheer complexity of neuronal structures and networks that he observed in the brain led him to formulate what became known as the "central dogma", which states that these networks can only be established in early developmental stages. When broken or damaged during the adult life, the nervous system cannot be regenerated. This idea remained unchallenged until the 1960s by Joseph Altman's study on the injured rat brain. Using radioactive thymidine analogues to detect dividing cells in the brain upon bilateral electrolytic lesioning, Altman observed label-positive neuroblasts, glial cells, and neurons (Altman, 1962). This controversial observation pioneered an ever-increasing number of adult neurogenesis studies with the aim to discover the regenerative capabilities of nervous tissues and to strategize the development of effective therapeutic methods.

Further radioautography studies with thymidine analogues provided solid evidence of adult born neurons in the rat (Kaplan and Hinds, 1977; Kaplan, 1981) and primate brain (Kaplan, 1983), followed by a series of studies that isolated neural progenitors from the mammalian brain (Richards *et al.*, 1992; Reynolds and Weiss, 1992). Later, the establishment of non-radioactive thymidine analogues, such as bromodeoxyuridine (BrdU) incorporation studies for tracing cell lineages accelerated the field (Kuhn *et al.*, 1996, Gross, 2000). At the beginning of the 21<sup>st</sup> century, it was accepted that an evolutionarily conserved and persistent life-long neurogenesis takes place in mammalian and non-mammalian vertebrates, including in humans (Eriksson *et al.*, 1998; Kaslin *et al.*, 2008; Zhao *et al.*, 2008, Bergmann *et al.*, 2015).

Under physiological conditions, constitutive neurogenesis in the adult brain of mammals takes place in the ventricular-subventricular zone (V-SVZ) of the lateral ventricles and the subgranular zone (SGZ) of the hippocampus (Gage, 2000). Adult born neurons from the V-SVZ then migrate as neuroblasts towards the olfactory bulb (OB) (Alvarez-Buylla and Garcia-Verdugo, 2002; Kaneko *et al.*, 2017; Ming and Song, 2011), where they mature into GABA-ergic interneurons (Alvarez-Buylla & Garcia-Verdugo, 2002; Lois & Alvarez-Buylla, 1994). In the SGZ, newborn neurons integrate into the neural tissue of the dentate gyrus (DG) in the adult life (Hayashi *et al.*, 2015).

Two characteristic features define stem cell identity: self-renewal and the ability to generate cells that can differentiate to obtain specialized terminal identities (Gage, 2000). This unique feat is accomplished through asymmetric cell divisions during which the generated daughter cells assume differential fates (Horvitz and Herskowitz, 1992). Two candidate cell types with these properties were found in rodent (Richards *et al.*, 1992; Reynolds and Weiss, 1992; Palmer *et al.*, 1999) and human brains (Palmer *et al.*, 1995; Kukekov *et al.*, 1999), glial fibrillary acidic protein (GFAP)-expressing radial glial cells and non-radial cells expressing the sex determining region Y-box 2 (Sox2) transcription factor (Alvarez-Buylla and Lim, 2004; Lugert *et al.*, 2010). Using retroviral lineage tracing methods in the intact brain GFAP-expressing radial glia-derived B1 cells were shown to give rise to cells in the OB where anti-mitotic treatments decreased the number of neuroblasts and proliferating glia (Doetsch *et al.*, 1999;). On the other hand, Sox2-expressing neural stem cells (NSCs) give rise to both glia and neurons in the SGZ (Suh *et al.*, 2007). More recent studies revealed that radial glia in the SVZ give rise to transit-amplifying cells that populate OB with various GABA-ergic interneuron types (Lledo *et al.*, 2006). In the SGZ, Sox2-expressing radial astrocyte precursors generate intermediate progenitors that give rise to neuroblasts that differentiate into granule cells of the dentate gyrus in the hippocampus (Zhao *et al.*, 2006). However, the precise lineage hierarchy between progenitor cells in these niches still remain partially elusive.

Several other regions of the brain were also proposed to possess NSCs, such as the hypothalamus, striatum and neocortex (Feliciano *et al.*, 2015; Inta *et al.*, 2015; Jin, 2016). However, these regions do not show the “canonical” neurogenic activity that takes place in the V-SVZ and SGZ and non-neuronal cell proliferation can be observed more commonly (Rusznak *et al.*, 2016). The question arises why the hippocampus and OB require this constitutive neurogenesis activity and lifelong production of new neurons? Studies show that the dorsal hippocampus is crucial in spatial learning and the formation of new memories (Deng *et al.*, 2010), an ability which could be facilitated by neurogenesis and the constant integration of new neurons into existing neuronal networks (de Miranda *et al.*, 2017). On the other hand, V-SVZ-originated cells that migrate towards the OB and function as interneurons may allow for establishment of new and altered synaptic connections in olfactory processing circuits to adapt to or to maintain changing sensory inputs (Alvarez-Buylla & Garcia-Verdugo, 2002). Persistent daily neurogenesis also takes place in the peripheral olfactory epithelium (OE; a topic that will be discussed in detail in the following sections) and increased plasticity of synaptic connections within the olfactory bulb may support persistent and meaningful odor perception (Graziadei and Graziadei, 1978; Hinds *et al.*, 1984).

Regenerative neurogenesis, on the other hand, describes the process of generating new neurons when the tissue integrity or homeostasis is severely disrupted. Distinct from constitutive neurogenesis, regeneration requires the restoration of both neuronal and non-neuronal cell populations in order to re-establish the functionality of the overall tissue or sense organ tissue. Thus, regenerative neurogenesis must somehow take priority in the damaged tissue context. One possibility could be that NSCs that contribute to maintenance neurogenesis could also give rise to distinct neuronal cell identities to integrate into other brain regions in response to injury or degeneration.

Further studies on vertebrate CNS neurogenesis revealed an inverse relationship between the neurogenic and regenerative capacity and the evolutionary complexity of the brain (Kizil *et al.*, 2012; Schmidt *et al.*, 2013). Typically, more zones with neural stem cells can be observed in lower vertebrates than in mammals (Alunni and Bally-Cuif, 2016). In adult medaka and zebrafish, for instance, there are active progenitors at the periphery of the optic tectum (Alunni *et al.*, 2010; Ito *et al.*, 2010). At the margins of the zebrafish pallium non-glia NCSs with constitutive neurogenesis activity were observed to be involved in injured tissue regeneration along with radial glial cells that are normally dormant under physiological conditions (Dirian *et al.*, 2014). Activation of dormant neural stem cells is also often accompanied by the recruitment of immune system function (Kyritsis *et al.*, 2012, Baumgart *et al.*, 2011).

Similar studies in other peripheral sensory tissue strongly suggest that regenerative neurogenesis largely depend on dormant progenitor cells that are not involved in daily maintenance of the tissue (Fausett and Goldman, 2006; Bernardos *et al.*, 2007; Leung *et al.*, 2007). Thus, constitutive and regenerative neurogenesis must be tightly controlled by distinct regulatory events and signals to activate the right type and number of progenitors to re-establish neural tissue or to preserve meaningful physiological function and tissue integrity.

Maintenance and regenerative neurogenesis events are evolutionarily conserved among species (Cayre *et al.*, 2002). Although the human brain shows neurogenic characteristics that is similar to other vertebrate models (Eriksson *et al.*, 1998; Gonçalves *et al.*, 2016; Spalding *et al.*, 2013), studies show that neurogenesis in human brain is mainly restricted to the SVZ (Bergmann *et al.*, 2015). On the other hand, there are conflicting reports about the activity in the SGZ. Some studies show that there may be no (or extremely rare) persistent neurogenic activity in the hippocampus after childhood (Sorrells *et al.*, 2018), while a different study found evidence for neurogenesis at 80 years of age (Boldrini *et al.*, 2018). However, other than studies on humans with psychiatric disorders showing abnormal hippocampal neurogenesis (Gonçalves *et al.*, 2016), there is no further evidence on the mechanism of neurogenesis in the human brain but suggests a link between disease and neurogenesis.

A lifelong persistent neurogenesis is required to maintain the meaningful function of the nervous systems against possible loss of neurons that might be encountered naturally throughout life or be accelerated during neurodegenerative disorders. As previously described, lower vertebrates, and especially the peripheral sensory tissues, could yield unique and meaningful insight by studying neurogenesis under physiological conditions or in damage context. Findings from these studies could help during the development of more effective treatments against gradual or acute neuronal loss caused by traumatic brain injuries, natural cognitive decline, and neurodegenerative diseases.

## 1.2. Olfactory system

Unlike other neuronal structures, the olfactory system is unique in the way that it shows lifelong neurogenesis from both the central OB (Altman, 1969, Lim and Alvarez-Buylla, 2016) in the forebrain and the peripheral sensory OE (Graziadei and Graziadei, 1978; Hinds *et al.*, 1984). While the auditory and visual systems deal with the detection and processing of physical stimuli, the olfactory system is responsible for the detection of external chemicals, also called odorants, through highly sensitive and specific chemoreceptors. Unlike sound vibrations and light that are distinguished by single attribute (frequency or wavelength, respectively), odorants are chemicals with wide structural variety and differences in complexity that require specific chemoreceptor cells, the olfactory sensory neurons (OSNs), to correctly analyze, interpret, and represent the environment. Odorants give valuable environmental information that are related to mating, sources of food and water, or the presence of predators. Due to their specific function in detecting outside chemicals, OSNs are in direct contact with the environment, which makes them highly susceptible to toxins or pathogens during odor sensation (Moulton, 1974). Thus, odor sensation is sustained with a lifelong maintenance neurogenesis in the OE, and OB is constantly supplied with new interneurons to preserve synaptic plasticity (Takahashi *et al.*, 2018) to match the dynamic OE maintenance and efficient regenerative neurogenesis that take place in the olfactory system (Brann and Firestein., 2014).

Odorants are recognized by specialized OSNs that line the outer surface of the olfactory epithelium (OE) located in the nasal cavity. Highly specific olfactory receptor (OR) proteins (Buck and Axel, 1991) that are abundant in the ciliated structures of apically protruding dendrites (Barnea *et al.*, 2004), mediate the molecular recognition of these chemical cues. These interactions are then transmitted as electrical signals in the OSNs to the OB as the next step of odor perception. Due to the diversity of candidate odorant ligands, the size of the OR repertoire is extremely large and comprises about 450 functional genes in humans or more than 1000 in rodent species (Niimura and Nei, 2004). OSNs that express the same ORs extend their axons into same regions of the OB (Vassar *et al.*, 1994; Buck, 2000) where axons coalesce into single or multiple spherical structures called glomeruli (Baier and Korshing., 1994; Mombaerts, 1996; Chen *et al.*, 2005; Braubach *et al.*, 2012). In these glomeruli, axons from OSNs form synapses with mitral cells and interneurons that relay odor information to higher-order cortical areas for conscious smell perception. This organization of the olfactory system is highly conserved among different species, but different organizations of olfactory organs are also observed. For instance, in rodents, main OE, septal organ of Maseria (SO) and Grueneberg ganglion (GG) innervate the main olfactory bulb (OB), whereas vomeronasal organ (VNO) innervates the accessory olfactory bulb (AOB) (Su *et al.*, 2009). In contrast, fish appear to possess only a single olfactory organ that includes multiple diverse chemosensory subtypes (Calvo-Ochoa *et al.*, 2021).

This specific wiring is also a representation of the functional OR repertoire of the OSNs in these organs. As previously described, OSNs expressing the same receptor innervate the same or multiple glomeruli in OB or AOB (Vassar *et al.*, 1994; Chen *et al.*, 2005), but may also rarely overlap (Mucignat-Caretta *et al.*, 2012). In addition to the specificity of the neuronal wiring, a single OSN only expresses one olfactory receptor protein (Mombaerts, 2004), and receptor gene choice is a unique phenomenon that is based on a complex “monogenic and monoallelic” expression mechanism (Chess *et al.*, 1994; Mombaerts *et al.*, 1996), meaning that only one of the maternal or paternal alleles of a single receptor gene from the whole repertoire is expressed by any given OSN.

ORs comprise the largest gene family of chemoreceptors in vertebrate genomes (Zhang and Firestein, 2002) and are mainly responsible for generic odorant recognition. ORs and also a small number of trace amine associated receptors (TAARs) responsible for detecting social cues and involved in gender recognition (Fleischer *et al.*, 2007; Liberles and Buck, 2006), are expressed mainly in the OE. In the VNO, V1r and V2r type receptors are responsible for detecting pheromones (Matsunami and Buck, 1997) that play an important role in sexually-guided behavior and aggression. A subset of ORs are expressed in the SO which can recognize changes in air pressure (Grosmaître *et al.*, 2007; Ma *et al.*, 2003). In the GG in addition to a subset of ORs (Fleischer *et al.*, 2007), one V2r type receptor that is involved in freezing behavior in mice is also expressed (Brechtbuhl *et al.*, 2018). Nevertheless, the most conserved olfactory structure for odor recognition across vertebrates seems to be the main OE. Although, distinct gene families are observed to be expressed in different olfactory organs, in the species where VNO is not present, required olfactory functions are accomplished by the OE.

The OE tissue is under a constant threat of environmental toxins (Sunderman, 2001), but also provides a gateway for pathogens into the CNS due to the direct axonal route between the OE and the OB of the forebrain (Kristensson *et al.*, 2013). OSNs appear to have a limited lifespan of around 30-90 days (Mackay-Sim and Kitter, 1991), and, consequently, effective maintenance and regenerative neurogenesis are a necessity to preserve the function of the OE. In this thesis, understanding the maintenance and regeneration of the zebrafish OE are the scope of the presented studies.

### **1.3. Organization of the Vertebrate OE and OSN Neurogenesis**

The inside of the nasal cavity of vertebrates shows a highly convoluted turbinate structure. The OE is positioned as a continuous multilayered epithelial sheet that lines the lumen of these convolutions. These turbinate organization provides a larger surface and has also been shown to determine airflow across the OE (Kimbell *et al.*, 1997) which might facilitate odorant detection. The OE itself has a pseudostratified cellular organization where nuclei of different cell types occupy discernable basal to apical layers.

Two main OSN types responsible for the odor detection, OR- and TAAR-expressing ciliated cells and V1R- and V2R- expressing microvillous cells, are positioned in the intermediate layers of the OE (Graziadei & Graziadei, 1979; Mombaerts *et al.*, 1996; Wagner *et al.*, 2006; Johnson *et al.*, 2012). Constitutively generated OSNs are added to the structure from basal layers and immature neurons comprise suprabasal OE layers (Graziadei & Graziadei, 1979). OSNs show a bipolar morphology and project a single dendrite decorated with multiple ciliary or microvillous structures to the apical surface and into the mucus that covers the epithelium (Graziadei & Graziadei, 1979; Mendoza, 1993). A single unmyelinated axon from each OSN extends from the basal soma and innervates a corresponding glomerulus in the OB, according to the previously described rules.

Bowman's glands are positioned in the mesenchyme underneath the OE and are in contact with the apical surface with duct cells piercing through the epithelium (Frisch, 1967, Graziadei & Graziadei, 1979). These cells are involved in the production of mucus that covers the epithelium and is reported also to be rich in enzymes involved in detoxification (Yu *et al.*, 2005).

Sustentacular cells (SCs) are the tissue-specific glial cells that show mainly columnar morphologies which extend from the apical surface to the basal layer where they form branched end feet that connect with the basal lamina (Graziadei & Graziadei, 1979). SCs provide structural support to the epithelium and are involved in the metabolism of odorants and other toxic compounds (Ding and Coon, 1988; Chen *et al.*, 1992; Yu *et al.*, 2005), but also in removal of debris of dead cells through phagocytosis (Suzuki *et al.*, 1995). SCs are also connected to OSN dendrites with tight junctions from their somata located at the apical layers (Vogalis *et al.*, 2005), which isolates the OSN cell bodies and the rest of the epithelium from the ionic outside environment (Miragall *et al.*, 1994). SCs characteristically express cytokeratin 8 and 18 (Ding *et al.*, 1991; Chen *et al.*, 1992) and can also be marked by their expression of sex determining region Y-box2 (Sox2) and paired box protein 6 (Pax6) (Guo *et al.*, 2010). The loss of SCs is also found to trigger regenerative neurogenesis in the vertebrate OE (Herrick *et al.*, 2017), suggesting a critical regulatory role in maintaining the tissue homeostasis.

Adult neurogenesis in the OE is supported by two key stem/progenitor cell populations that occupy basal layers of the tissue. Horizontal basal cells (HBCs) and globose basal cells (GBCs) are positioned at the adjacent basal layers and are responsible for regeneration and daily maintenance, respectively (Schwob *et al.*, 2017). HBCs, a quiescent population under physiological conditions, are activated in response to loss of structural integrity, which may include the loss of SCs (Leung *et al.*, 2007; Packard *et al.*, 2017). GBCs, on the other hand, constitute a heterogeneous group of cells that includes tissue specific stem/progenitor cell, transit-amplifying cell, and immediate neuronal precursors, some of which show constitutive mitotic activity under physiological conditions (Guo *et al.*, 2010; Chen *et al.*, 2014).

HBCs are multipotent dormant progenitors located at the basal most layer of the OE and can be visualized by their specific expression of cytokeratin 5 (Krt5) and 14 (Krt14), tumor protein 63 (p63) and intercellular adhesion molecule 1 (ICAM-1) (Carter *et al.*, 2004; Holbrook *et al.*, 1995; Fletcher *et al.*, 2011; Packard *et al.*, 2011) and by Sox2 expression generically (Guo *et al.*, 2010). Studies on the mitotic activity of HBCs and their contribution to OSN neurogenesis under physiological conditions are conflicting. One study suggests that HBCs are largely active only during developmental stages but undergo mitotic activity only twice in post-natal mice, once after four months and then 12 months of age but cease all activity later (Leung *et al.*, 2007). A different study suggested a cycle time of 30 – 60-days between mitotic events for each HBC (Mackay-Sim and Kittel, 1991; Iwai *et al.*, 2009). Although HBC activity in the intact tissue is not completely understood, it is clear that HBCs are mainly in a dormant state in the adult vertebrate OE. On the other hand, they are activated upon various *in vivo* damage conditions and quickly expand the progenitor pool up to three cell layers (Leung *et al.*, 2007). It has been demonstrated that loss of p63 expression (a member of p53 gene family) in HBCs, normally driven by Notch1/Jagged signaling from SC end feet at the basal layer, breaks dormancy and causes cell-cycle re-entry (Fletcher *et al.*, 2011; Packard *et al.*, 2011). Selective OSN ablation through OSN nerve transection (Graziadei and Graziadei, 1980; Costanzo, 1985; Packard *et al.*, 2011) does not seem to activate HBCs.

*In vivo* BrdU incorporation studies show that nasal irrigation of the OE with the toxic drugs zinc sulfate (Smith, 1938), dichlobenil (John and Key, 2003) and methyl bromide gas (Schwob *et al.*, 1995) can effectively activate HBCs by causing both OSN and SC death (Packard *et al.*, 2011). Upon chemical lesion to the OE, HBCs start to proliferate between 24 – 48 hours post lesion (hpl), and gradually return to basal levels after 4 weeks (Schwob *et al.*, 1995). Once activated, the multipotent HBC progenitor pool can reconstruct the entire OE in six to eight weeks (Schwob *et al.*, 1995). Apart from extensive *in vitro* studies (Schwob *et al.*, 2017), direct *in vivo* evidence of HBC multipotency comes from K5:CreERT2 transgenic lineage tracing in the mouse, which shows that HBCs stay dormant under physiological conditions but can give rise to OSNs and SCs by differentiating into GBCs and can also re-establish Bowman's duct/gland cells (Leung *et al.*, 2007). However, direct lineage relations between HBC and GBC progenitor pools under physiological conditions are difficult to establish with real certainty.

It is interesting to note that the OE only partially recovers after bullectomy (Costanzo and Graziadei, 1983; Schwob *et al.*, 1992). Newly generated OSNs either remain mostly immature (Schwob *et al.*, 1992) or innervate different glomeruli (Christensen *et al.*, 2001) and show different responses to odorants (Yee and Costanzo, 1998), pointing towards an alteration in odor perception. These observations suggest a requirement for trophic factors from the OB that support OSN differentiation or survival for the effective re-establishment of odor perception.

The main mode of neurogenesis that can be observed upon nerve transection originates from GBCs, which are also located at the basal layers (Carter *et al.*, 2004). Unlike HBCs, GBCs comprise a heterogeneous population that is mitotically active throughout life (Guo *et al.*, 2010; Chen *et al.*, 2014, Brann and Firestein, 2014). *In vitro* cell culture and cell transplantation studies show that according to specific transcription factor expression, GBCs can be divided into three groups within the same lineage hierarchy (Schwob, 2002). Multipotent GBCs (GBC<sub>MPP</sub>) are committed stem cells that can give rise to OSNs, SCs and also Bowman's duct/gland cells following transplantation into injured OE. These cells are marked by Sox2 and Pax2 expression (Goldstein *et al.*, 1998; Chen *et al.*, 2004).

Following differentiation, GBC<sub>MPP</sub> give rise to transiently amplifying GBC progenitors (GBC<sub>TA</sub>) which are committed to the OSN lineage and are characterized by achaete scute homolog-1 (*Ascl1*) expression (Cau *et al.*, 2002; Jang *et al.*, 2003; Caggiano *et al.*, 1994; Krolewski *et al.*, 2012). Increased expression of differentiation factors neurogenin1 (*Ngn1*) (Cau *et al.*, 1997) and NeuroD1 (Shaker *et al.*, 2012), forces GBC<sub>TA</sub> to differentiate into immediate neuronal precursor GBCs (GBC<sub>INP</sub>). GBC<sub>INP</sub> then differentiate into immature OSNs, which express GAP-43, a protein related to axonal growth (Holtmaat *et al.*, 1995). Mature functional OSNs can then be identified by their characteristic olfactory marker protein (OMP) expression that is required in formation of correct glomerular connections in the OB (Albeanu *et al.*, 2018) and functional odor sensation (Lee *et al.*, 2011). It is also shown in adult mice that *Lgr5*, a G-protein coupled receptor that was shown to be expressed by stem cells in the small intestine (Barker *et al.*, 2007), hair follicles (Jaks *et al.*, 2008) and the tongue (Yee *et al.*, 2013), is also expressed by actively dividing GBCs that can give rise to OSNs in the intact OE (Chen *et al.*, 2014). However, which GBC type in the lineage hierarchy expresses *Lgr5* is still obscure. Apart from the OSN lineage, GBCs can also give rise to SC precursor GBCs (GBC<sub>SC</sub>) marked by their expression of *Hes1*, instead of *Ascl1*, and which differentiate into SCs when transplanted into lesioned OE (Manglapus *et al.*, 2004), demonstrating the multipotency of GBCs.

It is also important to mention that transplantation studies also revealed that SCs and Bowman's duct /gland cells can self-renew (Huard *et al.*, 1998). Interestingly, detached duct cells showed migratory behavior along the surface of the epithelium and can become SCs (Schwob *et al.*, 1995). Due to their continuous lifelong activity that persists in aged animals (Brann and Firestein 2010), GBCs are accepted as the SC lineage origin under physiological conditions. Thus, in the vertebrate OE, two progenitor cell pools that are similarly positioned inside the epithelium, GBCs and HBCs, orchestrate the lifelong persistent maintenance and regenerative neurogenesis, respectively. While one is persistently active, the other one serves as a reserve stem cell population that is activated under extreme conditions (Herrick *et al.*, 2017). However, the specific lineage relationship between HBC and GBC is still obscure, and basally restricted positioning of the progenitor pools pose a challenge in these studies.

#### 1.4. Organization of the Zebrafish OE and OSN Neurogenesis

Compared to most other vertebrates that possess an OE and a separate VNO, the zebrafish has only a single olfactory organ, which is divided into separated bilateral OEs inside individual nasal cavities that are located dorsally to the mouth. Sealed from the ventral side, the OE faces dorsal and slightly anterior within the nasal cavity. In addition to ciliated OSNs, microvillous OSNs, that are characteristically found in the terrestrial vertebrate VNO, are present in the same zebrafish OE (Hansen and Zeiske, 1998; Sato *et al.*, 2005). Following the same one receptor one neuron (Mombaerts, 2004; Dang *et al.*, 2018) and monogenic/monoallelic expression (Chess *et al.*, 1994; Mombaerts *et al.*, 1996) rules as other vertebrates, OSNs innervate the OB located at the anterior telencephalon (Hansen and Zeiske, 1998). Water flow to the OE is achieved by anterior and posterior outlets of the nasal cavity as the fish propagate through water. The zebrafish OE shows an organization with stacked lamellae that project outwards from the median raphe which separates the OE into bilateral stacks (Figure 1.1; top).

The epithelial sheets span both surfaces of the lamellar structure by folding around the inner edge between lamella before the median raphe, effectively forming independent epithelial folds (EF) in between lamellae structures (Figure 1.1; bottom). Analogous to the turbinates in the rodent OE, these folds increase the surface area to enhance odor detection (Calvo-Ochoa *et al.*, 2021). In the adult zebrafish OE, new lamellae are constitutively produced and added to the anterior OE throughout life (Hansen and Zeiske, 1998). Depending on the age or the quality of the aqueous environment, usually 12-24 lamellae can be observed (Calvo-Ochoa *et al.*, 2021). The zebrafish OE is also functionally separated into two concentric circular regions according to the presence of OSNs. The inner circle, which corresponds to about two-thirds of each epithelial fold and is called the “sensory region” due to the restricted localization of OSNs to this region of the OE. The sensory region on each epithelial fold is flanked by the centrally located “interlamellar curve” (ILC) that faces the median raphe and the transient between inner and outer regions at the “sensory-nonsensory border” (SNS).

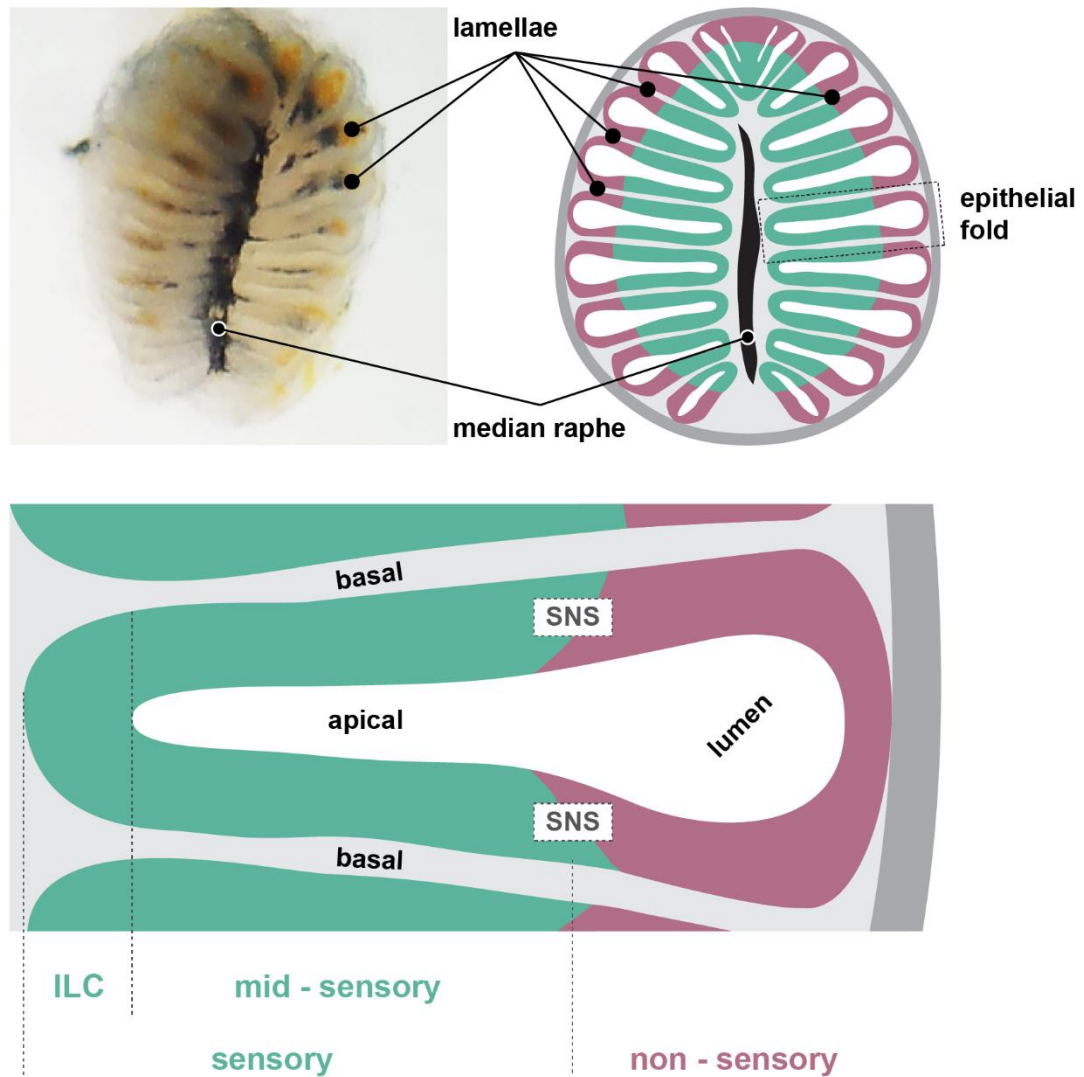


Figure 1.1. Structural overview of the zebrafish OE.

The outer “non-sensory” region does not harbor OSNs but is populated by beating ciliated cells that facilitate water flow inside the ventrally sealed OE (Reiten *et al.*, 2017) and goblet cells that are responsible for mucus production (Hansen and Zeiske, 1998), which are functional analogues to the respiratory OE in higher vertebrates (Morrison and Constanzo, 1992). The clear separation between sensory and nonsensory regions can easily be observed by antibody staining against the ELAV-like mature OSN marker HuC/D (Bayramlı *et al.*, 2017) or the expression of ciliated OSN marker OMP in the zebrafish OE (Çelik *et al.*, 2002).

OSNs in the zebrafish OE also show a specific basal to apical distribution. Unlike terrestrial and amphibious vertebrates, the zebrafish OE is the only olfactory organ and harbors all types of OSNs in the OE. To date, five types of receptor cells, the ciliated, microvillous, crypt, kappe and pear OSNs, have been described according to their characteristic morphology, OR, and marker expression (Hansen and Zeiske, 1998; Calvo-Ochoa and Byrd-Jacobs, 2019; Ahuja *et al.*, 2013; Ahuja *et al.*, 2015; Wakisaka *et al.*, 2017) (Figure 1.2).

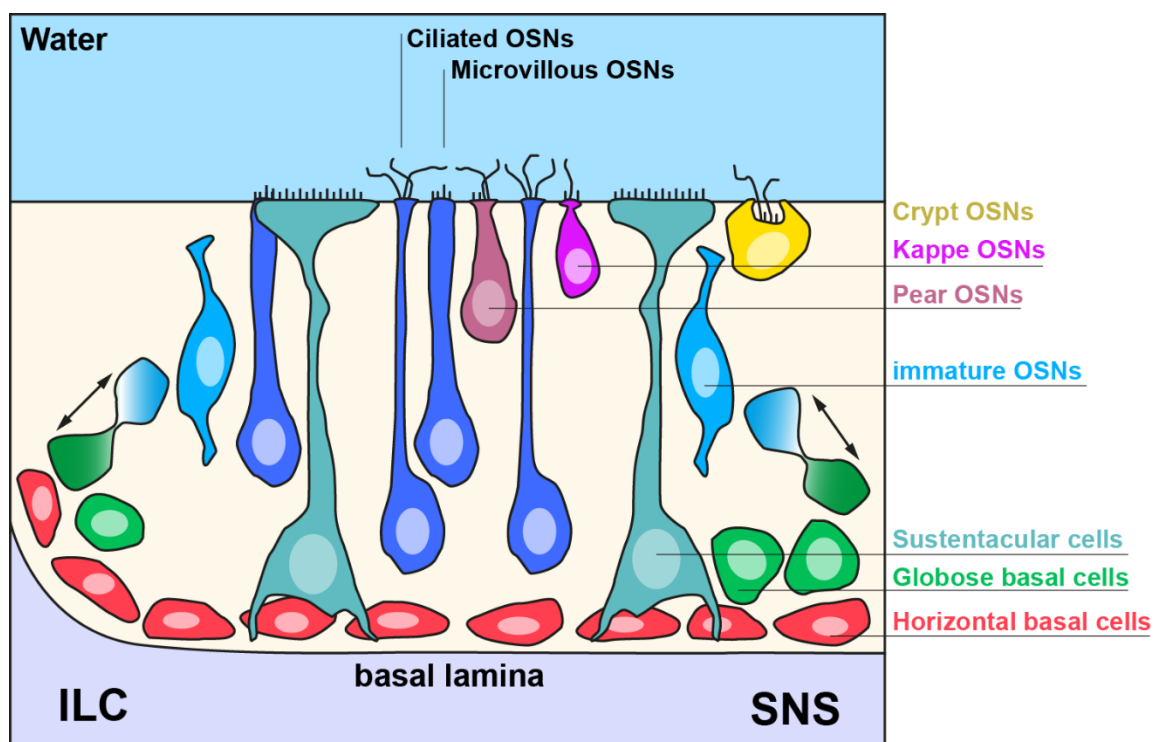


Figure 1.2. Cellular composition of the zebrafish OE.

Somata of bipolar ciliated OSNs are located in intermediate layers and closer to the basal layer (Figure 1.2). They show slender dendrites that protrude apically and a single axon at the basal portion that innervates the OB. Similar to mammals, ciliated OSNs express receptors of the OR or TAAR gene families (Niimura and Nei, 2005; Niimura, 2009; Hussain, 2009), and can be observed by specific OMP expression (Sato *et al.*, 2005).

Microvillous OSNs are also bipolar neurons located just apically to the ciliated neurons and have thicker and shorter apically protruding dendrites end with microvilli formations that expand into the outer lumen. This OSN type specifically express transient receptor potential cation channel type C2 protein (TrpC2) (Sato *et al.*, 2005) and show receptor expression preference to V1R and V2R receptor gene families (Saraiva *et al.*, 2007; Ahuja *et al.*, 2018)

The crypt, kappe and pear neurons, which describe minor OSN populations, are all polar OSNs that show direct contact with the apical surface of the epithelium. Depending on the cell type, they protrude either microvilli or cilia into the lumen (Calvo-Ochoa *et al.*, 2021). Crypt cells can be detected by their round cell morphology (Hansen and Zeiske, 1998) and cell type specific TrkA and S-100 expression (Catania *et al.*, 2003; Germana *et al.*, 2004), and unique expression of the V1R-type *ora4* receptor gene (Oka *et al.*, 2012). Kappe neurons show slightly longer morphology than crypt cells, present with a cap-like structure at the apical end of the cell and can be recognized by olfactory system specific G-protein *Gα-olf* expression (Ahuja *et al.*, 2015). Pear neurons exclusively express A2c receptor that is primarily sensitive to adenosine and also adenine nucleotides (Wakisaka *et al.*, 2017).

Analysis of BrdU incorporation into the zebrafish OE and chase of the BrdU pulse over different time intervals revealed that the average lifespan of OSNs is around 30-days (Bayramlı *et al.*, 2017), similar to the previously described rodent models. This OSN loss is neutralized by GBC progenitor activity in the rodent OE and the zebrafish OE also harbors OSN lineage-specific differentiation marker positive cells that resemble GBCs by their expression of *dla*, *ascl1* and *neurod* (Bayramlı *et al.*, 2017). However, unlike the rodent OE in which all progenitors are positioned in basal layers (Schwob *et al.*, 2006), zebrafish GBCs are restricted to unique proliferation zones at the ILC and SNS.

The zebrafish OE also has the ability to initiate a rapid increase in the proliferation activity upon Triton X-100 induced chemical lesion (Iqbal and Byrd-Jacobs., 2010), from a distinct progenitor cell population observed throughout the sensory region as early as 24 h (Kocagöz, 2021; Kocagöz *et al.*, under review), which resembles the HBC response in rodents (Leung *et al.*, 2007). Sox2 expressing cells in the zebrafish OE show a continuous band in the basal layer (Bali, 2015), but unlike the *Xenopus* and rodent OE (Hassenklöver, 2008; Guo *et al.*, 2010), an apical Sox2 layer formed by SCs is not present. Thus, a similar dual-progenitor system like in the higher vertebrates might be present in the zebrafish OE, where GBCs are spatially restricted to the ILC and SNS, and HBC-like cells reside throughout all positions of the sensory region.

Daily neurogenesis takes place in the zebrafish OE from the ILC and SNS where heterogenous GBC population can be observed (Bayramlı *et al.*, 2017). Adult born OSNs from the margins of the sensory OE, displace towards more central positions over time and die or are eliminated in the core of the mid-sensory region by unknown mechanisms (Bayramlı *et al.*, 2017). This lateral displacement of the OSNs is not observed in higher vertebrates, in which GBCs located at the basal layers and give rise to OSNs at their respective positions. Instead, *Ascl1a* (zebrafish functional homolog of mammalian *ascl1*)-expressing GBC<sub>TA</sub> progenitors of the zebrafish are located in radially separate proliferation zones and probably give rise to *neurod*-expressing GBC<sub>INP</sub> (Bayramlı *et al.*, 2017) that will transition into mature OSNs detected by their HuC/D expression. The zebrafish OE gets smaller towards ventral positions, and central displacement of the OSNs is conserved in the dorsal-to-ventral axis as well (Bayramlı *et al.*, 2017), suggesting that spatial restriction of the GBCs might be tightly regulated by unknown signals.

Similar with the OE of higher vertebrates, HBCs in the zebrafish OE can be labelled by targeting Krt5, p63 and Sox2 expression (Sakızlı, 2018; Demirler *et al.*, 2020; Kocagöz, 2021; Kocagöz *et al.*, under review). HBCs occupy the basal layer of the OE contacting the basal lamina (Sakızlı, 2018; Demirler *et al.*, 2020) and show horizontally elongated morphology (Sakızlı, 2018).

Under physiological conditions, HBCs were only rarely observed to show mitotic activity, but detailed studies on the nature of this HBC activity in the intact tissue were not available for the zebrafish OE. As previously described, HBCs can be effectively activated upon chemical lesioning by nasally irrigated Triton X-100 or other toxicants (Iqbal and Byrd-Jacobs, 2010; Kocagöz, 2021; Kocagöz *et al.*, under review). Upon chemical lesion, the near total loss of OSNs is observed at 24 hpl and HBCs show a symmetric expansion of the progenitor population over the same timeframe, followed by a gradually decreased rate of proliferation starting at 72 hpl (Kocagöz, 2021; Kocagöz *et al.*, under review). The tissue re-established the OSN population up to 80% by around 5 days following the injury and almost fully within a week (Kocagöz, 2021; Kocagöz *et al.*, under review). Selective ablation of OSNs by axon transection triggers an atypical latent HBC activation which is more pronounced in the ILC and SNS in the zebrafish OE (Kocagöz, 2021; Kocagöz *et al.*, under review).

SCs have been initially proposed to be present in the zebrafish OE by electron microscopy that only described columnar cells that span the OE in the vertical axis (Hansen and Zeiske, 1998). Molecular studies showed that SCs in the zebrafish OE can be labelled with *Xenopus* anti-cytokeratin type 2 antibody (Hassenklöver *et al.*, 2009; Bali, 2015). In the zebrafish OE, unlike other vertebrate models, cell bodies of SCs are located at the suprabasal layers and are uniformly distributed along the entire sensory OE (Bali 2015; Demirler *et al.*, 2020), and show morphometric correlation with a subgroup of Sox2-expressing basal cells.

In the zebrafish OE, HBC and GBC functionality closely resembles the dual-progenitor niche that is observed in the higher vertebrate models. While similar acute activation of the HBC pool upon damage and gradual transition to the quiescent state (Leung *et al.*, 2007) show that HBCs in the zebrafish OE could be constituting a similar dormant progenitor niche. On the other hand, atypical latent activation upon OSN ablation (Kocagöz, 2021) and spontaneous mitotic activity under physiological conditions has also been observed, which might suggest a broader niche or function for zebrafish HBC progenitors. Identity of the basally restricted Sox2-expressing cell population and lineage relations between HBCs, GBCs, GBC subtypes and SCs were also not available before this study.

The zebrafish OE could, however, provide us with a unique solution to study the tissue under physiological conditions due to the spatially restricted progenitor populations at least partially without the need of transgenic lineage tracing. Apart from the cell identities, interactions and signals that govern OSN maintenance and regeneration in the zebrafish OE are also largely unknown in the zebrafish OE. The lack of effective regeneration observed in the rodent model following OSN ablation (Schwob *et al.*, 1992) also suggests that independent of the progenitor type that is involved in the neurogenesis, external or internal signals and other regulatory events are required to preserve meaningful olfactory perception. This regulation might require external inputs or systemic paradigms involved to match the OB and OE maintenance and regeneration to effectively preserve or restore the nervous tissue function.

## 1.5. Molecular Regulation of Neurogenesis

To preserve the function of the OE over the life time of the organisms, the rate of neurogenesis both in intact and damaged conditions must be tightly controlled to balance the loss of OSNs that occurs either naturally or due to the injury. As too low levels of OSN generation might not be adequate to replace specific OSNs that are involved in vital behaviors such as predator avoidance or locating food sources, insufficient neurogenesis may lead to anosmia which could result not only in direct behavioral deficits but also in imbalanced emotional control and eventually anxiety or depression (Song and Leonhard, 2005; Glinka *et al.*, 2012). Excessive OSN generation in the intact tissue or following damage, on the other hand, may result in odor confusion or indiscrimination (Fleischmann *et al.*, 2008). Mechanistically, the incessant high OSN neurogenesis may also lead to progenitor pool depletion over time. Although rarely observed in the OE (Parker *et al.*, 2010; Gould *et al.*, 2020), neurogenesis, if unchecked, could also lead to neuroblastoma-like cancer formation. Yet, regulation of OSN neurogenesis in the OE is such a tightly controlled event that excess activity is only rarely observed even following severe damage and, typically, repair neurogenesis is downregulated as soon as a physiological density of OSNs is reestablished.

As previously described, studies in rodent OE showed that selective loss of OSNs following bulbectomy or genetic manipulation does not trigger HBC activity but enhances GBC proliferation rate (Leung *et al.*, 2007; Herrick *et al.*, 2017). It was later discovered using selective SC ablation that under physiological conditions, Jagged1 expressed by SCs stimulates the Notch signaling pathway in HBCs and drives p63 expression (Herrick *et al.*, 2017), which keeps the progenitor cells in a quiescent state (Fletcher *et al.*, 2011; Schnittke *et al.*, 2015). Distinct signaling molecules may affect OSN neurogenesis by agonistic or antagonistic effects.

Leukemia inhibitory factor (LIF) and transforming growth factor alpha (TGF- $\alpha$ ) stimulate neurogenesis differentially from GBCs and HBCs, respectively. LIF is normally expressed in OSNs and LIF-knock out mice show decreased GBC proliferation rate following bulbectomy since the LIFR $\beta$  receptor is only expressed in GBCs (Kim *et al.*, 2005). In contrast, promoter driven transgenic LIF expression enhanced GBC progenitor activity but does not activate HBC proliferation in the bulbectomized OE (Bauer *et al.*, 2003). A subset of OSNs, basal cells, and SCs also express TGF- $\alpha$  (Farbman and Buchholz, 1996; Ring *et al.*, 1997), which selectively stimulates HBCs and leads to increased proliferation caused by upregulated expression of EGFR (Getchell *et al.*, 2000).

Damage associated molecular patterns (DAMPs) are prominent signals that include various intracellular and extracellular components that are released from dying or damaged cells, and which are involved in activating immune responses but also cell proliferation or death (Venereau *et al.*, 2015). DAMPs are particularly interesting in this context, as their release would largely depend on the extent of cell loss in the tissue and could evoke proportional responses from progenitor cells. The proliferation-promoting effect of adenosine triphosphate (ATP) that is released from dying cells has been shown in both neuronal (Burnstock, 2016a) and various non-neuronal tissues (Burnstock, 2016b). In fact, a neurogenesis-promoting effect of ATP can be observed in the evolutionarily conserved neurogenic sites of the V-SVZ and SGZ (Suyama *et al.*, 2012; Cao *et al.*, 2013). Reports also have shown that the mouse and *Xenopus* OE express purinergic receptors and that ATP can induce Ca<sup>2+</sup>-transients in basal progenitor cells and SCs (Hegg *et al.*, 2003; Hegg *et al.*, 2009; Hassenklöver *et al.*, 2008), which leads to increased proliferation in the OE (Jia *et al.*, 2009). In this context, SCs that traverse the entire vertical axis of the OE could act as the detector of the rate of cell loss and relay this information to basal progenitors and induce proliferation. Furthermore, stimulation of the OE with ATP also results in the upregulated expression of FGF2 and TGF- $\alpha$  (Jia *et al.*, 2011) both of which have known proliferative effects. Studies from our lab also have shown that ATP can evoke Ca<sup>2+</sup>-transients in the zebrafish OE, predominantly through P2-type purinergic receptors (Bali, 2015). Initial results suggested that ATP stimulation has an enhancing effect on proliferative activity as well (Sakızlı, 2018). However, further studies are needed to accurately identify the purine sensitive cells and eventually the exact biological function of purine release in the context of neurogenesis in the zebrafish OE.

Apart from intra-epithelial regulation of regeneration or neurogenesis, the immune system is almost always involved in tissue repair (Karin *et al.*, 2016). Inflammation goes along with a release of pro-inflammatory cytokines and the recruitment of immune cells from the blood circulatory system into the tissue (Medzhitov, 2008). Studies from rodent models show that parenchymal immune cell activation decreases basal constitutive neurogenesis levels and also regeneration in the hippocampus (Monje *et al.*, 2003; Ekdahl *et al.*, 2003). Additionally, chronic release of IL-6 from astrocytes or exogenous induction of IL-1 $\beta$  decreases the rate of neurogenesis in the hippocampus (Vallieres *et al.*, 2002; Koo and Duman, 2008). Furthermore, maternal IL-6 administration, to mimic human maternal infections that could result in various cognitive disorders, results in disrupted olfactory neurogenesis and enlarged forebrain neuronal precursors in the adult mouse (Gallagher *et al.*, 2013). In contrast to mammals, acute inflammation caused by the release of pro-inflammatory cytokines is necessary to initiate regenerative responses by activating radial progenitors in the stab-lesioned zebrafish brain (Kyritsis *et al.*, 2012). A direct relationship between the immune system and OE regeneration has been reported in TNF- $\alpha$  receptor-deficient mice in a methimazole-induced damaged context (Chen *et al.*, 2017). In this study, the authors showed that TNF- $\alpha$  levels increase significantly following injury which can induce cytokine (IL-6 and TNF- $\alpha$ ) and chemokines (RANTES and IP-10) expression from HBCs. Consequently, TNFR1-deficient mice showed significantly lower cytokine and chemokine expression on the third day after a lesion and failed to recruit CD45-expressing T-cells. The study suggests that injury-related TNF- $\alpha$  release induced enhanced cytokine and chemokine release from HBCs to recruit the immune system cells into the injured tissue (Chen *et al.*, 2017). Thus, studying immune system activity and signals that are involved in both maintenance and regenerative neurogenesis may give further insight into the underlying molecular mechanisms and regulatory events that are required to fine tune neurogenesis activity.

## 2. PURPOSE

Neurogenesis, whether under physiological conditions or in a damage context, must be thoroughly orchestrated by internal and external regulatory/signaling components to ensure persistent olfactory function. Due to their nature, chemoreceptor cells in the OE are in direct contact with the external environment and susceptible to toxins, pathogens and other stressors. OSNs are continuously replaced by a process of maintenance neurogenesis that persists lifelong under physiological conditions. When homeostasis of the OE is disrupted, regenerative neurogenesis takes precedence over maintenance and ensures the structural and functional reconstitution of the zebrafish OE. Two distinct progenitor pools contribute to each of the two distinct modes of neurogenesis. However, functional characteristics of non-neuronal cell populations in the zebrafish OE have not been studied in detail to competently describe their role during OSN neurogenesis. The main aim of this study is to characterize the role of non-neuronal cells under physiological conditions with a special emphasis on the Sox2-positive cell populations and to discover signals that are responsible for triggering regenerative neurogenesis responses. The zebrafish OE provides a unique opportunity of identifying the prevalent mode of OSN neurogenesis based on the position of active progenitors within the tissue. Thus, the effect of signaling molecules and regulatory pathways can be studied, at least to an extent, without the explicit need of transgenic lines.

Purine sensitivity of the zebrafish OE suggests that ATP, released from dying or damaged OSNs, could regulate the rate of neurogenesis by either selectively activating or regulating the mitotic rate of neurogenic progenitors. However, the identity of purine-sensitive cells has not been studied rigorously. My first aim was to classify purine-sensitive cells and to examine the effect of purines on neurogenic activity in the zebrafish OE. To identify purine-sensitive cells, purine responses were systematically classified according to the differential sensitivity of OE cells to purine analogues, the temporal profiles of the response onsets, the morphology of the responding cells, and the vertical and radial positional distribution of these cells.

To match OE cell types with the various purine-sensitive cells, Sox2-positive cells were similarly classified according to their cell type-specific marker expression, their cellular morphology, and the vertical and radial positions of these cells. To investigate the biological outcome of the released ATP, I systemically applied ATP and positionally profiled the proliferation rate using BrdU incorporation assays and performed immunohistochemistry against cell type-specific markers.

In the zebrafish sensory OE, except for the subpopulation of GBC progenitors, the base level mitotic activity of Sox2-positive non-neuronal cells were not known. My second aim was to investigate the proliferation dynamics of dormant HBC progenitors and tissue specific glial SCs under physiological conditions and in a damage context. To accomplish this, short and long term BrdU incorporation assays were used to examine the activity of these cells over time and the positional displacement of HBCs and SCs in the intact tissue using immunohistochemistry against cell type specific markers. A combination of the lineage tracers BrdU and EdU was used to further investigate the lineage relationships of neuronal and non-neuronal cell types in the zebrafish OE.

Molecular signals that control maintenance neurogenesis and tissue regeneration are drawing increased attention. However, fundamental changes in the internal and/or external regulatory frameworks that are required to trigger regenerative neurogenesis are elusive. The last aim of this study was to identify which regulatory pathways, genes, and signaling molecules are unique or differentially regulated during the time course of de- and regeneration in the chemically lesioned zebrafish OE. For this purpose, global changes in gene expression by RNA-seq obtained from the different regeneration timepoints were analyzed. Using various transcriptome analysis packages, I mined for relevant upregulated pathways and candidate regulatory genes that are specifically upregulated immediately after the lesion.

Among those, the cytokine IL-6 was highly upregulated and expressed uniquely in the regenerating OE transcriptome and its *in vivo* effect on progenitor cell activity and neurogenesis in the intact tissue was functionally tested. To achieve this, the zebrafish OE was treated with IL-6 and the changes in positional proliferation rate were quantified using BrdU incorporation assays and immunohistochemistry against cell type-specific markers. I analyzed the OE at 24 hpi to see its proliferation promoting effect on the progenitor pools, and at 72 hpi to identify neurogenic activity by allowing newborn cells to differentiate into OSNs.

### **3. MATERIALS AND METHODS**

#### **3.1. Materials**

##### **3.1.1. Animals**

Adult (6 months of age or older) zebrafish (*Danio rerio*) of the AB/AB genetic background or fish derived from a local pet shop were used in this study. Animals were housed in the Vivarium Animal Facility of Boğaziçi University Center of Life Sciences and Technologies.

##### **3.1.2. Equipment and Supplies**

The lists of reagents and chemicals together with manufacturer information are detailed in tables in Appendix part A and B.

##### **3.1.3. Buffers and Solutions**

The generic buffers and solutions used in this study for standard biological techniques in zebrafish were prepared according to “The Zebrafish Book” (Westfield, 2007). Specialized or modified buffers have been described in the corresponding methods section.

## 3.2. Methods

### 3.2.1. Zebrafish Maintenance

Ethical approval to use zebrafish in this study was obtained from Institutional Ethics Board for Animal Experiments at Boğaziçi University (BÜHADYEK) with reference numbers 2012-11-28 (“Olfactory neurogenesis during tissue maintenance and repair”) and 2020-17 (“The role of heparin-binding epidermal growth factor (HB-EGF) signaling during regenerative neurogenesis in the zebrafish olfactory epithelium”). Zebrafish were kept in 1 l, 3 l or 10 l tanks containing artificial freshwater at  $28 \pm 2$  °C temperature with maximum of 5 fish/l. Light/dark cycles were set at 14h/10h. A professional pump-based housing system (Aquatic Habitats) with in-built UV-filtration, heater, aeration, and physical and biological filtering systems was used. Artificial freshwater was prepared using 100 l reverse osmosis water by dissolving 0.84 g calcium sulfate, 7.5 g sodium bicarbonate and 2.0 g sea salt. Fish were fed with flake food in the mornings and flake food supplemented with either live brine shrimp larvae (*Artemia spp.*) or frozen brine shrimp pellets in the afternoons.

### 3.2.2. Dissection of Zebrafish Olfactory Organ

Zebrafish were euthanized with an overdose (250 mg/l) with the anesthetic 3-amino benzoic acid ethylester (MS222; Sigma) dissolved in artificial freshwater in a beaker. Following the loss of opercular movements, the container was transferred into ice and kept for 10 min, followed by decapitation using surgical blades. Heads were placed into dissection plate containing ice-cold 1x PBS. Using fine forceps, parietal and frontal bones were cut into two lateral pieces with a series of shallow punctures from the median along the anterior-posterior axis and removed by holding posterior ends of cranial bones with forceps and gently twisting away from the median.

Olfactory organs together with nasal cavity bones were removed from the head and cleaned from remaining bone and skin tissues. For functional  $\text{Ca}^{2+}$  imaging, heads were placed in chilled zebrafish ACSF (131 mM NaCl, 2 mM KCl, 1.25 mM  $\text{KH}_2\text{PO}_4$ , 2 mM  $\text{MgSO}_4$ , 10 mM D-Glucose, 2.5 mM  $\text{CaCl}_2$ , 20 mM  $\text{NaHCO}_3$ , pH: 7.4) solution and same procedure was applied.

### **3.2.3. Cryosectioning of the OE**

Dissected OEs were immediately embedded into optimal cutting temperature (OCT) embedding medium-filled rubber molds and left to freeze for 15-20 min at  $-20^\circ\text{C}$ . For long-term storage, molds were wrapped with aluminum foil and kept at  $-80^\circ\text{C}$ . Frozen OCT bricks were mounted onto the stage of pre-cooled cryostat (Leica) at  $-22^\circ\text{C}$  object and  $-20^\circ\text{C}$  chamber temperatures. 12  $\mu\text{m}$  horizontal cross-sections were obtained and collected carefully onto positively charged glass slides. Prepared slides were then transferred individually into plastic petri dishes and dried at  $65^\circ\text{C}$  for 1-2 h. At this point preparations were either re-cooled to room temperature (RT) for immediate use or kept at  $-80^\circ\text{C}$  for long term storage by sealing the petri dish using parafilm or cling film.

### **3.2.4. Labeling of Dividing Cells by Thymidine Analogue Incorporation**

Solutions containing 30 mg/L 5-Bromo-2'-deoxyuridine (BrdU) were prepared freshly with aerated artificial freshwater prior BrdU incorporation assay. Fish were transferred into BrdU solution and kept in a dark container or an incubator with maximum 5 fish/l density at  $28^\circ\text{C}$  for up to 24 h in the same solution. Due to light sensitivity of BrdU, fish were always kept in the dark after the incubation when analyzed at later time points. Every 24 h, the solution was changed with a freshly prepared BrdU in accordance with the timescale of the relevant experiment. In chemical lesion experiments, fish were immediately transferred to the BrdU solution following the experimental damage explained in section 3.2.7.

For long term BrdU chase experiments, the fish were transferred into aerated artificial freshwater, which was replaced every 24 h. For BrdU/EdU sequential labelling, BrdU incorporated fish were anesthetized using 160 mg/L MS222 solution and transferred to the grooved surface of a sponge ventral side up. Intraperitoneal injections were performed by penetrating the abdomen with insulin syringe (U100 - 30G) 1 mm anterior to the midline of pelvic fins at a 45° angle by driving the needle parallel to the abdomen for about 3 mm towards the anterior side from just beneath skin. A maximum volume of 50µl 5mM EdU was injected. Fish were transferred to aerated artificial freshwater immediately following the injection.

### **3.2.5. Tissue Dissociation Assay**

For tissue dissociation, zebrafish OEs were dissected using ice-cold Ringer's solution (140 mM NaCl, 5 mM KCl, 10 mM HEPES, 1mM CaCl<sub>2</sub>, 1 mM MgCl<sub>2</sub> and 10 mM D-Glucose, pH: 7.2) Isolated OEs were first acclimatized in Ringer's solution at room temperature (RT) for 10 min, followed by 15 min incubation at RT in low-Ca<sup>2+</sup> Ringer's solution (140 mM NaCl, 5 mM KCl, 10 mM HEPES, 10 mM EDTA, 10 mM D-glucose, and 1 mM L-cysteine; pH 7.2). 1U papain (Sigma) was added to the same low-Ca<sup>2+</sup> Ringer's. Samples then incubated for 5 min at 28°C to enhanced papain reactivity and 5 min at RT with gentle agitation to facilitate papain diffusion, which was repeated for a total of 30 min incubation.

Afterwards, OE were transferred to fresh low-Ca<sup>2+</sup> Ringer's supplemented with 0.1% BSA (mg/ml) and left at room temperature for up to 10 min. OE were then transferred onto glass slides and sliced by hand using surgical blades, minced with heat-sealed glass Pasteur pipettes and gently triturated using 100 µL micropipettes. Preparations were dried at 65°C for up to 1 h before immunohistochemistry.

### 3.2.6. Immunohistochemistry

Freshly prepared or stored frozen sections were incubated at RT for 10 min inside plastic petri dishes and rehydrated for 5 min by filling the dish with 1 x PBS solution. Then, rehydrated samples were fixed using 4% cold paraformaldehyde (PFA), dissolved in 1x PBS for 10 min at RT. Slides were placed into Coplin jars and washed three times with 0.1% (v/v) Tween-20 supplemented PBS (1 x PBST) for 10 min by gentle agitation on an orbital shaker. To effectively permeabilize the nuclei and to denature DNA for anti-BrdU immunohistochemistry, preparations were treated with 4 N HCl for 10-15 min at RT and subsequently washed with 1x PBST three times for 15 min at RT by gentle agitation. Preparations were incubated with blocking solution, 3% bovine serum albumin (BSA) (m/v; in PBST), for 1h at RT to prevent unspecific interactions. 1% BSA was used for immunohistochemistry on tissue dissociation preparations. After 1 h, the blocking solution was replaced with fresh 300  $\mu$ l blocking solution containing primary antibodies at the desired dilution (Table 3.1). Primary antibody incubation was performed overnight (16-18 h) at 4°C temperature.

Table 3.1. List of primary antibodies.

<b>Antigen</b>	<b>Dilution</b>	<b>Host</b>	<b>Manufacturer</b>	<b>Cat. no.</b>
BrdU	1:250	Mouse	Beckon Dickinson	347580
BrdU	1:300	Rat	Abcam	Ab6236
Sox2	1:500	Rabbit	Genetex	GTX124477
PCNA	1:500	Mouse	Sigma-Aldrich	O84M4776
HuC/D	1:500	Mouse	Life Technologies	1661237
P63	1:500	Rabbit	Genetex	GTX124660
Krt5	1:500	Rabbit	BioLegend	905501
CKII	1:500	Mouse	DSHB	1h5

The next day, the primary antibody solution was re-collected either by 1000  $\mu$ L micropipette or pouring directly into a 1.5 ml tube and stored at  $-20^{\circ}\text{C}$  for later use. Preparations were rinsed once with PBS and washed three times with 1x PBST for 15 min at RT or 30 min if anti-Krt5 or anti-CKII antibodies were used. Secondary antibody solutions were prepared by diluting secondary antibodies in fresh 300  $\mu$ L blocking solution (Table 3.2) and samples were incubated for 2h at RT and subsequently rinsed once with 1x PBS and washed three more times with 1xPBS for 30 min at room temperature. If TO-PRO-3 or DAPI was used to label nuclei, incubation with the counterstain was performed after the first wash with 1x PBS that followed the secondary antibody incubation. TO-PRO-3 or DAPI were diluted in PBS and incubation was performed for 15 or 5 min, respectively. Detection reaction for EdU Click-iT™ was done according to manufacturer's instructions at the end of all immunostaining steps.

Table 3.2. List of secondary antibodies and nuclear markers.

<b>Antigen</b>	<b>Fluorophore / Excitation</b>	<b>Dilution / Concentration</b>	<b>Manufacturer</b>
Mouse/rabbit/rat IgG	Alexa Fluor® 488	1:800	Thermo Fischer
Mouse/rabbit/rat IgG	Alexa Fluor® 555	1:800	Thermo Fischer
Mouse/rabbit/rat IgG	Alexa Fluor® 633/637	1:800	Thermo Fischer
Mouse IgG	Cyanine®2 (CY2 – 647)	1:250	Jackson Immuno.
Rabbit IgG	Cyanine®5 (CY5 – 488)	1:250	Jackson Immuno.
-	DAPI (405)	0.1 g/L	Thermo Fischer
-	TO-PRO-3 (647)	1:1000 (1 mM)	Thermo Fischer

### **3.2.7. Chemical Lesion of the OE using Triton X-100**

Fish were anesthetized by immersion in 160 mg/mL MS222 solution until opercular movements ceased to ensure deep anesthetic stage. Fish were then transferred to a make shift groove between wet paper towels or a sponge and placed under a stereomicroscope with the dorsal side up. 1% Triton X-100 dissolved in 1x PBS supplemented with coloring agent 0.1% phenol red was prepared as damage solution (TrX). The left nasal cavity was irrigated with approximately 2  $\mu$ l of TrX from the naris using a 1 mm heat-pulled glass capillary needle and incubated for 90 seconds. At the end of the application, TrX was flushed out by rapid application of 3 ml artificial freshwater using a Pasteur pipette and fish were immediately transferred to BrdU-containing water.

### **3.2.8. Functional Ca<sup>2+</sup> Imaging and Analysis**

Zebrafish OEs were dissected in cool zebrafish artificial cerebrospinal fluid (ACSF) solution and embedded into 2% low melting agarose gel. OEs were oriented in a dorsal side-down position and cooled down to RT. The agarose was trimmed into a block using surgical blades and mounted onto the stage of a VT1200S vibratome (Leica) with superglue and sectioned at 140  $\mu$ m thickness. Acute OE slices were transferred into hand-made 1.5cm to 0.5 cm rectangular chambers filled with ACSF and kept on ice until fresh 50  $\mu$ M Fluo4-AM staining solution was prepared. Fluo4-AM solution was prepared by resuspension in 5  $\mu$ L DMSO supplemented with 10  $\mu$ L Pluronic-127 initially and further diluted to 500  $\mu$ l with ACSF solution. 250  $\mu$ l of this solution was diluted 1:2 again with ACSF and remaining 250  $\mu$ l was stored at +4°C for future use. 5  $\mu$ l MK571 was added to the diluted working solution. The ACSF solution was then replaced with 125-250  $\mu$ l of working Fluo4-AM solution and incubated for 35 min at RT. Once dye loading was complete, slices were washed with ACSF and transferred onto the stage of a LSM780/Axio Examiner (Zeiss) confocal microscope and supplied with a constant stream of ACSF solution throughout experiment. Imaging was done at 1 frame/s over 60 s for each application at 512x512 pixel resolution.

Tissue slices were stimulated by injecting 500  $\mu$ l of 100  $\mu$ M purine solutions (ATP, 2-MeSATP) or 50 mM KCl solution at the 10<sup>th</sup> frame into the ACSF stream. For repeated stimulations, 3 min intervals were given between each application to prevent the exhaustion of cellular Ca<sup>2+</sup>. Image analysis was performed in FIJI (Schindelin *et al.*, 2012) using a custom macro. Each responding cell was traced using a free-hand drawing tool and the mean pixel value for each frame in the cell selections was taken as the response intensity (F) of the cell in that frame. Mean intensity of the first 10 frames were taken as baseline intensity value (F<sub>0</sub>). Change in fluorescence intensity ( $\Delta F/F_0$ ) over the time course of the experiment was calculated by dividing the response intensity of each frame relative to the baseline intensity.

### **3.2.9. Staining with CellTrace™**

Following dissection in cooled ACSF solution, intact OEs were incubated with 500  $\mu$ L CellTrace™ working solution (100  $\mu$ M), resuspended according to manufacturer's instructions, at RT for 30 min with gentle agitation. OE were then washed twice with 1% BSA (m/v) dissolved in ACSF solution for 15 min and sectioned on a vibratome as described in section 3.2.8.

### **3.2.10. Confocal Microscopy and Positional Quantification**

Immunostaining samples were imaged with LSM780/Axio Examiner (Zeiss), Leica SP5-AOBS, or Leica TCS SP8 (Leica Microsystems) confocal microscopes using 20x or 40x water immersion lenses. Imaging was performed using 1024x1024 or 2048x2048 pixel resolution, mainly with 400 Hz acquisition frequency or 200 Hz for detailed CKII and Krt5 labeling. To remove background, 0.2% (in SP8) or 2% (in SP5) smart offset adjustment and, 4x line averaging for each channel were applied. To prevent loss of image information during volumetric Z-stack imaging, Z-Step size was set to half value of the optical section size provided by the software.

Sequential imaging setting was used to prevent cross talk between channels, quenching, or self-quenching in co-immunostained samples and all samples were imaged individually for each fluorophore according to the secondary antibody used in the experiment.

Leica image files (lif) were processed with FIJI software (Schindelin *et al.*, 2012) and, following brightness contrast adjustments, saved as tagged image file format (TIFF) to prevent data loss. Individual epithelial folds (EF) were oriented to the horizontal axis with the ILC on the left side and either cropped (CTRL+SHIFT+X) or copied and cropped (CTRL+SHIFT+D) as individual multi-channelled images and saved as TIFF file.

Positional analysis was performed for each co-labeled or single-labeled (up to 3 criteria could be analyzed at the same time) cells using a custom macro. Macro sequentially prompts the user to mark labeled cells with the point tool (size medium) manually for each channel and saves the markings as separate region of interest (ROI) files into the ROI manager. Upon completion, three ROIs are given RGB colors by the macro and projected onto a separate, equally sized black image. Then, this *in silico* representation of the original image that contains the positional information of each labeled cell was separated into 10 equidistant bins and the number of cells within each bin was counted. Data were corrected for cells positioned at the edge of bins and quantified with custom R codes (R Core Team, 2020).

### **3.2.11. Statistical Analysis and Graphing**

Student's t-test, One-way analysis of variance (ANOVA) with post hoc Tukey honestly significant difference (HSD) test, and two-way ANOVA with Sidak's multiple comparison test were performed using Prism Software v7 (Graph Pad, USA). Graphs were prepared using Prism Software v7 and edited with Illustrator CC v17 (Adobe, USA).

### 3.2.13. Transcriptome Analysis

Total RNA extracts from OEs bilaterally lesioned with 1% Triton X-100 from 10 fish for each timepoint (4, 12, 24, 72, 120 hpl) and OEs from 10 unlesioned control fish for two biological replicates were available in the lab and subjected to Illumina HiSeq 2000 sequencing (Kocagöz, 2021).

Quality control of the sequencing runs was performed using the FastQC tool v0.11.7. Ribosomal RNAs were removed using SortmeRNA v2.1b (Kopylova *et al.*, 2012) by aligning reads to the SILVA database (Quast *et al.*, 2013). Low-quality reads and adapter sequences were removed using Trimmomatic v0.3.6 (Bolger *et al.*, 2014). FastQC was used again to check the quality improvement of cleaned read files and quality control graphs were obtained.

RNA-seq reads were aligned to the zebrafish reference genome GRCz11 (obtained from Ensembl) using HISAT2 v2.1.0 (Kim *et al.*, 2015). Aligned transcripts were then assembled and annotated using HTSeq v0.9.1 (Anders, *et al.*, 2014) to the annotation file obtained from Ensembl (Danio\_rerio.GRCz11.92.gtf). Annotated count files were further analyzed using the Integrated Differential Expression Pathway Analysis (idep.92) suite (Ge *et al.*, 2018).

Count data from 12 samples were transformed using the EdgeR:log2 procedure based on minimum CPM value of 0.5 with added pseudo counts of 4 and the gene median was used for missing value imputation. Heatmaps were generated from 5000 most variable genes (MVG) where genes were centered by subtracting mean and distances between samples and genes were calculated with Pearson correlation for hierarchical clustering. The 2500 MVG option was selected for k-means clustering that were normalized to mean center and sorted into 6 clusters. DESeq2 (Love *et al.*, 2014) option was used to normalize and obtain log2 fold-change (log2-FC) values of differentially expressed genes (DEGs). Only DEGs show more than 2 log2-FC and with FDR cutoff of 0.05 were included for pathway analysis.

Analysis of GO terms on biological process, molecular function, and KEGG pathways for 4h, 12h and 24h was performed with generally applicable gene set enrichment (GAGE) selection method (Luo *et al.*, 2009) and criterions were set to 100-500 gene set size interval and adjusted p value (adj.pval) significant cutoff of 0.1.

#### **3.2.14. Systemic ATP Administration**

Adult fish were anesthetized with 160 ng/mL MS222 solution and injected intraperitoneally with 50  $\mu$ l of 1xPBS, ATP (10 mM) in 1x PBS, or ATP/Suramin (10 mM / 5.6 mM) in 1xPBS for three biological replicates. Immediately following the injection, fish were transferred to 30 mg/L BrdU containing water and incubated for 12 h in the dark. Then, fish were transferred into aerated BrdU-free artificial freshwater until 72 hpl. Fish were euthanized by MS222 overdose (250 mg/L) as previously described (see section 3.2.2) and olfactory organs were dissected at 72 hpl and immunostained as described in section 3.2.6.

#### **3.2.15. IL-6 Administration to the OE**

Adult fish were anesthetized with 160 mg/L MS222 solution and cooled down to 10°C by placing the beaker on ice and monitoring the temperature. Anesthetized and cooled fish were transferred into grooved surface of a sponge at a dorsal up position and covered with cooled wet paper towel for temperature control. The left nasal cavity of the fish was drained with a paper towel and irrigated with 1  $\mu$ L IL-6 (250 ng/ $\mu$ L) using a heat pulled glass capillary needle and incubated for 15 min. During this process, 80 mg/L MS222 solution at 10°C was applied to gills and into the mouth of the fish by a micropipette tip (compatible with 20-100-200  $\mu$ l micropipettes) every 3 min. After 15 min, the nasal cavity was drained again and 1  $\mu$ L IL-6 (250 ng/ $\mu$ L) was re-applied. Fish subjected to IL-6 for a total of 30 min were then immediately transferred to 30 mg/L BrdU containing artificial freshwater and kept in the dark. IL-6 applied fish were either subjected to a 24 h BrdU pulse and immediately analyzed or a 48 h BrdU pulse and analyzed at 72 h by immunohistochemistry.

## 4. RESULTS

The zebrafish is considered to be an important vertebrate research model and widely used in numerous experimental fields due to its outstanding regenerative capabilities. Understanding the molecular and cellular similarities and differences between zebrafish and other vertebrate models could offer critical insight into regenerative processes, including nervous system repair and neurogenesis at tissue level. To highlight an important interspecies difference, in response to injury, Müller Glia cells of the retina play a major neurogenic role in fish that is not observed in mammals (Fausett *et al.*, 2008; Goldman, 2014; Lenkowski and Raymond, 2014; Lahne and Hyde 2015; Lust and Wittbrodt, 2018).

In rodents, non-neuronal cells in the OE consist of reserve stem cell, transiently amplifying stem cell, tissue specific sustentacular glial cell and duct/gland cell populations (Schwob *et al.*, 2016). Even though there is an abundance of studies on the physiological and regenerative function of these cell populations in the mouse, knowledge about the identity of candidate progenitor pools and their dynamic activity during OSN neurogenesis are limited in zebrafish. The study presented in this thesis provides a cellular and functional analysis of the contribution of different OE cell types to maintenance and repair neurogenesis in the zebrafish OE. Aspects of the findings may form a basis for future studies that will provide an in-depth understanding of the dynamics and responsiveness of non-neuronal cells and reveal whether there are characteristic and functional similarities and differences between zebrafish and other model organisms.

The results of the work undertaken in this thesis will be reported in three sections. In the first section, the identification of purine-responsive cells and the specific effects of the purine ATP on olfactory neurogenesis will be reported. In the second section, a detailed characterization of the activity of the different non-neuronal cell types during maintenance neurogenesis will be presented. Lastly, the transcriptional changes that occur during tissue injury and which might be involved in regulating tissue regeneration will be analyzed by global transcriptome analysis.

Of the various candidate molecular signals, the effects of IL-6, which is found to be one of the most highly upregulated genes following tissue injury, on OSN neurogenesis will be described.

#### **4.1. Identification of ATP-responding Non-neuronal Cells and the Effect of ATP in Zebrafish OE Neurogenesis**

Purines are prominent damage associated molecular pattern (DAMP) molecules that have been implicated in activating immune responses and regenerative processes, including OSN neurogenesis in the mouse (Jia *et al.*, 2009). DAMPs that are released by dying OSNs, either because they are damaged by severe environmental conditions or because of old age, could subsequently modulate progenitor cell activity. In the zebrafish OE, there are two progenitor cell types that may respond to purines, which are either involved in maintenance or regenerative neurogenesis. The aim of this section is to examine the effect of purine signals on the zebrafish OE and to provide an in-depth analysis of the effect of ATP signaling on cell proliferation. Identification of purine-sensitive cell populations could consequently provide a link between stem cell identity and related biological effects during different modes of neurogenesis.

Previous work from our laboratory has shown that the zebrafish OE responds to purine compounds by signal transduction through P2-type purinergic receptors and subsequent generation of  $\text{Ca}^{2+}$  transients by the release of  $\text{Ca}^{2+}$  from internal stores into the cytoplasm (Bali, 2015). While  $\text{Ca}^{2+}$  signals are largely restricted to the basal layers of the OE, the work also suggested that a subgroup of ATP-responding cell profiles could be SCs by measuring the distances between CKII-immunoreactive cells and ATP responding cells. In addition, the proliferation-promoting effect of ATP on the intact tissue, which is reversible by application of the unspecific P2-type receptor inhibitor Suramin, was described (Sakızlı, 2018). These combined results somehow suggest a link between neurogenic responses and the activity of SCs in the zebrafish OE. Hence, a more rigorous, and systematic approach was necessary to understand the cell type specific regulatory effect of ATP.

In this part of the thesis, additional findings on purine-responsive non-neuronal cell populations of the zebrafish OE will be presented. The responding cell types will be identified using a systematic characterization of the purine responses by sub-categorizing them according to response onsets, sensitivity, morphology, and epithelial positions. Finally, the effect of ATP on neurogenic activity in the zebrafish OE will be presented.

#### **4.1.1. Purine-sensitive Cells are Predominantly Non-neuronal in the Zebrafish OE**

To measure physiological responses to purine compounds, an *ex vivo* slice preparation of the zebrafish OE loaded with the Ca<sup>2+</sup>-sensitive dye Fluo-4/AM was used. Slices were mounted onto the stage of a LSM780/Axio Examiner confocal microscope and constantly perfused with a stream of ACSF solution. Imaging was done with 1 Hz frequency over 60 seconds and 100  $\mu$ M ATP or 80mM high K<sup>+</sup> were intercalated into the perfusion stream at the 10<sup>th</sup> frame while simultaneously recording changes in fluorescence intensity. The first 10 frames were used to calculate the average baseline fluorescence intensity and temporal response profiles were quantified as fold-increase in intensity over baseline and time (shown in right side of the figure as  $\Delta F/F$ ).

Fluo-4/AM fluorescence showed a rapid increase in intensity upon exposure to 100  $\mu$ M ATP, indicative of cytoplasmic Ca<sup>2+</sup> influx, and slowly returned to baseline levels over 20-30 seconds. Induced Ca<sup>2+</sup> transients were most prominent in basal layers but could also be observed in occasional cells in intermediate layers of the epithelium (Figure 4.1a). Upon closer inspection, basally located profiles (indicated by arrowheads in the figure) and profiles located in more suprabasal layers (indicated by arrows in the figure) could be identified. The two distinct cell populations were named according to their relative positions along the apicobasal axis of the OE as “basal” (arrowheads) and “intermediate” cells (arrows).

Purines have been previously shown to be potent odorants in fish (Friedrich and Korsching, 1998; Wakisaka *et al.*, 2017). To understand whether any of the responding cell populations includes neurons, the same preparations were subsequently stimulated with 80

mM KCl, which depolarizes OSNs and results in the formation of neuronal  $\text{Ca}^{2+}$  transients (Figure 4.1a, bottom right and Figure 4.1b, red).

Thus, cells that respond to ATP but also to depolarization most likely would constitute OSNs. Yet, apart from a small number of apically located ATP-sensitive cell profiles, all the response profiles in basal and intermediate layer of the epithelium did not overlap with high  $\text{K}^+$  -induced  $\text{Ca}^{2+}$  signals. The observation of apically located ATP-responding neuron is in line with the recent description of a novel class of adenosine-sensing A2c chemosensory neurons, which have been reported to be highly conserved and specific to fish and amphibians (Wakisaka *et al.*, 2017).

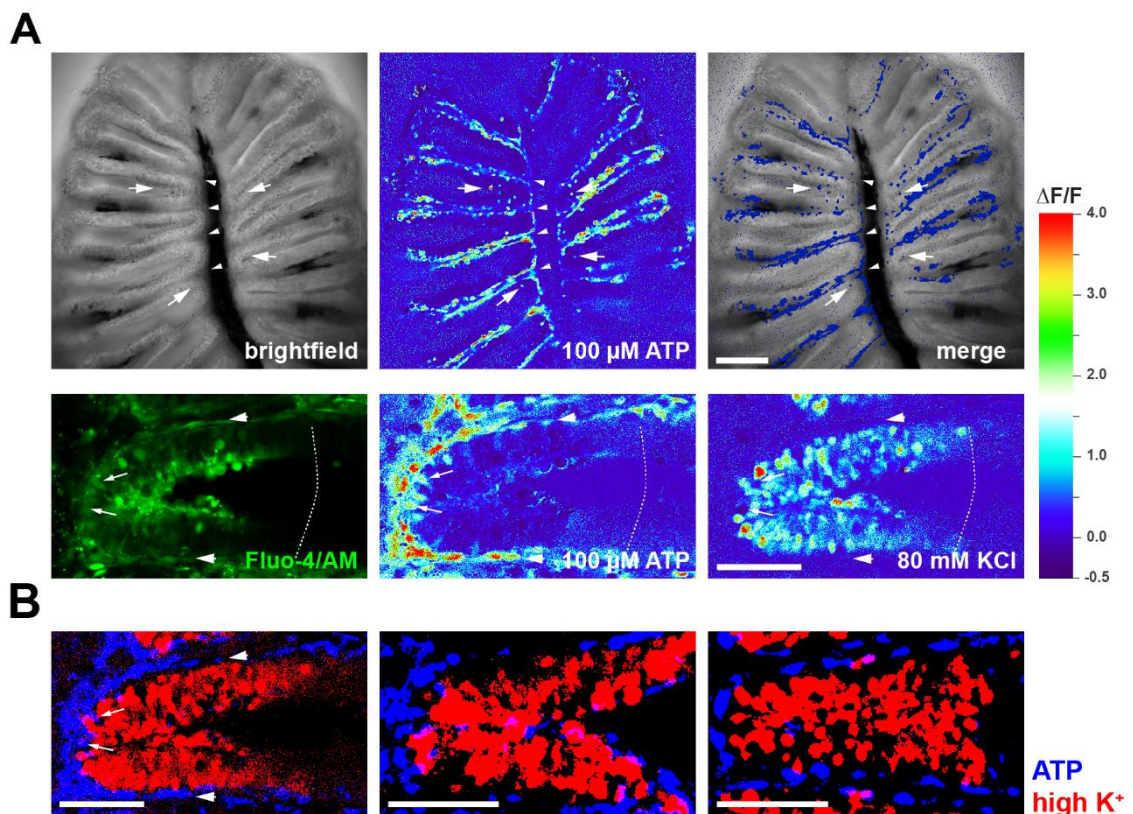


Figure 4.1. Stimulation of the OE slices with ATP or KCl. A.  $\text{Ca}^{2+}$  transients projected onto brightfield images (top, scale bar: 100  $\mu\text{m}$ ); dye fluorescence (bottom left) and  $\text{Ca}^{2+}$  responses (middle, right; scale bar: 50  $\mu\text{m}$ ). B. Merged peak responses. Scale Bar: 50  $\mu\text{m}$ .

These results show that,  $\text{Ca}^{2+}$  transients induced by ATP located in basal and intermediate layers of the OE are mutually exclusive from high  $\text{K}^{+}$ -induced transients and, therefore, predominantly constitute a non-neuronal cell population. Unlike observations in the OE of *Xenopus* and mice, in which ATP-responsive cells can also be observed in the most apical layers of the OE, ATP-responsive non-neuronal cells in the zebrafish OE seem to exclusively populate basal and suprabasal layers.

#### **4.1.2. The Sensory OE is Populated by OSNs and Sox2-positive Cells**

The exact identification of ATP-responsive non-neuronal cell profiles requires an in-depth understanding of the tissue composition and placement of cells within the intact epithelial structure. In all amphibians and mammals, OSNs are sandwiched between Sox2-immunoreactive, basally located HBC and GBC progenitors and SC layer that spans the apical OE. Thus, the observation that ATP responses occur exclusively in the basal OE might either reflect the absence of an apical layer of SCs or the unresponsiveness of zebrafish SCs to purine stimulation.

To better understand the cellular architecture of the zebrafish OE, 12  $\mu\text{m}$  cryo-sections through the zebrafish OE were immunohistochemically stained against the neuronal marker HuC/D to detect the nuclei of mature OSNs and the unspecific stem cell marker Sox2 (Figure 4.2). To observe additional cells that were not labeled by HuC/D (blue) and/or Sox2 (red) expression, the nuclear label TO-PRO-3 (blue) was used as a counterstain. Microscopic analysis of these samples showed the presence of Sox2-positive cells exclusively within basal strata, while HuC/D expression could be detected in intermediate and apical layers. Both, Sox2- and HuC/D-positive cells are restricted to the sensory OE starting from the ILC, indicated with asterisk, until the end of S/NS border indicated by arrowheads (Figure 4.2a). On the other hand, cells that were only stained by TO-PRO-3 but not HuC/D or Sox2 expression were scarce within this region. However, rare double-negative cells could be observed in basal epithelial strata which were shared with HuC/D- expressing cells and showed a positional preference towards the ILC and SNS (Figure 4.2a, right; arrows).

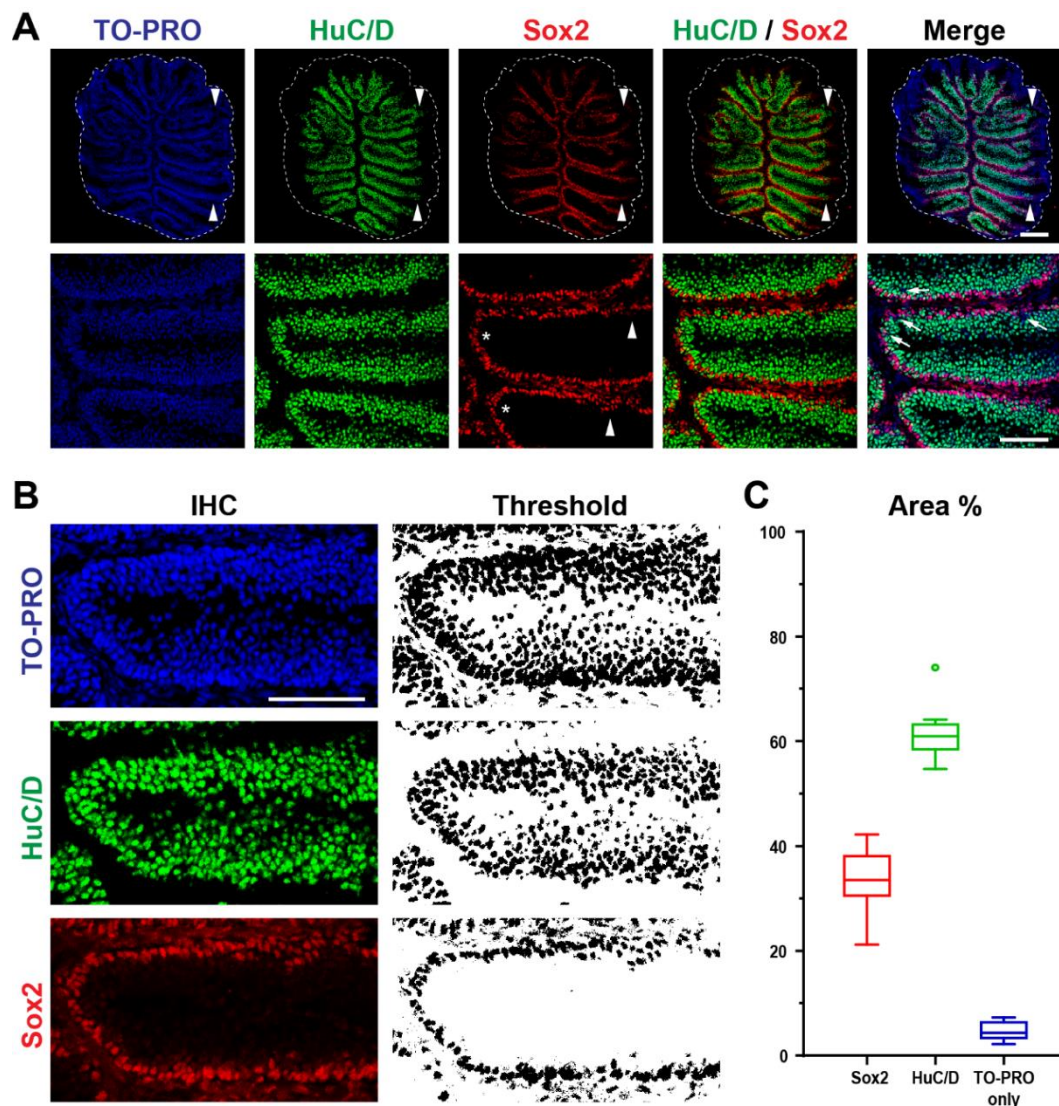


Figure 4.2. Cellular architecture of the sensory epithelium. A. Antibody-stained sections (top) and enlarged sensory region (bottom). Scale bar: top: 100  $\mu$ m; bottom: 50  $\mu$ m. B. Signal thresholding for area analysis. C. Quantification of occupied tissue areas of cells.

To obtain an estimate of the prevalence of Sox2/HuC/D double-negative cells, the sensory regions of epithelial folds were cropped and thresholded to remove background signals (Figure 4.2b). The area occupied by Sox2 and HuC/D labeled cells were measured and subtracted from the TO-PRO-3 labeled area for each image. The area labeled only by TO-PRO-3 was then expressed as the percentage of the total area of the sensory region (Figure 4.2c). The analysis revealed a mean occupied area for Sox2 expressing cells of  $33.6 \pm 1.8\%$  (mean  $\pm$  SEM) and of  $61.7 \pm 1.6\%$  for HuC/D expressing OSNs.

In contrast, only  $4.7 \pm 0.5$  % accounted for cells labeled only by the nuclear marker TO-PRO-3. The percentage of TO-PRO-3 only-positive cells ranged between 2.1% to 7.3% of the total area of the sensory region (5 epithelial folds/section, 2 sections of 1 fish). Due to their proximity to basal layers and to the neurogenic zones, it is very likely that these TO-PRO-3 only cells include immature sensory neurons that transition between Sox2-positive GBCs and HuC/D-positive OSNs.

In summary, between 95% - 98% of all cells in the sensory region of the zebrafish OE can be labeled for HuC/D and Sox2 expression with almost full confidence of covering all non-neuronal cells and only between 2 – 5% of cells do not express any of the two markers. Interestingly, staining for Sox2 expression does not label the most apical nuclear layers, but is restricted to basal layers in the zebrafish OE. These results also confirm that ATP-responding basal and intermediate cells may include predominantly non-neuronal cells, because of their positional overlap. Heterogeneity of the Sox2 expressing cells will be reported in following sections.

#### **4.1.3. ATP Responding Non-neuronal Cells are a Heterogenous Population**

Ca<sup>2+</sup> transients induced by purine analogues in the zebrafish OE were described previously in a preliminary study from our lab. Among the tested analogues (ATP, 2-MeSATP, UTP, UDP, ATP $\gamma$ S), ATP and 2-MeSATP evoked the most differential transients between basal and intermediate cell profiles. Basal cells showed high sensitivity to both ATP and 2-MeSATP, whereas intermediate cells showed higher sensitivity to ATP, but a much lower Ca<sup>2+</sup> signal was evoked by 2-MeSATP (Bali, 2015). This preliminary study suggested that additional distinct characteristics of purine-responding cells could be identified.

Similar analyses were made on Fluo-4/AM loaded 140  $\mu$ m tissue slices that were prepared with a vibratome. Purine analogues 100  $\mu$ M ATP, 100  $\mu$ M 2-MeSATP, or 80mM high K<sup>+</sup> applications were applied at the 10<sup>th</sup> frame, indicated by dashed lines (Figure 4.3a) during imaging. Each subsequent application was done with 3 min intervals and Ca<sup>2+</sup> transients were imaged over 60 seconds.

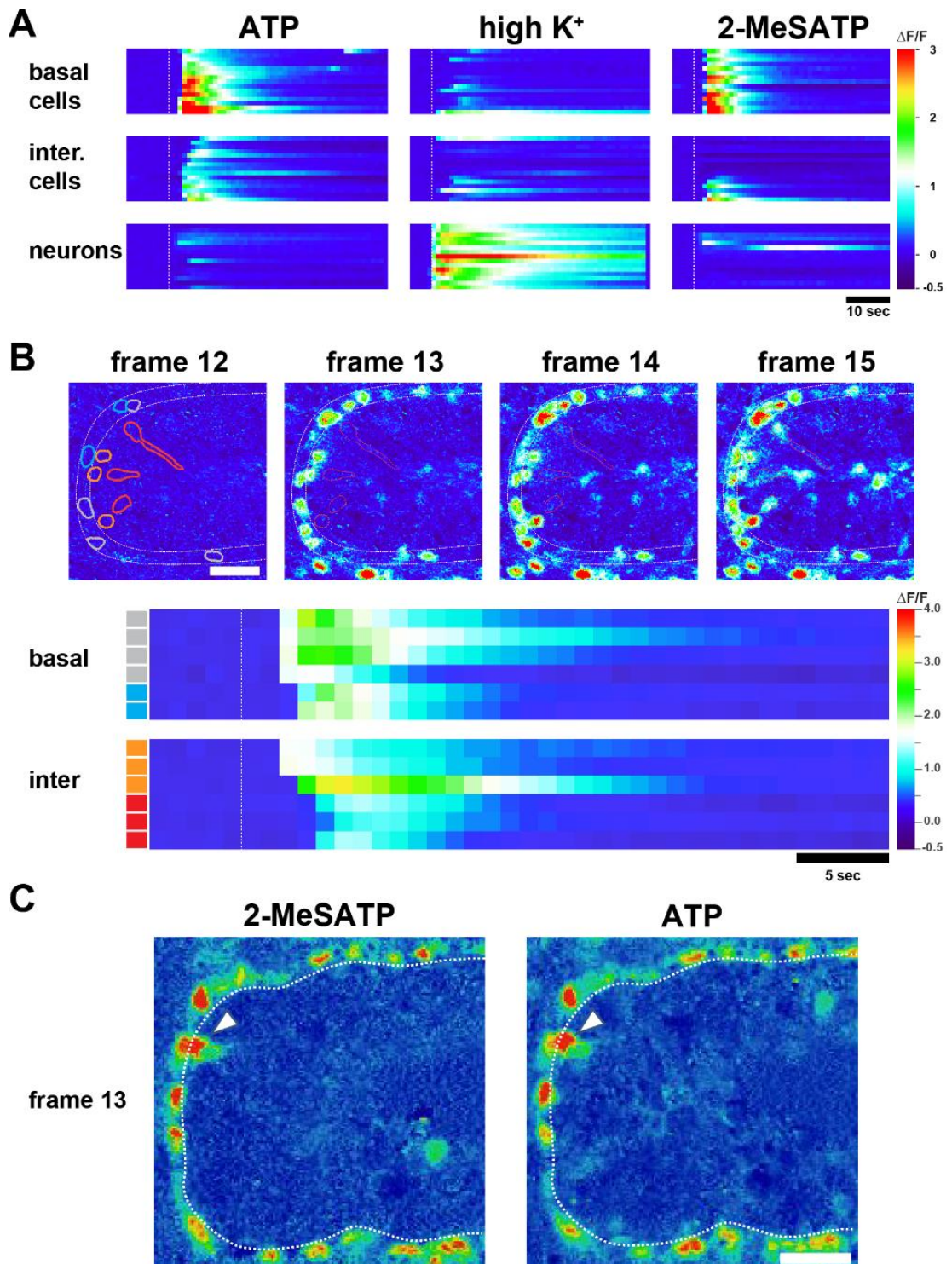


Figure 4.3. 2-MeSATP responding cells show earlier response onsets to ATP. A. Temporal response profiles show  $\text{Ca}^{2+}$  transients upon induction. B. Timeframe of 100  $\mu$ M ATP induced transient development. C. 2-MeSATP responding intermediate cell. Bars: 10  $\mu$ m.

In agreement with previous results, observations made from tissue preparations of three different fish confirm the sensitivity difference between basal and intermediate cells in response to ATP and 2-MeSATP. Figure 4.3a shows 15 randomly selected response profiles collected from three independent preparations of cells stimulated with ATP, 2-MeSATP, and high-K<sup>+</sup>. The responding cells were sorted to their relative position in the OE. Over the 60 sec time-course, 100 μM ATP-induced changes in fluorescence intensity were up to 6.1-fold in basal cells and up to 3.6-fold in intermediate cells across all specimens. Interestingly, only a subset of intermediate cells showed up to 3.7-fold increase in fluorescence intensity upon stimulation with 100 μM 2-MeSATP whereas up to 4.8-fold increase was observed in all basal cells. Stimulation with a high concentration potassium solution was used to identify neurons. Occasional adenosine-sensing neurons could be seen responding to ATP and/or 2-MeSATP applications as well. On the other hand, the apparent intensity increases in basal and intermediate cells upon high-K<sup>+</sup> application were probably caused artificially by neuronal cells in out-of-focus planes.

Apart from the differential sensitivity of intermediate cells to ATP and 2-MeSATP, analysis of the temporal onset of ATP-evoked Ca<sup>2+</sup> transients also indicated variance within the intermediate cell population (Figure 4.3b). The time point of 100 μM ATP delivery is indicated by dashed lines in the temporal profiles located in the bottom panel of the figure. In the ILC region, response onsets to ATP induction from basal cells showed short latencies of approximately one second. These cells are indicated with gray and blue outlines in the top panel of Figure 4.3b and labeled with respective colors in the temporal profile in the bottom panel. Intermediate cells in the ILC showed higher variance in their response onsets upon 100 μM ATP induction (orange and red outlined cells). Curiously, intermediate cells exhibiting the same response onsets with basal cells were located more basally among the population and had strikingly globular morphology (orange) compared to late onset cells. Cells that showed up to three-second delay in response onsets were positioned in more intermediate epithelial strata. Interestingly, these cells showed columnar morphologies and recognizable apical protrusions (red) as compared to the spherical profiles of more basal and fast-responding cells. Additionally, some of these early onset intermediate cells also showed sensitivity to 2-MeSATP (Figure 4.3c).

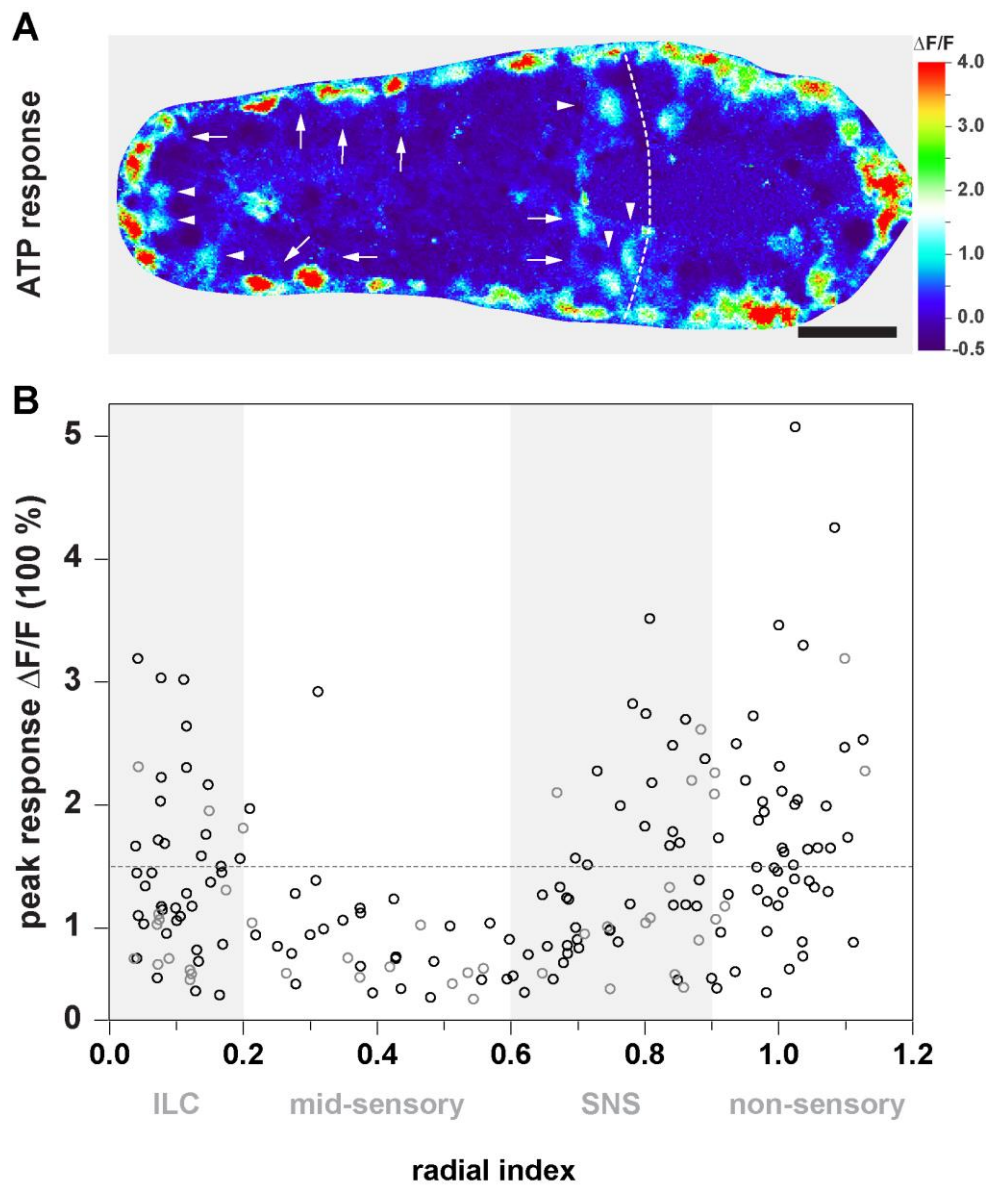


Figure 4.4. Positional profile of ATP responding intermediate cells. A.  $\text{Ca}^{2+}$  transients induced by ATP show varied levels of intensity. Scale bar:  $25\mu\text{m}$ . B. Positional profile of peak response intensities of intermediate cells (191 cells, 12 EFs, 8 sections, 5 fish).

The differential sensitivity to 2-MeSATP and differences in response onset and cell morphology indicate intrapopulation heterogeneity in intermediate cells around the ILC. Since this region is one of the neurogenic zones in the intact zebrafish OE, understanding the ATP sensitivity along different epithelial positions may reveal functional principles of progenitor cell regulation. Therefore, the response intensities of all intermediate cells along

the radial axis were quantified to understand if there is any correlation between response strength and the occurrence of a neurogenic zone along the radial dimension of the OE. A representative epithelial fold is shown in Figure 4.4a and the positional quantification of individual peak responses of intermediate cells is shown as a scatter plot along the axial dimension of the epithelial fold in Figure 4.4b.

The neurogenic zones, the ILC and SNS, are indicated with gray boxes in the graph. Positions of data points were normalized to the center of the SNS (dashed line in EF image) in preparations with subsequent high K<sup>+</sup> application (black) or to 70% of total radial length (gray). The plot clearly shows an upper limit at 1.5-fold increase in fluorescence intensity in the mid-sensory region (gray dashed line in graph). These cells with low sensitivity are indicated with arrows in Figure 4.4a. On the other hand, around the neurogenic zones at the ILC and SNS, a subset of cells exhibited higher ATP sensitivity and showed more than 1.5-fold increase in response intensities. These cells are indicated with arrowheads in Figure 4.4a. Thus, a specific subset of cells with high sensitivity to ATP appears to be selectively positioned at the ILC and SNS.

These last results suggest, but do not prove, that progenitor cells at the ILC and SNS may respond to ATP or related purine compounds with high sensitivity. In contrast, out of 35 measured responses in the mid-sensory region, only a single cell showed a 3-fold increase in intensity, while the response intensities of all other cells remained below 1.5-fold.

#### **4.1.4. Spatially Restricted GBCs are Highly ATP Sensitive**

So far, a positional preference for highly ATP-sensitive intermediate cells towards the ILC and SNS could be identified. These cells also show a spherical morphology in contrast to other ATP-responsive cells, a more rapid response onset and distinct 2-MeATP sensitivity. Location and morphological characteristics suggest that those highly ATP-sensitive cells in neurogenic zones could include GBC progenitors. Fast cycling progenitor GBCs can be identified by their characteristic *ascl1* expression in the mouse (Murray *et al.*, 2003; Chen *et al.*, 2004) and zebrafish OE (Bayramli *et al.*, 2017). In zebrafish, *ascl1a*-

expressing cells are spatially restricted to the ILC and SNS and are mitotically active (Bayramlı *et al.*, 2017; Kocagöz, 2021). To examine whether *ascl1a*-expressing GBCs show similarity with the ATP-responsive cell pools, the basal to apical position of *ascl1a*-positive cells was compared to the position of cells that responded to 100  $\mu$ M ATP application (Figure 4.5).

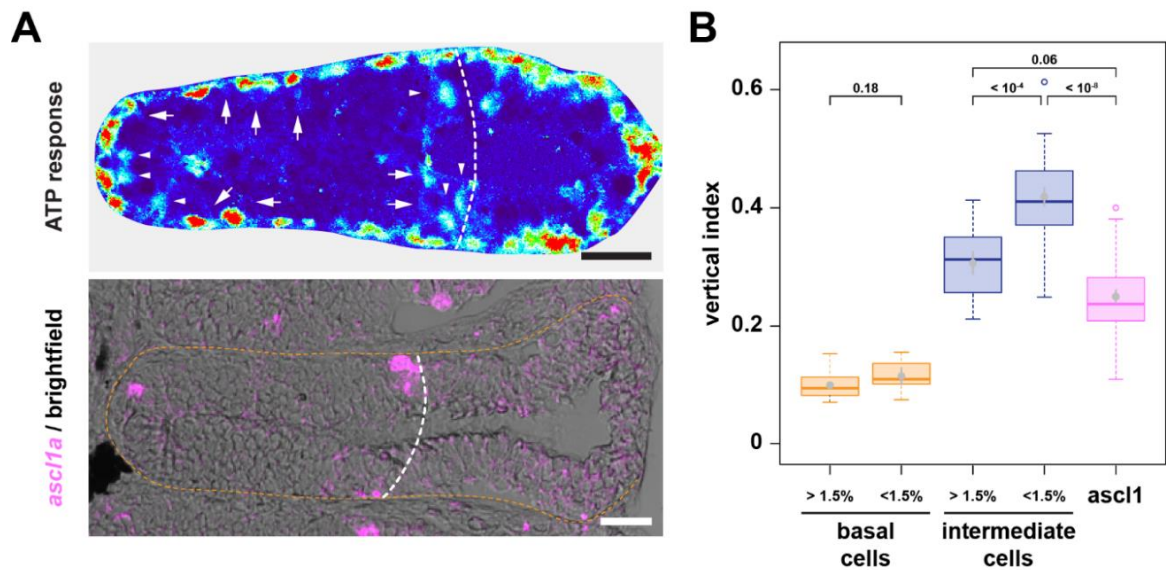


Figure 4.5. GBCs correlate with radial and vertical positions of high ATP sensitive cells.

A. ATP induced Ca<sup>2+</sup> transients (top), ISH against *ascl1a* (bottom, performed by Xalid Bayramlı). Bars: 25 $\mu$ m. B. Vertical positions of *ascl1*-positive and ATP-responsive cells.

A vertical index was calculated by normalizing the individual cell position along the basal-to-apical axis to the height of the epithelial sheet at the position of the analyzed cell. Profiling was performed for 69 basal (orange) and intermediate (blue) cells from five tissue preparations, grouped according to the previously described 1.5-fold threshold in intensity increase, and 28 cells labeled for *ascl1*-expression (pink) from four OE sections (Figure 4.5b). Basal cells showed no significant difference between low and high sensitivity groups (two tailed Student's t-test,  $P = 0.18$ ). On the other hand, statistical analysis with one-way ANOVA, *post hoc* Tukey HSD test ( $F_{(2,62)} = 41.4$ ,  $P_{intermediate / ascl1} < 10^{-11}$ ) on vertical profiles of thresholded intermediate cell groups and *ascl1*-expressing GBCs clearly

showed that GBCs are located at the same epithelial strata as cells with sensitivity to ATP ( $P_{>1.5/ascl1} = 0.6000$ ,  $P_{<1.5/>1.5} < 10^{-4}$ ,  $P_{<1.5/ascl1} < 10^{-8}$ ).

These results, while further extending the heterogeneity of ATP-responding intermediate cells, also suggest that *ascl1a*-expressing GBCs are included in the highly ATP-sensitive intermediate cell group. In addition, 2-MeATP sensitive intermediate cells with rapid response onsets have a considerable chance to be a subset of GBCs that could help distinguish transiently amplifying GBCs from multipotent progenitor GBCs that are still elusive in the zebrafish OE or from immediate neuronal precursors. Additionally, recent discovery from our lab showed that *ascl1a*-expressing GBCs are also positive for Sox2 expression (Kocagöz *et al.*, under review), which means that Sox2-positive cells require further characterization to understand the cellular composition of the zebrafish OE.

#### **4.1.5. Sox2-positive Non-neuronal Cells Constitute a Heterogenous Population**

The results of the analysis in part 4.1.2 demonstrated that immunohistochemical staining against Sox2 expression labels nearly all cells that are not OSNs. However, based on the observation of differences in ATP-responsiveness in the basal OE, the pool of Sox2-positive cells may be heterogeneous and include distinct subpopulations.

Closer inspection of 12  $\mu\text{m}$  cryosections that were stained against Sox2 by immunohistochemistry (Figure 4.6) revealed a multilayered organization of Sox2-positive cells in basal strata of the epithelium (top). Sox2-positive cells with distinct nuclear morphologies showed a clear preference along vertical positions within the sensory region (bottom). Cells adjacent to the basal lamina are dominated by flat horizontal profiles, i.e. a longer width in the horizontal and a shorter height in the vertical dimension (filled arrowheads), whereas cells in suprabasal layers showed more columnar morphologies (empty arrowheads). These characteristic features could be observed continuously throughout the sensory region, starting from the ILC until the beginning of the SNS where Sox2-positive cells begin to occupy additional layers. Up to three cell layers could be observed in the center of the ILC region and around the SNS, as opposed to only two layers throughout the remainder of the sensory OE.

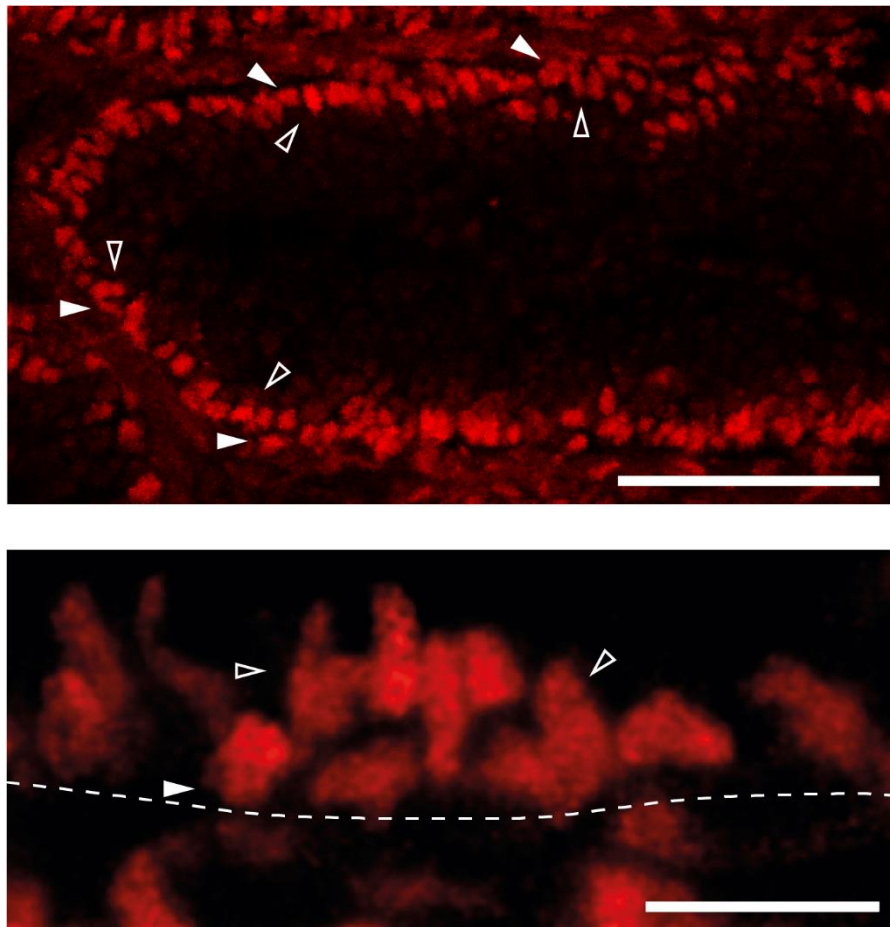


Figure 4.6. Sox2-positive cells with different morphologies define distinct epithelial strata.

Multilayered cells with distinct morphologies along the sensory epithelium (top) and higher power magnification of Sox2 labeling in sensory region (bottom). Bars: 50, 10  $\mu\text{m}$ .

A quantitative morphometric analysis was performed previously in collaboration with Uğurcan Sakızlı by measuring the vertical and horizontal dimensions of individual Sox2-positive cells and of cells expressing the HBC markers p63 (Fletcher, 2011; Packard *et al.*, 2011) and Krt5 (Holbrook *et al.*, 1995). The results were combined with morphometric measurements of ATP-induced responses to pinpoint the molecular identity of ATP-responsive cells. Nuclear measurements of Sox2-labeled cells demonstrated two distinct groups: a horizontal group with longer width in the horizontal and shorter length along the vertical dimension and cells with columnar features with inverted morphometric properties (Sakızlı, 2018).

Measurements of cytoplasmic  $\text{Ca}^{2+}$  transient also demonstrated two distinct groups of cells with similar but larger dimensional ratios, confirming a close morphometric relation with Sox2-positive cells and ATP-sensitive cells.

Taken together, cells labeled for Sox2 expression clearly show distinct morphological characteristics and have positional preference in the basal and suprabasal epithelial strata in the zebrafish OE. Additionally, ATP response morphometrics from basal and intermediate cells shows direct correlation with Sox2-positive nuclei at basal and suprabasal epithelial strata, suggesting that most physiological purine responses originate from Sox2-positive cells.

#### **4.1.6. Sustentacular Cells Constitute the ATP-sensitive Suprabasal Sox2 Layer**

Sustentacular glial cells of the zebrafish OE were previously identified by immunohistochemistry against CKII (Bali, 2015). Surprisingly, these cells show an inverted morphology when compared to mammalian SCs. While mammalian SCs occupy the apical layer of the OE in mammals and *Xenopus*, zebrafish SCs possess basally located somata in close proximity to the basal lamina. However, previous efforts failed to confirm with certainty whether SCs also express Sox2 due to dense packing of CKII-labeled keratin filaments. To understand whether SCs constitute a subpopulation of Sox2-expressing cells, a more rigorous approach was required.

After a rigid trial and error process, immunostaining against CKII exclusively double-labeled the suprabasal epithelial stratum of Sox-2 positive cells in the sensory region (Figure 4.7). Sox2-positive nuclei of SCs were observed to be encapsulated in columnar or tall pyramidal profiles defined by perinuclear CKII labeling (arrows). Sox2-positive horizontal cells were generally mutually exclusive from CKII-labeled SCs (arrowheads) and occupied more basal strata. To distinguish HBCs from SCs in the zebrafish OE, immunostaining against HBC-specific markers Krt5 and p63 was performed in combination with anti-CKII antibody staining. Both Krt5 and p63 labeling marked morphologically distinct cells positioned in the basal epithelium (Figure 4.8) and showed

mutually exclusive labelling from characteristic spherical somatic features of CKII-labeled cells (arrowheads).

Thus, apart from protruding endfeet of sustentacular cells that contact the basal lamina (Bali, 2015), anti-CKII and anti-Krt5 antibodies labeled morphologically and positionally distinct cell populations.

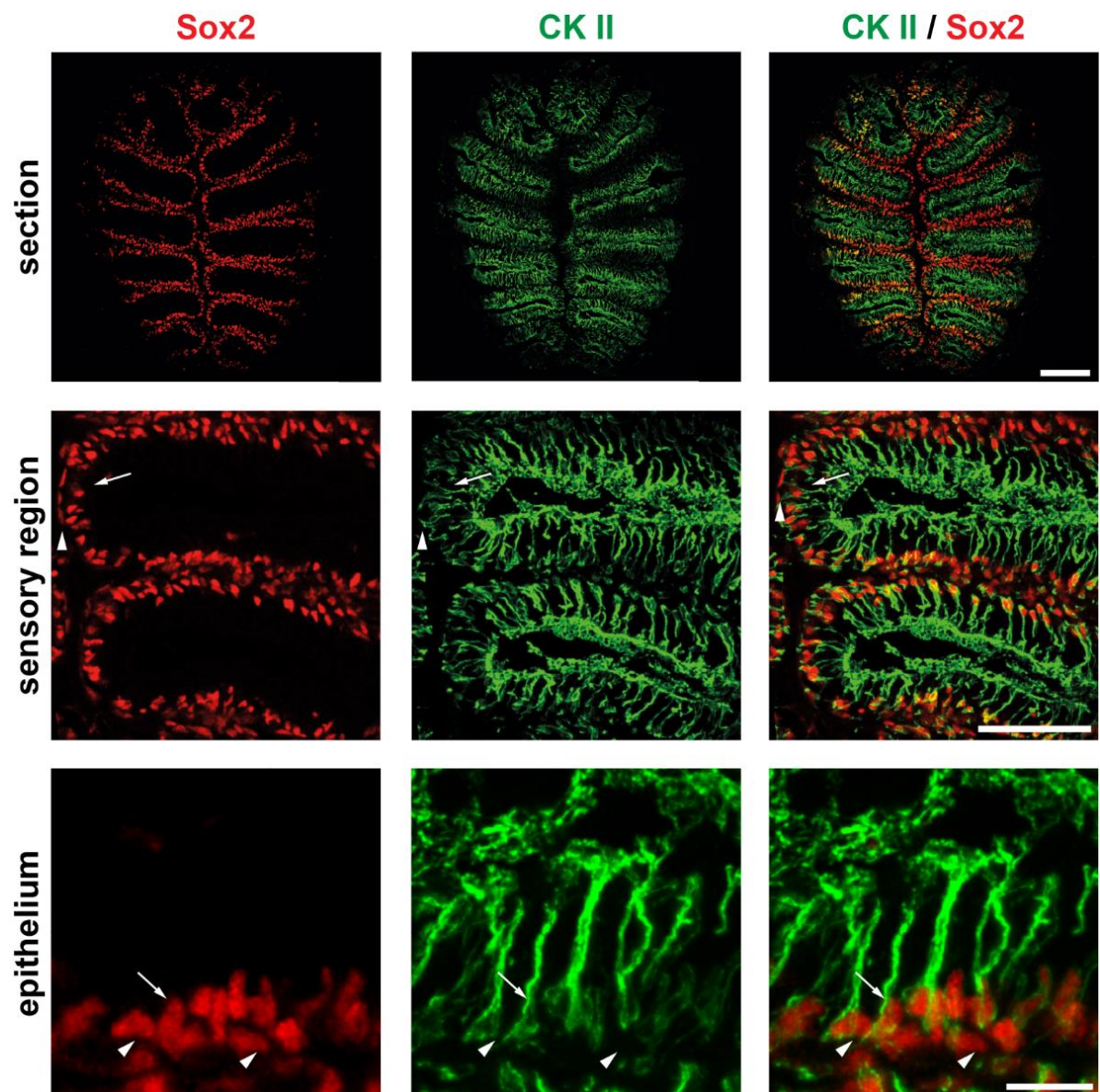


Figure 4.7. Suprabasal Sox2-positive cells are SCs. Immunostaining against Sox2 and CKII identifies the suprabasal layer of Sox2<sup>+</sup> cells as sustentacular cells (arrows) with columnar nuclei. Arrowheads: Basal Sox2<sup>+</sup> cells. Bars: top: 100; mid: 50; bottom: 10  $\mu$ m.

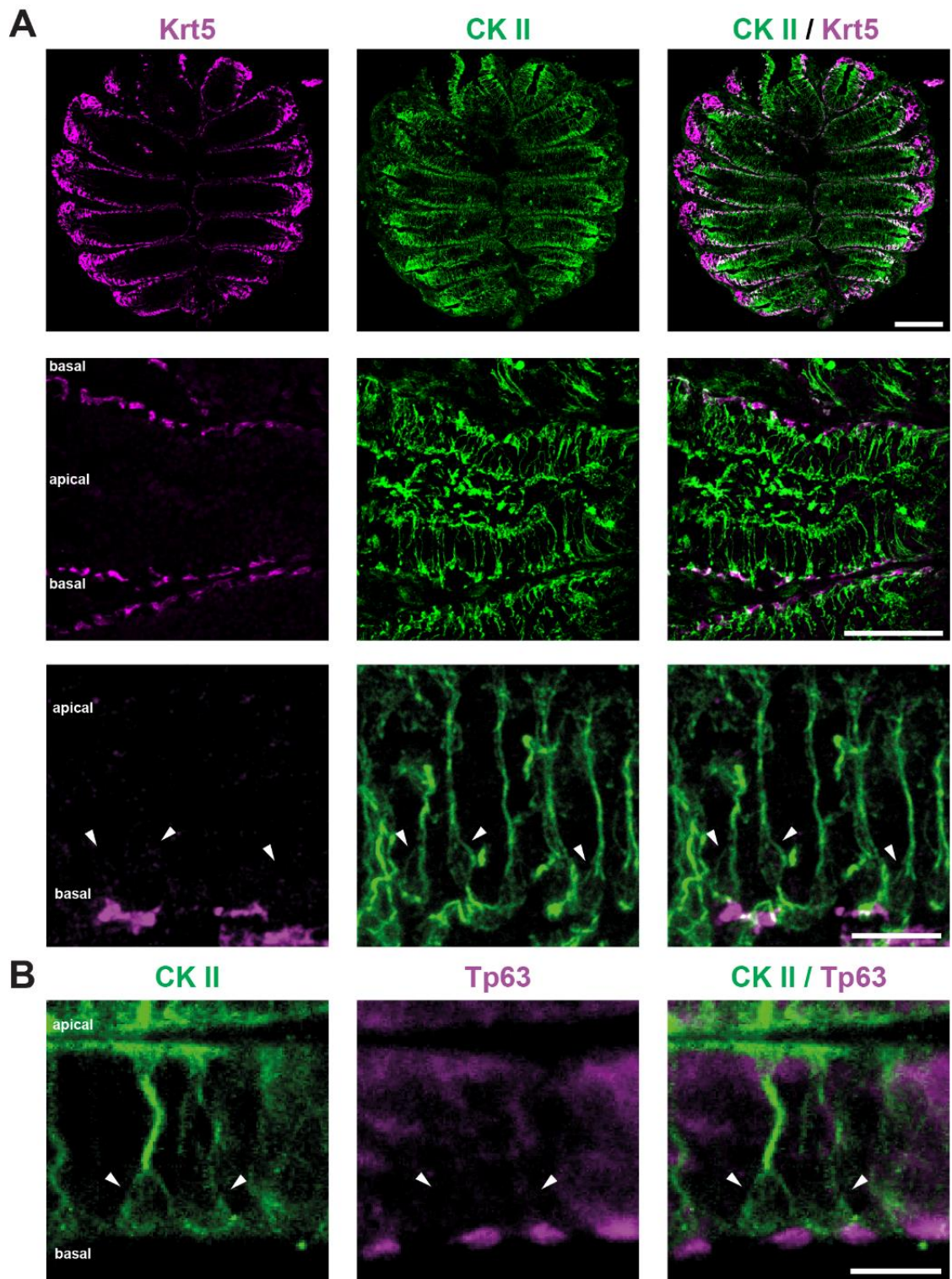


Figure 4.8. CKII exclusively label SCs in sensory region. Immunostaining against SC marker CKII and HBC markers Krt5 (A) and tp63 (B) show mutually exclusive labeling.

Scale bars: top: 100  $\mu\text{m}$  (section); middle: 50  $\mu\text{m}$ , bottom: 10  $\mu\text{m}$  (sensory region).

To gain independent confirmation that SCs are Sox-2-positive and are mutually exclusive from HBCs, double-immunostaining was performed against CKII in combination with Sox2 or Krt5 on mildly dissociated tissue chunks (Figure 4.9). To do so, the zebrafish OE was dissociated with 1U papain enzyme for 5 min at 28°C temperature in low-Ca<sup>2+</sup> Ringer's solution to form small epithelial cell clusters. The immunostained tissue chunks inarguably revealed Sox2-positive nuclei that are encapsulated by CKII-labeled cells (Figure 4.9a). On the other hand, Krt5-positive cells showed mutually exclusive labelling with CKII-positive cells other than weak unspecific interactions (Figure 4.9b).

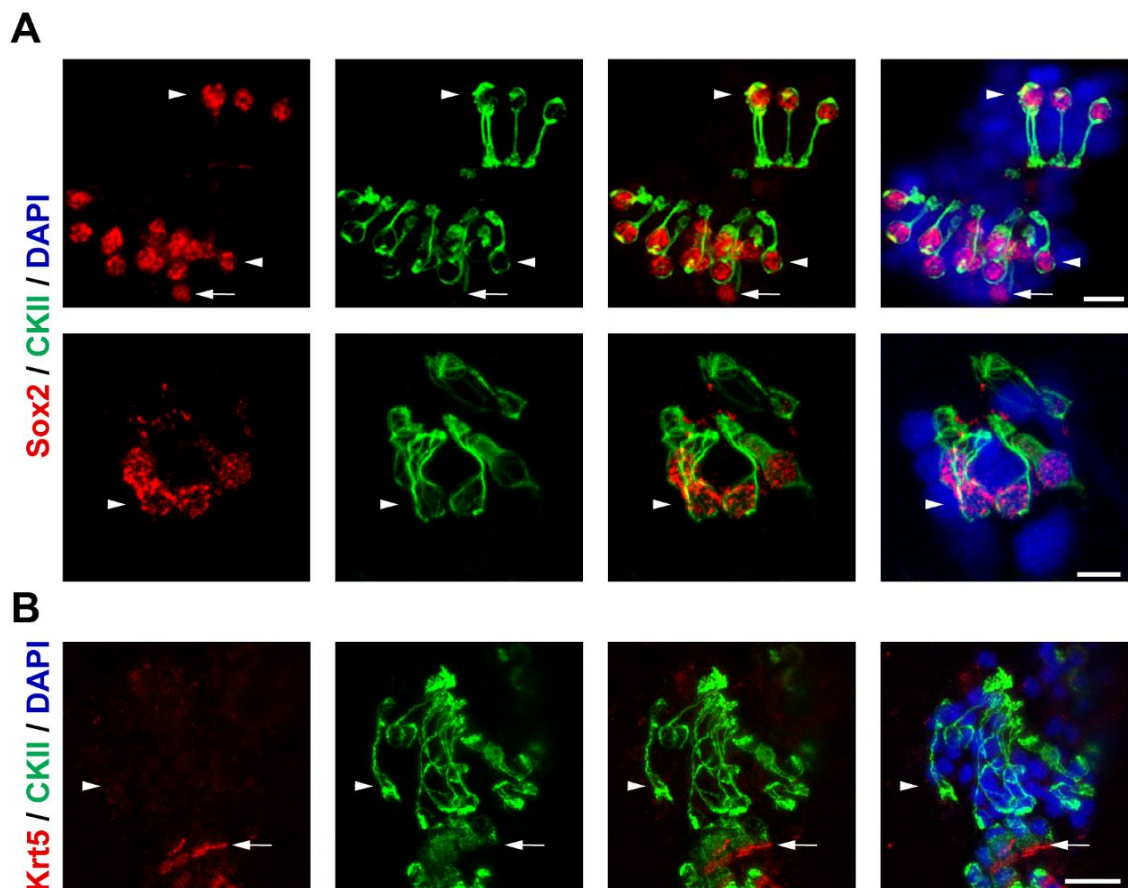


Figure 4.9. Immunostaining on dissociated tissue chunks. Sox2-positive SCs (A) and HBCs (A and B) are labeled in a mutually exclusive fashion with CKII and Krt5. Arrows: basal HBCs, arrowheads: SCs in suprabasal layers of zebrafish OE. Scale bars: 10  $\mu$ m.

These observations show that immunostaining against CKII-expression distinctly labels SCs, which constitute the suprabasal Sox2-expressing cell pool, and can be distinguished from Krt5-expressing HBCs. Sox2-positive intermediate cells also show a close correlation with the morphometric profiles of ATP-responsive cells (Sakızlı, 2018), which suggests that weak ATP responses among intermediate cells originate from zebrafish SCs.

#### **4.1.7. HBCs Form the Basal Layer of Both Sox2-positive Cells and ATP-induced Transients**

HBCs in the zebrafish OE are immunoreactive to p63 and Krt5 and can be stained against Sox2 expression (Kocagöz, 2021). This result was already predicted from the previously described morphometric analysis, as both nuclear p63 and cytoplasmic Krt5-labelling measurements showed close similarity with the horizontal group of Sox2-positive cells (Sakızlı, 2018). As cells with Sox2 expression were identified as the majority of ATP-sensitive intermediate cells, it was imperative to further identify the cells that contribute to ATP-induced responses in the basal layer of the OE. A direct approach based on immunostaining the tissue previously used in Ca<sup>2+</sup> physiology failed to provide reliable results. Thus, a fixable vital dye CellTrace™ that can be used in Ca<sup>2+</sup> physiology and withstands the conditions of immunohistochemistry was used to bridge between the two experimental approaches.

Since the dye was applied to intact epithelia, only cells that have contact with the apical border of the OE were labeled with CellTrace™ prior to cryosection or vibratome slicing (Figure 4.10). Olfactory organs were either frozen and cryo-sectioned to obtain 12 µm sections for immunostaining, or vibratome-sectioned to get 140 µm live-tissue slices for Ca<sup>2+</sup> physiology trials (Figure 4.10b). CellTrace™ treatment clearly exposed cells in the most basal layer of the epithelium that were devoid of staining (arrows).

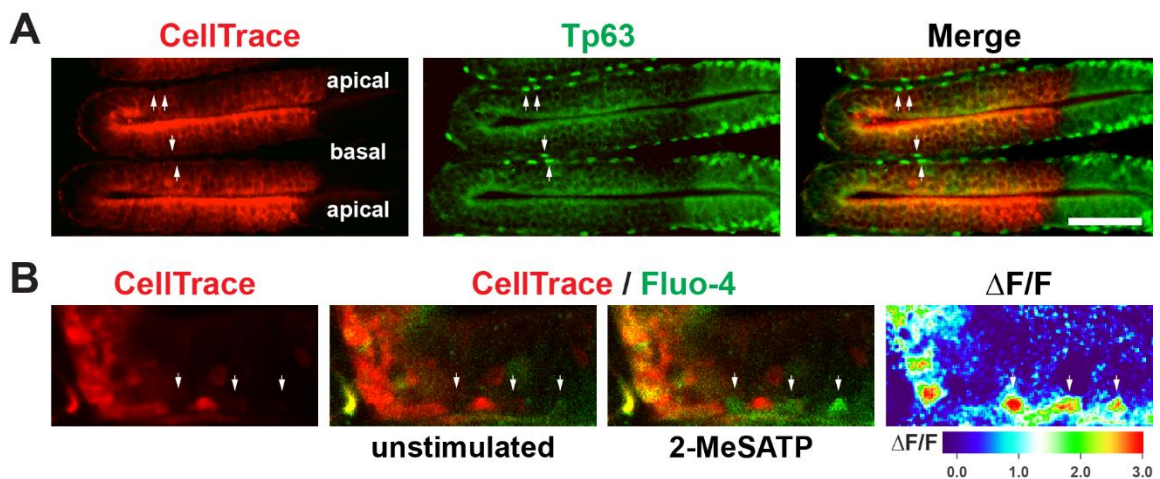


Figure 4.10. Purine sensitive basal cells are HBCs. A. CellTrace<sup>TM</sup> does not stain cells in the basal layer of the OE (arrows), which are positive for tp63 expression (arrows, B and C) and respond to 2-MeSATP. Scale bars: 50  $\mu$ m.

As expected, these cells could be labeled by immunostaining against the HBC marker p63 (Figure 4.10a). The same CellTrace<sup>TM</sup> devoid cells could be observed in vibratome sectioned tissue preparations (Figure 4.10b). Ca<sup>2+</sup> transients induced exclusively from basal layer by 2-MeSATP application and often correlated with cells that were devoid of CellTrace<sup>TM</sup> labeling in Ca<sup>2+</sup> physiology trials. Thus, HBCs that make up the basal layer of Sox2-expressing cells constitute the majority, if not the entire complement, of the basal subset of ATP-responsive cells.

#### 4.1.8. ATP Induces Spatially Restricted Proliferative Activity Through GBCs

All results so far provided the identities of non-neuronal cells in zebrafish OE and their differential physiological characteristics. In the zebrafish OE, ATP induces Ca<sup>2+</sup> transients almost exclusively from non-neuronal cell types in the sensory region. A preliminary study found that ATP stimulation of the OE induces increased cell proliferation from all radial positions of zebrafish OE (Sakızlı, 2018). GBCs, which show high sensitivity to ATP, however, are spatially restricted to the ILC and SNS, where they contribute to persistent maintenance neurogenesis (Bayramlı *et al.*, 2017).

In contrast, HBCs are distributed along the basal stratum of the entire epithelial fold. These cells are typically activated in response to tissue damage (Kocagöz *et al.*, under review). Hence, examining the cell type specific neurogenic effect of ATP on zebrafish OE could reveal the implications of purinergic signaling in distinct neurogenesis events, either daily tissue maintenance or under regenerative conditions.

To more accurately dissect the effect of ATP on OSN neurogenesis, 10 mM ATP was administered by intraperitoneal (IP) injection either separately or in combination with a 5.6 mM solution of the P2-receptor blocker Suramin. Injection of the vehicle PBS was used in a control group. Following injection, fish were kept in 5-bromo-2'-deoxyuridine (BrdU-) containing water for 12 h to label cells that have undergone cell division during this interval. Fish were then transferred to freshwater and analyzed 72 h after the injection by immunohistochemistry against BrdU, Krt5 and HuC/D to examine the neurogenic effect of the manipulation (Figure 4.11).

Initial observations from confocal images of OE sections suggest a spatially restricted effect of ATP on cell proliferation in the zebrafish OE (Figure 4.11a; top panel). In this experiment, ATP treatment resulted in an increased number of BrdU-labeled cells selectively at the ILC (arrowheads in middle panel) and SNS (asterisks in middle panel). Ruler in bottom panel of part A of the figure indicates the radial index of the graphs in part B of the Figure 4.11 and Figure 4.12. The neurogenic effect could be efficiently blocked by simultaneous application of the P2-receptor blocker Suramin (right column).

The number of BrdU-positive proliferating cells and of newly generated HuC/D/BrdU double-positive OSNs were quantified positionally by counting labeled cells in 10 equidistant bins between the ILC and peripheral margin of the OE (54 EF/condition: 6 EF/section, 3 section/fish, 3fish/condition). HuC/D/BrdU and Krt5/BrdU double-positive, and only BrdU-positive cells were counted in these bins by a custom macro in the FIJI environment and corrected for multiple counting of cells at the edge of the bins in RStudio.

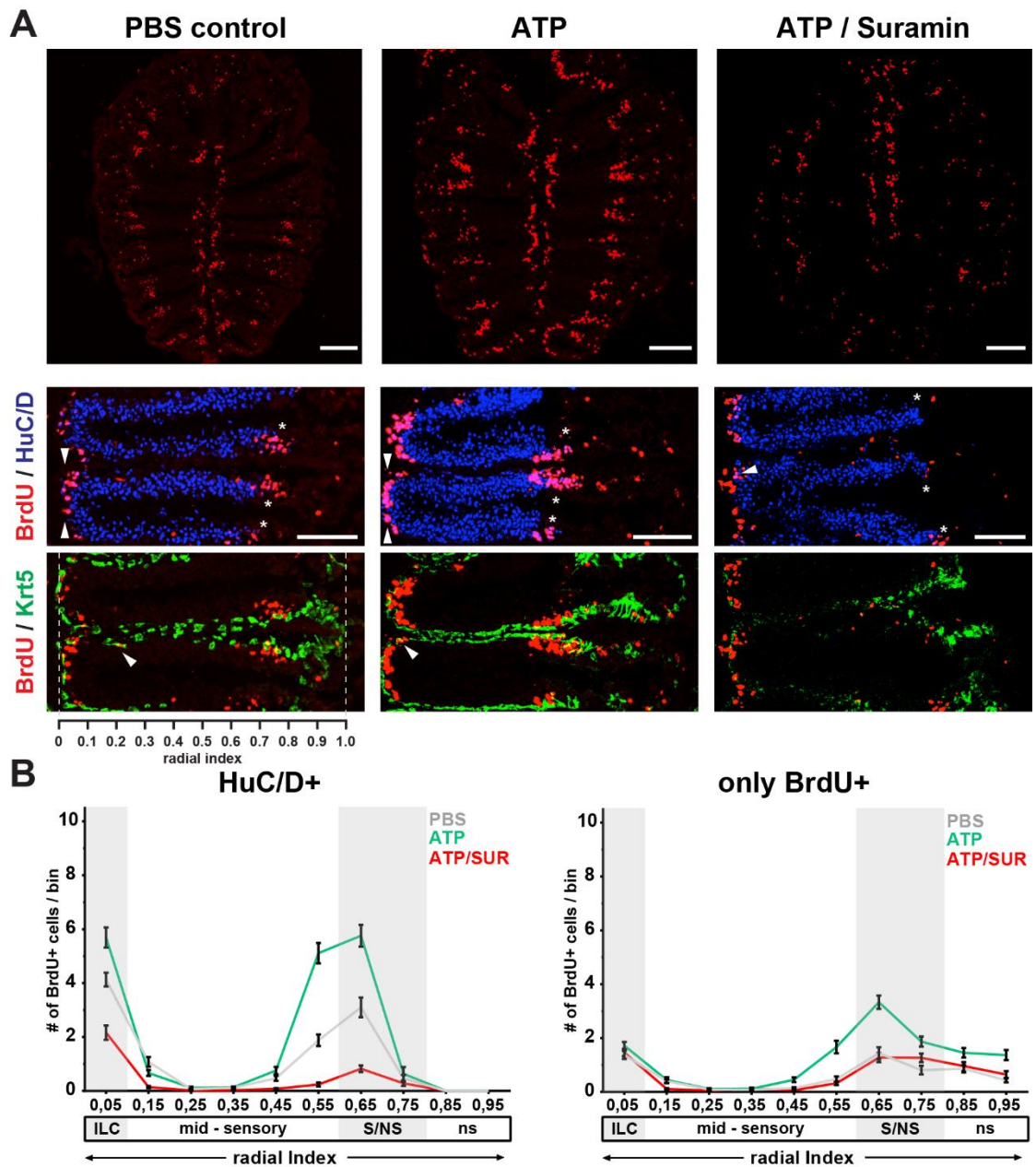


Figure 4.11. ATP-induced proliferative activity at 72hpi. A. Confocal images of whole sections (top, Scale bar: 100  $\mu$ m) and individual epithelial folds (bottom; Scale Bar: 50  $\mu$ m). B. Positional quantification of BrdU+ cells along the same radial index as in A.

The average number of labeled cells that were in each radial bin for EFs are represented as line graphs in Figure 4.11b and Figure 4.12. In this representation, the sensory region extends between positions 0.05-0.65, while the ILC occupies the bins denominated by a radial index of 0.05. The SNS occupies positions 0.65-0.75, while the remainder of the tissue between 0.85 and 0.95 corresponds to the non-sensory OE. The mid-sensory region in which spontaneous mitotic activity is rare or absent in the intact OE was defined as the region between radial positions 0.15 and 0.55.

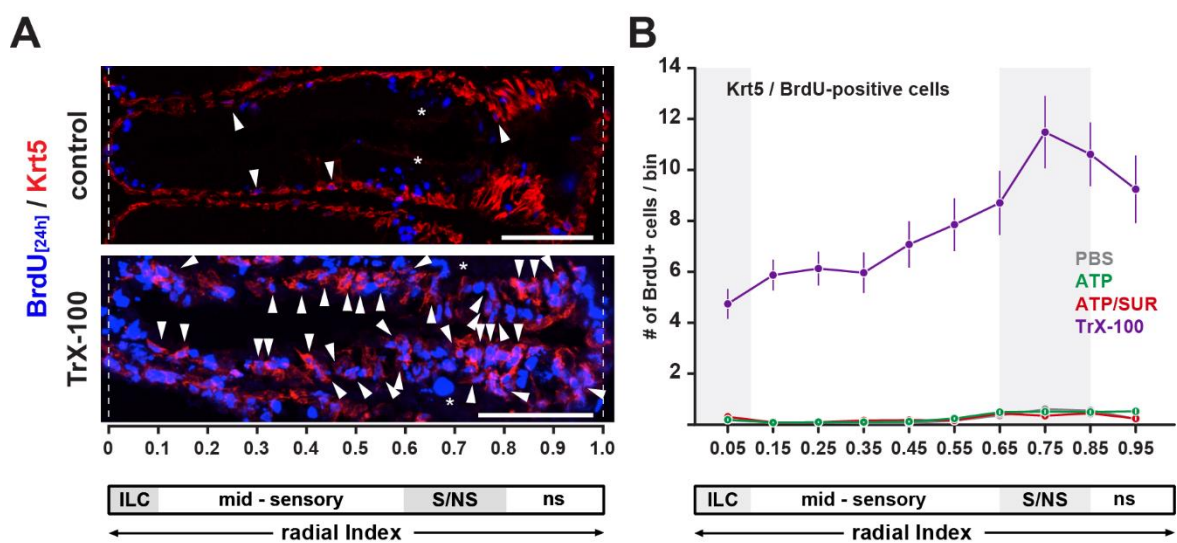


Figure 4.12. ATP does not activate HBC proliferation at 72 hpi. A. Tissue lesioned with 1% Triton-X100 compared to control. Scale bars: 50  $\mu$ m. B. Profile of Krt5<sup>+</sup>/BrdU<sup>+</sup> cells in lesioned tissue compared to PBS-, ATP-, or ATP/Suramin-injected fish at 72 h.

The quantification shows that ATP stimulation induced an increased number of BrdU-positive cells, many of which co-labeled for HuC/D (Figure 4.11b and Figure 4.13). At the ILC, the number of newly generated HuC/D/BrdU double-positive OSNs in PBS control increased from  $4.13 \pm 0.26$  (mean  $\pm$  SEM) to  $5.69 \pm 0.4$  upon ATP injection but decreased to  $2.16 \pm 0.26$  in ATP and Suramin co-injection (ATP/SUR) condition. A more robust increase in the number of mitotically active cells could be observed at the SNS at position 0.65, where the number of cells increased from  $3.1 \pm 0.37$  in PBS controls to  $5.7 \pm 0.4$  in ATP-stimulated fish but decreased to  $0.8 \pm 0.12$  when Suramin was applied.

Cells also displaced from the SNS to more mid-sensory positions at 0.55 (PBS:  $1.9 \pm 0.21$ ; ATP:  $5.1 \pm 0.38$ ; ATP/SUR:  $0.24 \pm 0.08$ ) in different conditions. Cells that labeled only for BrdU but not HuC/D, which may include proliferating progenitors and transient-amplifying precursors cells showed an increase at the 0.05 position of the ILC (PBS:  $1.4 \pm 0.16$ ; ATP:  $1.7 \pm 0.13$ ; ATP/SUR:  $1.4 \pm 0.13$ ) and 0.65 position of SNS (PBS:  $1.4 \pm 0.22$ ; ATP:  $3.3 \pm 0.24$ ; ATP/SUR:  $1.3 \pm 0.17$ ) but failed to show any observable decrease for ATP/SUR co-injection. On the other hand, apart from sporadic activity, BrdU/Krt5 double-positive cells did not present any change in ATP or ATP/SUR conditions (Figure 4.12b).

These results indicate that the stimulatory effect of ATP on cell proliferation is restricted to the zones of maintenance neurogenesis at the ILC and SNS. Krt5 was selected to label HBCs in basal epithelial stratum of sensory region. Therefore, in this experiment, only BrdU-positive cells could represent SCs or GBCs in the sensory region (positions between 0.05-0.65 in radial index). Since SCs have the similar radial distribution with HBCs in sensory region, the spatially restricted neurogenic effect induced by ATP, if not from HBCs, could only originate from GBCs localized to these positions. All in all, the observations suggest that ATP has a modulatory effect by promoting neurogenesis from GBCs but not HBCs or SCs.

#### **4.1.9. ATP does not Activate HBC Proliferation in Intact Tissue**

To show that ATP indeed does not induce HBC activation, the tissue was lesioned by irrigation with the non-ionic detergent Triton X-100 for comparison (Figure 4.12). 1% Triton X-100 (TrX) dissolved in PBS solution was used to chemically lesion the zebrafish OE (Iqbal and Byrd Jacobs, 2010). When applied nasally over the course of 90 seconds, TrX was shown to efficiently induce HBC activity (Demirler *et al.*, 2020; Kocagöz, 2021).

Activated HBCs can be observed in every radial position upon chemical lesion (Figure 4.12b) which exhibited 30-fold increase in total number of Krt5/BrdU double-positive cells on the epithelial folds (Figure 4.13; 18 epithelial folds/fish, 3 fish/condition). On the other hand, ATP failed to display any indications of HBC activation at any radial positions or in cumulative number of BrdU/Krt5 double-labeled cells in the epithelial

folds. A one-way ANOVA test revealed a significant increase in the number of all BrdU labeled, BrdU/HuC/D double-labeled, and only BrdU-positive cells upon ATP injection for analyzed epithelial folds (BrdU total:  $F_{(2,105)} = 71.3$ ,  $P < 10^{-19}$ ; BrdU only:  $F_{(2,105)} = 21.8$ ;  $P < 10^{-7}$ , BrdU/HuC/D:  $F_{(2,105)} = 133.6$ ,  $P < 10^{-28}$ ; BrdU/Krt5:  $F_{(2,105)} = 0.624$ ,  $P = 0.538$ ). Statistical difference between ATP, ATP/SUR and PBS injection conditions were evaluated with post hoc Tukey HSD test and p values are shown in the graph (Figure 4.13). ATP injection compared to PBS control showed significant difference in all BrdU labeled cell types except HBCs. The test also shows this effect is reversible with ATP/SUR co-injection in HuC/D/BrdU double-labeled cell numbers.

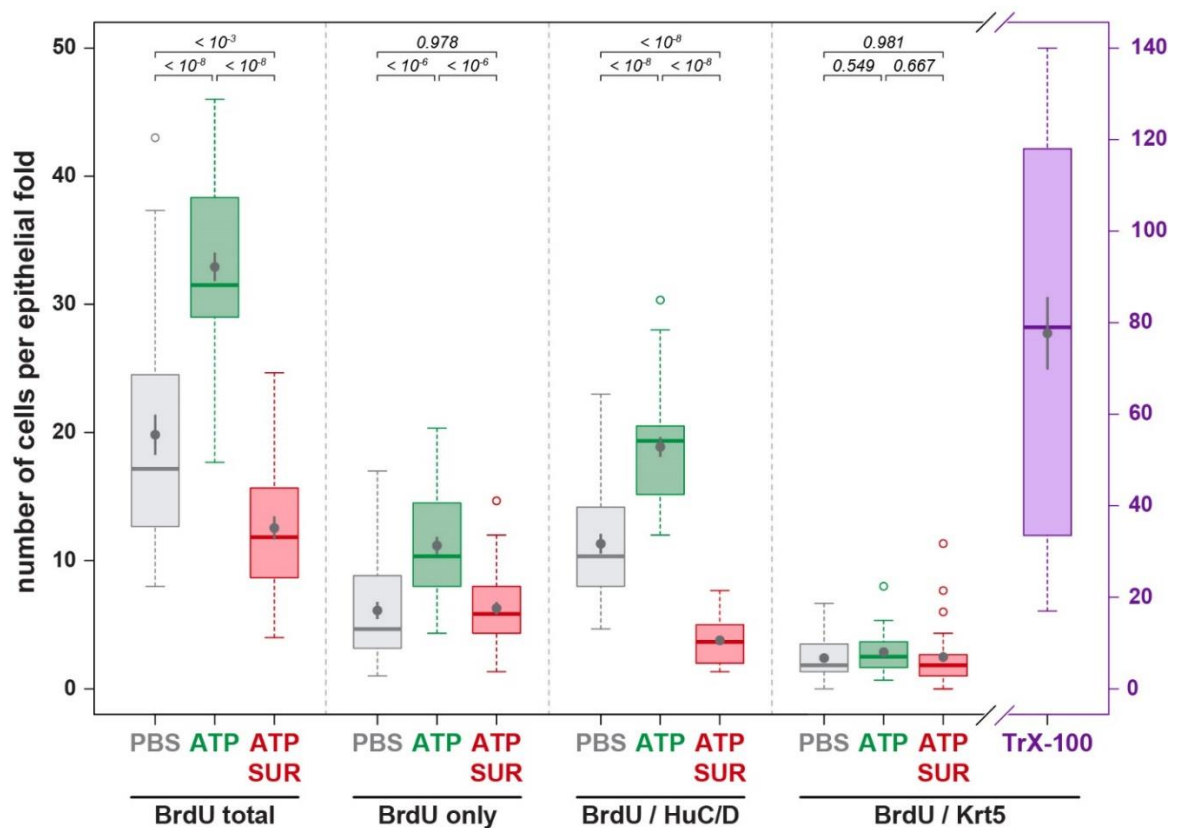


Figure 4.13. Cumulative cell type specific effect of fish injected with PBS, ATP, or ATP and Suramin at 72 hpi. Krt5 cells compared to TrX-100 induced damage (right y axis). Box and Tukey style whisker plot of BrdU<sup>+</sup> cells.

While ATP can induce differential  $\text{Ca}^{2+}$  transients from non-neuronal cells including HBCs, systemic ATP injection has a specific neurogenic effect on GBCs spatially restricted to the maintenance neurogenesis zones in the zebrafish OE. HBC activation could not be observed in any conditions other than direct chemical insult, which shows rapid expansion of BrdU-positive cells from all radial position of the epithelial folds. This suggests that ATP selectively stimulates maintenance neurogenesis through promoting GBC activity but not repair neurogenesis, which requires HBC activation (Kocagöz, 2021). All findings in section 4.1 were published in the FEBS Journal (Demirler *et al.*, 2020).

## **4.2. Characterization of Intact Tissue Dynamics of Sox2-positive Cells in the Zebrafish OE**

The second part of this thesis focuses on detailing the dynamic changes of Sox2-positive cells while also describing the intrapopulation differences in the intact zebrafish OE. First, the proliferative activity of Sox2-positive cells will be characterized in combination with cell proliferation assays that cover different time intervals. Distinct morphological and proliferative features of HBCs and SCs will be described by histology experiments. Then, the possible origin of SCs and proliferative events in the OSN lineage hierarchy will be proposed using a combination of proliferation markers to trace successive cell divisions within the same lineage.

### **4.2.1. Proliferative Activities of Sox2-positive cells in the intact tissue**

Immunohistochemistry against Sox2 and HuC/D expression alone labels up to 98% of all cells in the sensory region of the zebrafish OE (Figure 4.2), which implies that cells of the early neurogenic lineage are largely contained within the Sox2-positive cell population. Therefore, identifying the sources and location of proliferative activity in the sensory region is imperative to understand the extent of cell types that are involved in daily maintenance neurogenesis in the intact zebrafish OE. Proliferative cells can be observed by combining antibody staining against Sox2 expression and the mitotic marker proliferating cell nuclear antigen (PCNA). PCNA was selected for this analysis because it labels acutely dividing cells, starting from S-phase until the end of cell division (Dietrich, 1993) as opposed to BrdU incorporation assays, which integrate into proliferative cells over the entire duration of the BrdU pulse.

Cells that stain positive for PCNA-immunohistochemistry in the intact OE can be observed at the ILC, SNS, and within the non-sensory region of the zebrafish OE (Figure 4.14). These results confirm previous observations, which showed that the ILC and SNS are the main proliferative and neurogenic sites in the intact OE (Bayramlı *et al.*, 2017; Kocagöz, 2021).

As expected, in the sensory region, all PCNA-immunoreactive cells also stain positive for Sox2 expression. Accordingly, double-positive cells are located mainly at the neurogenic zones around the ILC (arrowheads) and SNS (asterisks). The observation also identifies Sox2-expressing cells in these positions to be the cell group that underlies proliferation activity under physiological conditions. GBCs are the progenitor cells of origin for maintenance neurogenesis in the zebrafish OE and might account for a fraction or all the PCNA and Sox2 double-labeled cells. However, the contribution of the two other Sox2-expressing cell types, HBCs and SCs, to the proliferative activity has not been studied in the intact tissue.

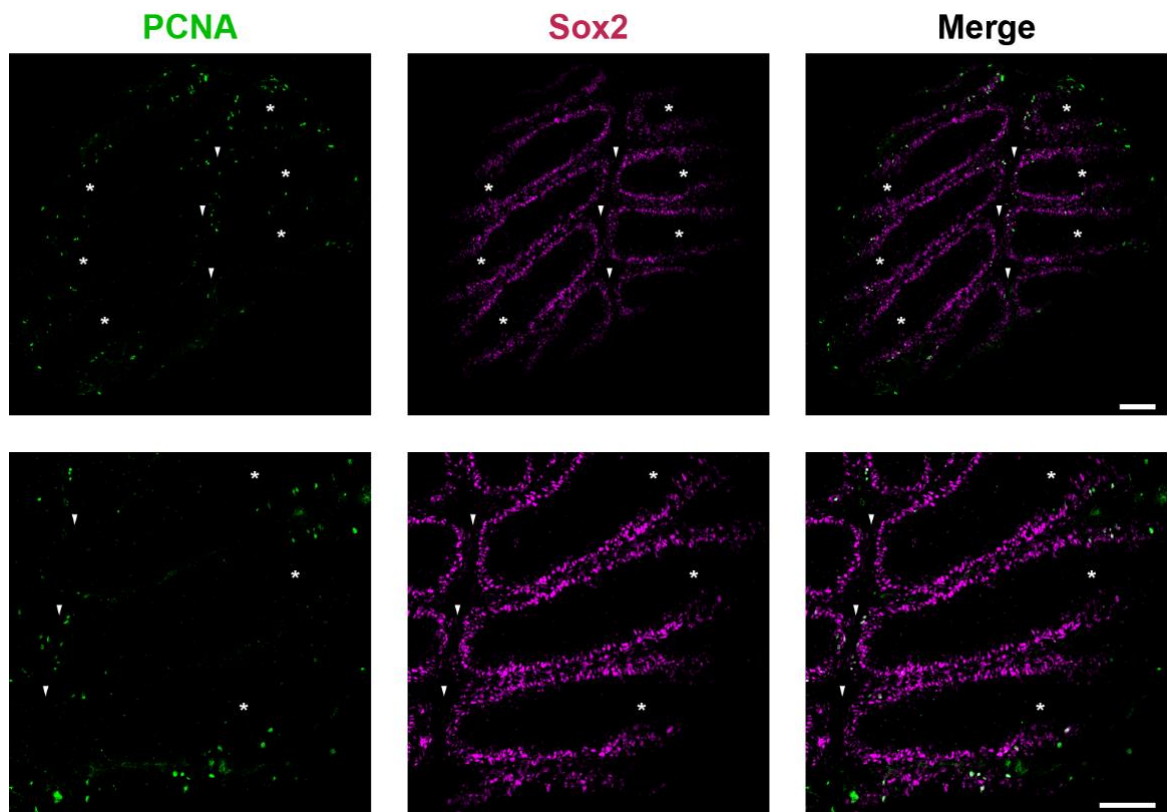


Figure 4.14. PCNA-immunoreactive cells are Sox2-positive in the sensory region. Arrowheads: space between interlamellar curves. Asterisks: SNS border. Scale bars 50  $\mu\text{m}$ .

To gain further insight into the proliferative activity of HBCs and SCs in the intact OE, animals were incubated in BrdU-containing tank water for 24 h to label mitotically active cells and subsequently subjected to immunohistochemical analysis with the HBC- and SC-specific molecular markers Krt5 and CKII, respectively (Figure 4.15). Interestingly, both Krt5/BrdU double-positive (arrowheads) and CKII/BrdU double-positive cells (arrows) could be observed at the ILC and SNS after a 24 h BrdU incubation period. Both HBCs and SCs were observed with a BrdU-positive nucleus that is encapsulated by Krt5- or CKII-labeled somatic fibers, respectively (Figure 4.15a). Krt5/BrdU double positive cells were observed rarely in the sensory region but could be observed almost always in the non-sensory region. CKII/BrdU double-positive cells were never observed in the mid-sensory but were encountered in the non-sensory along with Krt5/BrdU double-positive cells.

Thus, in addition to generating OSNs at high rate, the ILC and SNS appear to be also sites of HBC and SC proliferation. However, the direct lineage relationship between these different cell types remains obscure.

Interestingly, in the non-sensory OE, Krt5/CKII double-positive cells could also be observed (Figure 4.15b). Within the sensory region, immunostaining against Krt5 expression strictly labels cells with horizontal morphology in the basal OE, while CKII labels pyramidal cell bodies in suprabasal layers. However, in the surrounding nonsensory OE, cells with vertically elongated profiles (Figure 4.15b, asterisks) and somatic structures in intermediate epithelial strata can be observed. Closer examination of labeled cells around the SNS indicates a gradual morphological transformation of Krt5-positive cells in this region (Figure 4.16). Centrally to the SNS Krt5-positive cells are characterized by flat horizontal morphologies and do not express CKII, while Krt5/CKII double-positive cells can be observed on the non-sensory side of SNS. Krt5/CKII double-positive cells show bipolar morphology with CKII-labeling that spans the entire apico-basal axis of the epithelium (asterisks in Figure 4.16).

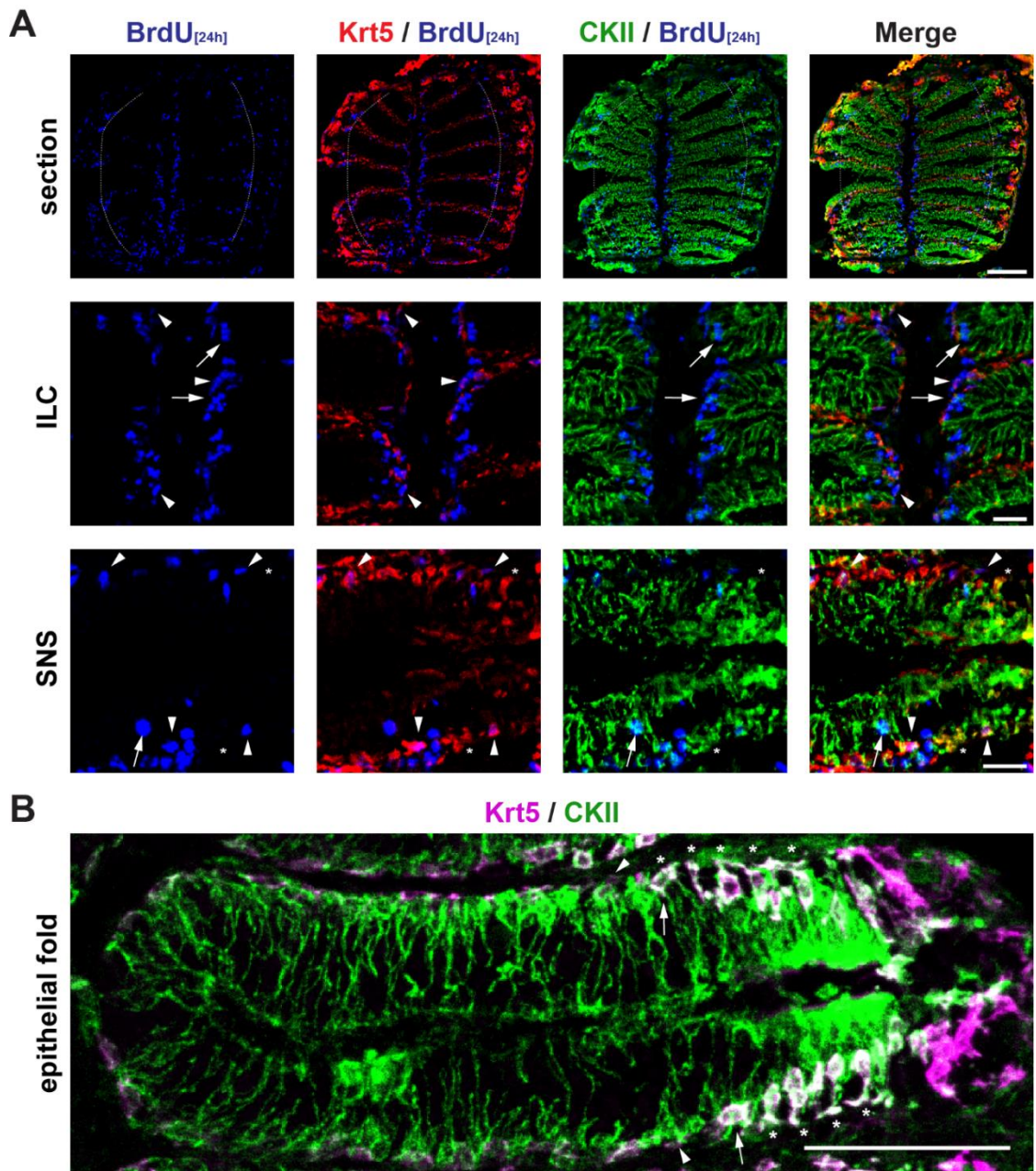


Figure 4.15. 24h proliferative activity of HBCs and SCs in the intact tissue. A. BrdU-labeled cells after a 24h BrdU pulse stained against Krt5(A: red, B: magenta) and CKII (green). B. Double-positive cells occur at the SNS. Scale bars: from top; 50, 20, 20, 50  $\mu$ m.

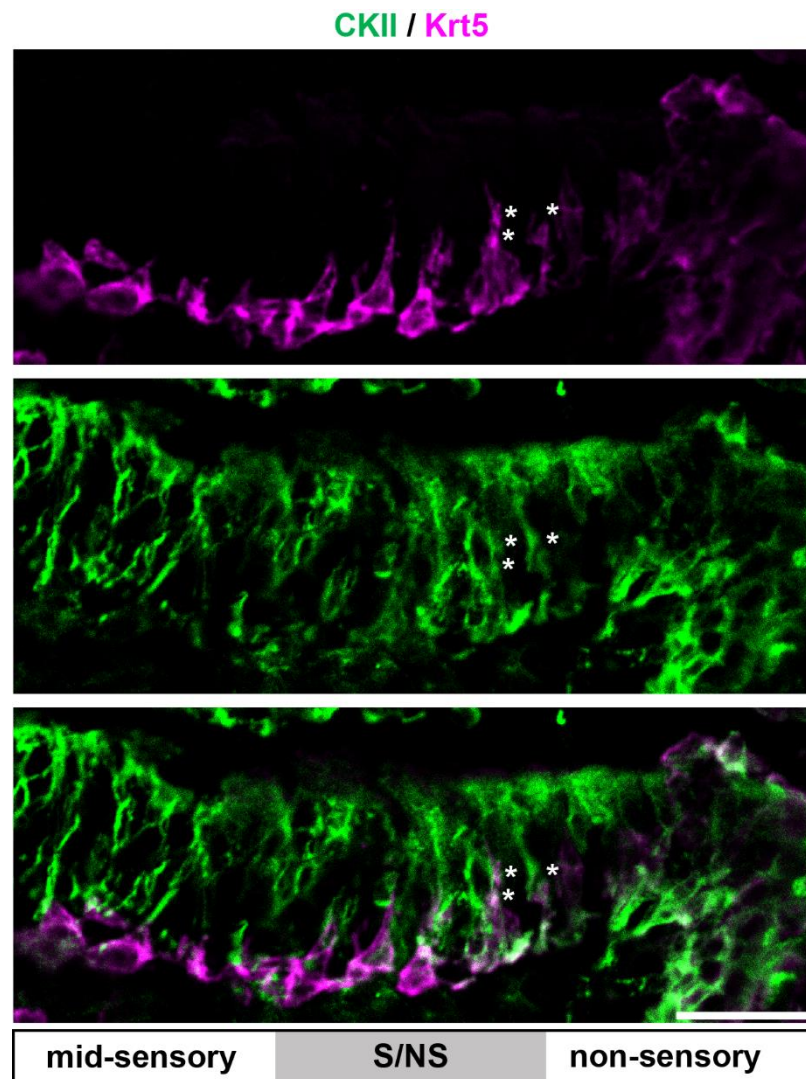


Figure 4.16. Transition of cell morphology at the SNS. Mid-sensory regions shows exclusive labeling for Krt5, while Krt5/CKII double-positive cells are predominant in the non-sensory OE. Scale bar: 20  $\mu\text{m}$ .

The observation of double-labeled cells with distinct bipolar morphology suggests that, apart from HBCs and SCs, another non-neuronal cell type could be populating the SNS. These cells are characteristically labelled with Krt5 at their basal portion while show complete CKII immunoreactivity and located between the ciliated beating cells in the non-sensory region (Hansen and Zeiske, 1998) and the basal HBC progenitors in the SNS.

The proliferation of Krt5-labeled HBCs in the intact tissue was described previously in this study (Figure 4.11 and Figure 4.15a), and a gradual morphological transformation from spherical to columnar morphologies could be observed in the neurogenic zone of the SNS (Figure 4.16). Next, the link between morphological changes in Krt5-positive cells and proliferative activity was studied more closely along the radial dimension on OE tissue subjected to a 24 h BrdU pulse.

Examination of the epithelial sheet of intact tissue following a 24h BrdU pulse revealed the morphological change of Krt5-labeled cells along the radial dimension, most notably at the transition zone between sensory and non-sensory regions and their relationship with the proliferative activity (Figure 4.17). Since the ILC and SNS are the neurogenic zones with high proliferative activity (Bayramlı *et al.*, 2017), BrdU-positive cells were primarily observed in these regions. A large portion of these cells were positioned at the intermediate layers of the epithelium and were only BrdU-positive. Although the proliferative activity of Krt5-positive cells was low over the 24 h labeling period, a small number of Krt5/BrdU double positive cells were mainly observed in the ILC and SNS (arrowheads in Figure 4.17a). On the other hand, sporadic Krt5/BrdU double positive cells could also be observed in the mid-sensory region (arrowhead located in the 0.3 position in Figure 4.17a).

While most of the Krt5-positive cells showed a horizontal morphology in the sensory OE (0-0.7 regions in Figure 4.17a), a few cells with more pyramidal profiles could also be observed and this (Figure 4.17b). These cells were endowed with vertical extensions that protruded into intermediate epithelial strata (arrows) and showed retained BrdU-labeling as well. Krt5-expressing cells with horizontal morphology (arrowheads) are prominent at the ILC and mid-sensory regions whereas the beginning of the SNS is marked by cells with enlarged and more globular profiles or pyramidal morphology that are accompanied by apical protrusions (arrows).

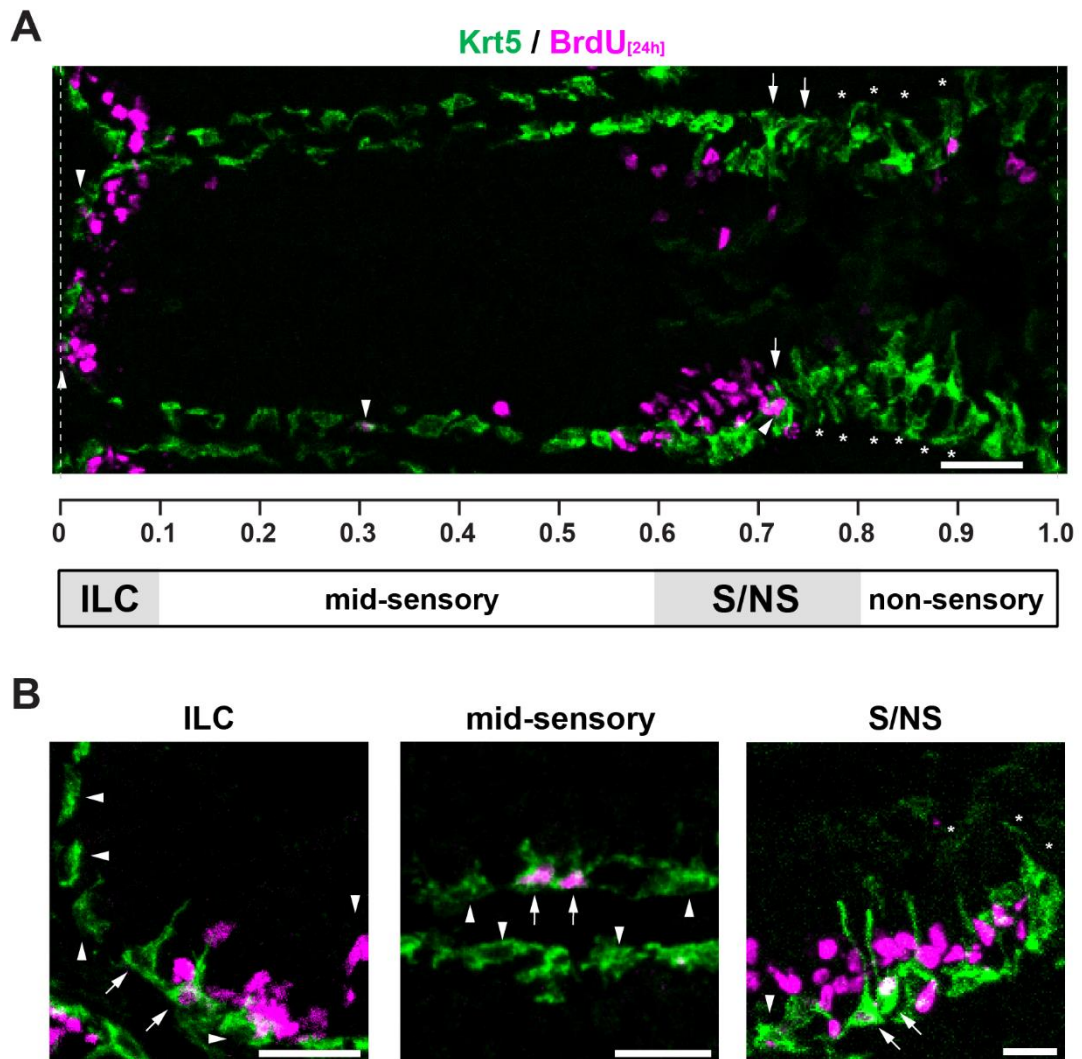


Figure 4.17. OE tissue stained against Krt5 and BrdU following a 24h BrdU pulse. The morphology of Krt5-labeled cells varies along the radial dimension. A. Epithelial fold. Scale bar: 20  $\mu$ m. B. High-power views of ILC, mid-sensory, and SNS. Scale bars: 10  $\mu$ m.

At the SNS, the position of the observed high proliferative activity matched with the transition zone and changes in morphology of Krt5-expressing cells (arrows in Figure 4.17b; but also see Figure 4.16 and Figure 4.19b top panel). A pyramidal Krt5/BrdU cell can be seen in the SNS and marked with both an arrow and an arrowhead at the 0.7 position in Figure 4.17a. Further into the SNS, these protrusions change into basal end feet and the nuclei are positioned in intermediate layers of the epithelium, showing an inversion of the cell morphology (asterisk at SNS and non-sensory).

This change coincides with an upward-directed bending of the basal lamina. The beginning of non-sensory region could be described by the presence of Krt5-cells with elongated columnar morphologies with apical nuclear arrangement that have apical and basal contacts (asterisks in non-sensory region in the Figure.17; but also see Figure 4.16 and Figure 4.19b top panel).

Thus, in physiological conditions, HBCs are presented with mainly horizontal dimensions in the mid-sensory regions but can also show occasional elongated pyramidal morphology that can be attributed to mitotic activity at the ILC and rarely in mid-sensory region. On the other hand, HBCs mark the beginning of the SNS by gradual change in morphology from horizontal to globular and eventually pyramidal cells with apical protrusions. However, further to the non-sensory side, Krt5-labeling marks cells with inverted somata located in intermediate layers of the epithelium with obscure identity.

#### **4.2.2. Proliferative Activities of Sox2-positive Cells in Response to Damage**

In the intact OE, occasional Krt5/BrdU double-positive HBCs could be identified after a 24 h BrdU incubation period. Proliferatively active HBCs were often characterized by morphological changes that included epithelial protrusions and a more pyramidal appearance. The morphology of these cells could, thus, be a hallmark of its acute proliferative state and could serve as an excellent identifier for actively dividing HBCs. In the mouse OE, injury-activated HBCs were also reported to show pyramidal morphologies when they become PCNA-immunoreactive (Brann, 2014). The morphological change might reflect detachment from the basal lamina and regaining apico-basal polarity, which could be required for asymmetric divisions and an indication that HBCs lose their quiescence and enter S-phase. Hence, studying the HBC morphology in physiological conditions and in lesioned tissue could help to understand if a correlation exists between changes in cellular morphology and the activity of HBCs.

To characterize the morphology of activated HBCs, immunohistochemistry against BrdU and Krt5 was performed at 24 h post-lesion (hpl) on tissue irrigated with 1% TrX. The specimens were subjected to a 24 h BrdU pulse immediately after the damage (Figure 4.18). Staining against HuC/D expression was used to evaluate the extent of the chemical injury and untreated OEs of the same fish were used as internal controls.

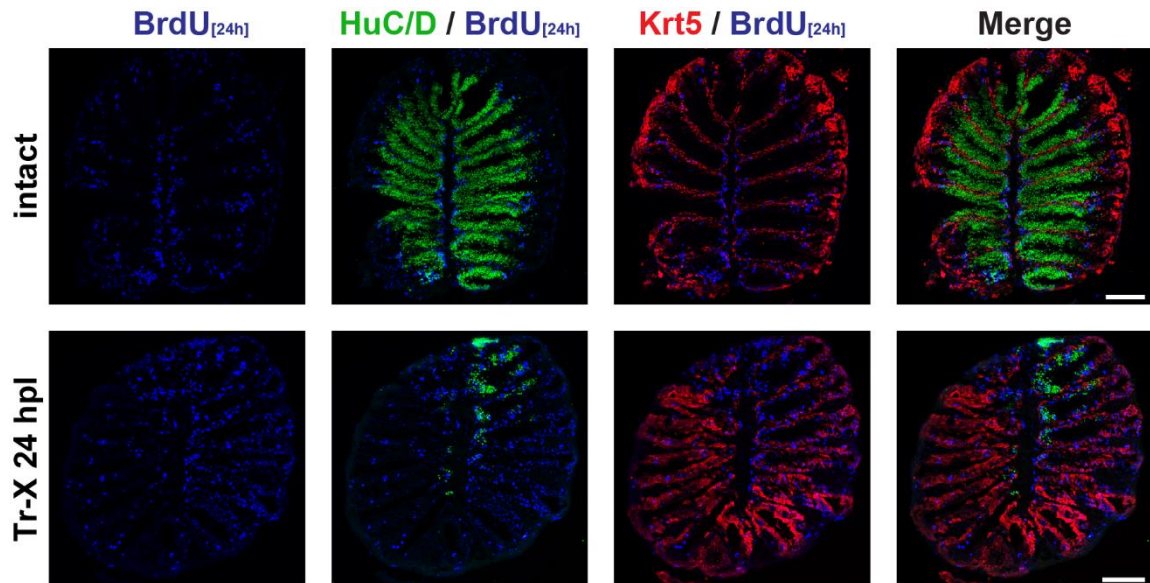


Figure 4.18. Chemically lesioned OE compared to intact tissue at 24hpl. Immunostaining against Krt5 (red), HuC/D (green) and BrdU (blue) on intact (top) and chemically lesioned tissue by 1% Triton-X100 (bottom). Scale bars: 100  $\mu$ m.

Upon tissue damage, characteristic morphological arrangement of Krt5-positive cells along the radial axis was lost and Krt5-labeled, mitotically active HBCs in the sensory region adopted a globular shape with more intense cytoplasmic labelling at 24 hpl in every position. Activated HBCs expanded and invaded the intermediate epithelial strata to form suprabasal layers, which is also observed in rodent OE following lesion (Leung *et al.*, 2007). Thus, a change in the morphological appearance can also be observed in damage-activated HBCs and can serve as a proxy for mitotic activity. Dormant HBCs are characterized by smooth, horizontally flat profiles, whereas actively dividing HBCs become spherical and often extend apical protrusions.

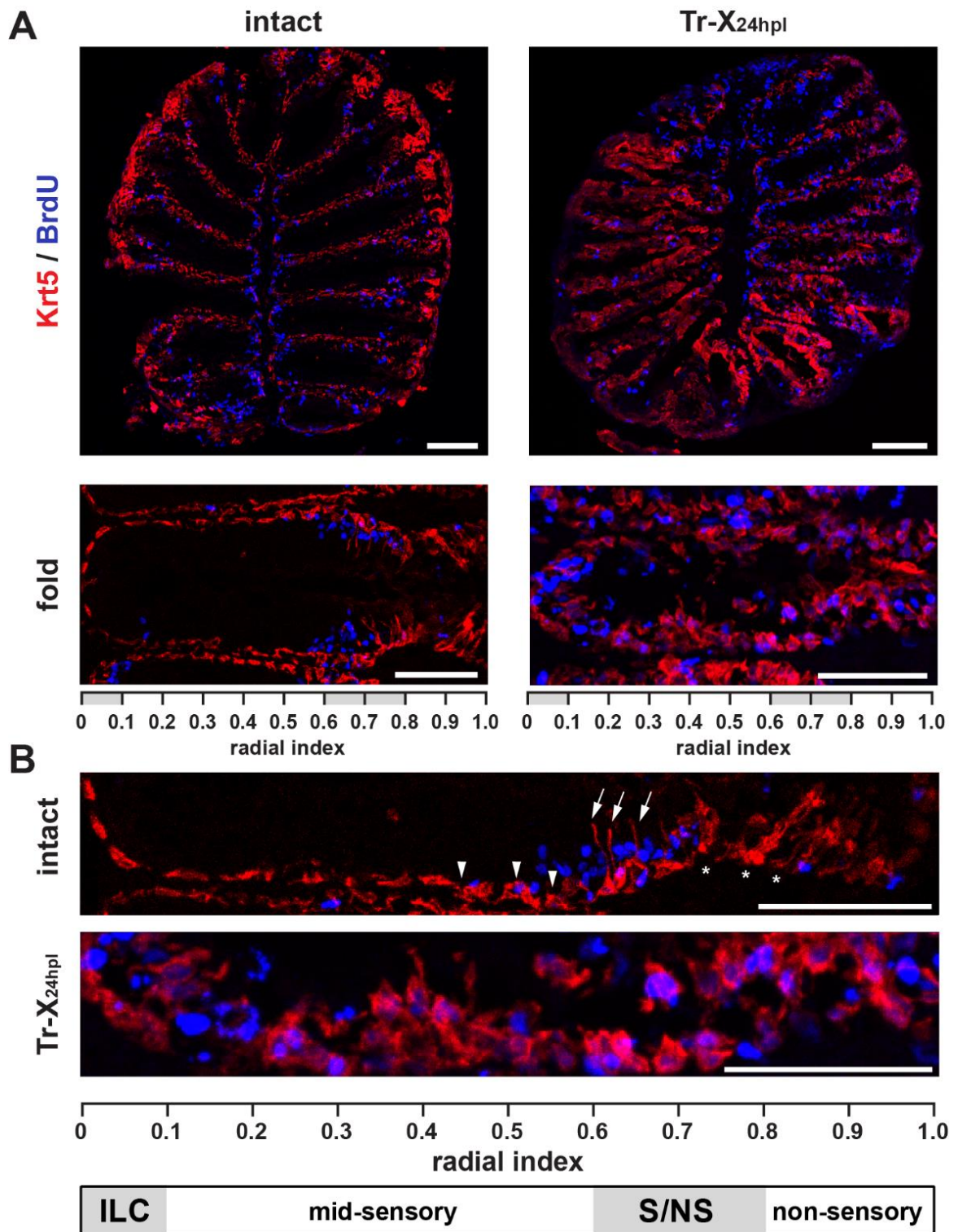


Figure 4.19. Lesion activated HBCs show changes in morphology and invade the tissue. A. Krt5<sup>+</sup> (red) cell in lesioned compared to intact tissue. A. Section (top:100  $\mu$ m; bottom:50  $\mu$ m). B. Morphological differences in HBCs. Scale bars: 20  $\mu$ m.

To examine the proliferative activity of regenerating SCs, immunostaining against BrdU and the SC-specific marker CKII was performed at 24 hpl following a 24h BrdU pulse (Figure 4.20). Both, surviving SCs labeled only with CKII but not BrdU (arrows) and newborn BrdU/CKII double-positive SCs (arrowheads) could be observed without any positional preference in the OE, suggesting a rapid expansion of the SC pool. However, Krt5/CKII double-positive cells were again only observed at the SNS and within the non-sensory region (asterisks), while CKII and Krt5 expression labels distinct cell types in the ILC and mid-sensory region.

Although there is clear evidence that SCs are also rapidly generated in the damaged tissue, CKII-labelling is diffuse and restricted to intracellular filaments, making it difficult to obtain clear images required for quantification of individual cells. Immunostaining against glial cell markers from other model organisms or tissues such as homeotic transcription factor paired box protein 6 (Pax6) (Tomita *et al.*, 1996; Furukawa *et al.*, 2000; Roesch *et al.*, 2008), Notch1 (Herrick *et al.*, 2017), vimentin and glial fibrillary acidic protein (GFAP) (Chapouton *et al.*, 2007; Kizil *et al.*, 2012), or other possible markers sine oculis homeobox 1 homolog (Six1) and orthodenticle homeobox (OTX) was used in an attempt to label SCs more effectively in the zebrafish OE but did not provide reliable staining results. Because of this reason, my studies further focused on analyzing the intact tissue for possible origins of SC generation, which will be detailed in section 4.2.8.

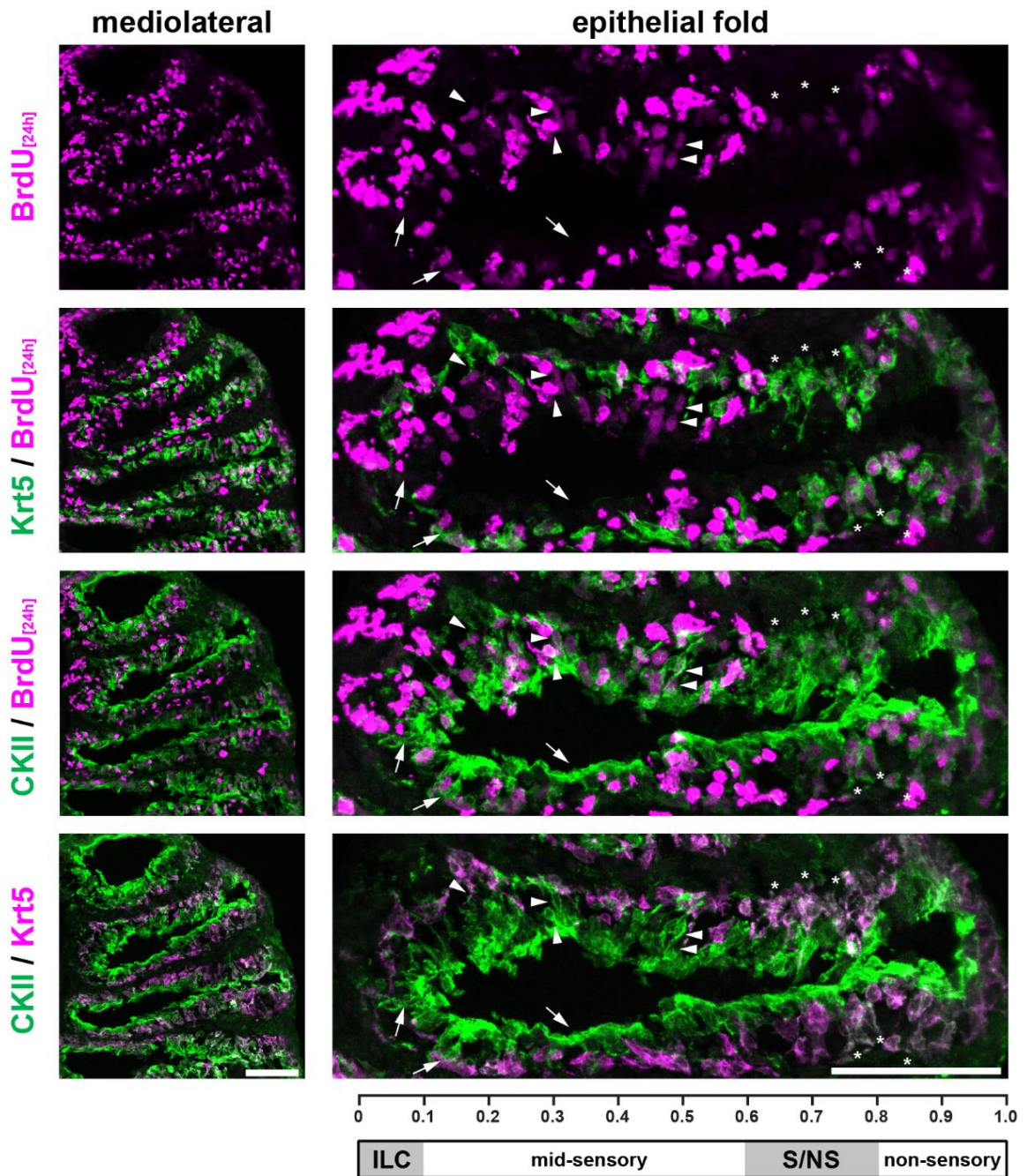


Figure 4.20. Sustentacular cells regenerate following a chemical lesion. Arrowheads: newborn SCs ( $CKII^+/BrdU^+$ ); arrows: SCs that survived chemical damage ( $CKII^+/BrdU^-$ ); asterisks: Krt5 and CKII double labeled cells at SNS. Bars: 50  $\mu m$ .

### 4.2.3. HBCs Show Continuous Proliferative Activity with Varied Frequencies Along Radial Positions

Adult-born OSNs are generated by spatially restricted GBCs at the ILC and SNS in the intact OE. The newborn cells show radial displacement towards the mid-sensory region and are eliminated in the middle of mid-sensory region by an unknown mechanism (Bayramlı *et al.*, 2017). Since HBCs occupy the basal stratum in all radial positions, including the middle of the sensory region but appear to divide more frequently at the ILC and SNS in the intact tissue (Figure 4.15, Figure 4.17, Figure 4.19), it was curious to determine if HBCs also shift from marginal proliferation zones towards more central positions.

To understand whether adult-born HBCs follow a similar flow as adult-born OSNs, fish were subjected to 24 or 168 h of continuous exposure to BrdU and were analyzed by immunohistochemistry against Krt5-expression and BrdU labelling in the sensory region (Figure 4.21). BrdU/Krt5 co-labeled cells (arrowheads in part A of the related figure) were analyzed for their position and compared to all Krt5-labeled cells. Around 40 HBCs occupy the sensory region between radial positions 0.05 and 0.65 ( $HBC_{24h} = 40.6 \pm 0.8$ ;  $HBC_{168h} = 42 \pm 0.9$ ; data collected from 90 epithelial folds: 30 epithelial folds/fish, 3 fish/condition). The average number of all Krt5-expressing HBCs and BrdU/Krt5 double-positive proliferating HBCs is shown in graphs according to their radial distribution along the epithelial folds for each condition in Figure 4.21b.

Out of ~40 Krt5-positive cells only  $5.94 \pm 0.16$  (mean  $\pm$  SEM) were Krt5/BrdU double-positive in the whole sensory region (0.05-0.65) after 24 h (Figure 4.21, left). Most of these cells were observed in the ILC (0.05 position) and SNS (0.65-0.75) as expected ( $ILC_{(Krt5/BrdU)/Krt5} : 1.24 \pm 0.16 / 7.39 \pm 0.21$ , mean  $\pm$  SEM;  $SNS_{(Krt5/BrdU)/Krt5} : 1.24 \pm 0.16 / 8.46 \pm 0.65$ ) and average number of Krt5/BrdU double-positive cells in each mid sensory positions (0.15-0.55) was  $0.54 \pm 0.12$  out of  $4.89 \pm 0.23$  Krt5-positive cells. After continuous 168 h BrdU pulse (Figure 4.21, right), 76.4 % of all Krt5-positive cells were also BrdU in the ILC and SNS, and on average 53.1 % of cells were Krt5/BrdU double-positive for each position in the sensory region.

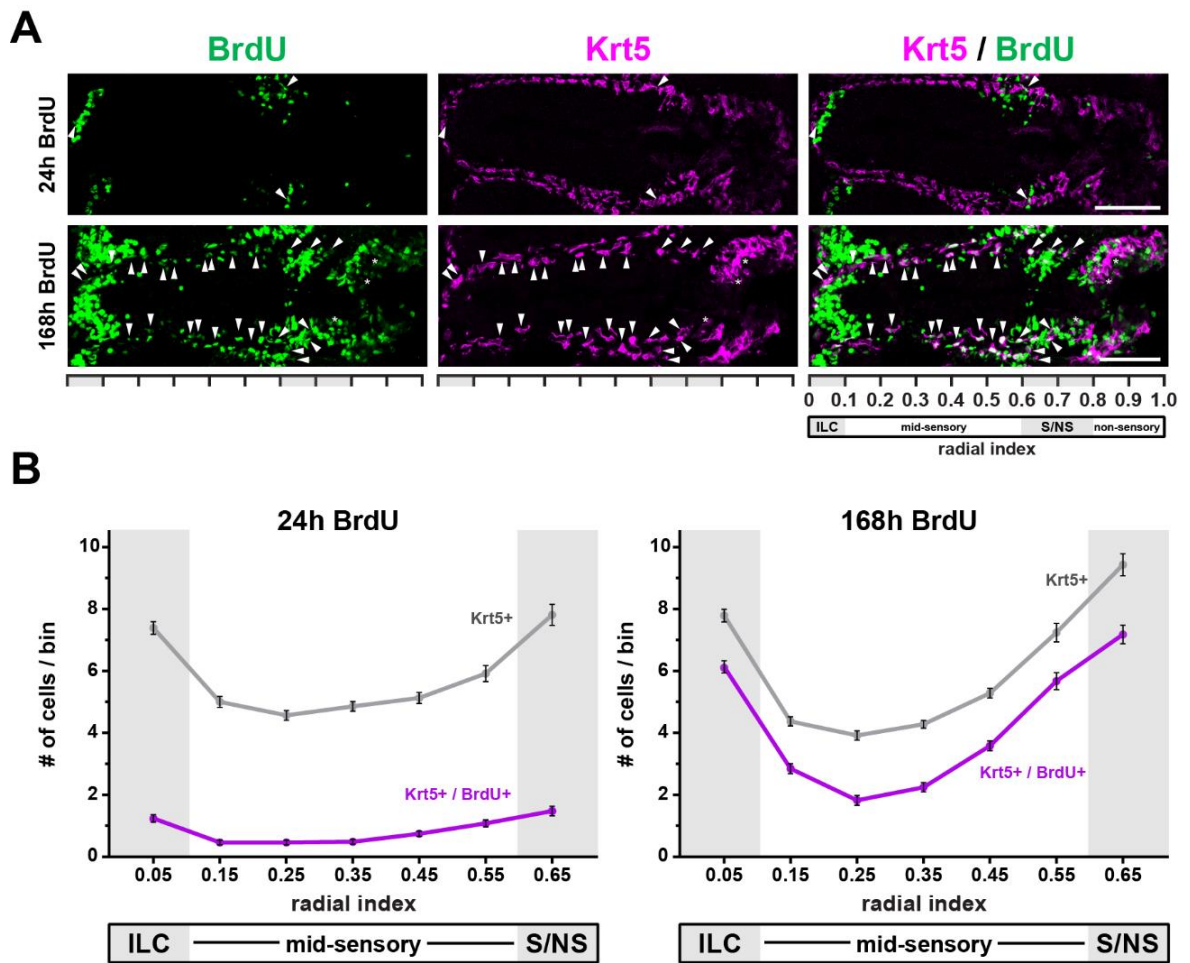


Figure 4.0.21. Radial distribution of Krt5/BrdU cells after a 24 and 168 h BrdU pulse. A. Confocal images. Scale bars: 50  $\mu$ m. B. Positional profiling of Krt5 and Krt5/BrdU cells after continuous BrdU labeling in intact tissue.

The number of BrdU/Krt5 double-labeled cells increased for every radial position between 24 and 168 h, suggesting an unusually rapid turnover or expansion of HBCs. Proliferating HBCs could be observed in the core of the mid-sensory region but were more numerous at the ILC and SNS.

To understand if HBCs indeed originated from neurogenic zones at the ILC and SNS (gray areas in graphs) and displace towards mid sensory region or proliferate at their site of detection, immunostaining was performed on tissue following 168 h BrdU pulse using 25  $\mu\text{m}$  vertical sections instead of the standard 12  $\mu\text{m}$  horizontal sections along the dorsal-ventral axis (Figure 4.22a). Gray dashed lines indicate the end of the ILC towards the mid-sensory region and the middle of the SNS. The dorsal to ventral axis is indicated by an arrow. The HBC layer in mid-sensory regions is shown in the right column in Figure 4.22a. A large number of Krt5/BrdU double-positive cells can be identified in the mid sensory OE (arrowheads). This confirms that HBCs divide in any radial position as BrdU/Krt5 co-labeled cells were not mutually exclusive at the ILC and SNS. Isolated BrdU/Krt5 co-labeled cells surrounded by only Krt5-labeled cells could be observed in the core of the mid-sensory region, suggestive of local mitotic activity.

Since HBCs appear not to undergo displacement but instead to proliferate in their respective positions, the time between HBC divisions could be predicted by the changes in the number of double-positive cells between 24h to 168h. Active HBC ratios were calculated for 24 and 168 h BrdU incubation periods by dividing the number of BrdU/Krt5 co-labeled cells to all Krt5-labeled cells for each radial position (Figure 4.22b). Active HBCs increased from around 20% to up to 80% at the neurogenic zones and from around 10% to at least 43% in mid-sensory region (24h<sub>0.05</sub>:  $18.1 \pm 0.02\%$ , mean  $\pm$  SEM; 24h<sub>0.15</sub>:  $10.2 \pm 0.02\%$ ; 24h<sub>0.25</sub>:  $11.8 \pm 0.02\%$ ; 24h<sub>0.35</sub>:  $10.9 \pm 0.02\%$ , 24h<sub>0.45</sub>:  $16.5 \pm 0.02\%$ ; 24h<sub>0.55</sub>:  $20.9 \pm 0.02\%$ ; 24h<sub>0.65</sub>:  $22.4 \pm 0.02\%$ ; 168h<sub>0.05</sub>:  $79.1 \pm 0.02\%$ ; 168h<sub>0.15</sub>:  $64.4 \pm 0.03\%$ ; 168h<sub>0.25</sub>:  $43 \pm 0.03\%$ ; 168h<sub>0.35</sub>:  $51.9 \pm 0.03\%$ , 168h<sub>0.45</sub>:  $68.2 \pm 0.02\%$ ; 168h<sub>0.55</sub>:  $78.9 \pm 0.02\%$ ; 168h<sub>0.65</sub>:  $76.7 \pm 0.01\%$ ). A linear regression model was used to calculate the time required for each position to have all HBCs divided at least once. The model predicted  $8.68 \pm 0.59$  days for ILC  $8.75 \pm 1$  days for SNS and up to  $15.71 \pm 0.89$  in the mid-sensory region (0.05:  $8.68 \pm 0.59$ , mean  $\pm$  SEM; 0.15:  $10.9 \pm 0.1$ ; 0.25:  $15.71 \pm 0.89$ ; 0.35:  $13.29 \pm 0.47$ , 0.45:  $10.0 \pm 0.68$ ; 0.55:  $8.66 \pm 0.84$ ; 0.65:  $8.75 \pm 1.01$ ).

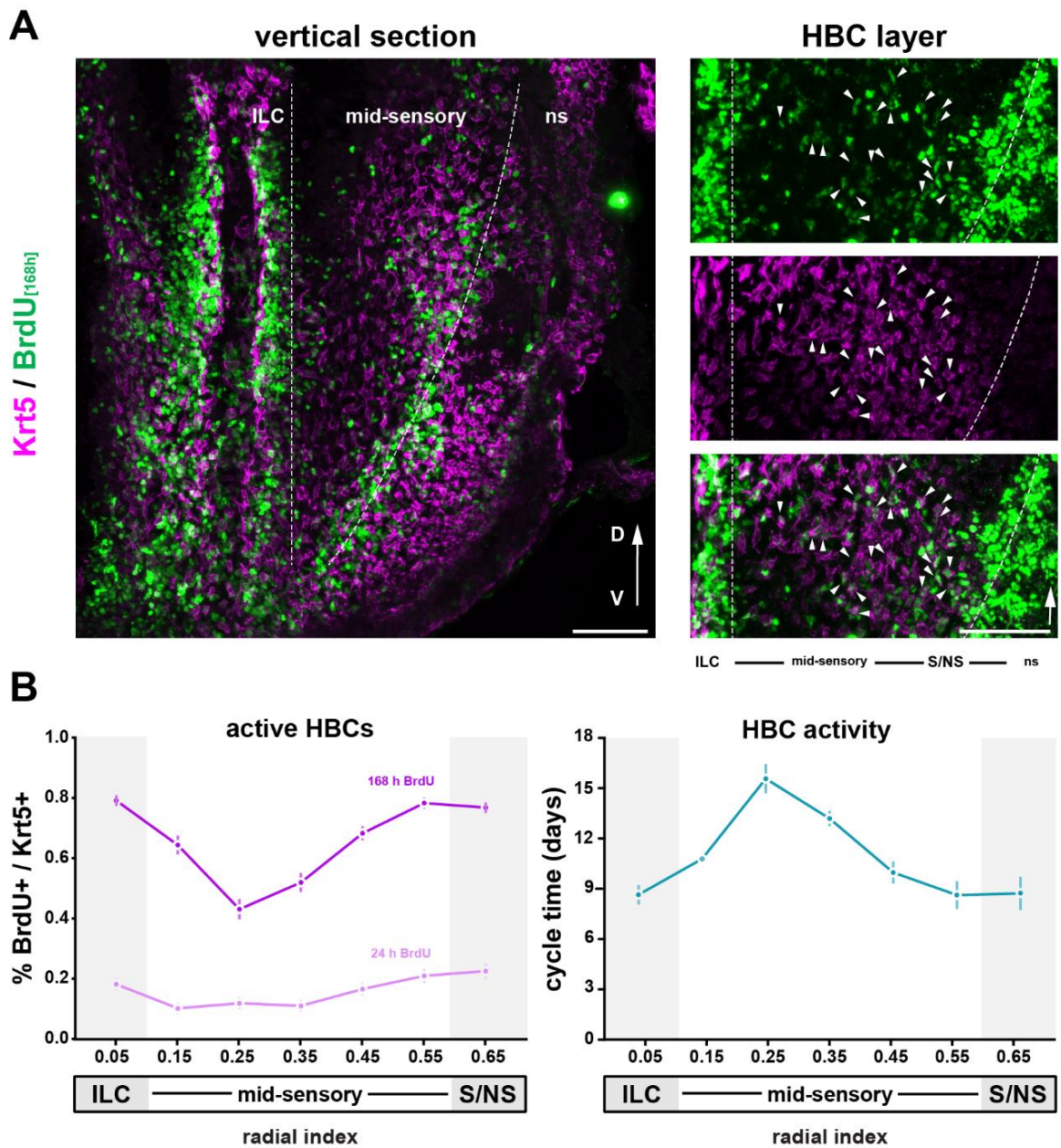


Figure 4.22. Quantification of active HBCs and prediction of HBC cell cycle time. A. Confocal images of vertical sections. Scale bar: 50  $\mu$ m B. Comparison of BrdU<sup>+</sup> HBCs at 24h and 168 h (left), linear regression model of HBC activity in radial positions (right).

Thus, HBCs divide in different radial positions in the zebrafish OE instead of following a flow towards the mid-sensory region like OSNs. However, the frequency of HBC proliferation at the ILC and SNS is higher than in mid-sensory regions, suggesting a different regulation of proliferation at these positions in the zebrafish OE.

#### 4.2.4. HBC Activity Cannot be Detected Three Months After Labeling

Analysis of mitotic activity in HBCs showed an unusually high HBC proliferation rate of 9 to 16 days in the zebrafish OE. The functional contribution of this activity to the available progenitor pool is unknown. Investigation of mitotically active HBCs in the long term could help to better understand the function of the frequent division of HBCs. To examine whether HBCs proliferate just once and return to quiescence or continuously divide in the mid-sensory region, a 168 h BrdU pulse was chased for three months and analyzed by immunostaining against BrdU in combination with analysis of Krt5 and HuC/D expressions to observe any radial displacement.

The number of BrdU co-labeled cells was quantified according to their distance to the tip of the ILC which was normalized to the total length of each epithelial fold (Figure 4.23). The graph in part A of the figure is aligned to images of epithelial folds in part B and the gray box in the graph indicates the middle of the SNS and extends through non-sensory region until the edge of the tissue. After three months, HuC/D-expressing OSNs were found mainly at the core of the mid-sensory region while numbers dropped sharply towards the ILC and SNS, as expected (Bayramli *et al.*, 2017; Kocagöz, under review). Cells labeled only with BrdU but not HuC/D or Krt5 were consistently found in low numbers throughout the sensory region (0.05-0.95). On the other hand, the average number of BrdU/Krt5 double-positive cells encountered in this experiment was only  $8.42 \pm 0.82$  per epithelial fold, most of which were found in the non-sensory region (12 epithelial folds: 2 epithelial fold/section, 3 section/fish, 2 fish). In contrast, the number of double-positive cells was low within the sensory OE and cells were distributed without any positional preference.

Thus, under physiological conditions, HBCs that divide during a 168 h interval are almost untraceable after three months in the sensory OE. In contrast displaced BrdU-labeled OSNs with strong BrdU intensity can be observed in mid-sensory regions. The loss of BrdU-labelled DNA in Krt5 cells could be explained by successive proliferation events undergone by these progenitor cells after BrdU supply is ended at 168h. This suggests that

HBCs could have a self-renewing mitotic activity to ensure steady availability of the progenitor pool.

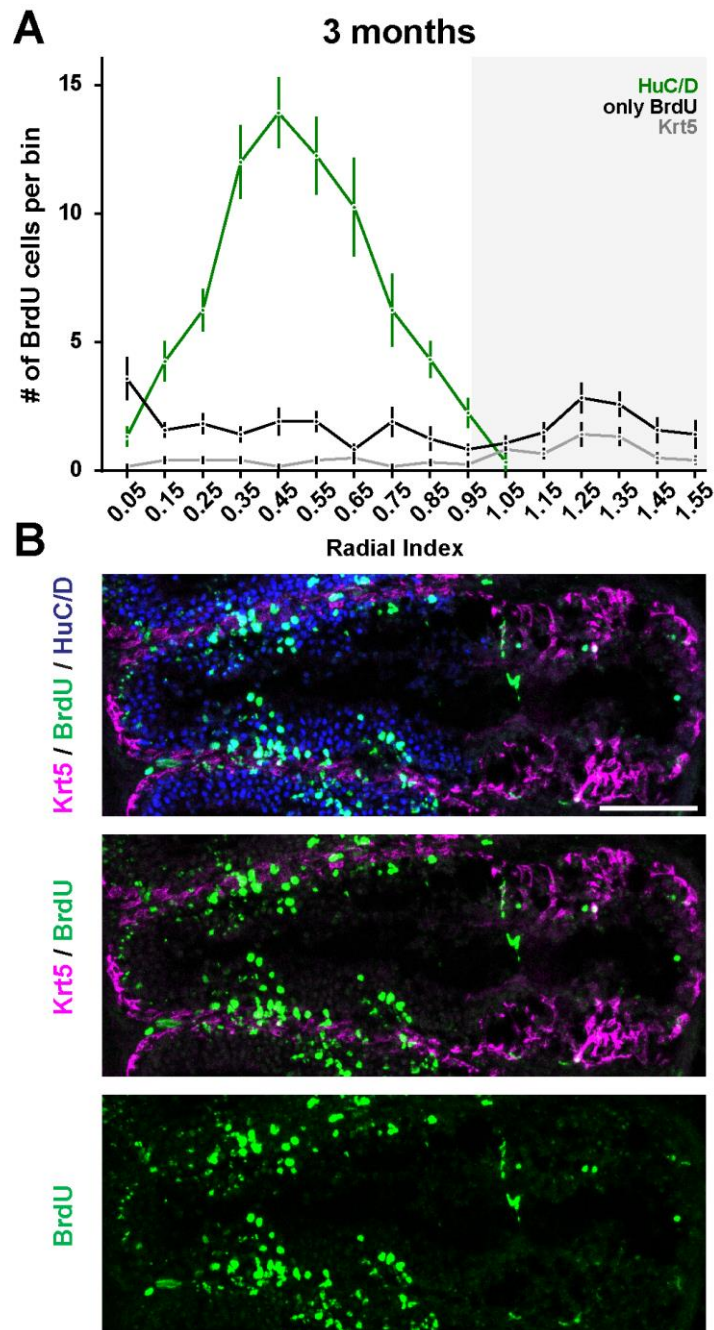


Figure 4.23. 168 h BrdU pulse chased for 3 months in the intact OE. A. Positional profiling of BrdU<sup>+</sup> OSNs (green), HBCs (gray) and SCs or GBCs (black). B. Confocal images of epithelial folds. (2 folds /section, 3section/fish, 2 fish). Scale bar: 50  $\mu$ m.

On the other hand, this unusually high activity also suggests that HBC numbers increase constantly under physiological conditions. A previous study from our lab showed that there is a cell death mechanism at the central positions of the mid sensory region, and it is possible that displaced OSNs are recycled in these positions (Bayramlı *et al.*, 2017). Constantly generated cells could also be recycled in these locations as well. Another possibility is that, in the embryonic rodent OE, HBCs can divide and contribute to the growth of the developing tissue. However, fate of the HBCs are yet to be discovered in the zebrafish OE.

#### **4.2.5. BrdU-labelling Could Indicate Relative Proliferative Activity of Non-neuronal Cells**

Tissue subjected to a continuous 168 h BrdU pulse and chased for three months also displayed interesting features of the fluorescence intensity of BrdU-labeled cells. The BrdU-label shows specific affinity to specific regions inside some cell nuclei when counterstained with DAPI, forming single or multiple specks other than homogeneous labelling that fills the whole nucleus as observed in in mid-sensory regions (Figure 4.24). Interestingly, at the ILC only speckled BrdU labeling could be observed, which could be remnants of the BrdU label inherited from labeled chromosomes during successive cell divisions.

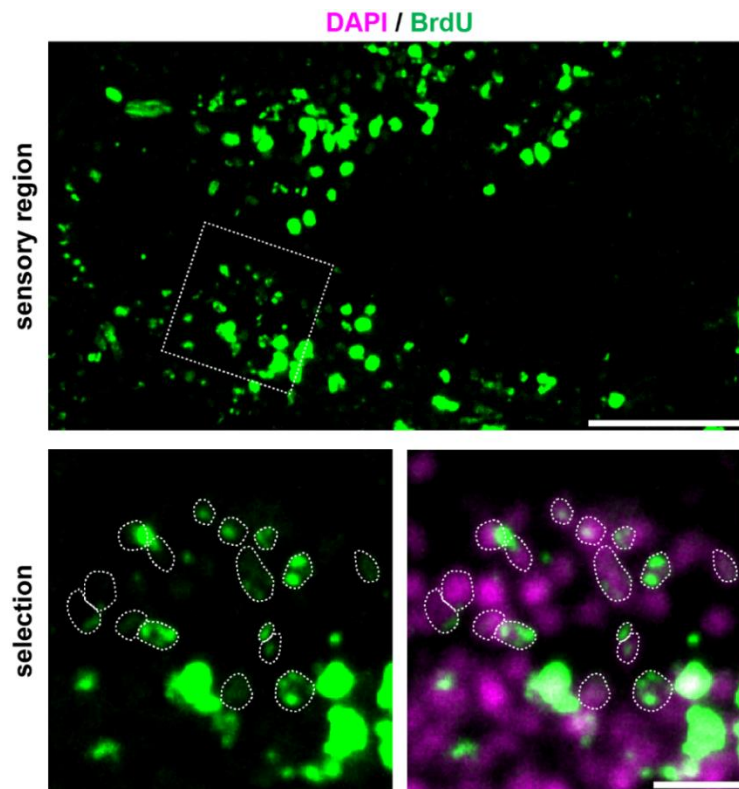


Figure 4.24. BrdU-labeling shows variability after 3 months of BrdU staining (green). Full nuclear, partial, and speck-like labeling can be observed on DAPI stained nuclei (magenta). Scale bars: 50  $\mu\text{m}$ .

Quantification of BrdU intensity in each BrdU-positive cell nucleus might, thus, allow for the identification of different generations of adult-born cells. Mean pixel intensity values for all cells in each radial position are shown as bar graphs superimposed on the number of cells counted for each radial position (Figure 4.25). While cells positive for BrdU-only showed an even number of cells and label intensity for the BrdU-label ( $n=338$ ), Krt5-positive cells ( $n=101$ ) exhibited lower intensity values and a smaller number of them retained BrdU in their DNA after three months (Figure 4.25a). Given that up to 80% of HBCs can be labeled with BrdU after a 168 h pulse, this might suggest that the timescale of this experiment exceeded the number of divisions that would leave detectable amounts of BrdU in each cell for analysis by immunohistochemistry. On the other hand, as mature OSNs do not divide, a high but gradual decrease in normalized BrdU intensity can be observed towards the ILC and SNS in HuC/D/BrdU double-positive cells (Figure 4.25b; left,  $n=881$ ).

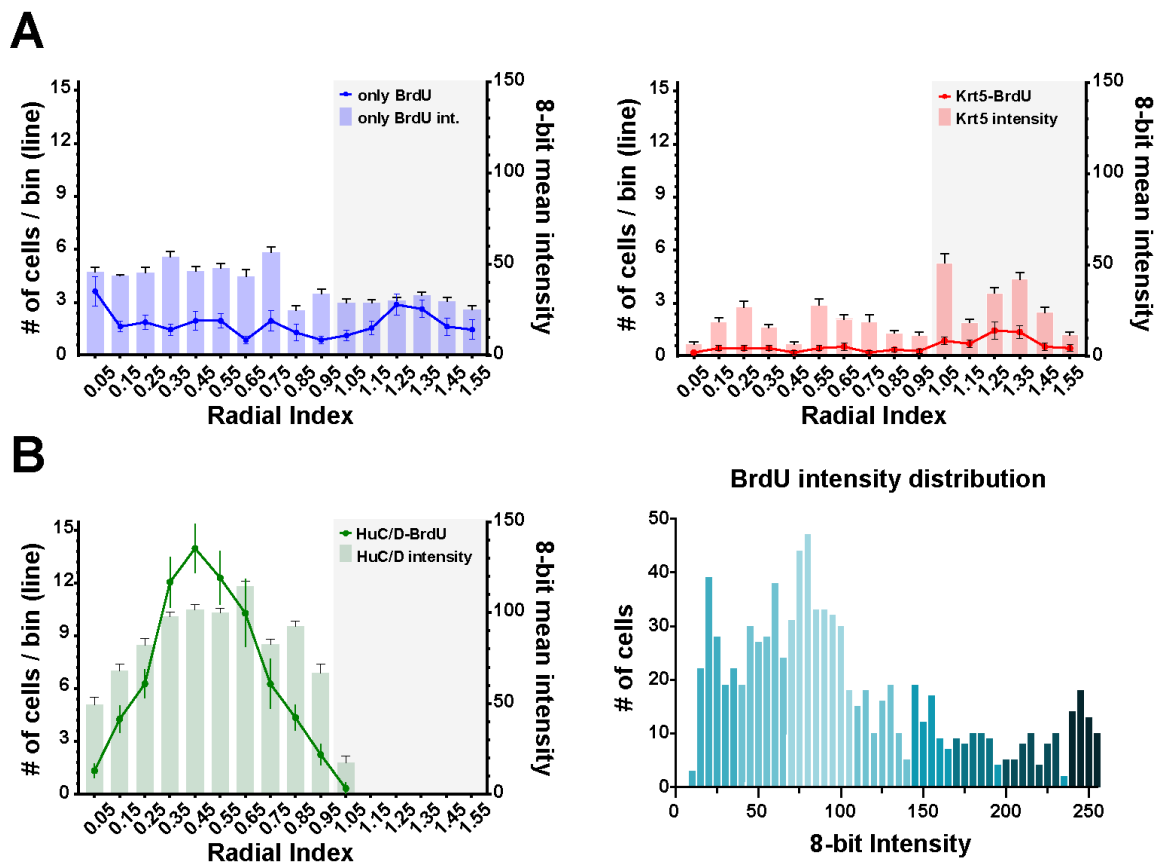


Figure 4.25. BrdU-label intensities of BrdU+ only and double-labeled cells after 3 months. Positional quantification of BrdU signal intensity (bar) and cell numbers (line) for HBCs (Krt5<sup>+</sup>), OSNs (HuC/D<sup>+</sup>) in A and B. Histogram in B shows the BrdU intensity of OSNs.

The frequency distribution of BrdU intensities from each HuC/D/BrdU double-positive cells is further categorized in a histogram that is shown on the right side in Figure 4.25b. Each bin in the histogram represents 5 points in 8-bit intensity values (0-255). Curiously, groups of cells with similar BrdU intensities were observed to form discernable modes around 20, 55, 80, 125, 150, 180, 215 and 245 mean pixel intensity values. These possible groups are indicated with successively darker colors, starting from the largest group around 80 intensity value in the graph. Number of cells in groups that show high BrdU label intensity were smaller in numbers, whereas groups with lower individual intensity values were more populated.

The analysis of adult born OSNs after three months suggests that differences in labeling intensity could signify generations of cell divisions before OSNs are formed. Highest BrdU intensity was observed in the center of the mid sensory region (Figure 4.25b, left) but high BrdU-retaining cells were lower in numbers (Figure 4.25b, right). Lower number of high BrdU retaining OSNs could be explained by older generations of neurons that reached their lifespan in the center of the mid sensory region and started to get recycled by unknown mechanisms (Bayramlı *et al.*, 2017).

Towards the ILC and SNS, different generations of OSNs show gradually lower mean BrdU intensity due to multiple rounds of cell divisions and successive depletion of BrdU-labeling in the progenitor cell DNA. This shows that successive generations can be identified by their BrdU intensity, depending on the timescale of the experiment.

However, the low number of detectable HBCs that retain reliable levels of the BrdU label does not allow to distinguish between HBC generations. This is consistent with the continuous and high proliferative activity of HBCs. On the other hand, cells labelled with BrdU-only may include GBCs or SC, as HBCs and OSNs constitute almost all populations apart from suprabasal Sox2 positive population in the sensory OE.

Spatial restriction of GBCs to the ILC and SNS suggests that BrdU-only positive cells in the mid-sensory region are mostly SCs, which shows a relatively uniform distribution of cell numbers and mean BrdU label intensity values. Retained higher BrdU label intensity compared to HBCs after three months suggests that SCs do not have an HBC-like proliferative activity in the sensory OE or have a different lineage origin in physiological conditions.

#### **4.2.6. SCs are BrdU-positive Mainly in Mid-sensory Regions After Three Months Following BrdU labeling**

To be able to confirm the presence of BrdU retaining SCs in the long term, CKII immunohistochemistry was performed on tissue after a continuous 168 h BrdU pulse and a three months chase for SC activity. SCs were identified by labeling against CKII expression and Sox2-expression to enhance the validity of BrdU co-labelling (Figure 4.26). BrdU/CKII/Sox2 co-labeled cells were observed mainly in the mid-sensory region at low numbers as expected. Radial distribution of SCs showed close similarities to BrdU/HuC/D double-labeled cells. BrdU retaining cells showed a similar differential labeling in the ILC and SNS. Sox2/CKII double positive cells with gradually decreasing BrdU labelling could be observed towards the ILC and SNS but not with high confidence due to the filamentous nature of the CKII label.

Thus, after three months, SCs generated in the OE are mainly located at the core of the mid sensory region. These observations, although not quantified, suggest that SCs may also follow a similar displacement process as OSNs in the zebrafish OE under physiological conditions.

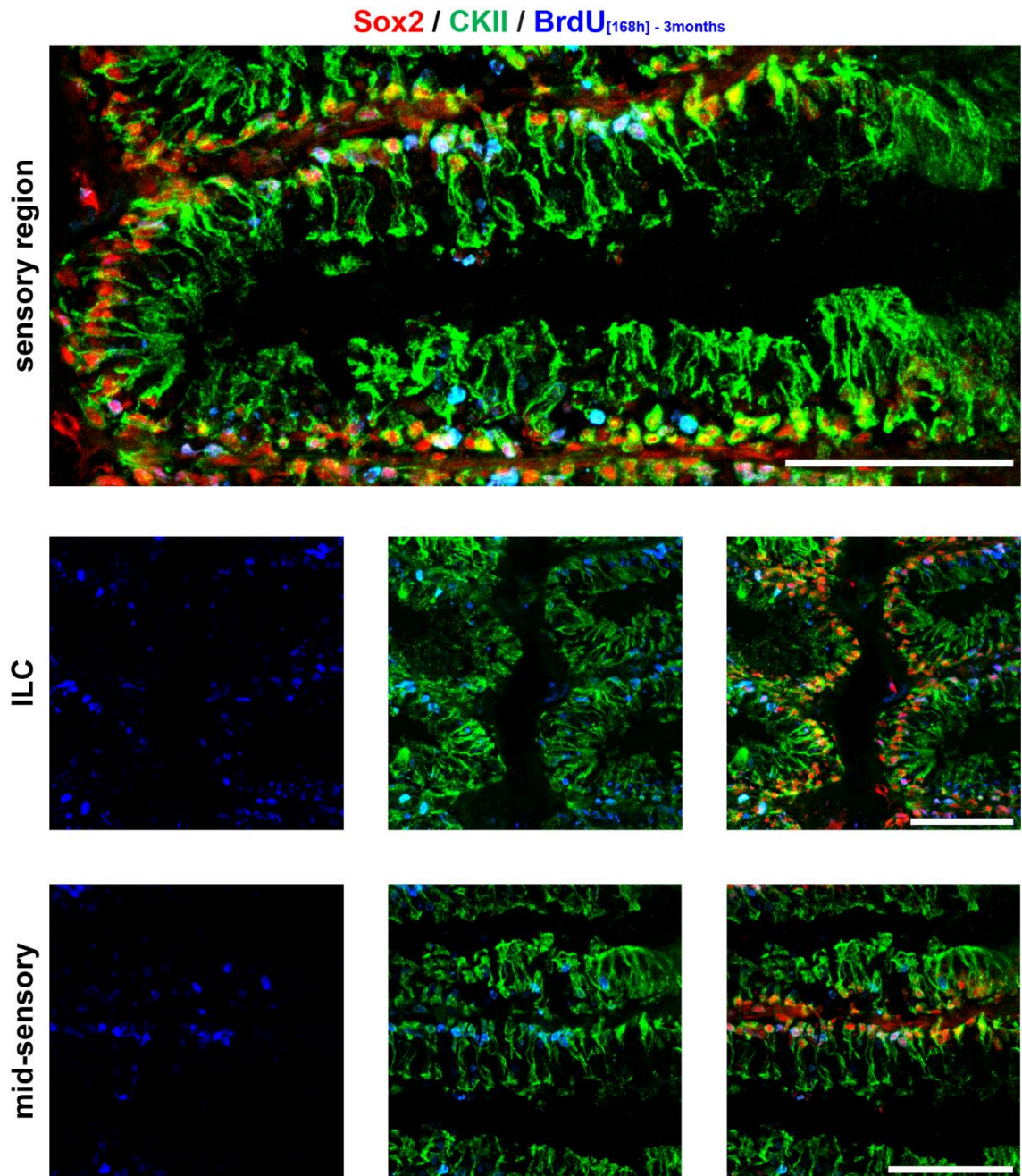


Figure 4.26. Sustentacular cell activity in tissue labeled with BrdU for 168 h after 3 months. Immunostaining on OE after 3 months against Sox2 and CKII (SCs). Mitotic SCs can be found in the sensory region but are scarce at the ILC and SNS. Scale bars: 50  $\mu$ m.

#### 4.2.7. HBCs are Almost Completely Renewed within Two Weeks with Rare Neurogenic Activity

HBCs are activated and rapidly expanding after chemical insult by 1% Triton X-100 as previously described (Iqbal and Byrd Jacobs 2010; Demirler *et al.*, 2020; Kocagöz, 2021), but do not respond to ATP stimulation with proliferative activity. HBCs also display an unusually high proliferative activity in mid-sensory regions under physiological conditions in the zebrafish OE. However, whether HBCs can directly contribute to neurogenesis in the zebrafish OE or only proliferate to preserve progenitor pool is elusive. To understand the contribution of HBC proliferation to OSN neurogenesis, the zebrafish OE was subjected to two-week continuous BrdU pulse during which almost all HBCs are expected to proliferate at least once by the linear regression model described in section 4.2.3. At the end of two-week period, the OEs were analyzed by immunohistochemistry against BrdU and the cell type specific markers Krt5 and HuC/D (Figure 4.27).

BrdU labeled cells were observed with highest density at the ILC and SNS border, since adult born OSNs are generated here and displace radially towards mid-sensory region. The bilateral displacement fronts of BrdU-positive cells that originated from the ILC and SNS are indicated by crosshairs on a representative epithelial fold in the Figure 4.27. As expected, Krt5-labeled HBCs in the sensory region frequently showed BrdU double-staining in their nuclei and only a fraction of Krt5-labeled cells was found to be negative for BrdU labeling (arrowheads).

Positional quantification of BrdU-positive cells was performed for the number of HuC/D/BrdU and Krt5/BrdU double-positive, and all BrDU- and Krt5-positive cells in each radial position. Profiles are shown in Figure 4.28a (45 EFs, 5 folds/section, 3 section/fish, 3 fish). HuC/D/BrdU double-positive and total number of BrdU-positive cells were quantified by thresholding either colocalized signals or all BrdU signals, respectively, and counted by a custom macro in FIJI environment. Colocalized signals were obtained by generating composites of grayscale images with inverted LUT, which isolates co-labeled pixels with low intensity values on the image. As expected, adult-born OSNs comprise the majority of all BrdU-labeled cells and displace towards mid-sensory (Figure 4.28a, left).

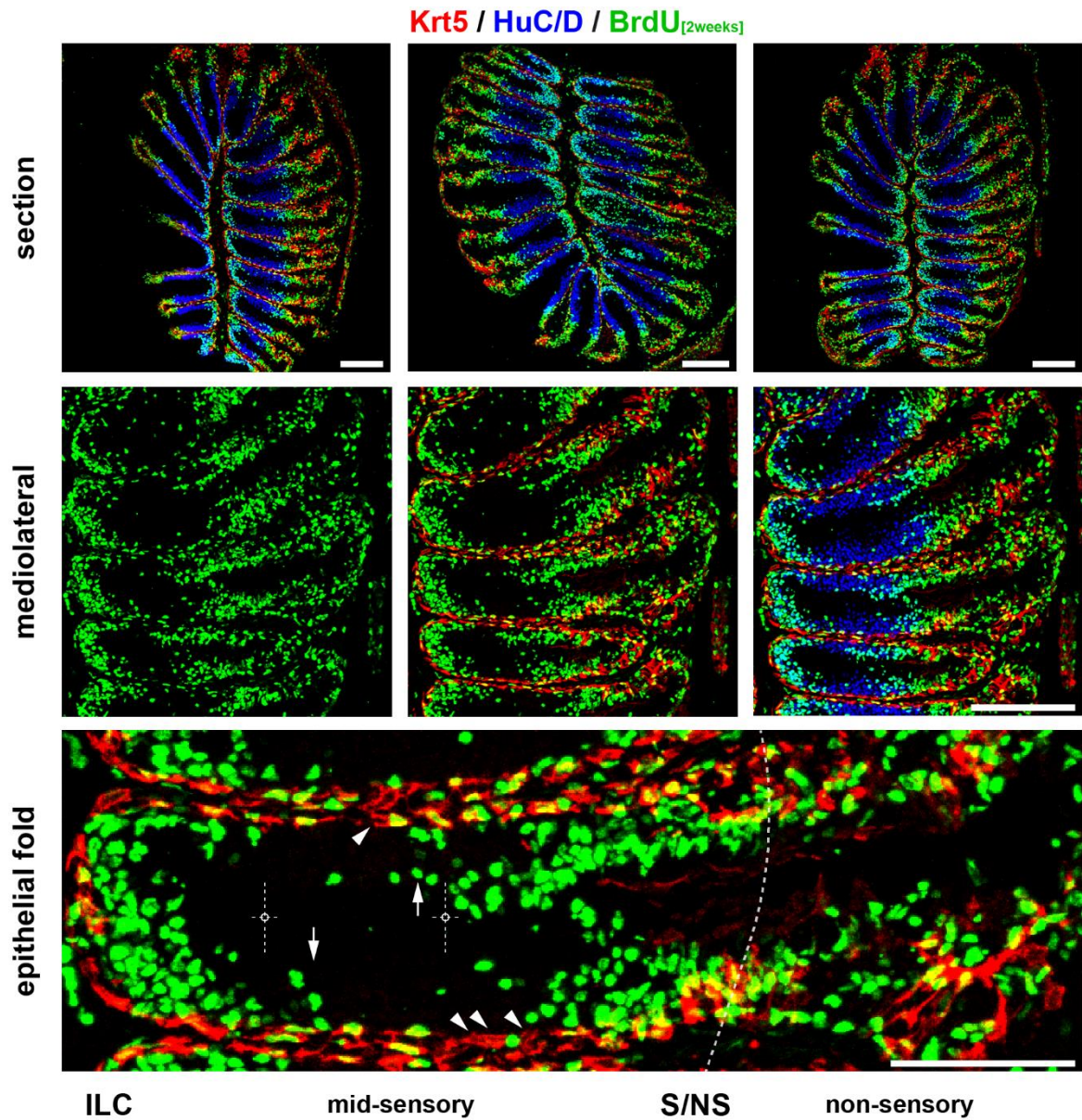


Figure 4.27. HBC activity in OEs labeled with BrdU (green) for two weeks counterstained with Krt5 (red) and HuC/D (blue). Almost all HBCs have divided. crosshairs: BrdU propagation fronts from the ILC and SNS; arrows: clonal cell clusters. Scale bars:50  $\mu$ m.

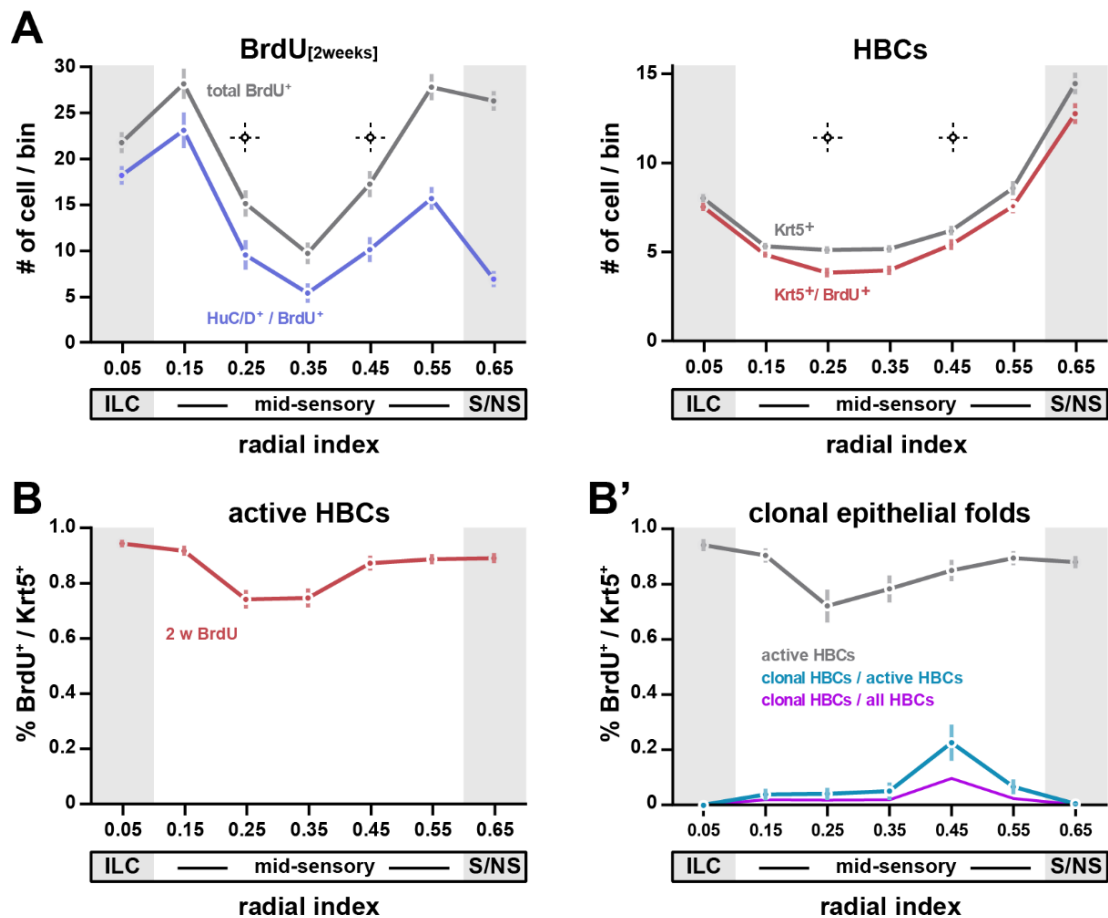


Figure 4.28. Positional quantification of BrdU+ cells continuously labeled for 2 weeks. A. All BrdU labeled cell counts and generated OSNs (blue) (left); all or BrdU+ HBCs (right). B. Proliferative activity of HBCs. B'. Clonal HBC activity normalized for each fold.

Krt5/BrdU double-positive cells, all Krt5-positive cells and BrdU fronts were marked manually, and positions of manual markings were counted in 10 equidistant bins in FIJI environment as previously described, and graphed separately (Figure 4.28a, right).

Quantified BrdU-positive cell displacement fronts were marked with crosshairs in the graph. Krt5/BrdU double-positive cells can be observed frequently in all positions of the sensory region (0.05-0.65) as expected (Figure 4.28b), ranging from  $73.8 \pm 0.03\%$  in the core regions of mid sensory up to  $93.9 \pm 0.01\%$  at the tip of the ILC (0.05:  $93.9 \pm 0.01\%$ , mean  $\pm$  SEM; 0.15:  $91.3 \pm 0.02\%$ ; 0.25:  $73.8 \pm 0.03\%$ ; 0.35:  $74.3 \pm 0.03\%$ ; 0.45:  $86.8 \pm 0.03\%$ ; 0.55:  $0.88 \pm 0.02\%$ ; 0.65:  $0.88 \pm 0.2\%$ ).

Almost all Krt5 cells in each radial position were also BrdU retaining cells after two weeks. Compared to the ~80% in the ILC and SNS, and at least ~50% in the mid sensory activity observed in 168 h continuous BrdU pulse (Figure 4.22), continuous HBC activity shows almost complete turnover in 2 weeks as previously predicted.

Intriguingly, distinct from the primary neurogenic waves displacing towards the mid-sensory region, clusters of BrdU-labeled cells proximal to each other but positioned within the core sensory OE and at a distance from the displacement fronts could also be observed (arrows in Figure 4.27). These BrdU-positive cell clusters are oriented along the vertical axis and suggest a clonal origin based on their resemblance of basal cell originated OSN lineages in the rodent OE (Guo *et al.*, 2010). More critically, these clonal cell clusters contain Krt5/BrdU co-labeled cells in basal epithelial strata and HuC/D/BrdU double-positive cells in apical positions. This suggests that HBC activity can result in asymmetric cell divisions and eventually contribute to OSN neurogenesis under physiological conditions. Studying the prevalence of this activity could help to understand whether HBCs have a direct contribution to neurogenesis in the intact tissue.

Only 18 epithelial folds displayed clonal clusters (called as “clonal epithelial folds”) out of previously analyzed 45 in the sensory OE. The ratio of all Krt5/BrdU double-positive cells among all Krt5-positive cells in clonal epithelial folds, had a similar positional distribution (grey line in Figure 28b’) (0.05:  $93.98 \pm 0.01\%$ , mean  $\pm$  SEM; 0.15:  $91.32 \pm 0.02\%$ ; 0.25:  $73.77 \pm 0.03\%$ ; 0.35:  $74.31 \pm 0.03\%$ ; 0.45:  $86.81 \pm 0.03\%$ ; 0.55:  $88.28 \pm 0.02\%$ ; 0.65:  $88.28 \pm 0.2\%$ ) compared to the active HBCs calculated from the total set of 45 epithelial folds (Figure 28b).

Prevalence of clone-associated Krt5/BrdU cells were calculated out of all Krt5/BrdU double positive active cells in the clonal epithelial folds and presented as the cyan colored line, in Figure 4.28b’. Positional quantification of Krt5/BrdU double-positive cell prevalence showed a biased high clonality towards the positions with higher rate of Krt5/BrdU co-labeling observed in mid-sensory regions.

Highest clonal Krt5/BrdU double positive cell frequency (0.45 position) was  $22.6 \pm 0.7\%$  among clonal epithelial folds, which only accounts for 9.67% of all Krt5-expressing cells at the same radial position (magenta line in Figure 4.28b') (Frequency of clonal Krt5/BrdU positive cells in 18 clonal epithelial folds, cyan line; 0.05:  $0 \pm 0\%$ , mean  $\pm$  SEM; 0.15:  $3.75 \pm 0.02\%$ ; 0.25:  $4.01 \pm 0.02\%$ ; 0.35:  $5.05 \pm 0.03\%$ ; 0.45:  $22.61 \pm 0.06\%$ ; 0.55:  $6.55 \pm 0.55\%$ ; 0.65:  $0 \pm 0\%$ )(Frequency of clonal Krt5/BrdU positive cells in all 45 folds, magenta line: 0.05: 0% 0.15: 1.8%; 0.25: 1.7%; 0.35: 1.9%; 0.45: 9.6%; 0.55: 2.3%; 0.65: 0%). This result shows that only a small fraction of active HBCs gave rise to clones. Additionally, out of 1368 total Krt5-expressing cells counted in mid-sensory region, total number of clonal Krt5/BrdU cells were only 50, which means that asymmetric division of Krt5-expressing cells has only a 3.7% incidence.

The results show that after two weeks, almost all HBCs are renewed in the sensory region by symmetric divisions to sustain a steady progenitor pool in the zebrafish OE. Rarely, with a 3.7% incidence, HBCs can also divide asymmetrically and form cells of the OSN lineage and contribute to neurogenesis. This discovery is interesting because without the need of engraftment or cell culture experiments, OSNs with HBC lineage origin could be observed under physiological conditions in the zebrafish OE largely due to the spatial restriction of the progenitor pools.

#### **4.2.8. SCs Originate from ILC and SNS in the Intact OE and Displace with OSNs**

Apart from basal GBC and HBC progenitors and duct cells that have the ability to give rise to SCs, it has also been shown that SCs have the ability to self-originate in the rodent OE (Schwob *et al.*, 2016). In the studies presented in this thesis, newborn SCs were observed predominantly at the ILC and SNS after a 24 h BrdU pulse (Figure 4.15a). Lineage tracing with BrdU after three months suggest that SCs also follow displacement towards mid-sensory positions. However, the SC lineage origin or their lineage relationship to HBCs remains elusive in zebrafish. As almost all HBCs were observed to divide at least once in the mid-sensory region around two weeks, we can use a similar approach to understand whether SCs have a lineage relation to HBCs by searching for newborn SCs in the mid-sensory region after two weeks.

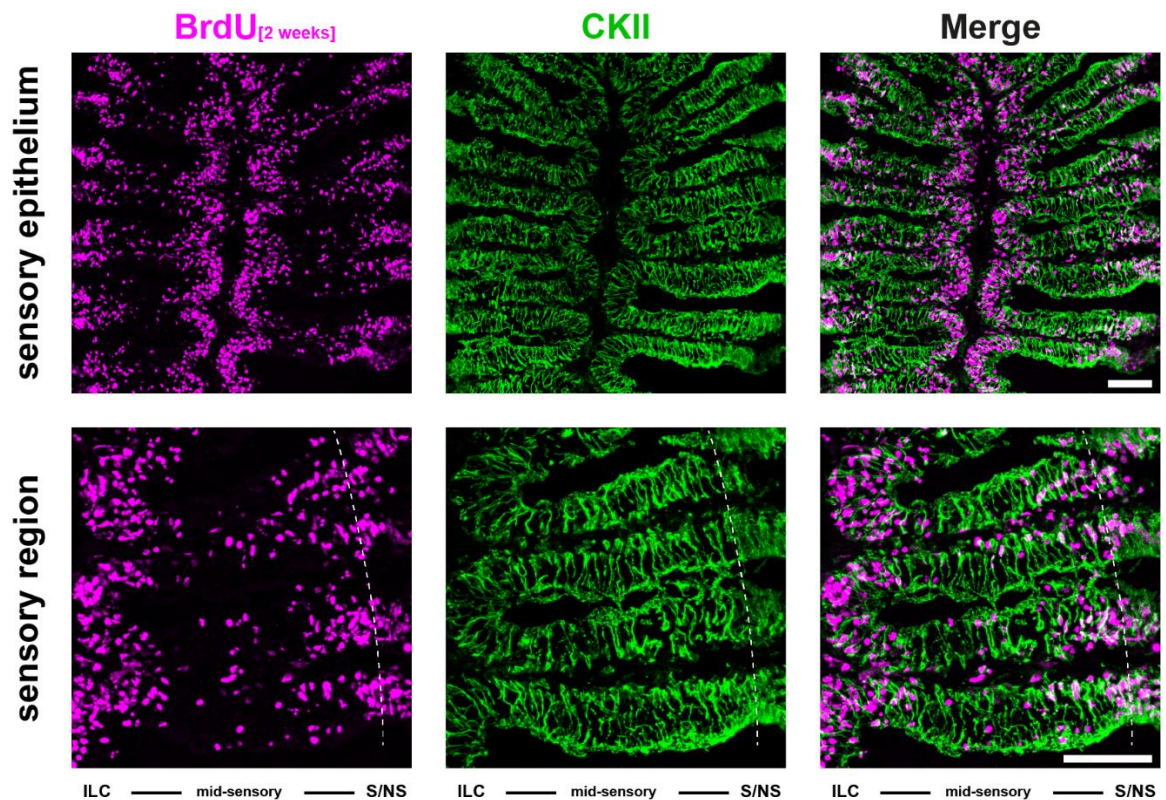


Figure 4.29. SC activity on 2-week continuously BrdU labeled OE. IHC against BrdU (magenta) and CKII (green) showing sustentacular cells (BrdU<sup>+</sup>/CKII<sup>+</sup>) are also originate from ILC and SNS. Bars: 50  $\mu$ m

Using a similar approach, immunohistochemistry against BrdU and CKII-expression for SC identification was performed on OEs subjected to two-week continuous BrdU incubation to observe the SC dynamics in the intact tissue (Figure 4.29). Initial observations on confocal images provided no evidence of newly generated CKII/BrdU double-positive cells in the mid-sensory regions after two weeks but showed BrdU/CKII co-labeled cells at ILC and SNS (Figure 4.29).

Positional quantification of CKII/BrdU double-positive cells (line) and the frequency of centripetal displacement fronts of BrdU-positive cells are shown in Figure 4.30 (27 epithelial folds; 3 epithelial folds/section, 3 section/fish, 3 fish).

Positions were quantified from the tip of ILC until the beginning of non-sensory region indicated by previously described bulge in basal lamina to have a better resolution of sensory region (0.05-0.65 in previous quantifications, 0.05-0.85 in this quantification). Frequency for each radial position was calculated by taking the ratio of total number of counted points in each bin to the total number of points.

CKII/BrdU-labeled adult born SCs were seen with gradually decreasing numbers from ILC and SNS towards the core of the mid-sensory region (Figure 4.30b). Interestingly, CKII/BrdU co-labeled cells observed to be furthest away from ILC or SNS either found in the same radial position with BrdU front in the same epithelial folds or formed the BrdU front on the either side of displacement. Quantified positions of BrdU front frequency from ILC (0.25: 27.6%, 0.35: 16.7%, 0.45: 3.7%) or SNS (0.55: 2.7%, 0.65: 34.1%, 0.75: 11.4%) also coincided with the CKII/BrdU co-labeled cells towards the core of mid-sensory region in the graph (0.05:  $3.64 \pm 0.37$ , mean  $\pm$  SEM; 0.15:  $2.92 \pm 0.52$ ; 0.25:  $1.24 \pm 0.89$ ; 0.35:  $0.18 \pm 0.07$ , 0.45:  $0.20 \pm 0.85$ ; 0.55:  $0.16 \pm 0.08$ ; 0.65:  $1.39 \pm 0.31$ ; 0.75:  $5.35 \pm 0.46$ ; 0.85:  $9.01 \pm 0.42$ ; 0.95:  $2.98 \pm 0.59$ ).

Clone-like BrdU-positive cell clusters were also observed in this analysis and quantified positionally for the HBC-like BrdU-labeled cells (Figure 4.30b, right). However, due to lack of HuC/D labelling, clones were described as any group of cells in proximity to each other with apparent directionality towards intermediate epithelial strata, which are in between bilateral BrdU fronts and can be traced back to an HBC-like BrdU-labeled cell in the basal OE. 18 out of 27 epithelial folds showed clonal clusters, and frequency of clonal clusters was calculated against cluster presenting epithelial folds (magenta) and all epithelial folds (cyan). Interestingly, none of the clones displayed any CKII/BrdU co-labeled cells in the mid-sensory region. Additionally, highest clone frequency could be observed in similar position as Krt5/BrdU originated clones in Figure 4.28b', and clonal clustering was encountered as a rare event since frequency suggested minimum of only one clone, not necessarily neurogenic, in around every third epithelial fold after two weeks ( $\text{bin}_{0.45}$ :  $28.47 \pm 0.06$  %).

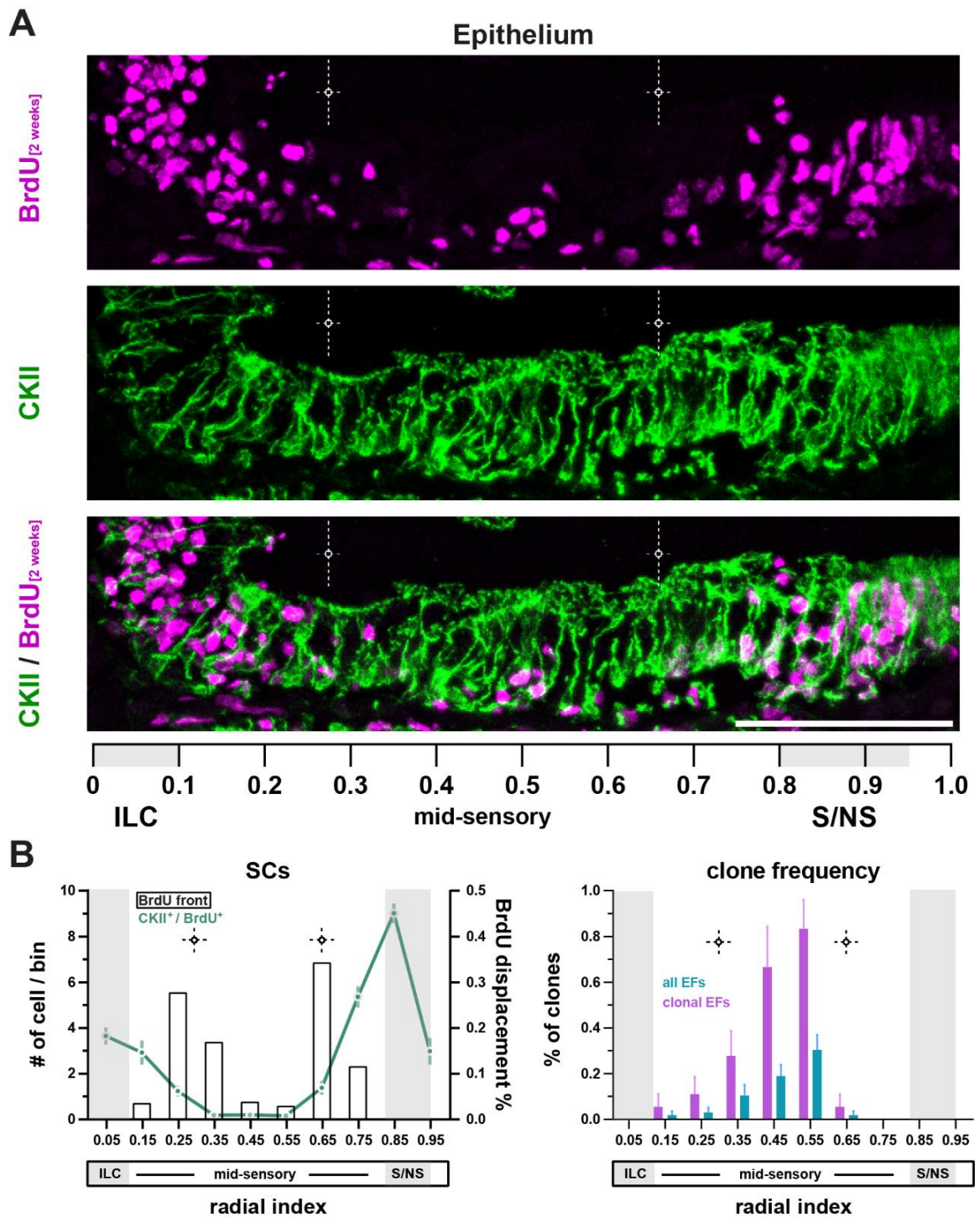


Figure 4.30. Sustentacular cells originate from the ILC and SNS. A. Confocal images; Crosshairs: bilateral BrdU fronts. Scale Bar: 50  $\mu$ m. B. Quantification of BrdU<sup>+</sup> SCs; and histogram of clones, normalized to epithelial folds.

As newly generated SCs were never observed in mid-sensory regions, the ILC and SNS were inspected in detail on higher power magnification of confocal images (Figure 4.31). CKII/BrdU co-labeled SCs (arrowheads) can be observed in any part of the ILC (Figure 4.31a). Interestingly, some CKII-labeled cells displayed multiple BrdU-labeled nuclei (arrows) separated by a thinly CKII-labeled structure which can be traced to a junction (asterisks) which led to a single protrusion that connects the cell to apical edge of the epithelium. Cell cluster outlined with a dashed line in Figure 4.31a indicates a possibly neurogenic clone without any newborn SC. This pattern can be observed in any section in the dorsal-ventral axis, suggesting a lineage origin of SCs with a different cell identity, rather than HBCs.

SCs display a gradual nuclear translocation, probably for successive generations as they show a mid-sensory directed displacement, from intermediate epithelial strata (arrows) to suprabasal stratum (arrowheads), where SCs are normally located in the mid sensory region (Figure 4.31b). CKII/BrdU co-labeled cells that have contact to basal and apical edges (asterisks) of the epithelium with BrdU-positive nuclei (arrows) were observed at intermediate strata in the non-sensory side of SNS. Then, nuclei of CKII/BrdU co-labeled cells with similar basal and apical contacts, as they approach to mid-sensory side of SNS, were seen to gradually occupy more basal layers in the intermediate epithelial strata, eventually translocate to suprabasal positions and connect with the cells in basal stratum.

Thus, SCs originate from the ILC and SNS but does not show self-originating mitotic activity under physiological conditions. SCs also show the characteristics of interkinetic nuclear translocation (Lust and Wittbrodt, 2017) in the SNS. Müller glia of the zebrafish retina can translocate its nucleus and proliferate upon lesion (Lust and Wittbrodt, 2017). Since SCs also displace towards the mid-sensory region, this translocation characteristic in the SNS might indicate a mitotic event taking place in the intermediate layers that could give rise to SCs. Newly generated SCs would then translocate to the basal layers gradually as the cell matures. This interpretation could suggest a separate lineage origin for the SCs in the SNS.

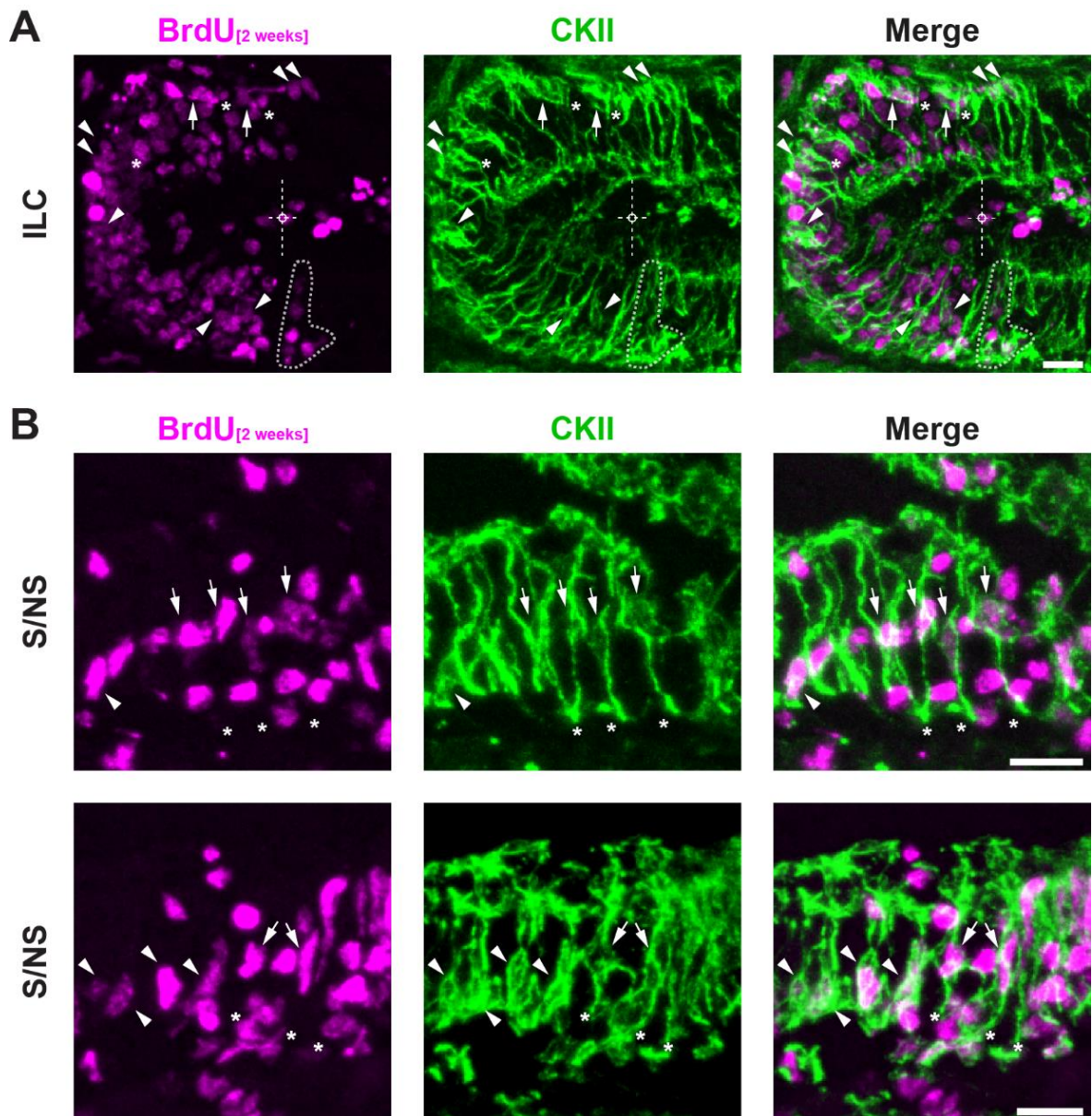


Figure 4.31. Sustentacular cells originate from ILC and SNS. IHC against CKII and BrdU on 2-week continuously BrdU labeled tissue, ILC (A) and SNS (B). In SNS, SCs originated from middle show nuclear displacement towards basal stratum. 10  $\mu$ m.

#### 4.2.9. Lineage Tracing with EdU and Two-week Continuously BrdU Labeled Intact Tissue

As shown in part 4.2.7, at least  $73.77 \pm 0.03\%$  of HBCs in the mid-sensory region were positive for BrdU labelling after a two-week continuous BrdU pulse. To detect if HBCs divide asymmetrically in mid-sensory region and eventually form OSNs at these positions besides the symmetric divisions observed so far, 5-ethynyl-2'-deoxyuridine (EdU) was injected intraperitoneally to add a second lineage tracer at the end of the two-week continuous BrdU pulse. Immediately following the EdU injection, fish were transferred to freshwater and analyzed with immunohistochemistry after 24h, 48h and 72h. Antibody staining against BrdU and non-neuronal cell marker Sox2 was coupled with Click-iT™ EdU reaction to observe the products of successive HBC proliferations in the mid-sensory region (Figure 4.32). After the 24h chase, EdU expectedly showed the same pattern as a 24h BrdU pulse, labelling primarily cells at the ILC and SNS with some exceptions in mid-sensory region. Some BrdU/Sox2 double-positive basal cells were also observed to be EdU positive at the ILC and SNS, showing the second proliferation cycle experienced by HBCs with higher activity at these positions. Clonal cell clusters (arrowheads) were also observed in mid-sensory region after 24h chase, albeit at low frequency (Figure 4.32, bottom panel).

More informative clones could be observed following a 48h and 72h chase (Figure 4.33). After a 72h chase, Sox2-positive cells in the suprabasal layers were seen to be co-labeled with EdU and BrdU. Respective mean pixel intensity values of selections were indicated next to the cells in single channel images for BrdU (blue) and EdU (green) labelling in the figure. This cluster was related to the horizontal cell at the bottom of the images and BrdU intensities suggested successive proliferation events eventually followed by the division of Sox2/EdU/BrdU triple-labeled daughter cells in suprabasal layer. In the case of the 48 h chase (Figure 4.33a, bottom panel), Krt5/BrdU cells at the basal stratum were also co-labeled with EdU and showed similar EdU intensity, suggesting a single origin due to similar level of BrdU and EdU labels with the cell located in the intermediate layer. A consistent observation, on the other hand, is the proliferation of suprabasal Sox2-expressing cells for the case of EdU positive clusters. Additionally, clone related CKII-

labeled cells were never observed. An example of BrdU-negative SC (arrow) was shown surrounded by clonal cells in Figure 4.33b.

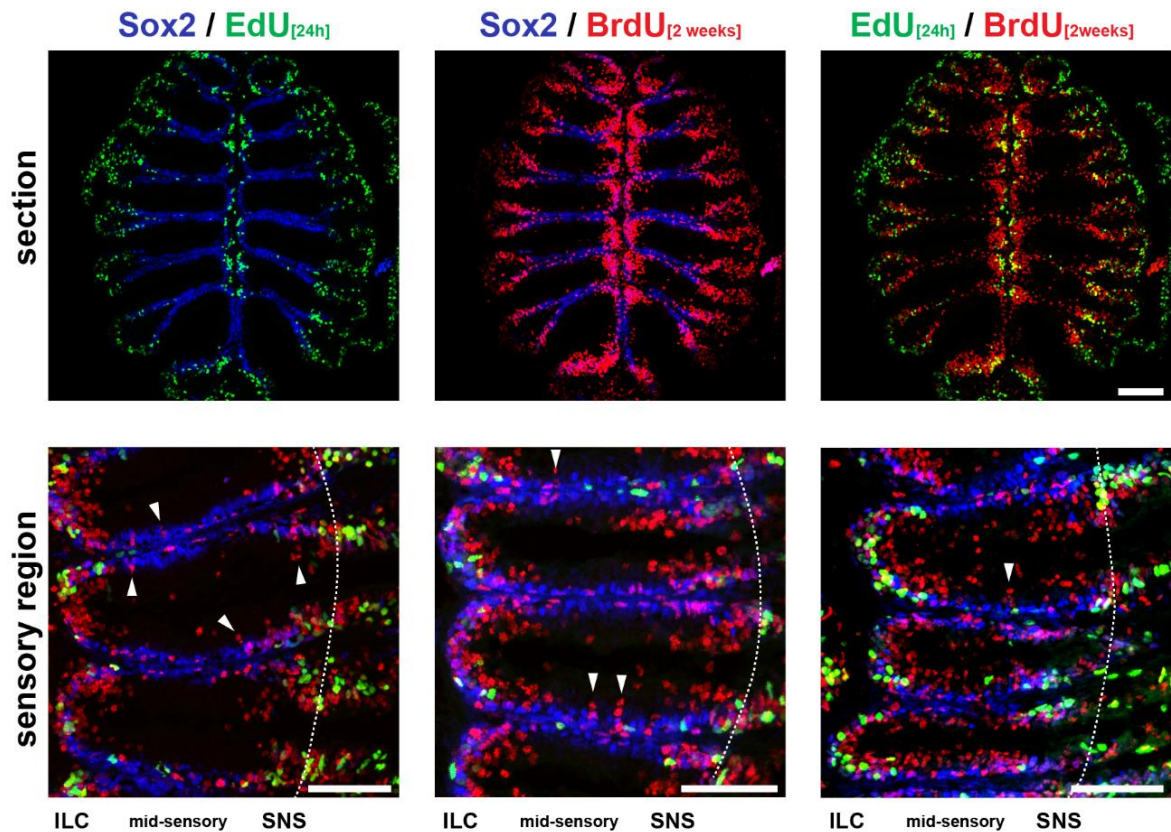


Figure 4.32. Single pulse EdU on 2-week continuously BrdU incorporated tissue after 24h.

A. Overview of sections stained against Sox2, EdU and BrdU. Scale bar: 100  $\mu$ m. B.

BrdU-positive Clonal cell clusters from sensory region (top). Scale bar: 10  $\mu$ m.

These results support that under physiological conditions, SC lineage is not originated from HBCs. In fact, product of asymmetric proliferation of HBCs are probably fast cycling progenitor GBCs which lead to sporadic clonal neurogenesis events by an independent proliferation of GBCs.

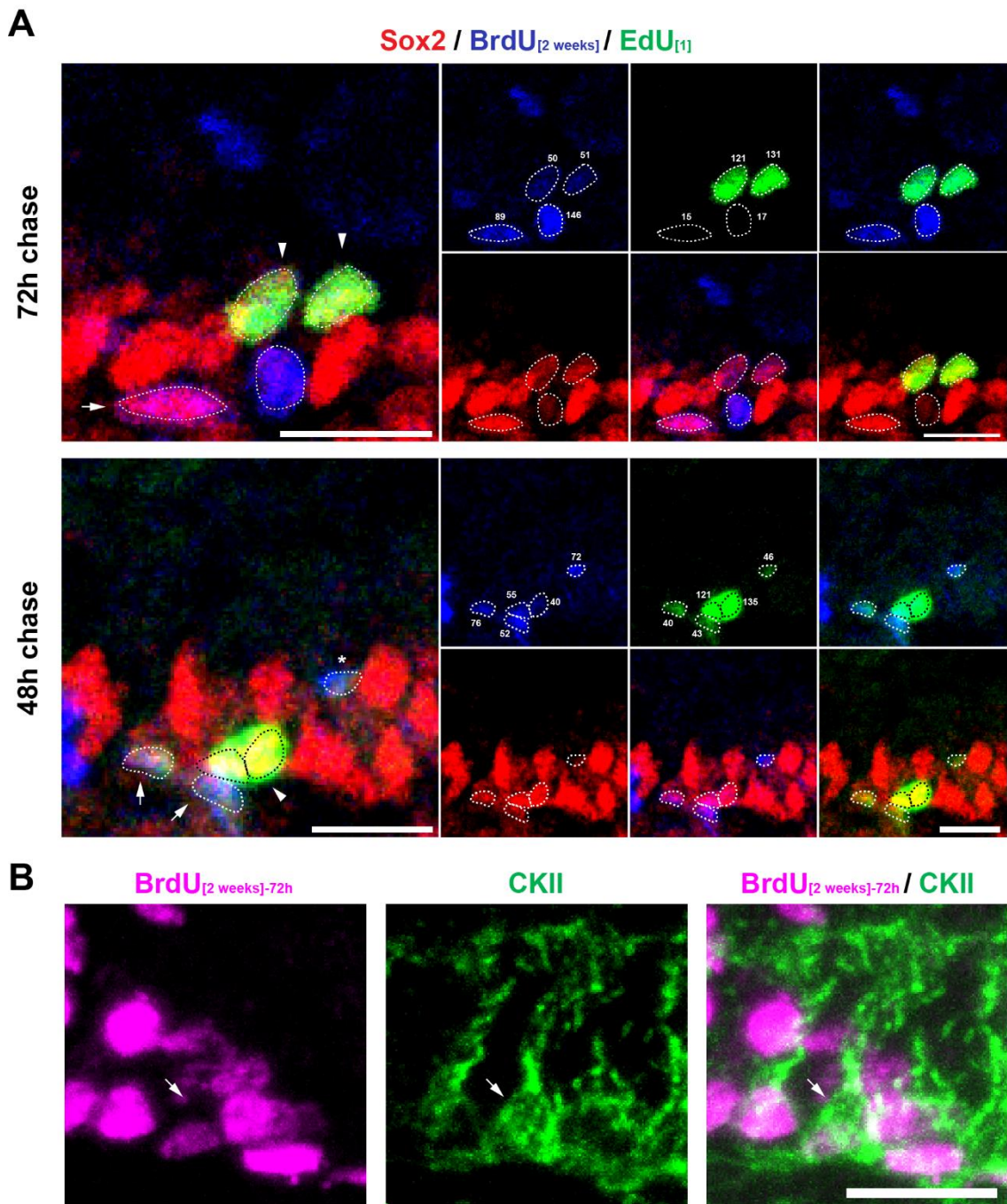


Figure 4.33. Asymmetric HBC division only forms GBCs in sensory region. A. 2-week BrdU pulse followed by single EdU injection chased for 72h and 48h. (numbers: signal intensity) B. Immunostaining on 2-week BrdU pulse chased for 72h. Bars:10  $\mu$ m.

#### **4.2.10. Clonal BrdU-positive Cells can Help Uncover OSN Cell Lineage Dynamics in Zebrafish OE**

The results so far showed that HBC activity in the mid-sensory region of zebrafish OE does not generate SCs. Therefore, studying the cell type composition of all clonal cells could help to understand the OSN lineage dynamics from HBCs. GBC progenitor cells at distinct levels of lineage hierarchy require to undergo an unknown number of mitotic events before generating immediate neuronal precursors of the OSN lineage (Schwob *et al.*, 2016). Further analysis of HBC-originated clones could uncover the number of mitotic events that are required to obtain OSNs from HBC lineage in the zebrafish OE.

To achieve this goal, clonal cell clusters from 4.2.7 (Figure 4.27) were further analyzed for the composition of cell types since they were immunostained against HBC marker Krt5 and the mature OSN marker HuC/D. Frequency of cell types that comprise clonal clusters encountered at radial index were calculated for each bin (sum of each bin = 1) and shown in the left graph of Figure 4.34. Cells only positive for BrdU- labelling could only have GBC-like identity in the suprabasal layer, since SCs are not originated from HBCs in mid-sensory region.

Clonal GBC-like cell frequencies were almost always higher than HBC frequency in each position, except in the 0.25 position where frequencies were the same. OSN frequencies were generally higher between the 0.15-0.35 regions and slightly lower in the 0.45-0.65 positions among all OSNs in the position of clusters. In contrast, GBC frequencies along the radial axis showed the opposite distribution in the respective positions with generally lower frequencies between 0.15-0.35 but higher between 0.45-0.65 positions. This result could suggest that GBCs might be depleting by giving rise to OSNs in the HBC originated clones in the mid sensory region.

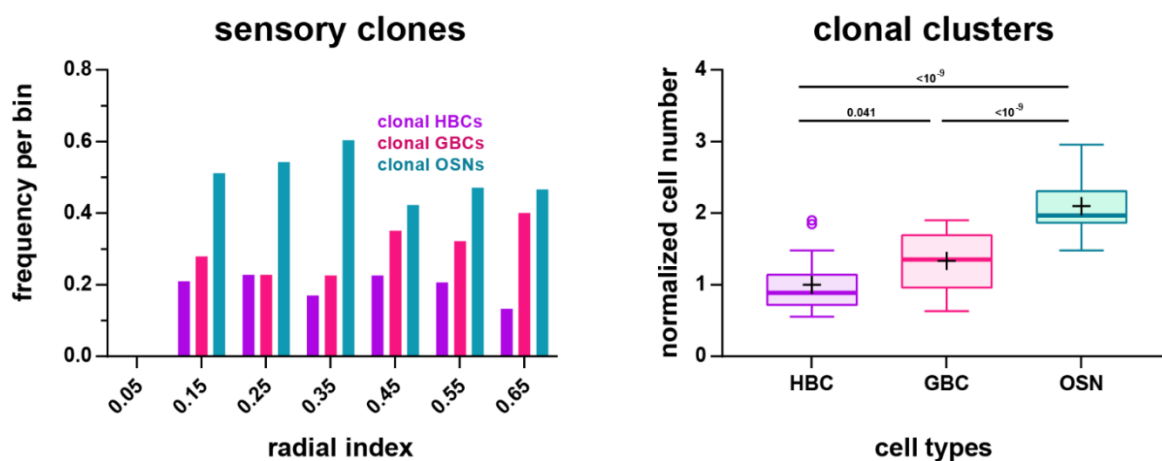


Figure 4.34. Normalized number of cell composition of clonal clusters. Frequency of  $Krt5^+$  (HBCs),  $HuC/D^+$  (OSNs) and GBC-like cells ( $Krt5^+/HuC/D^-$ ) encountered in each radial position (left), and normalized cell numbers encountered in clonal clusters (right).

Normalizing the number of clonal OSNs and GBC-like cells for clonal HBC, could predict the proliferation events required to obtain OSNs from a single HBC origin. Number of cells normalized for each fold further normalized to the average number of normalized clonal HBCs for each epithelial fold from all clone presenting epithelial folds ( $n=18$ ) are shown in a box and Tukey style whisker plot, located at the right side of Figure 4.34. Mean values were indicated by black plus signs, and medians were indicated by darker horizontal stripes. One-way ANOVA revealed statistical significance between normalized numbers of cell types ( $F_{(2,51)} = 35.567$ ,  $P < 10^{-9}$ ). A *post hoc* Tukey test was done for multiple comparison between each cell types and revealed significant difference between HBCs and GBCs ( $F_{(2,51)} = 3.5368$ ,  $P = 0.041$ ), and highly significant difference between HBCs and OSNs ( $F_{(2,51)} = 11.633$ ,  $P < 10^{-9}$ ) and between GBCs and OSNs  $F_{(2,51)} = 8.0968$ ,  $P < 10^{-5}$ ).

For each HBC ( $1 \pm 0.09$ ; mean  $\pm$  SEM),  $1.33 \pm 0.09$  GBCs and  $2.01 \pm 0.1$  OSNs were observed in the cell clusters. The difference between HBCs and GBCs, although significant, does not suggest a depleted HBC progenitor to give rise to two daughter GBCs. On the other hand, double the number of OSNs than other cells could suggest at least one symmetric division event transpired in the OSN lineage.

As GBC number is higher than HBCs and each cluster shows an indirect correlation between the frequency of GBCs and OSNs (Figure 4.34, left), GBCs might be symmetrically dividing at least once. Thus, this result could suggest that HBC originated GBCs in the mid sensory region might be dividing at least once before differentiating into OSNs.

When HBCs divide asymmetrically and form GBC in the mid-sensory region, daughter GBC undergoes a division at least once to form another two GBC-like daughter cells before forming an OSN. This proliferation event was also observed in Figure 4.33a, as the BrdU-positive suprabasal cells, which were originated from a basal cell, were positive for successive EdU-labeling. Although progenitor lineage hierarchy of GBCs is still elusive, clusters dominated by OSNs show decreased level of GBCs. This suggests that GBCs generated as the asymmetric division products of HBCs deplete over time in the zebrafish OE and might not have self-renewal capabilities.

### 4.3. Transcriptome Profiling of the Regenerating Zebrafish OE

The zebrafish OE contains constitutively active and dormant progenitor cells that undergo mitotic activity in the intact and injured OE, respectively, as outlined in the previous sections. The spatial disparity of these cells suggests that they not only occupy distinct positions but also unique progenitor cell niches. Their differential response properties make it likely that they are activated by different molecular signals or cell-cell interactions. As shown in sections 4.1.9 and 4.1.10, constitutively active GBC progenitors but not HBCs respond with increased cell proliferation to purine compounds. However, molecular signals that directly affect HBC activity are less well understood.

Transcriptome profiling by RNA-sequencing (RNA-seq) allows for a system-wide and comprehensive analysis of transcriptional changes at quantitative levels. Ranging from simple analysis of changes in gene expression to discovery of novel molecular pathways, RNA-seq has become a common and valid approach to understand regulatory events during specific developmental or cellular processes (Stark *et al.*, 2019). Generating a quantitative and qualitative transcriptome profile of the regenerative response in the zebrafish OE will help describe the dynamics of these events in detail and to pinpoint relevant regulatory pathways for the different phases of cell expansion during regeneration.

To better understand the molecular determinants of HBC activation and the processes that orchestrate the dynamic changes during regenerative neurogenesis in the zebrafish OE, intact and regenerating tissue were analyzed at different timepoints by RNA sequencing. Timepoints were selected as 4, 12, 24, 72, and 120hpl to cover the entire time course of de- and regeneration (Kocagöz, 2021) and compared to undamaged control samples. The chosen time points include the early proliferative activity of HBCs and the late events of OSN neurogenesis. Correlating the transcriptome of early regeneration timepoints with physiological tissue conditions is expected to reveal signaling molecules and pathways that are include signals for HBC activation and governing the de- and regeneration phases of regenerative neurogenesis mode in the zebrafish OE.

In this part, gene expression changes in the regenerating zebrafish OE will be described for different experimental timepoints, and an *in-vivo* study of one identified prominent signaling factor will be presented. First, results of RNA read processing and genomic alignment will be reported, then, discoveries of highly differentially expressed genes and GO-Term analysis from transcriptome data will be presented. Finally, the effect of interleukin 6, which is highly upregulated during the early phase of regeneration, will be tested *in vivo* and its effect on proliferation and neurogenesis will be reported.

#### 4.3.1. Quality Control and Genomic Alignment Rates

To obtain a global picture of differentially expressed genes and regulated molecular pathways in the regenerating zebrafish OE, whole olfactory organs were isolated from 10 intact fish and 10 fish with bilaterally TrX-lesioned OEs for each of the different analysis timepoints (control, 4, 12, 24, 72, and 120 hpl) . Time point samples were pooled for RNA isolation and two independent biological replicates for each condition were sequenced by Illumina HiSeq 2000 system to obtain raw reads (Appendix Table C.1). These reads were then subjected to a stepwise quality improvement process and subsequently analyzed by alignment to the zebrafish genome and establishment of read counts for individual transcripts (Figure 4.35).

The FastQC tool (Babraham Bioinformatics) was used to determine the overall quality of RNA reads before alignment to the genome. To visualize the difference between subsequent cleaning steps of raw reads, such as ribosomal RNA sorting, low quality sequence removal, and sequencing adapter sequence trimming, quality control plots were generated (Figure 4.36). Following these quality improvement steps, the overall sequencing depth obtained from the 6 sets of two biological replicates was determined to be at least 28.7 million reads (Appendix Table C.1), which was considered to be sufficient for alignment and further analysis. Cleaned read files were then aligned to the GRCz11 zebrafish genome with overall alignment rates ranging between 90.13% - 92.10%. Finally, the aligned read files were annotated, and gene expression read counts were generated using the HTSeq tool (Anders *et al.*, 2015). Further analysis of the expression data was performed using the idep.92 environment (Ge *et al.*, 2018).

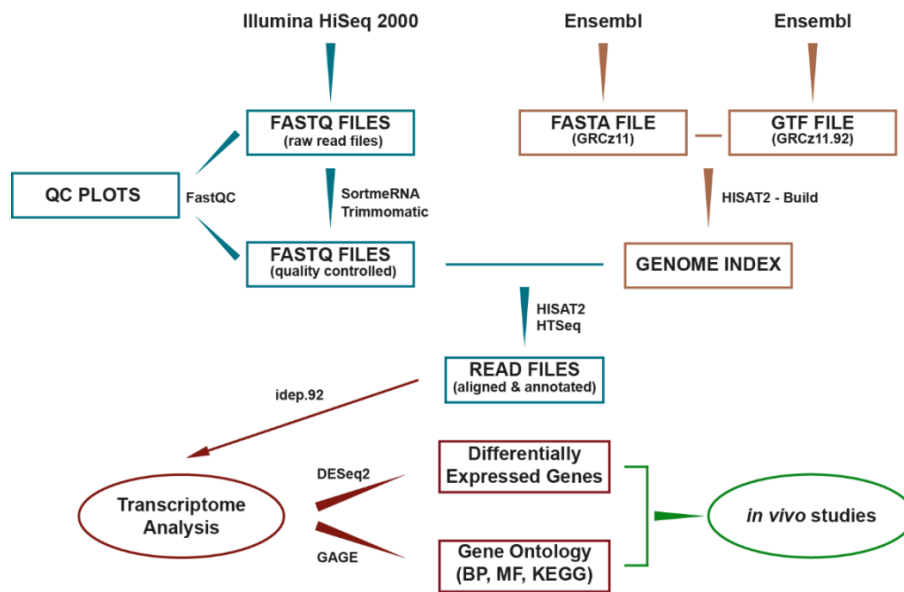


Figure 4.35. Genomic alignment and transcriptome analysis pipeline. Genomic index file preparation (yellow), RNA-read cleanup and annotation (cyan), and transcriptome profiling methods (red) are indicated in the diagram.

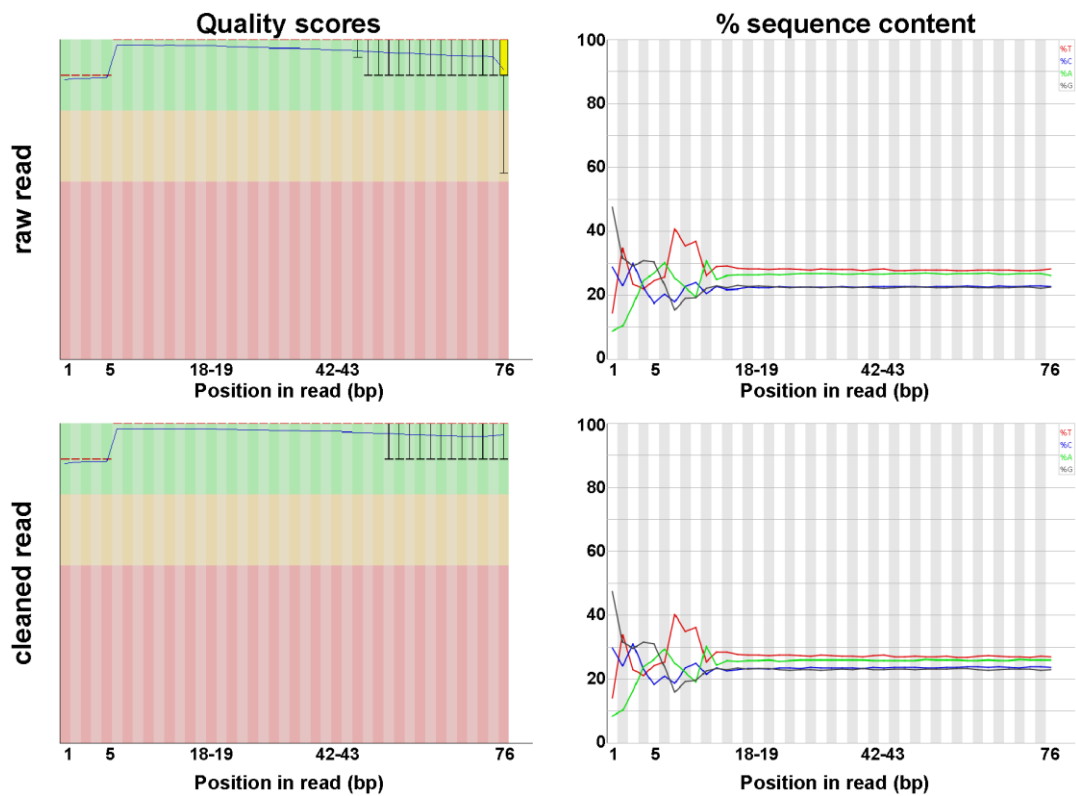


Figure 4.36. Quality of RNA reads before and after FastQC cleaning.

Following the elimination of genes with no read counts across all samples, 21303 genes with matched Ensembl IDs in the database were retained for further analysis.

#### 4.3.2. PCA and Hierarchical Clustering of Gene Expression Reveal Distinct Phases of Regeneration

A principal component analysis (PCA) was used to assess the overall changes in gene expression for different timepoints and the similarity of biological replicates as shown in Figure 4.37a. A correlation matrix was generated to observe the similarities between each analyzed gene count set (lowest correlation: green, highest correlation: orange).

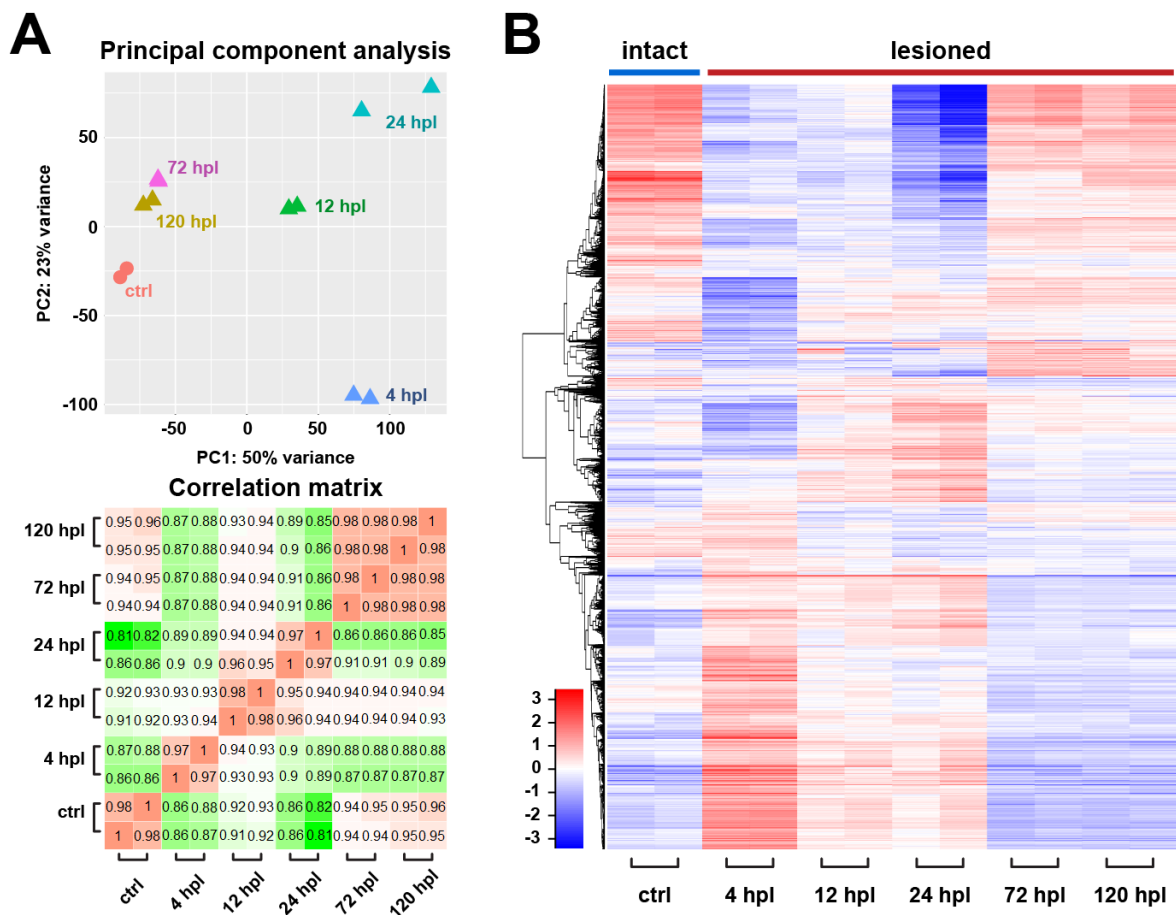


Figure 4.37. PCA, correlation matrix and hierarchical clustering of gene expression. A. PCA (top), correlation matrix (bottom) and B. Gene expression hierarchy heatmap of RNA reads in intact and chemically lesioned tissue at different time points after injury.

The two biological replicates showed similar rapid changes in gene expression in response to 1% Triton X-100 lesion can be easily observed as an elliptical counterclockwise rotation pattern in the PCA plot. Relative to the position of control samples, 4 hpl timepoint showed significant changes along PC1, which account for 50% of the observed variance. The early change was followed by changes along PC2 at 12 and 24 hpl, which describes an additional 23% of changes in gene expression between time points. Then, between 72 and 120 hpl a gradual return to control conditions could be observed, first along PC1, followed by changes along PC2.

The correlation matrix heatmap of similarities between each sample and timepoint for the 2500 most variable genes obtained similar results (Figure 4.37a, bottom). According to the matrix, the 4, 12 and 24 hpl showed the least correlation with control samples. Subsequently, a shift in gene expression is initiated around 72 hpl that is characterized by a slow gradual increase in similarity with the control tissue.

Construction of a hierarchical cluster heatmap for the same subset of genes (Figure 4.37b) provided a clearer distinction between timepoints in terms of gene expression. Upon lesion, an almost complete reversal of the pattern of gene expression is at 4hpl. Change in pattern expression pattern again was followed by gradual changes at 12hpl and 24hpl but displayed higher resemblance to intact conditions at 72 and 120 hpl.

Thus, in response to chemical lesion, gene expression pattern changes rapidly in the OE, marking the switch between maintenance to regenerative neurogenesis. The regenerative response can be characterized by three phases, a rapid change in a specific subset of genes described by PC1, followed by an orthogonal change along PC2 and slow reversal along both components towards control conditions. Thus, at 120 hpl, the transcriptome profile of the tissue is almost, albeit not fully, identical to undamaged control tissue. This further supports the transient nature of the regeneration response, which is also described by the differential mitotic activity of progenitor cells at these timepoints (Kocagöz, 2021; Kocagöz *et al.*, under review).

### **4.3.3. k-means Clustering Revealed Early and Late Enriched Genes in the Regenerating OE**

The 2,500 most variable genes were normalized to mean center (sum of each row = 1) and sorted into six clusters by a k-means clustering analysis (Figure 4.38a). Results of the analysis displayed differential expression profiles of genes for all de- and regeneration time points. Subsequent GO-term analysis on these groups of genes in each cluster also revealed prominent molecular events, shown in ascending order of adjusted p-values from top to bottom (Figure 4.38b and Table 4.1). Clusters A, B and C were composed of genes with high expression levels under physiological conditions which were lost or downregulated immediately after the chemical insult but recovered at later time points. Clusters D, E and F on the other hand were upregulated at different time points following the lesion that were described as distinct phases of regeneration in previous parts of this thesis.

The A-cluster predominantly displayed GO-terms related to olfactory functions such as sensory perception of smell as biological process, olfactory receptor activity as molecular function and neuroactive ligand-receptor interaction as KEGG pathway term (Figure 4.38b). Downregulated genes in A-cluster were indicative of OSN loss upon lesion, which are regained at the later stages of regeneration. The C-cluster showed the earliest downregulation at 4 hpl for genes of extracellular matrix regulation related GO-terms, which could be a hallmark for the loss of cell-to-cell contacts and disruption of tissue integrity caused by the chemical insult.

Genes in the B-cluster were related to cilia function and internal dynein-kinesin based transportation. Genes in this cluster are probably related to axon extension, and reconstitution of ciliated OSNs and non-neuronal ciliated cells of the respiratory epithelium in the non-sensory region, hence, upregulation is observed in the late phases of regeneration.

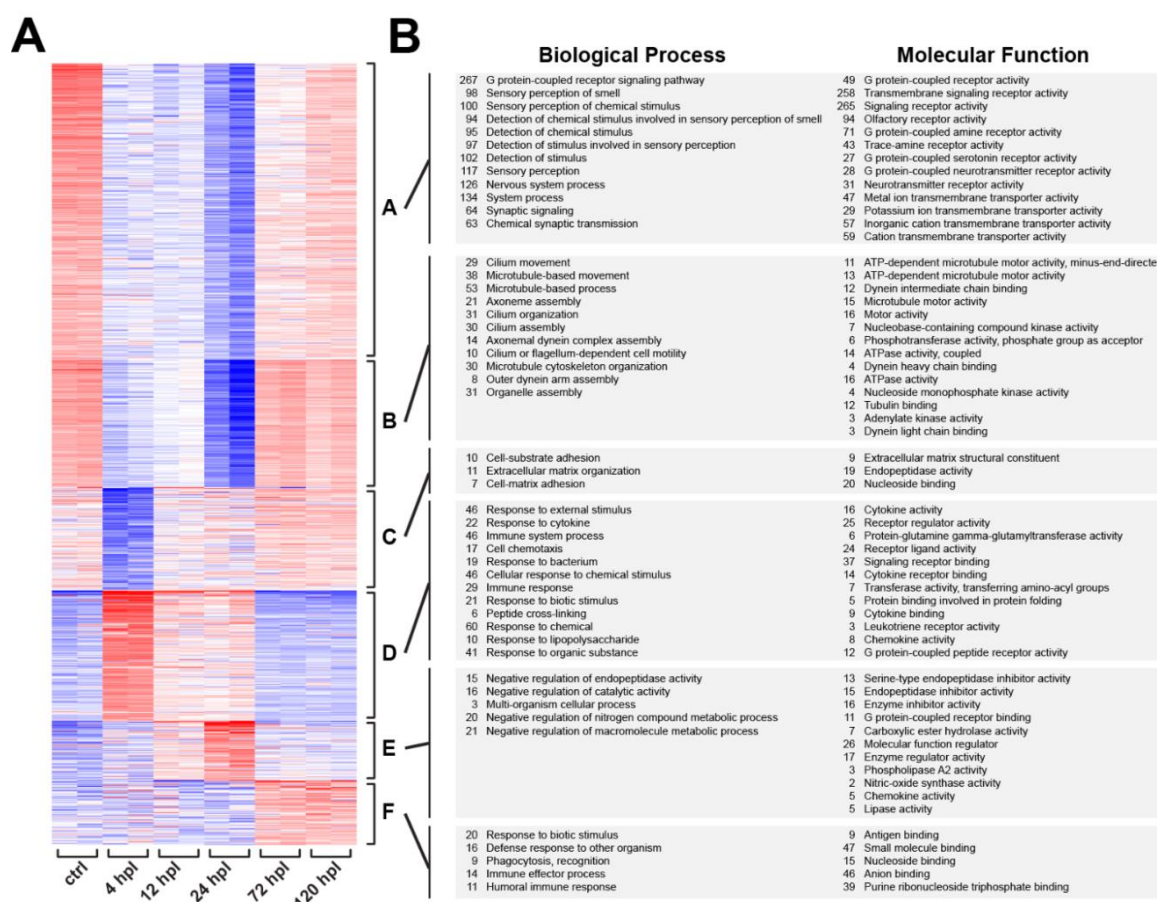


Figure 4.38. k-means clustering of differentially expressed genes. A. k-means heatmap showing high (red) and low (blue) gene expression levels centered to mean expression values for each gene in rows. B. Significant GO-terms related to clusters in part A.

Additionally, primary cilia is also necessary for progenitor cell proliferations (Han and Buylla, 2010; Jafaar Marican *et al.*, 2016) and establishment of polarity during asymmetric cell divisions (Komatsu and Mishina, 2013; Venkei and Yamashita, 2018), but due to generation algorithm of k-means clusters (row sum = 1) initial loss of ciliated OSNs and ciliated non-neuronal cells in the non-sensory region (Hansen and Zeiske, 1998) might be masking the upregulation of non-motile cilium genes in progenitor pools during early stages. To sum up, genes in the B-cluster could also be indicative of cell divisions in the committed progenitor pools and repopulation of neuronal and non-neuronal cells with ciliary structures during the later phases of regeneration.

In this study, asymmetric division was observed as the hallmark of HBC activity in the ILC and SNS and rarely in the sensory region under physiological conditions (Figure 4.19). Also, recent study from our lab shows that neurogenesis is prominent at 72 hpl and activated HBCs return almost completely to slow cycling state at 120 hpl (Kocagöz, 2021; Kocagöz *et al.*, under review).

Clusters D, E and F, on the other hand were constituted by upregulated genes during the early (D and E) and late phases (F) of regeneration. Genes in these clusters displayed specific upregulation at distinct time points and may signify regulatory events unique to different phases of regenerating neurogenesis. Cluster-D was constituted by genes upregulated immediately after the chemical insult at 4 hpl and remained relatively high until 24 hpl. GO-terms related to this cluster predominantly indicated the involvement of cytokine signaling (also see Table 4.1) and immune system activation as an immediate response to tissue injury. Upregulation of genes in cluster E was observed to be most prominent at 12 hpl and further upregulated at 24 hpl. Pathways significantly regulated in this cluster among all time points found to be apelin signaling that regulates mTOR, JNK and ERK pathways (O'Carroll *et al.*, 2013) and linoleic acid metabolism. Finally, cluster-F implied the late regulatory functions, which still showed mainly immune responses as biological process GO-terms in regenerating zebrafish OE but did not reveal associated pathway terms.

Among these groups, group D contained the immediate response genes upon chemical lesioning at 4 hpl, which is most likely a critical time point for HBC activation. Related biological process and molecular function GO-terms showed highest intragroup significance for cytokine related immune system processes (Figure 38.b). GO-term analysis for KEGG pathways showed 13 genes of cytokine-cytokine receptor interaction as the only pathway to be significantly regulated for all regeneration timepoints. Clusters D, E and F also showed upregulation of genes involved in immune system related cytokine, chemokine, and innate immune response activities at 4hpl, 24hpl, 72hpl and 120hpl.

Table 4.1. KEGG pathway GO-terms of k-means clusters.

<b>Cluster</b>	<b>adj.pval</b>	<b>Genes</b>	<b>Pathways</b>
<b>KEGG</b>			
<b>A</b>	1.90E-08	44	Neuroactive ligand-receptor interaction
<b>D</b>	1.20E-04	13	Cytokine-cytokine receptor interaction
<b>E</b>	7.90E-03	3	Linoleic acid metabolism
	7.90E-03	7	Apelin signaling pathway

#### 4.3.4. Differentially Expressed Cytokines Could Have a Signaling Role in Regenerative Neurogenesis

Time points that best represent the early phase of the response to chemical insult were described to be 4hpl, 12hpl and 24hpl according to k-means clusters. To get a better understanding of early regulatory events taking place during the initial phases of regenerative responses, a Differentially Expressed Genes (DEG) analysis was performed using the DESeq2 algorithm (Love *et al.*, 2014) in the idep.92 environment. Genes with at least two log<sub>2</sub> fold-changes in expression were subjected to GO-term analysis for the 4, 12 and 24 hpl timepoints, obtained by generally applicable gene set enrichment (GAGE) for pathway analysis method (Luo *et al.*, 2009). A full list of biological process, molecular function and KEGG pathway GO-terms for these timepoints can be found in appendices (see Appendix D, Appendix E and Appendix F).

A synopsis of regulatory events from this analysis showing the top regulated pathways for all time points of the early response is presented in Table 4.2. MAPK signaling pathway was only observed to be significantly upregulated at 4hpl as an immediate response. Upregulated TGF-beta and NOD-like receptor signaling pathways at 4, 12 and 24 hpl also emerged as highly regulated pathways during the early response. In addition, activation of the Wnt signaling pathway was observed during the second wave of early responses at 12 and 24 hpl. On the other hand, cytokine cytokine-receptor interaction was observed consistently with the highest adjusted p value for the entirety of early response phases.

The top 15 differentially expressed genes, either for all regeneration time points compared to control (Figure 4.39a) or for 4 hpl and 12 hpl time points (Figure 4.39b), highlighted the *interleukin-6 (il6)*, *leptin-a (lepa)* and *leptin-b (lepb)* genes. Among these genes, *il6* and *lepb* was expressed uniquely in chemically lesioned tissue and *il6* expression persisted among the top 30 DEG until 120 hpl.

Table 4.1. GO-term analysis summary of interesting KEGG pathways significantly regulated at 4, 12 and 24h post lesion.

Direction	Pathways	statistic	Genes	adj.pval
<b>4 hpl vs ctrl</b>				
<b>Down</b>	Neuroactive ligand-receptor interaction	-	-	-
<b>Up</b>	Cytokine-cytokine receptor interaction	3.7189	176	0.00087
	MAPK signaling pathway	3.601	349	0.00097
	AGE-RAGE signaling pathway in diabetic complications	3.2002	120	0.0034
	TGF-beta signaling pathway	3.0051	106	0.006
	NOD-like receptor signaling pathway	2.6497	153	0.014
	Wnt signaling pathway	-	-	-
	mTOR signaling pathway	-	-	-
<b>12 hpl vs ctrl</b>				
<b>Down</b>	Neuroactive ligand-receptor interaction	-4.5644	303	0.00014
<b>Up</b>	Cytokine-cytokine receptor interaction	3.7696	176	0.00084
	MAPK signaling pathway	-	-	-
	AGE-RAGE signaling pathway in diabetic complications	3.0836	120	0.0056
	TGF-beta signaling pathway	2.7155	107	0.013
	NOD-like receptor signaling pathway	2.5043	153	0.022
	Wnt signaling pathway	2.3973	185	0.027
	mTOR signaling pathway	-	-	-
<b>24 hpl vs ctrl</b>				
<b>Down</b>	Neuroactive ligand-receptor interaction	-5.5325	304	1.1E-06
<b>Up</b>	Cytokine-cytokine receptor interaction	2.8769	176	0.008
	MAPK signaling pathway	-	-	-
	AGE-RAGE signaling pathway in diabetic complications	2.745	120	0.011
	TGF-beta signaling pathway	3.0078	107	0.0072
	NOD-like receptor signaling pathway	2.877	153	0.008
	Wnt signaling pathway	2.3235	185	0.03
	mTOR signaling pathway	1.6944	178	0.087

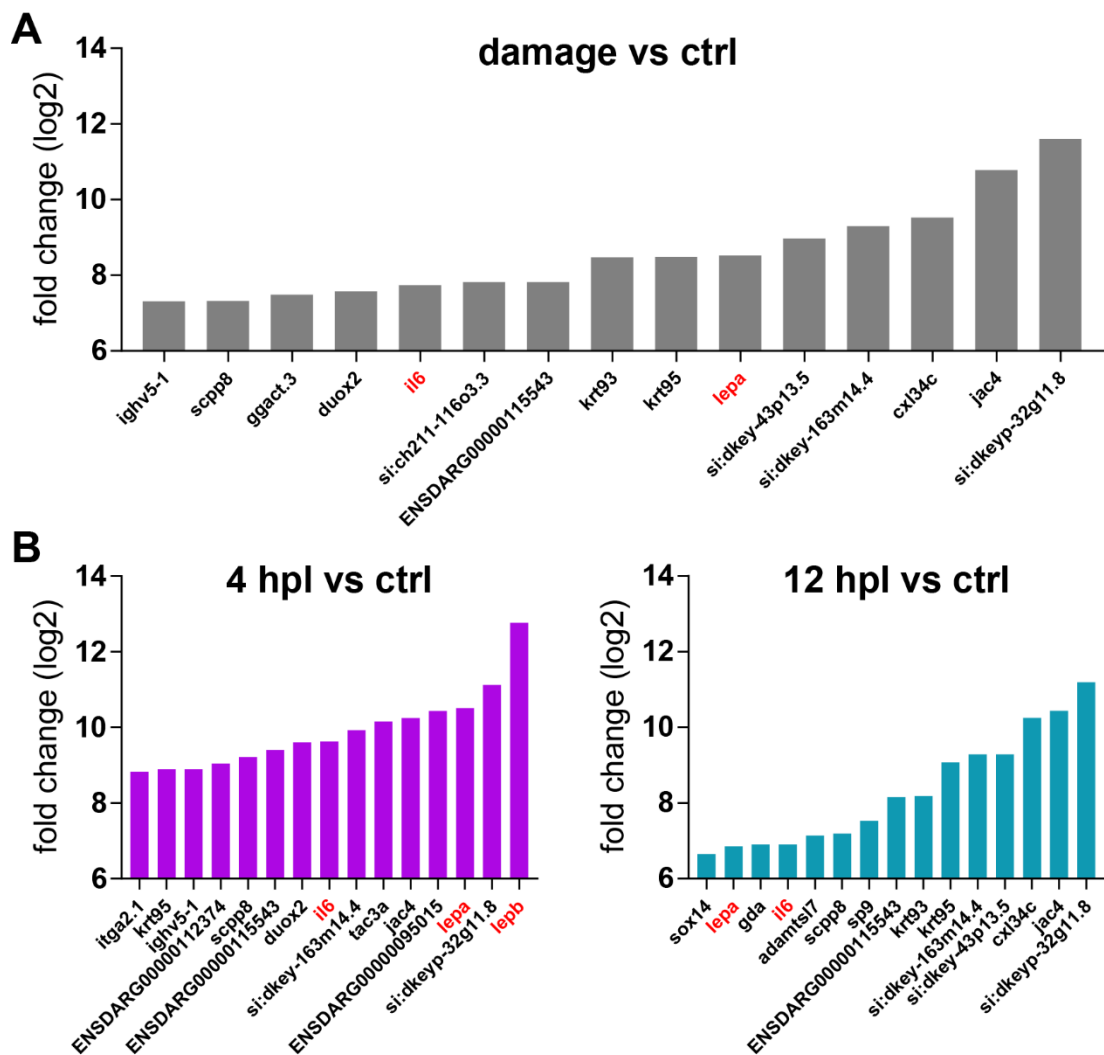


Figure 4.39. Cytokines are among the most upregulated genes in regenerating OE. A. Most upregulated 15 genes of all damage timepoints compared to controls. B. Most upregulated 15 genes at 4 hpl (left) and 12 hpl (right).

Thus, extracellular signaling related pathway components of cytokine-cytokine receptor interactions, NOD-like receptor signaling and TGF-beta signaling pathways and intracellular signaling components of MAPK signaling and Wnt signaling pathways are significantly upregulated in early phase of regenerating tissue. Upregulation of immune system related GO-terms among all time points, pathways for early phases of regeneration and unique expression of IL-6 makes them an interesting signaling route that has received little attention in the OE.

#### 4.3.5. Il6 Promotes Cell Proliferation in the Intact OE

Il6 was selected for further *in vivo* analysis due to its high differential expression in early and late phases of regenerative neurogenesis. Additionally, Il6 has been implicated to have a regulatory role in tissue regeneration in liver, heart, and CNS (Taub *et al.*, 1996; Leibinger *et al.*, 2013; Tang *et al.*, 2018). Interestingly, expression of *il6* was unique to lesioned tissue condition with virtually no expression in the intact OE. This suggests that Il6 might have a function during the acute response to chemical lesioning. If Il6 was involved in activation of regenerative neurogenesis mode, an increased proliferative activity in the zebrafish OE would be expected upon exogenous stimulation with recombinant Il6 protein.

The effect on proliferative activity in the intact zebrafish OE was studied *in vivo* by irrigating the left nasal cavity of three fish with 250 ng/ $\mu$ L of recombinant human IL-6 continuously for 30 min. The right OE was used as internal control of the effect. Immediately after nasal irrigation, fish were incubated in BrdU-containing water for 24 h. All three zebrafish OEs were analyzed at 24 h following the treatment by immunohistochemistry against BrdU to show the immediate effect on proliferation (Figure 4.40). Also, the cell type-specific mature OSN marker HuC/D (54 epithelial folds, 3 fish/condition), and HBC marker Krt5 (18 epithelial folds, 1 fish/condition) were analyzed immunohistochemically to understand whether IL-6 treatment stimulates HBC proliferation and OSN generation (Figure 4.41).

Antibody staining against BrdU, showed an increase in the number of cells in the zebrafish OE upon stimulating the OE with recombinant IL-6. An even increase in cell proliferation activity could be observed for each radial position (Figure 4.40a). Most importantly, the average number of BrdU-positive cells was increased 1.9-fold in the ILC (0.05 position; ctrl:  $9.19 \pm 0.79$ , IL-6:  $17.56 \pm 1.05$ ), 2.6-fold in mid-sensory (0.15-0.55 positions; ctrl:  $2.11 \pm 0.04$ , IL6:  $5.59 \pm 0.06$ ) and 1.4-fold in the SNS (0.65-0.75 positions; ctrl:  $11.22 \pm 0.63$ , IL6:  $15.29 \pm 0.74$ ), which can be observed in the graph at the left side in Figure 4.40b.

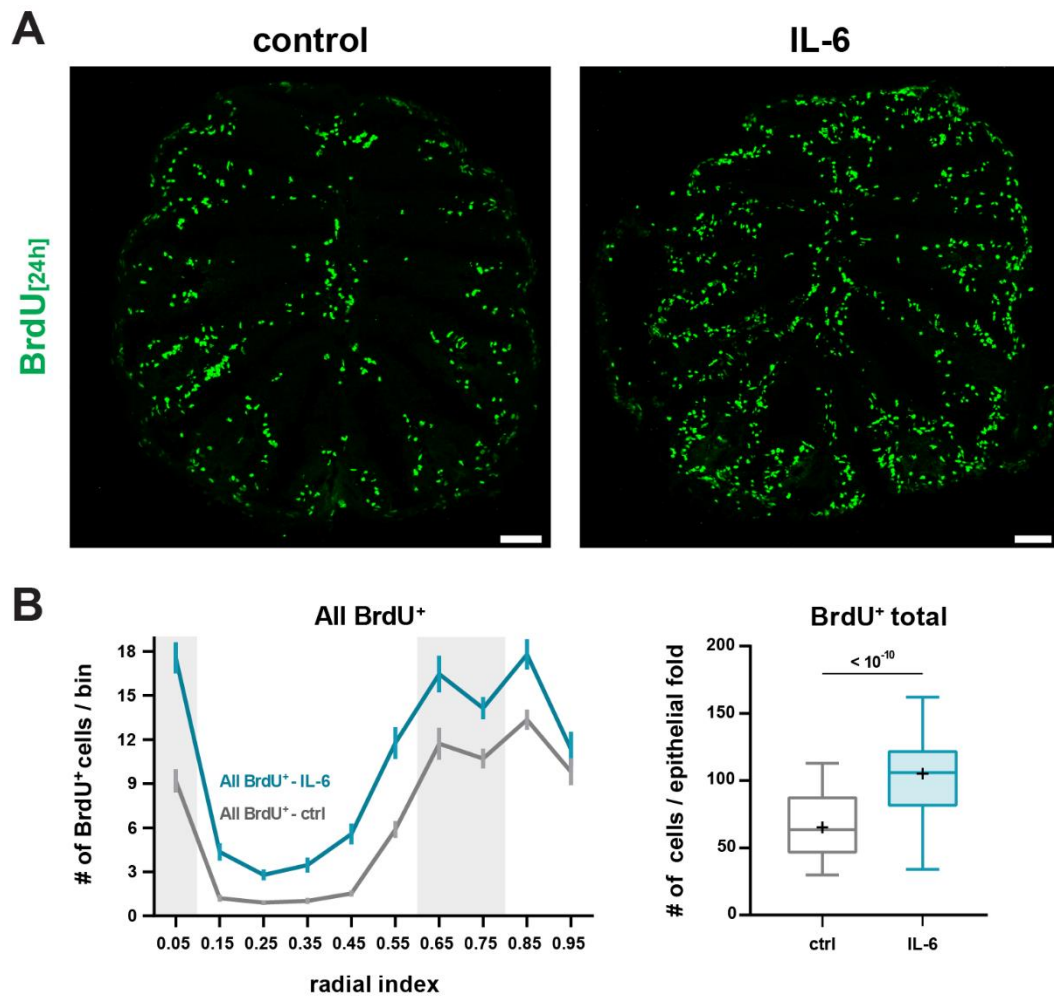


Figure 4.40. Effect of IL-6 on proliferation at 24 hpi. A. Confocal images of IHC against BrdU after 24 hpi. Scale bars: 50 $\mu$ m B. Positional (left) and cumulative (right) quantification of BrdU<sup>+</sup> cells (18 folds/fish, 3fish/condition; two tailed Student's t-test).

The total number of BrdU-positive cells in epithelial folds increased 1.6-fold upon IL-6 application at 24 hpi compared to control (54 epithelial folds/condition: 6 epithelial folds/section, 3 section/fish, 3fish/condition; Two-tailed Student's t-test;  $t_{IL-6/control} = 8.4702$ ,  $P < 10^{-10}$ ). Mean values are indicated by black plus signs in the graph (control:  $65.33 \pm 3.09$ , mean  $\pm$  SEM; IL-6:  $105.22 \pm 3.99$ ). To dissect the source of acute proliferation, the quantification was extended to HuC/D/BrdU and Krt5/BrdU double-positive cells (Figure 4.41).

HuC/D/BrdU double-positive OSNs increased in numbers at radial positions 0.05 (ctrl:  $3.06 \pm 0.55$ ; IL-6:  $4.52 \pm 0.69$ ), 0.55 (ctrl:  $1.68 \pm 0.32$ ; IL-6:  $2.63 \pm 0.47$ ) and 0.65 (ctrl:  $1.97 \pm 0.40$ ; IL-6:  $2.87 \pm 0.60$ ) but did not show a noticeable increase in the sensory OE.

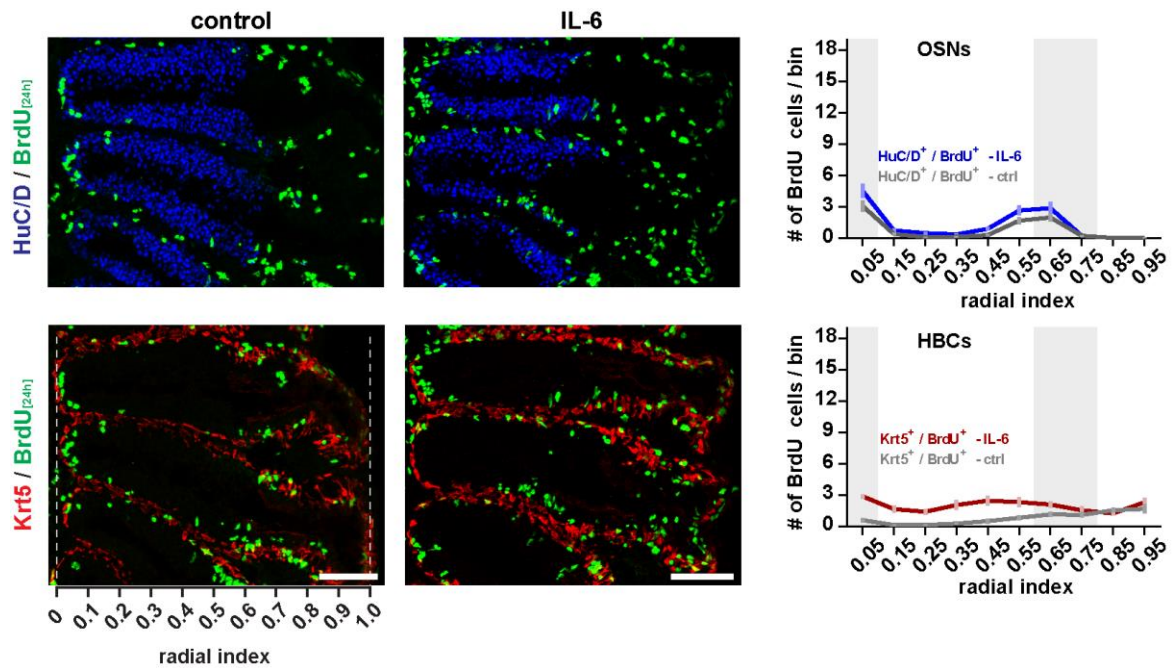


Figure 4.41. Cell type specific immediate effect of IL-6 stimulation at 24 hpi. Confocal images (left) and positional quantification of HuC/D+/BrdU+ and Krt5+/BrdU+ double-positive cells (right). Scale bars 50 $\mu$ m.

Interestingly, preliminary results from one fish showed an increase in the number of Krt5/BrdU double-positive cells for each radial position in the sensory region (0.05 - 0.65), which suggests that apart from ILC (0.05) and SNS (0.65) positions, increase in mid-sensory region (0.15 - 0.55) might be explained with the activated Krt5/BrdU double-positive HBCs (ctrl; 0.05:  $0.61 \pm 0.20$ , mean  $\pm$  SEM; 0.15:  $0.14 \pm 0.08$ ; 0.25:  $0.14 \pm 0.08$ ; 0.35:  $0.28 \pm 0.14$ ; 0.45:  $0.53 \pm 0.23$ ; 0.55:  $0.83 \pm 0.21$ ; 0.65:  $1.17 \pm 0.23$ ; and IL-6: 0.05:  $2.89 \pm 0.18$ ; 0.15:  $1.67 \pm 0.33$ ; 0.25:  $1.42 \pm 0.27$ ; 0.35:  $2.06 \pm 0.48$ , 0.45:  $2.47 \pm 0.46$ ; 0.55:  $2.33 \pm 0.45$ ; 0.65:  $2.11 \pm 0.32$ ).

Even though, the IL-6 induced Krt5/BrdU double-positive cells were only quantified for a single fish, these numbers may account for most of the BrdU-positive cell increase in 0.25-0.45 positions of the core-sensory region.

#### 4.3.6. IL-6 Induces Neurogenesis Through HBC Proliferation

IL-6 stimulation showed a proliferation-promoting effect in the zebrafish OE with some evidence of acute HBC activation. To further investigate if the IL-6-induced proliferative effect is ultimately neurogenic, OEs were analyzed at 72 hpi to give time for proliferated or newly generated cells to differentiate into OSNs after the IL-6 application.

Similar to previous experiments, the left zebrafish OE was irrigated with 250 ng/ $\mu$ l IL-6, while the right OE was used as internal control. Upon IL-6 treatment, fish were immediately transferred to BrdU containing water and subjected to a 48h BrdU pulse. Olfactory organs were collected at 72 hpi and tested with immunohistochemistry against BrdU, and the cell type specific markers HuC/D and Krt5 to visualize OSNs and HBCs, respectively (Figure 4.42). Positional quantification of newly generated HuC/D/BrdU double-positive, Krt5/BrdU double-positive and only BrdU-positive cells (Figure 4.43) revealed a similar proliferation pattern compared to control OE, but with higher numbers in almost every radial position in the sensory region (0.05-0.65).

The number of only BrdU-positive cells was increased by 1.6-fold, HuC/D/BrdU-positive cells by 2-fold, Krt5/BrdU double positive cells by 2.4-fold, and total BrdU-positive cells by 1.9-fold in IL-6 treated zebrafish OE (control<sub>(BrdU only)</sub> =  $30.79 \pm 1.42$ , IL-6<sub>(BrdU only)</sub> =  $48.15 \pm 1.93$ ; control<sub>(HuC/D/BrdU)</sub> =  $17.33 \pm 1.06$ , IL-6<sub>(HuC/D/BrdU)</sub> =  $34.87 \pm 1.89$ ; control<sub>(Krt5/BrdU)</sub> =  $12.35 \pm 2.13$ , IL-6<sub>(Krt5/BrdU)</sub> =  $30.55 \pm 0.82$ ; control<sub>(total BrdU)</sub> =  $60.48 \pm 2.13$ , IL-6<sub>(total BrdU)</sub> =  $113.57 \pm 3.54$ ). One way ANOVA on BrdU-positive cells show statistical significance ( $F_{(5, 318)} = 85.8$ ,  $P < 10^{-15}$ ) for IL-6 treatment, and results of post hoc Tukey test for pairwise comparison revealed that increase in all groups were significant ( $P_{(BrdU \text{ only})} < 10^{-8}$ ,  $P_{(HuC/D/BrdU)} < 10^{-8}$ ,  $P_{(Krt5/BrdU)} < 10^{-9}$ ,  $P_{(total BrdU)} < 10^{-15}$ ; 54 epithelial folds/condition: 6 epithelial folds/section, 3 section/fish, 3fish/condition).

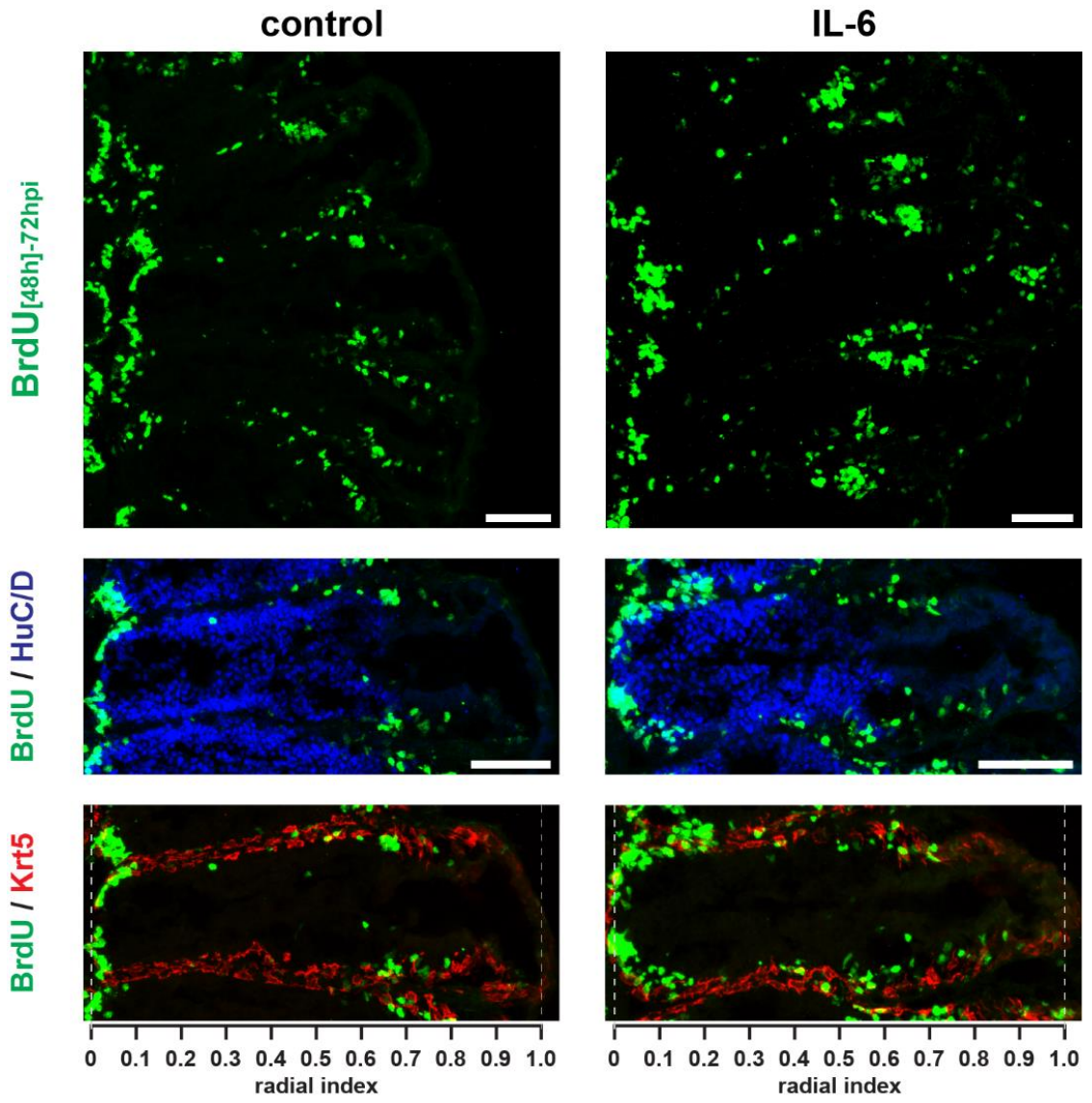


Figure 4.42. Effect of IL-6 on cell proliferation at 72 hpi. Images of immunostaining against BrdU, HuC/D (blue) and Krt5(red). Rulers indicate radial index, Scale bars: 50μm.

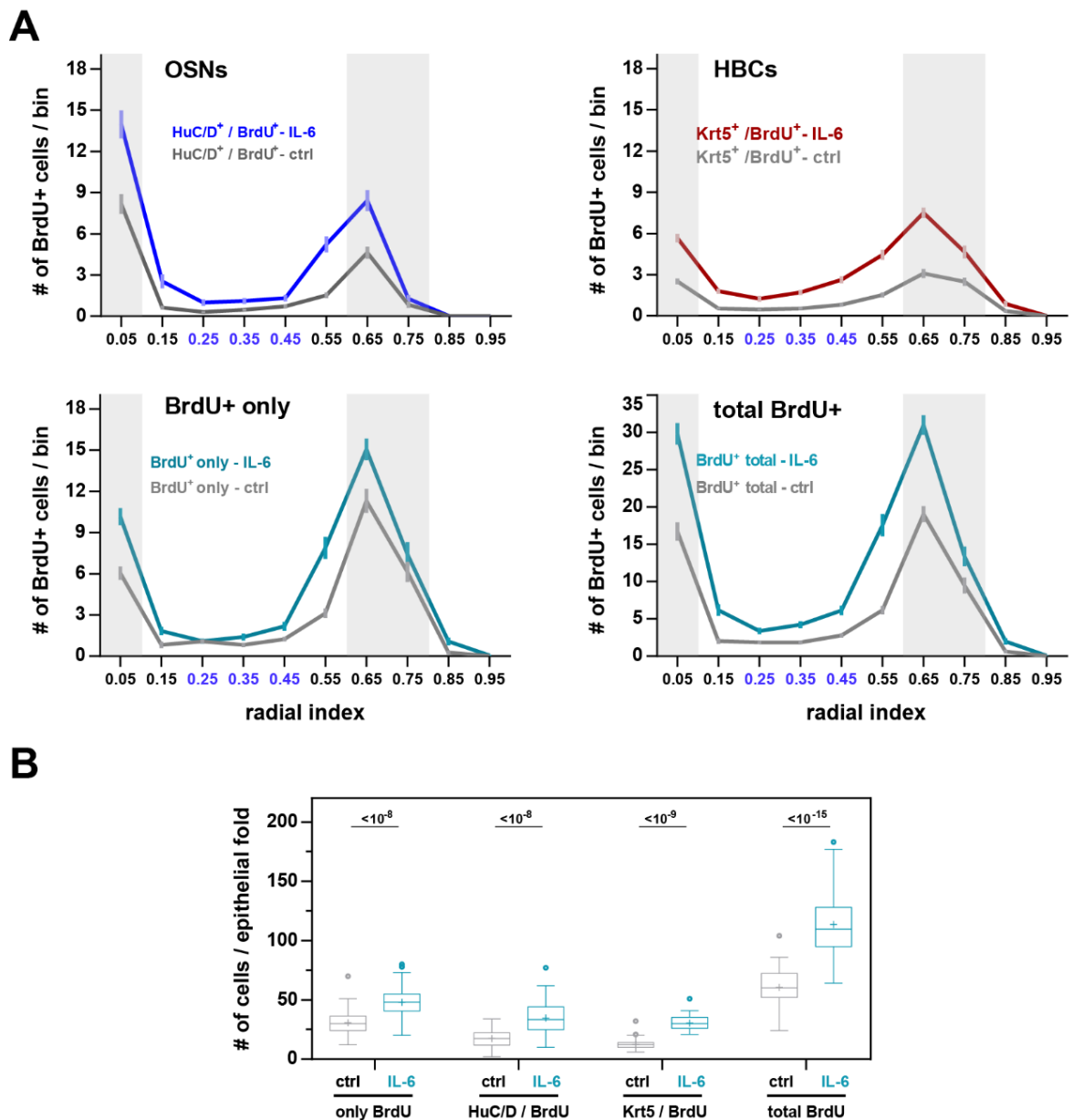


Figure 4.43. Quantitative analysis of the effect of IL-6 on proliferation at 72 hpi. A. Positional profile of only BrdU<sup>+</sup>, HuC/D<sup>+</sup>/ BrdU<sup>+</sup> and Krt5<sup>+</sup>/BrdU<sup>+</sup> double-positive cells.

B. Box and Tukey style whisker plots of BrdU-positive cells.

Curiously, active HBCs were increased 2.3-fold in the ILC, and on average 3-fold in each position. This increase was not accompanied with an increase of similar proportions in other BrdU-positive cells in these positions, suggesting that symmetric HBC divisions were favored upon IL-6 stimulation.

To assess whether the increase in the number of labeled cells were significant for the different radial positions as well, a two-way ANOVA was used to test the change for average number of cells in radial positions of each fish with Sidak's multiple comparisons test (Figure 4.44). Statistical analysis revealed significant overall effect for IL-6 treatment for each BrdU-positive cell group (BrdU only:  $F_{(6,14)} = 15.8282$ ,  $P = 1.6 \times 10^{-5}$ ; HuC/D+/BrdU+:  $F_{(6,14)} = 3.1826$ ,  $P = 0.034$ , Krt5+/BrdU+:  $F_{(6,14)} = 14.8044$ ,  $P = 2.4 \times 10^{-5}$ ). Differences in radial positions revealed a positional preference to ILC and SNS, favoring more increase from SNS position for only BrdU-positive cells (0.05:  $P = 5.6 \times 10^{-6}$ , \*\*\*\*; 0.15:  $P = 0.36$ , ns; 0.25:  $P = 0.9999$ , ns; 0.35:  $P = 0.8821$ , ns; 0.45:  $P = 0.44$ , ns; 0.55:  $P = 9.5 \times 10^{-7}$ , \*\*\*\*; 0.65:  $P = 1.7 \times 10^{-5}$ , \*\*\*\*) and HuC/D/BrdU double-positive OSNs (0.05:  $P = 0.0011$ , \*\*; 0.15:  $P = 0.5793$ , ns; 0.25:  $P = 0.9959$ , ns; 0.35:  $P = 0.9975$ , ns; 0.45:  $P = 0.9987$ , ns; 0.55:  $P = 0.0393$ , \*; 0.65:  $P = 0.0335$ , \*) in the mid-sensory region. Krt5/BrdU double-positive cells were also increased significantly in ILC and SNS, but additionally showed significant increase in core-sensory region indicated by blue labels in the Figure 4.44 (0.05:  $P = 1.7 \times 10^{-6}$ , \*\*\*\*; 0.15:  $P = 0.0178$ , \*; 0.25:  $P = 0.2659$ , ns; 0.35:  $P = 0.0320$ , \*; 0.45:  $P = 7.7 \times 10^{-4}$ , \*\*\*; 0.55:  $P = 4.5 \times 10^{-6}$ , \*\*\*; 0.65:  $P = 2.6 \times 10^{-8}$ , \*\*\*\*). Increased number of Krt5/BrdU cells favoring SNS side of the mid-sensory region.

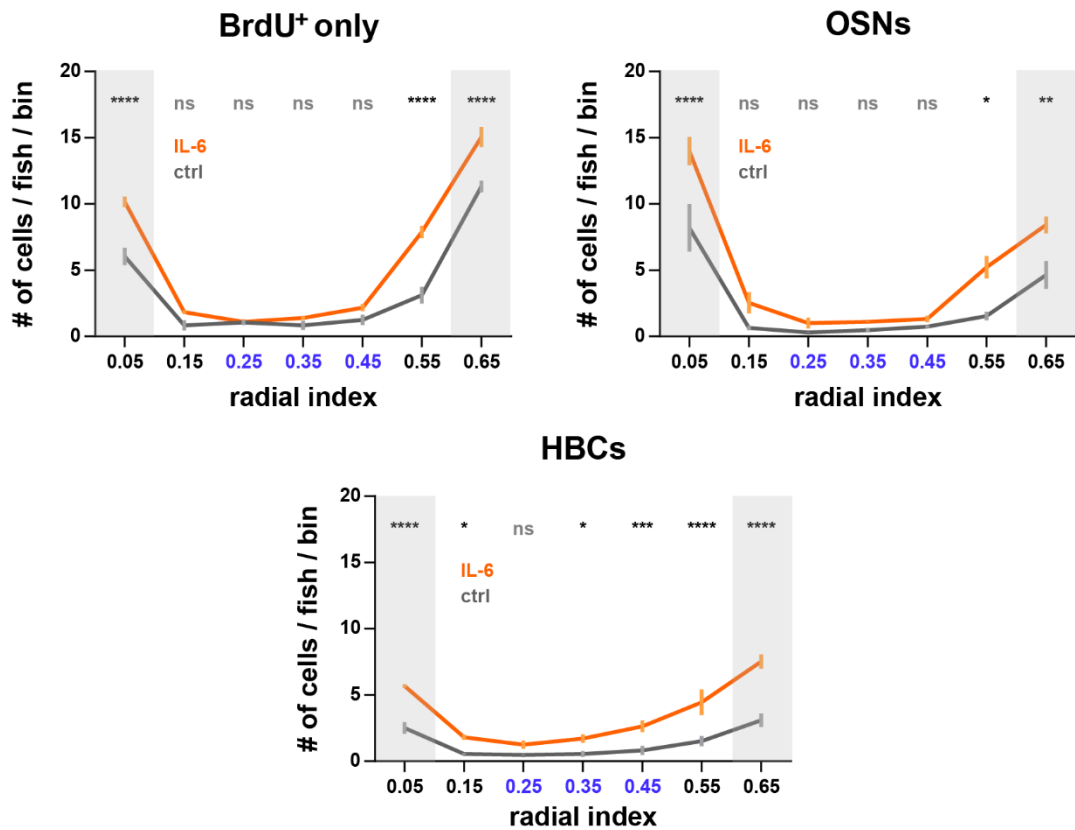


Figure 4.44. Statistical analysis of IL-6 effect on cell types in radial positions at 72 hpi. Positional statistics of average BrdU<sup>+</sup> cells numbers per control and IL-6 injected fish. Two-way ANOVA for IL-6 effect and Sidak's multiple comparison for radial positions.

This result suggests that proliferation promoting effect of IL-6 triggers symmetric division of HBCs in the intact zebrafish OE. When IL-6 stimulation ceases, the expanded HBC pool could give rise to an increased number of cells in the OSN lineage, including OSNs and transient GBCs. Yet, induction of SC activity cannot be ruled out from these experiments and remains elusive. On the other hand, although a more dominant effect could be observed at maintenance neurogenesis zones, a later differentiation into OSNs remains possible. While unique increase in HBC numbers in core-sensory region was evident of IL-6 induced HBC progenitor pool expansion, preferential increase at SNS side is curious and might suggest a broader indirect effect of IL-6 on zebrafish OE regeneration.

## 5. DISCUSSION

The OE is a neuronal tissue with unusually high cellular turnover and regenerative capacity. The main aim of this study was to characterize the role of non-neuronal cells in daily maintenance of the intact OE with a special emphasis on Sox2-positive cells. Based on their distribution, cellular morphology, molecular definition, and tissue function, Sox2-positive cells constitute a heterogeneous population that includes at least three different subtypes. Injury-sensitive HBCs uniformly line the basal OE, while SCs occupy more suprabasal layers to provide structural support. Specialized GBCs are restricted to the ILC and SNS, where OSNs are generated at high rate in the intact OE. Additional, less well defined Sox2-positive cells with columnar morphology and unknown function may exist around the ILC.

Mitotic activity of neurogenic progenitors needs to be tightly regulated to establish tissue maintenance. A candidate neurogenesis-promoting factor could be ATP and related purinergic compounds, which occur at high intracellular concentrations and could be liberated to the environment upon cell death or injury. In-depth analysis within the framework of this thesis revealed the identity and differential purine sensitivity of Sox2-positive non-neuronal cells. Most importantly, a differential proliferation-promoting effect of purine signals on maintenance neurogenesis through GBCs could be identified. In contrast, HBCs, although sensitive to ATP stimulation at the cellular level, do not undergo mitotic activity in response to systemic stimulation.

Long- and short-term lineage tracing studies revealed that SCs are also generated at the ILC and SNS, similar to OSNs in the intact OE. However, it remains currently unknown if SCs and OSNs are generated by the same multipotent progenitor or if distinct SC and OSN lineages exist. In addition, HBCs also show an unusually high proliferative activity at the ILC and SNS, suggesting a unique molecular definition of stem/progenitor cell niches in different epithelial regions. Even though HBCs may be spontaneously active in the sensory OE and can generate OSNs, they most likely do not give rise to SCs.

Transcriptome profiling of the regenerating zebrafish OE revealed a tri-phasic regenerative neurogenesis response during which immune system activity and cytokine signaling are prominently active immediately following experimental OE lesions. The pro-inflammatory cytokine IL-6 is expressed uniquely upon tissue injury and could be shown to selectively affect HBC progenitor pool expansion and OSN neurogenesis from GBCs in the intact zebrafish OE.

### 5.1. Purine-Sensitive Non-Neuronal Cells in the Zebrafish OE

The unprecedented capacity of continuous new OSN generation and efficient tissue regeneration upon acute damage requires a tight regulation of neurogenesis in the peripheral OE to preserve meaningful chemosensory function. Both the rate of OSN loss and compensatory OSN generation depend on the tissue condition, whether it is intact, infected, or injured, as well as the nature and the extent of the damage. However, molecular mechanisms governing the mode or the regulation of rate of OSN neurogenesis are largely elusive in the zebrafish OE. An attractive hypothesis tested in our lab is that the release of purine compounds from dying or injured OSNs could regulate the activation of progenitor pools, as purines were implicated in increased cell proliferation in the mouse and *Xenopus* OE (Jia *et al.*, 2006; Hassenklöver, 2009). Previous studies from our lab showed that neuronal and non-neuronal cells of the zebrafish OE are sensitive to purine compounds (Bali, 2015) and that ATP can increase cell proliferation in the tissue (Sakızlı, 2018), albeit the exact cell types that are affected by the ATP induction had not been characterized in detail.

Findings in this study show that exogenous application of ATP on in physiologically active tissue preparations evoke  $\text{Ca}^{2+}$  transients that originate predominantly from basally located cells but also from a few apically located OSNs (Figure 4.1). ATP-sensitive OSNs are probably the adenosine sensing A2c chemosensory pear neurons that have been described to be located in the most apical layers of the OE (Wakisaka *et al.*, 2017) and correlate with the tissue distribution of the responding cells. Mutually exclusive  $\text{Ca}^{2+}$  transients evoked by ATP and high  $\text{K}^+$  in the basal and intermediate OE layers strongly suggests that ATP induces  $\text{Ca}^{2+}$  responses mainly in non-neuronal cells.

Examination of the neuronal and non-neuronal cell composition of the zebrafish OE by immunohistochemistry against the ELAV-like HuC/D protein to label mature OSNs and the undifferentiated/stem cell marker Sox2 to label non-neuronal cells on tissue counterstained with TO-PRO shows a segregated distribution of non-neuronal cells in basal layers of the sensory epithelium (Figure 4.2). The distribution of non-neuronal cells strongly correlates with the basally restricted ATP responses and suggests that ATP-induced  $\text{Ca}^{2+}$  transients are generated predominantly, if not exclusively, in basally located non-neuronal cells in the zebrafish sensory OE.

Quantification of the respective area occupied by marker expressing cells shows that the sensory region of the zebrafish OE is constituted almost exclusively by Sox2 and HuC/D expressing cells, which together account for 94-98% of all cells (Figure 4.2c). However, in this analysis, TO-PRO is overrepresented due to the presence of cells that are located outside the epithelium proper and within the lamina propria in the center of each lamella (Hansen and Zeiske, 1998). Even so, inside the sensory OE, a small number of marker-negative but TO-PRO-positive cells can be observed close to the ILC and SNS, thus, in regions where *ascl1*-expressing GBCs are located (Bayramlı *et al.*, 2017). In rodents, basally located transiently amplifying GBCs can also be identified by their Sox2 and *ascl1* expression, which divide and give rise to immediate neuronal precursor cells and immature neurons of the late GBC lineage (Schwob, 2002). The analogy suggests that the rare HuC/D- and Sox2-negative cells in the zebrafish are also either neuronal precursors or immature neurons of the OSN lineage.

Sox2-expressing non-neuronal cells are heterogeneous and show morphologically distinct characteristics and layer segregation in the basal strata of the epithelium (Figure 4.6). Sox2-positive cells uniformly occupy two cell layers in most positions of the sensory OE, the most basal of which corresponds to HBCs, which have horizontal and flat cell profiles. More columnar cells with elongated morphology along the vertical axis can be seen in the suprabasal layers, either protruding from between HBCs or located directly in these positions.

This is different from the rodent OE in which Sox2-expressing cells are located in two separate layers at the apical and basal borders of the OE and form continuous lines constituted by SCs in apical and progenitor cells in basal positions (Chen *et al.*, 2004; Guo *et al.*, 2010). The basally restricted localization of all Sox2-expressing cells in the sensory region of the zebrafish OE made it more challenging to identify the distinct non-neuronal cell types in the ATP responses. Direct immunostaining of OEs that were used in physiological  $\text{Ca}^{2+}$  measurements failed to provide consistent and reliable results due to differential experimental demands. To overcome this difficulty, the characteristics of purine responses was compared to position of *in situ* hybridization or immunohistochemically labeled cells to identify the purine sensitive non-neuronal cells.

The basal layer of cells that respond to ATP shows the most dramatic distinction by their concurrent sensitivity to 2-MeSATP (Figure 4.3). This distinction is in line with previous observations from our lab (Bali, 2015). 2-MeSATP sensitive cells show a close resemblance to HBCs that occupy basal-most layer in a discontinuous line of evenly spaced flat cells throughout the sensory region of the zebrafish OE (Demirler *et al.*, 2020; Kocagöz, 2021). The HBC markers p63 and Krt5 have also been shown to be co-expressed with Sox2 exclusively in the most basal cells (Demirler *et al.*, 2020; Kocagöz, 2021). Measurement of 2-MeSATP responses to directly target the basal layer of cells in combination with vital dye CellTrace<sup>TM</sup> shows a strong morphological correlation and similarity in tissue distribution with HBCs identified by p63 expression on CellTrace<sup>TM</sup>-stained OEs (Figure 4.10). When exposed to the vital dye CellTrace<sup>TM</sup>, the intact tissue can only receive the dye through cells that are in contact with the environment at the apical surface of the epithelium and a small population of cells remains unlabeled in the basal tissue. CellTrace<sup>TM</sup>-devoid cells both respond to 2-MeSATP and express p63, are in direct contact to basal lamina, and show horizontally elongated dimensions and an identical distribution in the sensory OE. Thus, vital dye free p63-positive HBCs shows a very tight correlation which makes them very likely to be the 2-MeSATP sensitive basal layer of ATP responses.

According to their response kinetics, ATP sensitivity and tissue distribution, intermediate ATP-sensitive cells can be further characterized into cell groups with low intensity responses that are distributed evenly throughout the sensory region and spatially

restricted cells with rapid response onsets and high intensity responses (Figure 4.3 and Figure 4.4). Cell morphology, as well as the radial and vertical distribution within the tissue of the latter group closely resembled GBCs that are located at the ILC and SNS (Figure 4.5). Mitotically active cells at the basal cell layer in the *Xenopus* vomeronasal organ also show a similar ATP induced responses with around 2-fold higher signal intensity than cells in the SC layer (Dittrich *et al.*, 2014), suggesting a link between mitotically active progenitor cells and increased sensitivity to ATP. Similar stronger ATP responses are also observed in basal cells compared to intermediate cells in the zebrafish OE (Demirler *et al.*, 2020). To unequivocally show that these spatially restricted cells with high response intensity are not simply a group of displaced HBCs,  $\text{Ca}^{2+}$  measurements using a transgenic zebrafish line for *ascl1*-promoter (Wan *et al.*, 2012) could be performed. On the other hand, anti-Krt5 immunohistochemistry to visualize HBCs never presented with localization of cells outside the most basal layer and always consisted of a single layer. Thus, high intensity ATP responses within intermediate cells most likely originated from GBCs and not HBCs.

One further distinction arises from the detection of 2-MeSATP-responding intermediate cells. At most two but most commonly one intermediate cell presented with 2-MeSATP sensitivity in the ILC (Figure 4.3). The same cells were also observed as a subpopulation of rapidly and more intensely ATP responding sensitive cells (two to three cells in the ILC). These 2-MeSATP-sensitive cells were always located in the suprabasal layer and were always in direct contact with a basal cell. Response kinetics, positioning in the epithelium and exclusion from the basal layer suggests that these cells could have an identity in between HBCs and *ascl1*-expressing transiently amplifying GBCs ( $\text{GBC}_{\text{TA}}$ ) (Bayramlı *et al.*, 2017). In rodents, GBCs obtained by the dissociation of uninjured OE and cell sorting, when engrafted to another OE, have been shown to have clonal ability to form all cell types in the rodent OE (Chen *et al.*, 2004). Multipotent progenitor GBCs ( $\text{GBC}_{\text{MPP}}$ ) are identified by Sox2 and Pax6 expression and can be distinguished from HBCs and  $\text{GBC}_{\text{TA}}$ s in OSN lineage by the lack of p63 (Packard *et al.*, 2011) and expression of differentiation-related transcription factor *Ascl1* and *NeuroD1* expressions, respectively (Chen *et al.*, 2009; Guo *et al.*, 2010). Alternatively, through Notch signaling,  $\text{GBC}_s$  are diverted from OSN lineage and express *Hes1* instead of *Ascl1* and become SCs in the rodent OE (Herrick and Schwob, 2015).

Multipotent progenitor GBCs of the early lineage are elusive in the zebrafish OE. Extending the previously proposed  $\text{Ca}^{2+}$  physiology experiment on an *ascl1*-promoter transgenic zebrafish line could differentially show 2-MeSATP-insensitive, ATP-responsive *ascl1*-expressing GBCs. If the 2-MeSATP-sensitive cells were indeed negative for *ascl1*-expression, these cells could be proposed to be the GBC<sub>MPPS</sub> of the zebrafish OE.

At the same time, these cells should be positive for Sox2 and negative for p63 and Krt5 expression. The unknown lineage origin of SCs in the ILC (Figure 4.31) could also be explained by the presence of multipotent GBCs in the zebrafish OE as SCs do not show evidence of self-renewal, at least in the intact OE (Figure 4.30). The Hes1 orthologue of the zebrafish, Her6, has been studied in zebrafish brain and shown to have a strict role in regulating the neurogenesis onset as well as the identity of generated neurons in the thalamus (Schlopp *et al.*, 2009). The role of Her6 in the zebrafish OE is not known and could be studied further to characterize GBC subtype clonality via grafting experiments or *in situ*.

Using their previously described CKII immunohistochemistry as a cell type-specific marker (Bali, 2015), SCs could be clearly identified to be positive for Sox2 expression in their nuclei in this study (Figure 4.7). Sox2-expressing basally located somata of SCs could be confidently identified and differentiated from HBCs using tissue dissociation experiments (Figure 4.8 and Figure 4.9). In addition, a characteristic low intensity response from SCs in the mid-sensory region can be seen throughout the sensory OE of the epithelial folds, which is expected as SCs constitute the suprabasal layer of Sox2-positive cells and have been shown to respond to purine compounds in rodents (Hegg *et al.*, 2003; Jia *et al.*, 2009) and *Xenopus* (Hassenklöver *et al.*, 2008). Due to their similar density (Bali, 2015), Sox2 immunoreactivity, position, and distribution within the tissue, SCs are the prime candidates to be the intermediate layer of ATP responding cells that show low response intensities.

In the framework of this study, I was able to characterize and identify the ATP sensitive non-neuronal cells as the SCs, GBCs and HBCs in the zebrafish OE. GBCs with rapid response onsets and high sensitivity to ATP are spatially restricted to the ILC and

SNS. At least in the ILC, the presence of a possible multipotent GBC progenitor type can be proposed, which is characterized by its differential 2-MeSATP sensitivity. HBCs and SCs are similarly distributed along the sensory OE and constitute basal and suprabasal layer of Sox2-expressing cells, respectively. HBCs can be distinguished by their horizontally elongated dimensions, and concurrent 2-MeSATP sensitivity. On the other hand, SCs have more columnar or tall pyramidal nuclear dimensions and show low intensity responses to ATP induction in the sensory region of the zebrafish OE.

## 5.2. ATP Selectively Modulates Maintenance Neurogenesis

Two lifelong neurogenesis events persist during adulthood in the vertebrate OE. Regenerative and maintenance neurogenesis can be classified not only by their dependence on the condition of the tissue, but also by the main progenitor pools that are actively involved in each process. A dual progenitor pool system can be found in basal layers of the vertebrate OE, which contribute separately to the two modes of neurogenesis. GBCs are involved in daily maintenance under physiological conditions (Schwartz-Levey *et al.*, 1991; Huard and Schwob, 1995), whereas HBCs are involved in global regeneration of the tissue upon injury (Holbrook *et al.*, 2007). Distinct from other vertebrate organisms studied so far, in the zebrafish OE, the daily generation of adult born OSNs takes place in radially segregated zones, the ILC and SNS, which are located at the periphery of the sensory OE. Neurogenic activity in these positions originates from resident *ascl1*-expressing GBCs (Bayramlı *et al.*, 2017; Demirler *et al.*, 2020). Unlike HBCs that are evenly distributed throughout sensory region (Demirler *et al.*, 2020; Kocagöz, 2021; Kocagöz *et al.*, under review), spatial restriction of GBCs (Bayramlı *et al.*, 2017) provides a unique way of identifying the mode of neurogenesis activity in the zebrafish OE based on where proliferating cells can be observed. Thus, effects of molecules on proliferative activity can be dissected by activated progenitor pools at distinct zones and categorized into either regenerative or maintenance neurogenesis modes exclusively in the zebrafish OE without a need of lineage tracing experiments, at least for some aspects of the process.

In this study, systemic injection of ATP promoted proliferative activity selectively from the ILC and SNS (Figure 4.11), where *ascl1*-expressing GBC progenitors reside.

Compared to PBS-injected control animals, the number of newborn OSNs showed the largest expansion with 1.4-fold increase in the ILC and 1.8-fold increase in the SNS at 72 hpi, while HBCs did not show any change and BrdU-only cells with ambiguous identity only showed increase in the SNS. HBC activation upon damage clearly shows their characteristic involvement in regenerative responses with the rapid expansion of the progenitor pool. Lack of HBC progenitor activity and neurogenic expansion restricted to the ILC and SNS with resident GBC progenitors suggest that ATP promotes cell proliferation exclusively from GBCs but not HBCs. The selective effect of exogenous ATP application is also supported by the reversal of this effect and a significant reduction of base level of proliferative activity and neurogenesis by the P2-type purine receptor blocker Suramin (Figure 4.11 and Figure 4.13). This effect further reinforces the concept of modulatory effect of purinergic signaling on GBC progenitor activity as a naturally occurring event under physiological conditions. The observed reduction in OSN neurogenesis following Suramin treatment strongly suggests that zebrafish GBCs receive tonic purinergic stimulation to maintain their baseline activity.

Modulatory effect of ATP also does not seem to result in neurogenesis by primarily promoting GBC progenitor pool expansion, since BrdU-only cells were only observed with increased numbers in the SNS, but not in the ILC. BrdU-only cells can be *ascl1*-expressing GBCs (Bayramlı *et al.*, 2017), neuronal precursors or newly generated SCs from ILC and SNS (Figure 4.31). The cell composition of the SNS (Figure 4.15, Figure 4.16, Figure 4.17), albeit not completely known, is found in this study to be more heterogenous than previously realized. Additionally, Suramin does not drastically change the number of BrdU-only cells (Figure 4.11 and Figure 4.13). This is rather interesting because especially in the ILC, GBCs can be activated with systemic application of ATP by intraperitoneal injection but does not show any expansion or depletion of the progenitor pool with applied Suramin. Number of BrdU-only cells observed in the ILC in any condition, could be explained by proposed 2-MeSATP responsive multipotent progenitor GBCs and newborn SCs under physiological conditions, as an increase in BrdU-positive SCs is also observed upon ATP application in the mouse OE which is reversible by Suramin (Jia *et al.*, 2009). The lineage origin of these newborn SCs, whether from basal progenitor cells or from a self-renewal process, is obscure.

In the zebrafish OE, activation of purinergic signaling differentially modulates progenitor activity in the ILC and SNS. Although exact data on SC number are missing in this experiment, the observed central displacement of OSNs from the SNS suggests the possibility that BrdU-only cells that exit the SNS are SCs. Using a 2-week BrdU pulse showed that newborn SCs strictly follow the OSN flow in the zebrafish OE (Figure 4.30). Thus, purinergic signaling probably modulates progenitor activity exclusively from fast-cycling GBCs that are committed to the OSN lineage in the ILC but may have a broader effect in the SNS that includes generation of SCs either by stimulating their division directly or changing the outcome of a multipotent progenitor lineage. Thus, if SCs indeed increased in numbers, this could be the indirect effect of increased neurogenesis if a multipotent lineage existed. Nevertheless, SC generation being closely related to daily OSN generation does not change, if not strengthen, the notion that purines, probably released from dying cells, signal the need for enhanced cell proliferation to maintain structural integrity of the zebrafish OE. Additional studies are required to pinpoint the specific progenitor pool that is responsible for the enhanced neurogenic activity and to understand the effect on and overlap between OSN and SC lineages.

### **5.3. HBC Dynamics Under Physiological Conditions**

In rodents, HBCs constitute a reserve stem cell niche (Schnittke *et al.*, 2015; Herrick *et al.*, 2017). Although HBCs are considered to be dormant progenitors under physiological conditions, there are also conflicting reports showing a low rate of proliferative activity once in every 60 days (Mackay-Sim and Kittel, 1991; Iwai *et al.*, 2009), or that HBCs undergo only two proliferation events and cease activity after 12 months (Leung *et al.*, 2007). On the other hand, injury activated HBCs can be identified by a morphology change from horizontal to apically elongated pyramidal profiles (Brann *et al.*, 2015), and forming up to 3 layers in the OE upon tissue damage (Leung *et al.*, 2007). HBCs have been shown to escape quiescence due to the loss of contact-dependent Notch signaling with SCs that regulates p63 expression (Packard *et al.*, 2011).

In the zebrafish OE, HBC progenitors show an unusually high mitotic activity under physiological conditions (Figure 4.22 and Figure 4.28), without any evidence of restricted generation zones, albeit a preference for HBC mitotic activity could be observed in the ILC and SNS. Short- and long-term lineage tracing experiments shows that continuous HBC proliferation with cycle times between 8 - 15 days mainly show symmetric division properties throughout the sensory region. The rate of proliferation shows a lower base activity within the core-sensory region (between 0.25-0.45 positions in the radial index) but twice the activity towards the ILC and SNS. Although HBCs show overall high turnover rate in the zebrafish OE, higher activity bias towards the zones with high base rate of proliferation could suggest a spatially localized regulation of proliferative activity at the ILC and SNS. Wnt/ $\beta$ -catenin signaling is common in active stem cell niches and has widely characterized implications in the regulation of breaking stem cell dormancy for self-renewal or lineage specific cell division in other adult tissue models (Clevers *et al.*, 2014; Fletcher *et al.*, 2017). Interestingly, in the zebrafish OE, active Wnt/ $\beta$ -catenin pathway can be observed from cells with horizontal dimensions at the basal layer mainly at the ILC and SNS under physiological conditions, and throughout sensory region from increased number of basal cells under damage conditions (Kocagöz *et al.*, under review). This discovery suggests that Wnt ligands could be regulating HBC activity, albeit from an unknown origin.

Not necessarily mutually exclusive with Wnt signaling, there is also the possibility that other, as of yet unknown, asymmetric division-promoting signals might be prevalent at the ILC and SNS. This is highly probable due to the consistently observed gradual morphological changes in Krt5 labeling in the SNS. HBCs with pyramidal morphologies and apical protrusions that are observed in this (Figure 4.17 and Figure 4.19) or other studies (Sakızlı, 2018; Demirlir *et al.*, 2020; Kocagöz, 2021; Kocagöz *et al.*, under review) shows that this change marks the beginning of the SNS from the mid-sensory side and suggests localized frequent asymmetric division of these progenitor cells under physiological conditions. In the ILC, Krt5 labeling occasionally shows apical protrusions but resident cells with pyramidal morphologies are never observed, different from the SNS. It has been demonstrated in the adult mouse brain that overexpression of cdk4/cyclinD1 leads to symmetric expansion of neural stem cell populations by shortening the G1 phase

(Lange *et al.*, 2009; Artegiani *et al.*, 2011), where *cdk4* loss is associated with differentiation and premature neurogenesis (Lim *et al.*, 2012).

Intriguingly, in the mouse OE, *cdk4* expression is upregulated upon selective ablation of neurons by axotomy but when coupled with selective macrophage depletion, *cdk4* levels does not show a similar increase in expression and lead to delayed neurogenesis (Bretchell *et al.*, 2007). This finding suggests that macrophages in the mouse OE could have neurogenesis promoting regulatory functions. Unfortunately, the study was not extended to show the proliferative activity of the progenitors. On the other hand, resident macrophages are observed in the OE of zebrafish larvae (Palominos and Whitlock, 2021), but studies in adult zebrafish are not available yet. Thus, external control of the speed of cell cycle in HBCs could also occur in the zebrafish OE in a spatially restricted fashion, promoting neurogenesis only in the ILC and SNS. The molecular underpinnings of such a regulation are, however, currently unknown.

#### **5.4. HBC-derived Cell Clones Provides Insights into the OSN Lineage under Physiological Conditions**

Cell clones been studied extensively in the rodent OE to dissect the lineage capacity of non-neuronal cell types (Schwob, 2016). All these studies were based on genetic manipulations, cell engrafting experiments, or cell culture experiments (Schwob, 2016), to demonstrate the clonality of non-neuronal cells and the identity of the cell types that can be generated from the colony forming cells or differentiated progenitors, which are in itself, a form of damage and does not mimic physiological conditions. For example, the multipotency of GBC progenitors in mice OE was demonstrated by engrafting the dissociated and sorted cells that were isolated by GBC-2 antibody reactivity (Chen *et al.*, 2004). Engrafted cells gave rise to all cell types that derive from the olfactory placode, displaying the multipotency of GBCs, whereas engrafted SCs and Bowman's duct and gland cells gave rise to only themselves, showing these cell types can self-originate (Chen *et al.*, 2004). The reserve stem cell capability of the HBCs, apart from extensive studies on damaged tissue, was also described using cell culture conditions (Satoh and Yoshida, 2000; Carter *et al.*, 2004), colony forming unit (CFU) assays by transplantation (Schwars-Levey

*et al.*, 1991; Huard and Schwob, 1995; Chen *et al.*, 2004; Schnittike *et al.*, 2015) and genetic manipulations (Packard *et al.*, 2011). Due to the basal restriction of all progenitors, studying the differential activity of progenitor pools is not possible without such manipulations in rodent models.

In this study, HBCs can be observed to show rare neurogenic activity in the zebrafish OE under physiological conditions. This is particularly interesting, as clones occurring at a distance from the ILC and SNS cannot originate from GBCs but can be attributed to HBC activity directly without transgenic lineage tracing. Clonality of the HBCs in the mid-sensory region can be detected using a combination of lineage tracers, such as BrdU and EdU. HBCs give rise to GBC-like cells (Figure 4.32), which eventually lead to neurogenesis (Figure 4.33). Although the same conclusion cannot be drawn with confidence for ILC-derived SCs without genetic manipulations, there is no evidence of SCs being included in HBC-derived lineages in the mid-sensory region under physiological conditions. On the other hand, quantification of HBC-derived clonal cell clusters may reveal insight into the lineage hierarchy of OSNs.

Even though HBC mitotic progenitor activity is high in the zebrafish OE, asymmetric divisions are a rare event with 3.7% incidence (out of 1368 HBCs in mid sensory region only 50 HBCs gave rise to clonal clusters), and the product of this division is most probably a fast-cycling GBC due to the neurogenic nature of the clonal clusters (bottom panel in Figure 4.33a and Figure 4.34). Fast cycling GBCs in the mid-sensory region were not detected by *in situ*-hybridization using probes to target *ascl1*-expression (Figure 4.5) (Bayramlı *et al.*, 2017), or may have been overlooked due to the rare occurrence of clonal HBC expansion. On the other hand, only one intermediate cell out of 191 cells measured in mid-sensory region for ATP sensitivity shows high intensity response (Figure 4.4) just like *ascl1*-expressing neurogenic GBC progenitors at the ILC and SNS (Figure 4.5). In addition, cell composition of clonal clusters analyzed in this study shows that, on average, for every clonal HBC, there are  $1.33 \pm 0.09$  GBCs and  $2.10 \pm 0.10$  OSNs, but for each cluster, GBCs diminish in numbers in the clusters with higher number of OSNs (Figure 4.34). However, it should be noted that these cell counts only reveal snapshots of the lower estimate due to the potential self-consuming nature of GBC divisions and cell cycle exit and terminal differentiation of transit amplifying cells. The lack of 2-MeSATP-responding

intermediate cells in the mid-sensory region also suggests that HBC-originated clonal GBCs do not necessarily have the same identity as the cells in the ILC. Before generating neurons, clonal GBCs are also observed to undergo at least one symmetric division (Figure 4.33a, top panel).

These results suggest that HBC originated clonal GBCs could be transient and deplete upon entering neurogenic lineage after undergoing at least one symmetric division event. This transient nature and rarity of HBC originated GBCs at any given time could explain the inability to detect them consistently in the mid-sensory region. On the other hand, higher mitotic activity coupled with more rigid external regulation in the ILC and SNS could support the steady availability of HBC and/or GBC progenitor pools found at these positions through population asymmetry (Simon and Clevers, 2011). Ultimately, the continuous HBC activity in the zebrafish OE could have an epithelial growth function in the zebrafish OE (Hansen and Zeiske, 1998) and postnatal mice, while asymmetric divisions in the ILC and SNS could fuel OSN neurogenesis in these positions.

### 5.5. SC Dynamics Under Physiological Conditions

In the rodent OE, apart from their self-renewal capabilities (Chen *et al.*, 2004), SCs have been shown to have a dual origin from GBC<sub>MPPS</sub> and duct cells (Schwob *et al.*, 1995; Huard *et al.*, 1998; Packard *et al.*, 2011). The main characteristic for SC differentiation is Hes1 expression by precursor cells (Herrick and Schwob, 2015). As previously discussed, most of these studies, if not all, perturbed the tissue to a level that is identical to a damage response and does not necessarily represent their accurate behavior under physiological conditions. This means, it can only be assumed that SCs arise from mainly GBC<sub>MPPS</sub> in the intact rodent OE, as GBCs fill the main progenitor niche in the intact OE (Packard *et al.*, 2011). In the damaged rodent OE, it is assumed that Bowman's gland duct cells can also give rise to SCs by the results obtained from grafting studies (Huard *et al.*, 1998), but substantially more evidence is available for HBC-originated SCs in the lesioned OE using genetic lineage tracing (Leung *et al.*, 2007; Iwai *et al.*, 2009; Schwob, 2016).

In the zebrafish OE lesioned with Triton X-100, a rapid expansion of newborn SCs in the sensory region at 24 hpl suggests that SCs can self-originate under regenerating conditions (Figure 4.20). In contrast, HBC activity mainly shows symmetric progenitor pool expansion over the same 24h timeframe (Kocagöz, 2021; Kocagöz *et al.*, under review).

Unfortunately, CKII labeling is not a reliable method to quantify SCs in the damaged OE as background and disorganized fiber arrangement increases significantly upon chemical treatment due to loss of structural integrity of the tissue, and studies on transgenic animals or a nuclear SC label will be necessary to observe whether SCs self-originate or not under damage conditions.

In the intact zebrafish OE, however, SCs follow centrally displacing OSNs, sometimes can even serve as a proxy of this displacement originating from the ILC and SNS (Figure 4.30). On the other hand, SCs do not proliferate in mid-sensory region like HBCs and are not generated by HBC-derived clonal clusters (Figure 4.34). Thus, it is highly unlikely that SCs can self-originate under physiological conditions, but instead are generated from spatially restricted generation zones in the OE similar to OSNs that are generated during daily maintenance neurogenesis. The lineage origin of SCs in the ILC remains obscure but proposed multipotent type GBC progenitor with concurrent 2-MeSATP sensitivity with high ATP response intensity could fill this niche similar to the GBC<sub>MPPS</sub> in the rodent OE.

The mitotic activity surrounding the SNS is a bit more complicated. Centrally displaced SCs also show nuclear translocation from intermediate layers in the SNS to basal layers towards mid-sensory regions (Figure 4.31b), suggesting an origin cell type that is located or dividing in the intermediate layer in the SNS. Intriguingly, different from HBCs or HBC-derived basal GBCs, cells with distinct morphology and marker expression characteristics are present in the SNS. These cells with unknown identity are distinguished by their somata in the intermediate layer, showing bipolar CKII immunoreactive extensions to both basal and apical end of the epithelium and polar Krt5 immunoreactivity at their basal portion (Figure 4.15 and Figure 4.16).

Due to their positions in the epithelium and identity different from HBCs, these cells could be the lineage origin of SCs in the SNS. Established polarity of these cells could suggest that upon asymmetric cell division in the vertical axis, daughter cell from the apical side could lose Krt5 expression and transform into either SC or a progenitor that can divide further to give rise to SCs. Due to the loss of the Krt5 basal anchor, these cells would undergo nuclear translocation towards basal side while displacing towards mid-sensory regions and become mature SCs with somata located in the suprabasal layer.

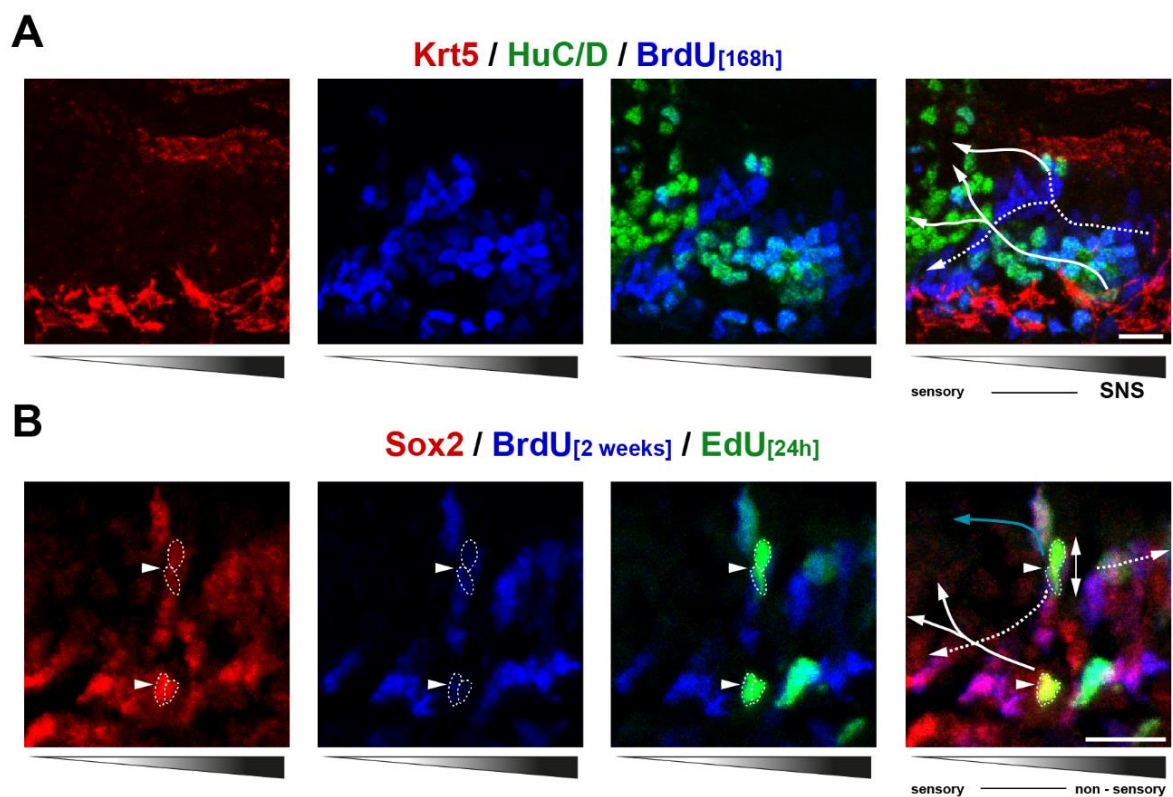


Figure 5.1. Distinct proliferation events taking place in the SNS under physiological conditions. A. Mid-sensory to SNS transition. B. Proposed basal neuronal and apical non-neuronal origin routes. Blue arrow: Alternative apical OSN route. Scale bars: 10  $\mu$ m.

Additionally, some high intensity ATP response profiles, not resembling multiple layers of cells, look more like elongated single cells or are localized in more intermediate strata of the epithelium in the SNS (arrowheads in Figure 4.4). These morphological characteristics also resemble the Krt5-immunoreactive basal portion of the Krt5/CKII double-positive cells at these locations. More globular and basally located high ATP response profiles are mutually exclusive from these cells and can still be observed in the SNS. In line with these observations, two separate lineages of BrdU-positive neuronal (green cells following full arrows) and non-neuronal (blue cells following dashed arrows) cells can be spotted and cross each other while exiting the SNS and displace towards mid-sensory region in the intact OEs subjected to 168h BrdU pulse (Figure 5.1a), suggesting a two-pronged proliferative activity to form neuronal and non-neuronal cell lineages. In line with previous observations, just like SCs, proxy cell of this SNS originated BrdU-positive cell group is a suprabasal cell with columnar nuclear morphology. Distinct proliferation events in intermediate and basal layers of the epithelium in the SNS can also be observed in the intact OE subjected to 2-week continuous BrdU pulse followed by intraperitoneally injected EdU and transferred to freshwater (arrowheads in Figure 5.1b). At 24 hpi (hours post EdU injection), two separate proliferation events (cells within dashed lines) can be observed in the intermediate layers and basal layer of the epithelium. These observations strengthen the possibility of a separate lineage origin for SCs in the zebrafish OE but require rigorous studies to confirm direct lineage relations.

### 5.6. A Proposed Maintenance Neurogenesis Model for the Zebrafish OE

The neurogenic events taking place in the intact OE can be summarized into the following model (Figure 5.2). There are two main neurogenic progenitor populations in the zebrafish OE, GBCs (Bayramlı *et al.*, 2017) and HBCs (Demirler *et al.*, 2020; Kocagöz, 2021). HBCs constitute the basal epithelial stratum that have discontinuous nuclear and cytoplasmic structures (Figure 4.1 and Figure 4.4) (Demirler *et al.*, 2020; Kocagöz, 2021) but are in contact to each other with horizontal protrusions strengthened with keratin (Figure 4.22a).

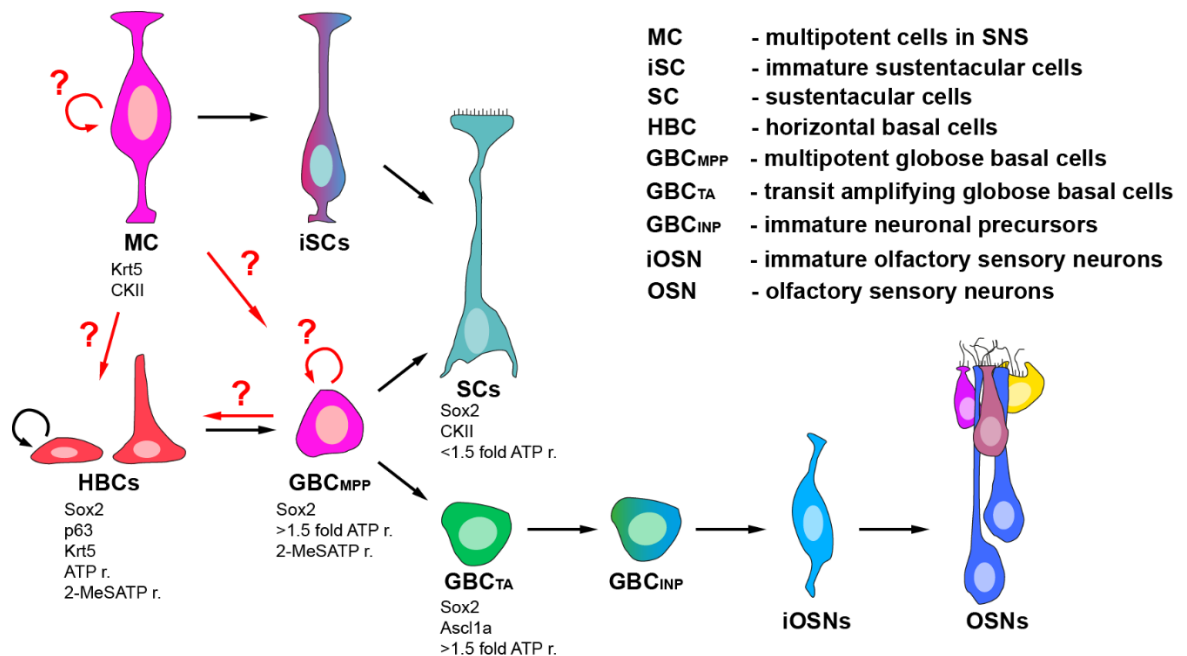


Figure 5.2. Lineage relation of different cell types in the zebrafish OE under physiological conditions. Red arrows represent currently unknown relations between progenitor cell types.

All HBCs divide within 8-15 days depending on their radial location in the zebrafish OE (Figure 4.22b). These cells predominantly divide symmetrically and form new HBCs to probably ensure the availability of a steady pool of dormant progenitors or to support continuous epithelial growth (Figure 4.21, Figure 4.27, and Figure 4.28). Incidentally, with

3-4% chance, HBCs can also divide asymmetrically in the mid sensory region (Figure 4.17b) and form GBC-like cells that do not have multipotency and cannot form SCs (clonal cluster in Figure 4.30a, Figure 4.33). Instead, asymmetrically dividing HBCs form probably *ascl1*-expressing fast cycling GBC progenitors (Bayramlı *et al.*, 2017) that may stay inactive for at least 3 days before division (Figure 4.33).

Clonal GBC proliferation in the ILC and SNS (Figure 4.33) might be dependent on the rate of OSN loss, which could be communicated by SCs through purinergic signaling (Demirler *et al.*, 2020). GBCs divide symmetrically once and may divide asymmetrically to form an immediate neuronal precursor (GBC<sub>INP</sub>) depending on the extent of neuronal loss. These GBCs eventually deplete in the mid-sensory region by turning into OSNs (Figure 4.34).

The main wave of OSNs in the zebrafish OE is generated by *ascl1*-expressing GBCs that are spatially restricted to two main neurogenic sites (Bayramlı *et al.*, 2017) (also see Figure 4.5 and Figure 4.11). First main residence of these cells is the tip of the centrally located ILC in the zebrafish OE, where they also show high intensity ATP responses. HBCs can also divide asymmetrically in the ILC (Figure 4.17b).

The product of this asymmetric division may also be 2-MeATP-sensitive cells in the suprabasal stratum (Figure 4.3). Although the presence of multipotent progenitor GBCs (GBC<sub>MPP</sub>) from the HBC lineage, or vice versa, in the zebrafish OE is still elusive, these cells could form the equivalent of the subpopulation of GBC<sub>MPP</sub> (one cell at a given time) of ATP-sensitive cells that exhibit >1.5 fold-increase in response intensity (two-three cells at most, Figure 4.3). These cells may generate SCs in ILC (Figure 4.30 and Figure 4.31) or *ascl1*-expressing GBCs. These 2-MeATP-sensitive cells may also give rise to SCs and OSNs. Other GBC subtypes formed by asymmetrically dividing HBCs could be responsible for only generating OSNs in the ILC. However, the concept that all GBCs located at the ILC and SNS are ultimately HBC derived cannot be ruled out. Newly formed cells then displace towards mid-sensory region, constituting the ILC-originated primary newborn cell wave.

The SNS is located around a position at two-thirds of the radial length of the zebrafish OE, which is marked by 0.65-0.75 radial positions in quantification method used (Demirler *et al.*, 2020). Lineage relationships in the SNS appear to be a bit more complicated as multiple mitotically active tissue layers and morphological cell types could be observed. HBCs that consistently show pyramidal morphologies with protrusions towards the middle epithelial strata could be evidence for the high rate of asymmetric division that fill a similar niche as in the ILC. Apart from only Krt5-expressing pyramidal HBCs that are located at the mid-sensory side of the SNS (arrows in Figure 4.17 and Figure 4.19), Krt5/CKII double-positive cells that show nuclear placement at the intermediate layers of epithelium and polarized Krt5-immunoreactivity at their basal segments, are located in the center of the SNS (asterisks in Figure 4.15b, Figure 4.16, Figure 4.17, and Figure 4.19, also see Figure 4.20). These double positive cells that have not previously been described, have higher nuclear positioning in the vertical axis (Figure 4.15 and Figure 4.16) and may undergo cell division in the apical-to-basal axis at the middle vertical positions or interkinetic nuclear movements. Adjacent and elongated Sox2/BrdU double-positive nuclei in middle epithelial strata that is distinct from the activity in the basal stratum, shares similarity with HBC or GBC activity (arrows in Figure 5.1b). These more apical divisions might be originating from, or generating a GBC<sub>MPP</sub> type progenitor, which could be identified by their high intensity ATP responses and apically elongated morphologies. Correlating with high intensity ATP responses, due to their distinct origin, GBC<sub>MPP</sub> might have elongated morphology in the vertical axis of the epithelium at the SNS (Figure 4.4).

These cells may give rise to the SC lineage (dashed route to the sensory) and maybe also to OSN lineages (colored full route in Figure 5.1b). Newborn SCs gradually translocate their nucleus towards mid-sensory region caused by the total loss of Krt5 expression (Figure 4.15), and fully mature into SCs (Figure 4.30 and Figure 4.31b). Unknown Krt5/CKII double-positive cells could also be generating the ciliated cells that eventually translocate their nucleus to the apical side towards non-sensory region (Figure 5.1b, dashed lines to the right) and show Krt5/CKII co-expression (Figure 4.15 and Figure 4.16).

It is uncertain if the proliferation events taking place in basal and intermediate layers in the SNS are linked to each other, since both events are taking place simultaneously and the 24 h analysis period used here is too long to dissect distinct events (Figure 5.1b). Apart from this caveat, Sox2/BrdU double-positive cells that are remnants of previous mitotic events can also be observed in between cells actively dividing in distinct layers. Thus, mitotic activity in the basally located HBCs or GBCs, and intermediate layers from cells with unknown identity may also originate from each other. Studies so far show a close relationship of basal activity with neurogenesis (Bayramlı *et al.*, 2017; Demirler *et al.*, 2020), and suggest a cell of origin for the SC lineage in the SNS at the intermediate layers (Figure 4.31b).

However, depending on the identity of the mitotically active cells in intermediate SNS layers, there could be an alternative explanation. Krt5/CKII double-positive cells could give rise to cells that are capable of generating a progenitor that has the capacity to make SCs and HBCs. One such cell type has been observed in the embryonic mouse OE, which has been called olfactory placodal progenitor GBCs (OPP/GBCs) (Packard *et al.*, 2011). OPP/GBCs are located at the more apical layers of the developing embryonic mouse OE and can give rise to cells expressing the lineage-specific markers p63, Hes1 or Ascl1, effectively covering both neuronal and non-neuronal lineages (Packard *et al.*, 2011). Intriguingly, during post-natal stages, basally translocating p63-expressing cells (Packard *et al.*, 2011) closely resemble the gradually changing morphology of HBCs at the SNS towards mid-sensory regions in the zebrafish OE (Figure 4.15b, Figure 4.16 and Figure 4.17b).

Thus, similar to the OPP/GBCs in the embryonic rodent OE (Packard *et al.*, 2011), the SNS in the zebrafish OE might have a progenitor population that is responsible for generating SCs in the intermediate layers with basally translocating nucleus, *Ascl1*-expressing GBCs, and also immature HBCs that require basal translocation which can be observed as gradual morphological changes with cell maturation towards mid-sensory. Thus, different from the ILC, the SNS may be a progenitor zone that has maintained embryonic characteristics and contributes to the persistent slow growth of the adult zebrafish OE. This might also explain the lack of more morphologically distinct HBCs in

the ILC, but does not change the fact that HBCs, under physiological conditions can give rise to GBCs in the zebrafish OE.

I propose the existence of a multipotent GBC type progenitor, a 2-MeSATP sensitive subgroup of cells with high sensitivity to ATP as the secondary progenitor cells during daily maintenance neurogenesis in the intact zebrafish OE. Products of GBC<sub>MPP</sub> proliferation are regulated by currently unknown means independently in the ILC and SNS to form GBCs in OSN or SC lineages, both of which are observed to be produced daily under physiological conditions and displace towards mid-sensory region. More frequently proliferating HBCs in the ILC and SNS can also contribute to neurogenesis. Alternatively, especially in the SNS, instead of GBC<sub>MPP</sub>, SC, OSNs and even HBCs could also be generated, eventually at low but persistent rate, by OPP/GBC-like multipotent stem cells. Newly generated and self-originating HBC populations, upon reaching a certain number, could trigger more frequent asymmetric divisions instead of self-renewal at the mid-sensory side of the SNS and contribute to daily neurogenesis from the basal layer under physiological conditions.

### 5.7. Transcriptome of the Lesioned OE Describes Distinct Phases of Regeneration

Transcriptome profiling and GO-term analysis was used in this study to analyze the different timepoints of de- and regeneration. K-means clustering is a method to reveal changes in gene expression patterns and to group subsets of genes by their similarity in behavior under different conditions (Ge *et al.*, 2018). The number of clusters can be increased or decreased to find the best fit but according to the elbow method, increased number of clusters decreases the reliability of the clustering analysis logarithmically, limits the number of meaningful groups (Ketchen and Shook, 1996). A number of 6 clusters best represent the patterns of differentially expressed genes at different regeneration timepoints (4, 12, 24, 72, 120 hpl). According to the similarity of gene expression pattern compared to intact tissue, early de- and late regeneration stages (4-12-24 hpl and 72-120 hpl) and immediate, early, and late response phases (4 hpl, 12-24 hpl and 72-120 hpl) can be observed.

The two main stages in this experiment can be identified as degeneration of the tissue at 4-12-24 hpl and regeneration at 72 and 120 hpl where the gene expression pattern of the intact tissue is partially regained. This distinction between de- and regeneration is correlated with the gradual loss and repopulation of OSNs in the zebrafish OE respectively (Kocagöz, 2021; Kocagöz *et al.*, under review). GO-term analysis on the six clusters also confirms the loss of OSNs and probably of cells with motile cilia in the non-sensory region (Hansen and Zeiske, 1998). The primary biological process and molecular function terms during the degeneration stage are related to sensory perception of odorants, intracellular trafficking and cilium organization and motility. On the other hand, non-motile cilium function is also implicated in the establishment of progenitor cell polarity and asymmetric divisions in vertebrate development (Levin *et al.*, 1995; Han and Buylla, 2010; Komatsu and Mishina, 2013), regenerating tissue (Jafaar-Marican *et al.*, 2016) and even in daily neurogenesis in the adult mouse hippocampus (Amador-Arjona *et al.*, 2011). During the degeneration stage, activation of HBCs, along with extension of apical protrusions, is observed to expand the progenitor pool (Figure 4.12 and Figure 4.19) (Kocagöz, 2021; Kocagöz *et al.*, under review). These progenitors are responsible for neurogenesis in the regeneration stage (Kocagöz, 2021; Kocagöz *et al.*, under review).

Thus, primary non-motile cilium related genes are not expected to have a major role during degeneration but could describe an increase in asymmetrically dividing progenitors after 72 hpl (Kocagöz, 2021; Kocagöz *et al.*, under review). Genes related to extracellular matrix organization and cell adhesion, are partially regained as early as 12 h, which is in line with acute loss of cell-to-cell contacts due to chemical lesion that could be regained by the rapid expansion of SCs (Figure 4.20).

According to the changes in gene expression patterns across samples, the 24 hpl timepoint is characterized by a breakpoint of upregulated responses upon chemical lesion. Three phases of regenerative neurogenesis responses are observed at 4 hpl as immediate, 12-24 hpl as early and at 72-120 hpl as late response phases by differentially upregulated gene expression patterns. KEGG pathways obtained from GO-term analysis on 4, 12 and 24 hpl timepoints shows externally activated cytokine, TGF- $\beta$  and Nod-like receptor signaling pathways and internal signal transduction Wnt/ $\beta$ -catenin and MAPK pathways seem to coordinate immediate and early responses in lesioned OE. Among these pathways, activated  $\beta$ -catenin is observed in activated progenitors upon damage in the zebrafish OE (Kocagöz *et al.*, under review), and in the mouse OE (Wang *et al.*, 2011; Chen *et al.*, 2014). Exogenous activation of Wnt/ $\beta$ -catenin signaling increases HBC proliferation and inhibition of Wnt signaling in the injured OE partially prevents the unfolding of a regenerative response (Eski, 2019). On the other hand, cytokine-cytokine receptor interaction is observed as the most significantly upregulated pathway across all samples and in the immediate and early regeneration phases in this study suggesting an acute activation of the immune system. Thus, one member of the identified upregulated cytokines was chosen for further functional analysis.

### 5.8. Regulatory Effect of IL-6 on the HBC Progenitor Pool

The pro-inflammatory cytokine *il6* is among the top upregulated genes across all samples and especially in the immediate and early regeneration response phases. *il6* is exclusively expressed upon tissue injury and no base expression can be detected in the zebrafish OE under physiological conditions. Broad-range of regenerative implications of IL-6 has been shown in tissue repair in multiple other research models that include partial hepatectomy or CCl<sub>4</sub>-induced liver injury (Cressman *et al.*, 1996; Taub *et al.*, 2004), cardiomyocyte proliferation during cardiac regeneration (Tang *et al.*, 2018), regeneration of injured intestinal mucosa (Neurath, 2014), and CNS axon regeneration (Leibinger *et al.*, 2013), which makes it an interesting candidate molecule to investigate that might be involved in the activation of regenerative neurogenesis responses in the OE.

Effect of IL-6 on the intact tissue was tested by nasally irrigating the zebrafish OE with 250 ng/μL recombinant human IL-6, followed by 24 h BrdU pulse and analyzed at 24 hpi to see the immediate effect on proliferation, or a 48 h BrdU pulse and analyzed at 72 hpi to see whether this effect is neurogenic by allowing newborn cells to differentiate into OSNs. IL-6 induced a 1.6-fold increase in cumulative proliferation activity evenly from each radial position along the epithelial folds without any noticeable neurogenic activity (Figure 4.40). A preliminary immunostaining against Krt5 and BrdU from one fish suggested that this increase in proliferation, especially in the mid-sensory OE can be attributed to expansion of the HBC pool (Figure 4.41). Analysis at 72 hpi showed a significant increase in total proliferation rate by 1.9-fold with a concomitant 2-fold increase in the number of newborn OSNs. A 2.4-fold increase in HBCs and 1.6-fold in GBCs, SCs and other non-neuronal cells cumulatively (BrdU- only positive cells) could also be observed (Figure 4.43). This increase was more pronounced in the ILC and SNS for OSNs and BrdU-only positive cells, but increased HBC activity was significant across all radial positions except only in one-third of the core sensory region (blue labeled numbers in the x-axis of graphs shown in Figure 4.44). Surprisingly, the increase in HBC activity in the mid-sensory OE is not followed by an increased number of OSNs, suggesting a specific effect of IL-6 induction on proliferation by triggering symmetric divisions of HBCs in the intact zebrafish OE.

This expansion of HBC pool could eventually lead to neurogenesis once IL-6 is no longer available in the tissue as pronounced during the late regeneration phase. An increase in newborn OSNs can be observed in the ILC and SNS along with BrdU-only positive cells, but activity or fate of SCs are still elusive and might be included in the BrdU-only positive population. HBC activity seems to be selectively higher at the SNS side, which could also suggest a localized enhanced effect of IL-6 induction.

IL-6 is expressed only upon tissue injury and stays at high levels in early phases of regenerative responses in the zebrafish OE (Figure 4.39). Resident low level of macrophages and neutrophils in intact tissues, can be activated upon disruption of tissue homeostasis such as damage (Eming *et al.*, 2017) and additional humoral or adaptive immune system cells can be recruited into the tissue from the blood circulation through released cytokines and chemokines (Godwin *et al.*, 2013; Mescher *et al.*, 2017; Huber-Lang *et al.*, 2018). Activated macrophages can release IL-6 in addition to various other pro-inflammatory cytokines (IL-1 $\beta$ , TNF), anti-inflammatory cytokines (TGF- $\beta$ , IL-10), chemokines, and proteolytic or anti-bacterial enzymes (Gordon *et al.*, 2017). In the larval zebrafish OE, resident neutrophils and macrophages have been demonstrated (Palominos and Whitlock, 2021) and involvement of macrophages has been established in various other zebrafish tissues during regeneration upon injury to CNS or peripheral tissues (Bohaud *et al.*, 2021). Thus, recruitment and/or activation of macrophages and neutrophils might be responsible for the release of IL-6 as an immediate response to chemical lesion to the zebrafish OE. In addition, previously discussed external regulation of higher asymmetric progenitor activity in the SNS through regulation of cdk4/cyclinD levels can also be explained by macrophages (Lange *et al.*, 2009; Artegiani *et al.*, 2011) in or around the adult zebrafish OE.

Tissue resident and circulating macrophages can be detected by immunostainings against cell type specific markers, such as the macrophage-expressed gene 1 (*mpeg1*) (Ellet *et al.*, 2011) or microfibrillar associated protein 4 (*mfap4*) (Walton *et al.*, 2015) in the zebrafish OE. Signal transduction of IL-6 requires two of each IL-6 effector molecules, the GP130 soluble signal transducing molecule and the IL6R $\alpha$  receptor, which forms a hexamer Jak-signal transducer molecule (Ward *et al.*, 1994), and internalized by STAT3 phosphorylation which can also drive *il6* expression by a feed-forward loop (Yu *et al.*, 2009; Chen *et al.*, 2012). If resident macrophages are present in the tissue, macrophage-derived IL-6 or IL-6 dependent IL-6 release can be tested by *in vitro* cell culture studies or pharmacological *in vivo* experiments. Immunostaining against receptor components and single cell transcriptomics for intact and injured OE could confirm the identity of IL-6-releasing and IL-6-responsive cells. If HBCs are a direct target of IL-6, inhibiting the signal transduction by blocking GP130 with bazedoxifene (Wei *et al.*, 2019), STAT3 with small molecule LLL12B (Chen *et al.*, 2021), or IL6R with tocilizumab (Ogata *et al.*, 2018) should prevent HBC activation and stall rapid expansion of the progenitor pool upon chemical lesion but should not change the HBC activity under physiological conditions, since *il6* expression is only available in the injured zebrafish OE.

Neurogenesis in the zebrafish OE is a complex process that involves the activity of multiple non-neuronal cell types and signaling routes. In the framework of this thesis study, the Sox-positive cell population that defines basal layers of the OE could be further dissected molecularly and functionally. Various signaling molecules and signaling pathways seem to selectively affect constitutively active and injury-sensitive progenitor pools. However, additional and important questions still remain, such as the exact lineage relationship of the distinct progenitor pools, and the identity and extend of external signals and/or cells that orchestrate differential activity progenitors under physiological conditions. A preliminary model of maintenance neurogenesis and cellular turnover in the intact OE could be developed that suggests the existence of a novel, yet to be characterized SC progenitor. The results of the studies presented here also imply that different molecular environments define unique and localized progenitor cell niches within the OE. Further molecular analysis will reveal the nature of these signals and how they contribute to balance OSN neurogenesis with the actual need of the tissue at different time points or under different conditions.

The concept of integral self-renewal and regenerative abilities have been developed by studying different organs and identifying distinct stem cell niches (Leblond and Walker, 1956). Distinct progenitor cells can be regulated externally to regain multipotency to initiate or extend the ability of tissue regeneration and sustainability of the stem cell niches in various tissue such as stomach, intestines and skin (Clevers *et al.*, 2014, Karin and Clevers, 2016).

Studying neurogenesis in the zebrafish OE, due to the unique distribution of neural progenitors in the tissue, could provide further insight on the differential regulation of stem cell niches. This thesis encompasses multiple aspects of regenerative studies. Functional characterization of non-neuronal cells, identification of possible progenitor cells and studies on the effect of various candidate regulatory molecules show that, in the zebrafish OE, progenitor cells are regulated by spatially restricted means. Results from this thesis, thus, can be utilized to generate more effective therapeutic strategies to negate neuronal loss or the activation of stem cell niches in neuronal tissues.

## REFERENCES

- Ahuja, G., I. Ivandić, M. Saltürk, Y. Oka, W. Nadler, and S. I. Korsching, 2013, “Zebrafish Crypt Neurons Project to a Single, Identified Mediodorsal Glomerulus.”, *Scientific Reports*, 3, no. 1.
- Ahuja, G., S. B. Nia, V. Zapilko, V. Shiriagin, D. Kowatschew, Y. Oka, and S. I. Korsching, 2014, “Kappe Neurons, a Novel Population of Olfactory Sensory Neurons.”, *Scientific Reports*, 4, no. 1.
- Ahuja, G., V. Reichel, D. Kowatschew, A. S. Syed, A. K. Kotagiri, Y. Oka, F. Weth, and S. I. Korsching, 2018, “Overlapping but Distinct Topology for Zebrafish V2R-like Olfactory Receptors Reminiscent of Odorant Receptor Spatial Expression Zones.”, *BMC Genomic*, 19, no. 1.
- Albeanu, D. F., A. C. Provost, P. Agarwal, E. R. Soucy, J. D. Zak, and V. N. Murthy, 2018, “Olfactory Marker Protein (OMP) Regulates Formation and Refinement of the Olfactory Glomerular Map.”, *Nature Communications*, 9, no. 1.
- Altman, J., 1969, “Autoradiographic and Histological Studies of Postnatal Neurogenesis. IV. Cell Proliferation and Migration in the Anterior Forebrain, with Special Reference to Persisting Neurogenesis in the Olfactory Bulb.”, *The Journal of Comparative Neurology*, 137, no. 4, pp. 433–57.
- Alunni, A., and L. Bally-Cuif, 2016, “A Comparative View of Regenerative Neurogenesis in Vertebrates.”, *Development*, 143, no. 5, pp. 741–53.
- Alunni, A., J. M. Hermel, A. Heuzé, F. Bourrat, F. Jamen, and J. S. Joly, 2010, “Evidence for Neural Stem Cells in the Medaka Optic Tectum Proliferation Zones.”, *Developmental Neurobiology*, 70, no. 10, pp. 693–713.

- Alvarez-Buylla, A., and D. A. Lim, 2004, “For the Long Run: Maintaining Germinal Niches in the Adult Brain.”, *Neuron*, 41, no. 5, pp. 683–686.
- Alvarez-Buylla, A., and J. M. García-Verdugo, 2002, “Neurogenesis in Adult Subventricular Zone.”, *The Journal of Neuroscience*, 22, no. 3, pp. 629–34.
- Amador-Arjona, A., J. Elliott, A. Miller, A. Ginbey, G. J. Pazour, G. Enikolopov, A. J. Roberts, and A. V. Terskikh, 2011, “Primary Cilia Regulate Proliferation of Amplifying Progenitors in Adult Hippocampus: Implications for Learning and Memory.”, *The Journal of Neuroscience*, 31, no. 27, pp. 9933–9944.
- Anders, S., P. T. Pyl, and W. Huber, 2014, “HTSeq, A Python Framework to Work with High-Throughput Sequencing Data.”, *Bioinformatics*, 31, no. 2, pp. 166–69.
- Artegiani, B., D. Lindemann, and F. Calegari, 2011, “Overexpression of cdk4 and cyclin1 Triggers Greater Expansion of Neural Stem Cells in the Adult Mouse Brain.”, *Journal of Experimental Medicine*, 208, no. 5, pp. 937–948.
- Baier, H., and S. Korsching, 1994, “Olfactory Glomeruli in the Zebrafish Form an Invariant Pattern and Are Identifiable across Animals.”, *The Journal of Neuroscience*, 14, no.1, pp. 219–230.
- Bali, B. “The Role of Sustentacular Cells in Adult Neurogenesis.”, M.Sc. Thesis, Boğaziçi University, 2015.
- Barker, N., J. H. van Es, J. Kuipers, P. Kujala, M. van den Born, M. Cozijnsen, A. Haegebarth, J. Korving, H. Begthel, P. J. Peters, and H. Clevers, 2007, “Identification of Stem Cells in Small Intestine and Colon by Marker Gene LGR5.”, *Nature*, 449, no. 7165, pp. 1003–1007.
- Barnea, G., S. O’Donnell, F. Mancia, X. Sun, A. Nemes, M. Mendelsohn, and R. Axel, 2004, “Odorant Receptors on Axon Termini in the Brain.”, *Science*, 304, no. 5676, p. 1468.

- Bauer, S., S. Rasika, J. Han, C. Mauduit, M. Raccurt, G. Morel, F. Jourdan, M. Benahmed, E. Moyse, and P. H. Patterson, 2003, “Leukemia Inhibitory Factor is a Key Signal for Injury-Induced Neurogenesis in the Adult Mouse Olfactory Epithelium.”, *The Journal of Neuroscience*, 23, no. 5, pp. 1792–1803.
- Baumgart, E. V., J. S. Barbosa, L. Bally-Cuif, M. Götz, and J. Ninkovic, 2011, “Stab Wound Injury of the Zebrafish Telencephalon: A Model for Comparative Analysis of Reactive Gliosis.”, *Glia*, 60, no. 3, pp. 343–57.
- Bayramli, X., Y. Kocagöz, U. Sakizli, and S. H. Fuss, 2017, “Patterned Arrangements of Olfactory Receptor Gene Expression in Zebrafish are Established by Radial Movement of Specified Olfactory Sensory Neurons.”, *Scientific Reports*, 7, no. 1.
- Bergmann, O., J. Liebl, S. Bernard, K. Alkass, M. S.Y. Yeung, P. Steier, W. Kutschera, L. Johnson, M. Landén, H. Druid, K. L. Spalding, J. Frisén, 2012, “The Age of Olfactory Bulb Neurons in Humans.”, *Neuron*, 74, no. 4, pp. 634–39.
- Bergmann, O., K. L. Spalding, and J. Frisén, 2015, “Adult Neurogenesis in Humans.”, *Cold Spring Harbor Perspectives in Biology*, 7, no. 7.
- Bernardos, R. L., L. K. Barthel, J. R. Meyers, and P. A. Raymond, 2007, “Late-Stage Neuronal Progenitors in the Retina Are Radial Muller Glia That Function as Retinal Stem Cells.”, *Journal of Neuroscience*, 27, no. 26, pp. 7028–7040.
- Bohauud, C., M. D. Johansen, C. Jorgensen, N. Ipseiz, L. Kremer, and F. Djouad, 2021, “The Role of Macrophages During Zebrafish Injury and Tissue Regeneration Under Infectious and Non-Infectious Conditions.”, *Frontiers in Immunology*, 12.
- Boldrini, M., C. A. Fulmore, A. N. Tartt, L. R. Simeon, I. Pavlova, V. Poposka, G. B. Rosoklija, A. Stankov, V. Arango, A. J. Dwork, R. Hen, and J. J. Mann, 2018, “Human Hippocampal Neurogenesis Persists throughout Aging.”, *Stem Cell*, 22, no. 4.

- Bolger, A. M., M. Lohse, and B. Usadel, 2014, "Trimmomatic: A Flexible Trimmer For Illumina Sequence Data.", *Bioinformatics*, 30, no. 15, pp. 2114–2120.
- Borders, A. S., M. L. Getchell, J. T. Etscheidt, N. van Rooijen, D. A. Cohen, and T. V. Getchell, 2007, "Macrophage Depletion in the Murine Olfactory Epithelium Leads to Increased Neuronal Death and Decreased Neurogenesis.", *The Journal of Comparative Neurology*, 501, no. 2, pp. 206–218.
- Brann, J. H., and S. J. Firestein, 2014, "A Lifetime of Neurogenesis in the Olfactory System.", *Frontiers in Neuroscience*, 8.
- Braubach, O. R., A. Fine, and R. P. Croll, 2012, "Distribution and Functional Organization of Glomeruli in the Olfactory Bulbs of Zebrafish (*Danio Rerio*).", *The Journal of Comparative Neurology*, 520, no. 11, pp. 2317–2339.
- Brechbuhl, J., M. Klaey, and M. C. Broillet, 2008, "Grueneberg Ganglion Cells Mediate Alarm Pheromone Detection in Mice.", *Science*, 321, no. 5892, pp.1092–1095.
- Buck, L. B., 2000, "The Molecular Architecture of Odor and Pheromone Sensing in Mammals.", *Cell*, 100, no. 6, pp. 611–618.
- Buck, L., and R. Axel, 1991, "A Novel Multigene Family May Encode Odorant Receptors: A Molecular Basis for Odor Recognition.", *Cell*, 65, no. 1, pp. 175–187.
- Burnstock, G., 2016, "An Introduction to the Roles of Purinergic Signalling in Neurodegeneration, Neuroprotection and Neuroregeneration.", *Pharmacology*, 104, pp. 4–17.
- Burnstock, G., 2016, "Short- and Long-Term (Trophic) Purinergic Signalling.", *Philosophical Transactions of the Royal Society B: Biological Sciences*, 371, no. 1700.

- Caggiano, M., J. S. Kauer, and D. D. Hunter, 1994, "Globose Basal Cells Are Neuronal Progenitors in the Olfactory Epithelium: A Lineage Analysis Using a Replication-Incompetent Retrovirus.", *Neuron*, 13, no. 2, pp. 339–352.
- Cajal, S. R. Y., 1913, *Degeneration & Regeneration of the Nervous System*. Oxford University Press, London.
- Calvo-Ochoa, E., C. A. Byrd-Jacobs, and S. H. Fuss, 2020, "Diving into the Streams and Waves of Constitutive and Regenerative Olfactory Neurogenesis: Insights from Zebrafish.", *Cell and Tissue Research*, 383, no. 1, pp. 227–253.
- Cao, X., L. P. Li, X. H. Qin, S. J. Li, M. Zhang, Q. Wang, H. H. Hu, Y. Y. Fang, Y. B. Gao, X. W. Li, L. R. Sun, W. C. Xiong, T. M. Gao, X. H. Zhu, 2013, "Astrocytic Adenosine 5'-Triphosphate Release Regulates the Proliferation of Neural Stem Cells in the Adult Hippocampus.", *Stem Cells*, 31, no. 8, pp. 1633–1643.
- Carter, L. A., A. J. Roskams, and J. L. MacDonald, 2004, "Olfactory Horizontal Basal Cells Demonstrate a Conserved Multipotent Progenitor Phenotype.", *Journal of Neuroscience*, 24, no. 25, pp. 5670–5683.
- Catania, S., A. Germanà, R. Laurà, T. Gonzalez-Martinez, E. Ciriaco, and J.A. Vega, 2003, "The Crypt Neurons in the Olfactory Epithelium of the Adult Zebrafish Express Trka-like Immunoreactivity.", *Neuroscience Letters*, 350, no. 1, pp. 5–8.
- Cau, E., G. Gradwohl, C. Fode, and F. Guillemot, 1997, "Mash1 Activates a Cascade of BHLH Regulators in Olfactory Neuron Progenitors.", *Development*, 124, no. 8, pp. 1611–1621.
- Cau, E., S. Casarosa, and G. François, 2002, "Mash1 and Ngn1 Control Distinct Steps of Determination and Differentiation in the Olfactory Sensory Neuron Lineage.", *Development*, 129, no. 8, pp. 1871–1880.

- Cayre, M., J. Malaterre, S. Scotto-Lomassese, C. Strambi, and A. Strambi, 2002, “The Common Properties of Neurogenesis in the Adult Brain: From Invertebrates to Vertebrates.”, *Comparative Biochemistry and Physiology Part B: Biochemistry and Molecular Biology*, 132, no. 1, pp. 1–15.
- Çelik, A., S. H. Fuss, and S. I. Korsching, 2002, “Selective Targeting of Zebrafish Olfactory Receptor Neurons by the Endogenous OMP Promoter.”, *European Journal of Neuroscience*, 15, no. 5, pp. 798–806.
- Chen, M., R. R. Reed, and A. P. Lane, 2017, “Acute Inflammation Regulates Neuroregeneration through the NF- $\kappa$ B Pathway in Olfactory Epithelium.”, *Proceedings of the National Academy of Sciences*, 114, no. 30, pp. 8089–8094.
- Chen, M., S. Tian, X. Yang, A. P. Lane, R. R. Reed, and H. Liu, 2014, “Wnt-Responsive Lgr5<sup>+</sup> Globose Basal Cells Function as Multipotent Olfactory Epithelium Progenitor Cells.”, *Journal of Neuroscience*, 34, no. 24, pp. 8268–8276.
- Chen, Q., H. Wang, Y. Liu, Y. Song, L. Lai, Q. Han, X. Cao, and Q. Wang, 2012, “Inducible MicroRNA-223 down-Regulation Promotes TLR-Triggered IL-6 and IL-1 $\beta$  Production in Macrophages by Targeting Stat3.”, *PLoS ONE* 7, no. 8.
- Chen, W. R., and G. M. Shepherd, 2005, “The Olfactory Glomerulus: A Cortical Module with Specific Functions.”, *Journal of Neurocytology*, 34, no. 3-5, pp. 353–360.
- Chen, X., H. Fang, and J. E. Schwob, 2004, “Multipotency of Purified, Transplanted Globose Basal Cells in Olfactory Epithelium.”, *The Journal of Comparative Neurology*, 469, no. 4, pp. 457–474.
- Chen, X., L. Pan, J. Wei, R. Zhang, X. Yang, J. Song, R. Bai, S. Fu, C. R. Pierson, J. L. Finlay, C. Li, and J. Lin, 2021, “LLL12B, a Small Molecule Stat3 Inhibitor, Induces Growth Arrest, Apoptosis, and Enhances Cisplatin-Mediated Cytotoxicity in Medulloblastoma Cells.”, *Scientific Reports*, 11, no. 1.

- Chen, Y., M. L. Getchell, X. Ding, and T. V. Getchell, 1992, “Immunolocalization of Two Cytochrome P450 Isozymes in Rat Nasal Chemosensory Tissue.”, *NeuroReport*, 3, no. 9, pp. 749–752.
- Chess, A., I. Simon, H. Cedar, and R. Axel, 1994, “Allelic Inactivation Regulates Olfactory Receptor Gene Expression.”, *Cell*, 78, no. 5, pp. 823–834.
- Christensen, M. D., E. H. Holbrook, R. M. Costanzo, and J. E. Schwob, 2001, “Rhintopy Is Disrupted during the Re-Innervation of the Olfactory Bulb That Follows Transection of the Olfactory Nerve.”, *Chemical Senses*, 26, no. 4, pp. 359–369.
- Clevers, H., K. M. Loh, and R. Nusse, 2014, “An Integral Program for Tissue Renewal and Regeneration: Wnt Signaling and Stem Cell Control.”, *Science*, 346, no. 6205.
- Costanzo, R. M., 1985, “Neural Regeneration and Functional Reconnection Following Olfactory Nerve Transection in Hamster.”, *Brain Research*, 361, no. 1, 2, pp. 258–266.
- Costanzo, R. M., and P. P. Graziadei, 1983, “A Quantitative Analysis of Changes in the Olfactory Epithelium Following Bulbectomy in Hamster.”, *The Journal of Comparative Neurology*, 215, no. 4, pp. 370–381.
- Cressman, D. E., L. E. Greenbaum, R. A. DeAngelis, G. Ciliberto, E. E. Furth, V. Poli, and R. Taub, 1996, “Liver Failure and Defective Hepatocyte Regeneration in Interleukin-6-Deficient Mice.”, *Science*, 274, no. 5291, pp. 1379–1383.
- Dang, P., S. A. Fisher, D. J. Stefanik, J. Kim, and J. A. Raper, 2018, “Coordination of Olfactory Receptor Choice with Guidance Receptor Expression and Function in Olfactory Sensory Neurons.”, *PLOS Genetics*, 14, no. 1.
- de Miranda, A. S., C. J. Zhang, A. Katsumoto, and A. L. Teixeira, 2017, “Hippocampal Adult Neurogenesis: Does the Immune System Matter?”, *Journal of the Neurological Sciences*, 372.

- Demirler, M. C., U. Sakizli, B. Bali, Y. Kocagöz, S. E. Eski, A. Ergönen, A. S. Alkiraz, X. Bayramli, T. Hassenklöver, I. Manzini, and S. H. Fuss, 2020, “Purinergic Signalling Selectively Modulates Maintenance but Not Repair Neurogenesis in the Zebrafish Olfactory Epithelium.”, *The FEBS Journal* 287, no. 13, pp. 2699–2722.
- Deng, W., J. B. Aimone, and F. H. Gage, 2010, “New Neurons and New Memories: How Does Adult Hippocampal Neurogenesis Affect Learning and Memory?”, *Nature Reviews Neuroscience*, 11, no. 5, pp. 339–350.
- Dietrich, D. R., 1993, “Toxicological and Pathological Applications of Proliferating Cell Nuclear Antigen (PCNA), a Novel Endogenous Marker for Cell Proliferation.”, *Critical Reviews in Toxicology*, 23, no. 1, pp. 77–109.
- Ding, X., and M. J. Coon, 1988, “Purification and Characterization of Two Unique Forms of Cytochrome p-450 from Rabbit Nasal Microsomes.”, *Biochemistry*, 27, no. 22, pp. 8330–8337.
- Ding, X., T. D. Porter, H. M. Peng, and M. J. Coon, 1991, “CDNA and Derived Amino Acid Sequence of Rabbit Nasal Cytochrome p450nmb (p450iig1), a Unique Isozyme Possibly Involved in Olfaction.”, *Archives of Biochemistry and Biophysics*, 285, no. 1, pp. 120–125.
- Dirian, L., S. Galant, M. Coolen, W. Chen, S. Bedu, C. Houart, L. Bally-Cuif, and I. Foucher, 2014, “Spatial Regionalization And Heterochrony in the Formation of Adult Pallial Neural Stem Cells.”, *Developmental Cell*, 30, no. 2, pp. 123–136.
- Dittrich, K., A. Sansone, T. Hassenklöver, and I. Manzini, 2014, “Purinergic Receptor-Induced Ca<sup>2+</sup> Signaling in The Neuroepithelium of the Vomeronasal Organ of Larval *Xenopus Laevis*.”, *Purinergic Signalling*, 10, no. 2, pp. 327–336.
- Doetsch, F., I. Caillé, D. A. Lim, J. M. García-Verdugo, and A. Alvarez-Buylla, 1999, “Subventricular Zone Astrocytes Are Neural Stem Cells in the Adult Mammalian Brain.”, *Cell*, 97, no. 6, pp. 703–716.

- Ekdahl, C. T., J. H. Claasen, S. Bonde, Z. Kokaia, and O. Lindvall, 2003, “Inflammation Is Detrimental for Neurogenesis in Adult Brain.”, *Proceedings of the National Academy of Sciences*, 100, no. 23, pp. 13632–13637.
- Ellett, F., L. Pase, J. W. Hayman, A. Andrianopoulos, and G. J. Lieschke, 2011, “Mpeg1 Promoter Transgenes Direct Macrophage-Lineage Expression in Zebrafish.”, *Blood*, 117, no. 4.
- Eming, S. A., T. A. Wynn, and P. Martin, 2017, “Inflammation and Metabolism in Tissue Repair and Regeneration.”, *Science*, 356, no. 6342, pp. 1026–1030.
- Eriksson, P. S., E. Perfilieva, T. Björk-Eriksson, A. M. Alborn, C. Nordborg, D. A. Peterson, and F. H. Gage, 1998, “Neurogenesis in the Adult Human Hippocampus.”, *Nature Medicine*, 4, no. 11, pp. 1313–1317.
- Eski, S. E. “The Role of Wnt Signaling during Regenerative Neurogenesis in the Zebrafish Olfactory Epithelium.”, M.Sc. Thesis, Boğaziçi University, 2019.
- Farbman, A. I., and J. A. Buchholz, 1996, “Transforming Growth Factor-Alpha and Other Growth Factors Stimulate Cell Division in Olfactory Epithelium in Vitro.”, *Journal of Neurobiology*, 30, no. 2, pp. 267–280.
- Fausett, B. V., and D. Goldman, 2006, “A Role for  $\beta$  Tubulin-Expressing Muller Glia IN Regeneration of the Injured Zebrafish Retina.”, *Journal of Neuroscience*, 26, no. 23, pp. 6303–6313.
- Fausett, B. V., J. D. Gumerson, and D. Goldman, 2008, “The Proneural Basic Helix-Loop-Helix Gene ASCL1A Is Required for Retina Regeneration.”, *Journal of Neuroscience*, 28, no. 5, pp. 1109–1117.
- Feliciano, D. M., A. Bordey, and L. Bonfanti, 2015, “Noncanonical Sites of Adult Neurogenesis in the Mammalian Brain.”, *Cold Spring Harbor Perspectives in Biology*, 7, no. 10.

- Fleischer, J., K. Schwarzenbacher, and H. Breer, 2007, “Expression of Trace Amine-Associated Receptors in the Grueneberg Ganglion.”, *Chemical Senses*, 32, no. 6, pp. 623–631.
- Fleischmann, A., B. M. Shykind, D. L. Sosulski, K. M. Franks, M. E. Glinka, D. F. Mei, Y. Sun, J. Kirkland, M. Mendelsohn, M. W. Albers, and R. Axel, 2008, “Mice with a ‘Monoclonal Nose’: Perturbations in an Olfactory Map Impair Odor Discrimination.”, *Neuron*, 60, no. 6, pp. 1068–1081.
- Fletcher, R. B., D. Das, L. Gadye, K. N. Street, A. Baudhuin, A. Wagner, M. B. Cole, Q. Flores, Y. G. Choi, N. Yosef, E. Purdom, S. Dudoit, D. Risso, J. Ngai, 2017, “Deconstructing Olfactory Stem Cell Trajectories at Single-Cell Resolution.”, *Stem Cell*, 20, no. 6, pp. 817–830.
- Fletcher, R. B., M. S. Prasol, J. Estrada, A. Baudhuin, K. Vranizan, Y. G. Choi, and J. Ngai, 2011, “P63 Regulates Olfactory Stem Cell Self-Renewal and Differentiation.”, *Neuron*, 72, no. 5, pp. 748–759.
- Friedrich, R. W., and S. I. Korsching, 1998, “Chemotopic, Combinatorial, and Noncombinatorial Odorant Representations in the Olfactory Bulb Revealed Using a Voltage-Sensitive Axon Tracer.”, *The Journal of Neuroscience*, 18, no. 23, pp. 9977–9988.
- Frisch, D., 1967, “Ultrastructure of Mouse Olfactory Mucosa.”, *American Journal of Anatomy*, 121, no. 1, pp. 87–119.
- Furukawa, T., S. Mukherjee, Z. Bao, E. M. Morrow, and C. L. Cepko, 2000, “Rax, hes1, and notch1 Promote the Formation of Müller Glia by Postnatal Retinal Progenitor Cells.”, *Neuron*, 26, no. 2, pp. 383–394.
- Gage, F. H., 2000, “Mammalian Neural Stem Cells.”, *Science*, 287, no. 5457, pp. 1433–1438.

- Gallagher, D., A. A. Norman, C. L. Woodard, G. Yang, A. Gauthier-Fisher, M. Fujitani, J. P. Vessey, G. I. Cancino, N. Sachewsky, K. Woltjen, M. P. Fatt, C. M. Morshead, D. R. Kaplan, F. D. Miller, 2013, “Transient Maternal IL-6 Mediates Long-Lasting Changes in Neural Stem Cell Pools by Deregulating an Endogenous Self-Renewal Pathway.”, *Stem Cell*, 13, no. 5, pp. 564–76.
- Ge, S. X., E. W. Son, and R. Yao, 2018, “IDEP: An Integrated Web Application for Differential Expression and Pathway Analysis of Rna-Seq Data.”, *Bioinformatics*, 19, no. 1.
- Germanà, A., G. Montalbano, R. Laurà, E. Ciriaco, M. E. del Valle, and J. A. Vega, 2004, “S100 Protein-like Immunoreactivity in the Crypt Olfactory Neurons of the Adult Zebrafish.”, *Neuroscience Letters*, 371, no. 2, 3, pp. 196–198.
- Getchell, T. V., R. K. Narla, S. Little, J. F. Hyde, and M. L. Getchell, 2000, “Horizontal Basal Cell Proliferation in the Olfactory Epithelium of Transforming Growth Factor- $\alpha$  Transgenic Mice.”, *Cell and Tissue Research*, 299, no. 2, pp. 185–92.
- Glinka, M. E., B. A. Samuels, A. Diodato, J. Teillon, D. F. Mei, B. M. Shykind, R. Hen, and A. Fleischmann, 2012, “Olfactory Deficits Cause Anxiety-like Behaviors in Mice.”, *Journal of Neuroscience*, 32, no. 19, pp. 6718–6725.
- Godwin, J. W., A. R. Pinto, and N. A. Rosenthal, 2013, “Macrophages Are Required for Adult Salamander Limb Regeneration.”, *Proceedings of the National Academy of Sciences*, 110, no. 23, pp. 9415–9420.
- Goldman, D., 2014, “Müller Glial Cell Reprogramming and Retina Regeneration.”, *Nature Reviews Neuroscience*, 15, no. 7, pp. 431–442.
- Goldstein, B. J., H. Fang, S. L. Youngentob, and J. E. Schwob, 1998, “Transplantation of Multipotent Progenitors from the Adult Olfactory Epithelium.”, *NeuroReport*, 9, no. 7, pp. 1611–1617.

- Gonçalves, J. T., S. T. Schafer, and F. H. Gage, 2016, “Adult Neurogenesis in the Hippocampus: From Stem Cells to Behavior.”, *Cell*, 167, no. 4, pp. 897–914.
- Gordon, S., and F. O. Martinez, 2010, “Alternative Activation of Macrophages: Mechanism and Functions.”, *Immunity*, 32, no. 5, pp. 593–604.
- Gould, A. C., M. Haulena, M. Pawlik, V. LePage, A. Mareschal, M. R. M. Manalang, and H. Snyman, 2020, “Rare Neural Crest Tumor in Teleost Species: Olfactory Neuroblastoma in a Spotted Pike-Characin *Boulengerella Maculata*.”, *Diseases of Aquatic Organisms*, 138, pp. 29–33.
- Graziadei, P. P., and G. A. Monti Graziadei, 1978, “Continuous Nerve Cell Renewal in the Olfactory System.”, *Handbook of Sensory Physiology*, pp. 55–83.
- Graziadei, P. P., and G. A. Monti Graziadei, 1979, “Neurogenesis and Neuron Regeneration in the Olfactory System of Mammals. I. Morphological Aspects of Differentiation and Structural Organization of the Olfactory Sensory Neurons.”, *Journal of Neurocytology*, 8, no. 1, pp. 1–18.
- Graziadei, P. P., and G. A. Monti Graziadei, 1980, “Neurogenesis and Neuron Regeneration in the Olfactory System of Mammals. III. Deafferentation and Reinnervation of the Olfactory Bulb Following Section of Thefila Olfactoria in Rat.”, *Journal of Neurocytology*, 9, no. 2, pp. 145–162.
- Grosmaître, X., L. C. Santarelli, J. Tan, M. Luo, and M. Ma, 2007, “Dual Functions of Mammalian Olfactory Sensory Neurons as Odor Detectors and Mechanical Sensors.”, *Nature Neuroscience*, 10, no. 3, pp. 348–354.
- Guo, Z., A. Packard, R. C. Krolewski, M. T. Harris, G. L. Manglapus, and J. E. Schwob, 2010, “Expression of Pax6 and Sox2 in Adult Olfactory Epithelium.”, *The Journal of Comparative Neurology*, 518, no. 21, pp. 4395–4418.

- Han, Y., and A. Alvarez-Buylla, 2010, "Role of Primary Cilia in Brain Development and Cancer.", *Current Opinion in Neurobiology*, 20, no. 1, pp. 58–67.
- Hansen, A., and E. Zeiske, 1998, "The Peripheral Olfactory Organ of the Zebrafish, *Danio Rerio*: An Ultrastructural Study.", *Chemical Senses*, 23, no. 1, pp. 39–48.
- Hassenklöver, T., P. Schwartz, D. Schild, and I. Manzini, 2009, "Purinergic Signaling Regulates Cell Proliferation of Olfactory Epithelium Progenitors.", *Stem Cells*, 27, no. 8, pp. 2022–2031.
- Hassenklöver, T., S. Kurtanska, I. Bartoszek, S. Junek, D. Schild, and I. Manzini, 2008, "Nucleotide-Induced  $Ca^{2+}$  Signaling in Sustentacular Supporting Cells of the Olfactory Epithelium.", *Glia*, 56, no. 15, pp. 1614–1624.
- Hayashi, K., K. Kubo, A. Kitazawa, and K. Nakajima, 2015, "Cellular Dynamics of Neuronal Migration in the Hippocampus.", *Frontiers in Neuroscience*, 9.
- Hegg, C. C., D. Greenwood, W. Huang, P. Han, and M. T. Lucero, 2003, "Activation of Purinergic Receptor Subtypes Modulates Odor Sensitivity.", *The Journal of Neuroscience*, 23, no. 23, pp. 8291–8301.
- Hegg, C. C., M. Irwin, and M. T. Lucero, 2009, "Calcium Store-Mediated Signaling in Sustentacular Cells of the Mouse Olfactory Epithelium.", *Glia*, 57, no. 6, pp. 634–644.
- Herrick, D. B., B. Lin, J. Peterson, N. Schnittke, and J. E. Schwob, 2017, "Notch1 Maintains Dormancy of Olfactory Horizontal Basal Cells, a Reserve Neural Stem Cell.", *Proceedings of the National Academy of Sciences*, 114, no. 28.
- Hinds, J. W., P. L. Hinds, and N. A. McNelly, 1984, "An Autoradiographic Study of the Mouse Olfactory Epithelium: Evidence for Long-Lived Receptors.", *The Anatomical Record*, 210, no. 2, pp. 375–383.

- Holbrook, E. H., K. E. Szumowski, and J. E. Schwob, 1995, “An Immunochemical, Ultrastructural, and Developmental Characterization of the Horizontal Basal Cells of Rat Olfactory Epithelium.”, *The Journal of Comparative Neurology*, 363, no. 1, pp. 129–146.
- Holtmaat, A. J., P. A. Dijkhuizen, A. B. Oestreicher, H. J. Romijn, N. M. Van der Lugt, A. Berns, F. L. Margolis, W. H. Gispen, and J. Verhaagen, 1995, “Directed Expression of the Growth-Associated Protein B-50/GAP-43 to Olfactory Neurons in Transgenic Mice Results in Changes in Axon Morphology and Extraglomerular Fiber Growth.”, *The Journal of Neuroscience*, 15, no. 12, pp. 7953–7965.
- Horvitz, H. R., and I. Herskowitz, 1992, “Mechanisms of Asymmetric Cell Division: Two BS or Not Two BS, That Is the Question.”, *Cell*, 68, no. 2, pp. 237–255.
- Huard, J. M. T., S. L. Youngentob, B. J. Goldstein, M. B. Luskin, and J. E. Schwob, 1998, “Adult Olfactory Epithelium Contains Multipotent Progenitors That Give Rise to Neurons and Non-Neural Cells.”, *The Journal of Comparative Neurology*, 400, no. 4, pp. 469–486.
- Huard, J. M., and J. E. Schwob, 1995, “Cell Cycle of Globose Basal Cells in Rat Olfactory Epithelium.”, *Developmental Dynamics*, 203, no. 1, pp. 17–26.
- Huber-Lang, M., J. D. Lambris, and P. A. Ward, 2018, “Innate Immune Responses to Trauma.”, *Nature Immunology*, 19, no. 4, pp. 327–341.
- Hussain, A., L. R. Saraiva, and S. I. Korsching, 2009, “Positive Darwinian Selection and the Birth of an Olfactory Receptor Clade in Teleosts.”, *Proceedings of the National Academy of Sciences*, 106, no. 11, pp. 4313–4318.
- Inaba, M., and Y. M. Yamashita, 2012, “Asymmetric Stem Cell Division: Precision for Robustness.”, *Stem Cell*, 11, no. 4, pp. 461–469.

- Inta, D., H. A. Cameron, and P. Gass, 2015, “New Neurons in the Adult Striatum: From Rodents to Humans.”, *Trends in Neurosciences*, 38, no. 9, pp. 517–523.
- Iqbal, T., and C. Byrd-Jacobs, 2010, “Rapid Degeneration and Regeneration of the Zebrafish Olfactory Epithelium after Triton X-100 Application.”, *Chemical Senses*, 35, no. 5, pp. 351–361.
- Iwai, N., Z. Zhou, D. R. Roop, and R. R. Behringer, 2008, “Horizontal Basal Cells Are Multipotent Progenitors in Normal and Injured Adult Olfactory Epithelium.”, *Stem Cell*, 26, no. 5, pp. 1298–1306.
- Jaafar Marican, N. H., S. B. Cruz-Migoni, and A. Borycki, 2016, “Asymmetric Distribution of Primary Cilia Allocates Satellite Cells for Self-Renewal.”, *Stem Cell Reports*, 6, no. 6, pp. 798–805.
- Jaks, V., N. Barker, M. Kasper, J. H. van Es, H. J. Snippert, H. Clevers, and R. Toftgård, 2008, “LGR5 Marks Cycling, Yet Long-Lived, Hair Follicle Stem Cells.”, *Nature Genetics*, 40, no. 11, pp. 1291–1299.
- Jang, W., S. L. Youngentob, and J. E. Schwob, 2003, “Globose Basal Cells Are Required for Reconstitution of Olfactory Epithelium after Methyl Bromide Lesion.”, *The Journal of Comparative Neurology*, 460, no. 1, pp. 123–140.
- Jia, C., A. R. Cussen, and C. C. Hegg, 2011, “ATP Differentially Upregulates Fibroblast Growth Factor 2 and Transforming Growth Factor Alpha in Neonatal and Adult Mice: Effect on Neuroproliferation.”, *Neuroscience*, 177, pp. 335–346.
- Jia, C., J. P. Doherty, S. Crudginton, and C. C. Hegg, 2009, “Activation of Purinergic Receptors Induces Proliferation and Neuronal Differentiation in Swiss Webster Mouse Olfactory Epithelium.”, *Neuroscience*, 163, no. 1, pp. 120–128.
- Jin, X., 2016, “The Role of Neurogenesis during Development and in the Adult Brain.”, *European Journal of Neuroscience*, 44, no. 6, pp. 2291–2299.

- John, J. A., and B. Key, 2003, "Axon Mis-Targeting in the Olfactory Bulb during Regeneration of Olfactory Neuroepithelium.", *Chemical Senses*, 28, no. 9, pp. 773–779.
- Johnson, M. A., L. Tsai, D. S. Roy, D. H. Valenzuela, C. Mosley, A. Magklara, S. Lomvardas, S. D. Liberles, and G. Barnea, 2012, "Neurons Expressing Trace Amine-Associated Receptors Project to Discrete Glomeruli and Constitute an Olfactory Subsystem.", *Proceedings of the National Academy of Sciences*, 109, no. 33, pp. 13410–13415.
- Kaneko, N., M. Sawada, and K. Sawamoto, 2017, "Mechanisms of Neuronal Migration in the Adult Brain.", *Journal of Neurochemistry*, 141, no. 6, pp. 835–847.
- Kaplan, M. S., 1981, "Neurogenesis in the 3-Month-Old Rat Visual Cortex.", *The Journal of Comparative Neurology*, 195, no. 2, pp. 323–338.
- Kaplan, M. S., 1983, "Proliferation of Subependymal Cells in the Adult Primate CNS: Differential Uptake of DNA Labelled Precursors.", *Journal für Hirnforschung*, 1, no. 24, pp. 23–33.
- Kaplan, M. S., and J. W. Hinds, 1977, "Neurogenesis in the Adult Rat: Electron Microscopic Analysis of Light Radioautographs.", *Science*, 197, no. 4308, pp. 1092–1094.
- Karin, M., and H. Clevers, 2016, "Reparative Inflammation Takes Charge of Tissue Regeneration.", *Nature*, 529, no. 7586, pp. 307–315.
- Ketchen Jr., D. J., and C. L. Shook, 1996, "The Application of Cluster Analysis in Strategic Management Research: An Analysis and Critique.", *Strategic Management Journal*, 17, no. 6, pp. 441–458.
- Kim, D., B. Langmead, and S. L. Salzberg, 2015, "Hisat: A Fast Spliced Aligner with Low Memory Requirements.", *Nature Methods*, 12, no. 4, pp. 357–360.

- Kim, E. J., P. J. Simpson, D. J. Park, B. Q. Liu, G. V. Ronnett, and C. Moon, 2005, “Leukemia Inhibitory Factor Is a Proliferative Factor for Olfactory Sensory Neurons.”, *NeuroReport*, 16, no. 3, pp. 25–28.
- Kimbell, J. S., M. N. Godo, E. A. Gross, D. R. Joyner, R. B. Richardson, and K. T. Morgan, 1997, “Computer Simulation of Inspiratory Airflow in All Regions of the F344 Rat Nasal Passages.”, *Toxicology and Applied Pharmacology*, 145, no. 2, pp. 388–398.
- Kizil, C., J. Kaslin, V. Kroehne, and M. Brand, 2012, “Adult Neurogenesis and Brain Regeneration in Zebrafish.”, *Developmental Neurobiology*, 72, no. 3, pp. 429–461.
- Kocagöz, Y. “Cellular and Molecular Analysis of Regenerative Neurogenesis in The Zebrafish (*Danio Rerio*) Olfactory Epithelium.”, Ph.D. Thesis, Boğaziçi University, 2021.
- Komatsu, Y., and Y. Mishina, 2013, “Establishment of Left–Right Asymmetry in Vertebrate Development: The Node in Mouse Embryos.”, *Cellular and Molecular Life Sciences*, 70, no. 24, pp. 4659–4666.
- Koo, J. W., and R. S. Duman, 2008, “IL-1 Is an Essential Mediator of the Antineurogenic and Anhedonic Effects of Stress.”, *Proceedings of the National Academy of Sciences*, 105, no. 2, pp. 751–756.
- Kopylova, E., L. Noé, and H. Touzet, 2012, “SortMeRNA: Fast and Accurate Filtering of Ribosomal RNAs IN Metatranscriptomic Data.”, *Bioinformatics*, 28, no. 24, pp. 3211–17.
- Kristensson, K., W. Masocha, and M. Bentivoglio, 2013, “Mechanisms of CNS Invasion and Damage by Parasites.”, *Neuroparasitology and Tropical Neurology*, pp. 11–22.

- Krolewski, R. C., A. Packard, W. Jang, H. Wildner, and J. E. Schwob, 2012, “Ascl1 (Mash1) Knockout Perturbs Differentiation of Nonneuronal Cells in Olfactory Epithelium.”, *PLoS ONE*, 7, no. 12.
- Kuhn, H. G., H. Dickinson-Anson, and F. H. Gage, 1996, “Neurogenesis in the Dentate Gyrus of the Adult Rat: Age-Related Decrease of Neuronal Progenitor Proliferation.”, *The Journal of Neuroscience*, 16, no. 6, pp. 2027–2033.
- Kukekov, V. G., E. D. Laywell, O. Suslov, K. Davies, B. Scheffler, L. B. Thomas, T. F. O'Brien, M. Kusakabe, and D. A. Steindler, 1999, “Multipotent Stem/Progenitor Cells with Similar Properties Arise from Two Neurogenic Regions of Adult Human Brain.”, *Experimental Neurology*, 156, no. 2, pp. 333–344.
- Kyritsis, N., C. Kizil, S. Zocher, V. Kroehne, J. Kaslin, D. Freudenreich, A. Iltzche, and M. Brand, 2012, “Acute Inflammation Initiates the Regenerative Response in the Adult Zebrafish Brain.”, *Science*, 338, no. 6112, pp. 1353–1356.
- Lahne, M., and D. R. Hyde, 2015, “Interkinetic Nuclear Migration in the Regenerating Retina.”, *Retinal Degenerative Diseases*, pp. 587–593.
- Lange, C., W. B. Huttner, and F. Calegari, 2009, “Cdk4/CyclinD1 Overexpression in Neural Stem Cells Shortens G1, Delays Neurogenesis, and Promotes the Generation and Expansion of Basal Progenitors.”, *Stem Cell*, 5, no. 3, pp. 320–331.
- Lee, A. C., J. He, and M. Ma, 2011, “Olfactory Marker Protein Is Critical for Functional Maturation of Olfactory Sensory Neurons and Development of Mother Preference.”, *Journal of Neuroscience*, 31, no. 8, pp. 2974–2982.
- Leibinger, M., A. Müller, P. Gobrecht, H. Diekmann, A. Andreadaki, and D. Fischer, 2013, “Interleukin-6 Contributes to CNS Axon Regeneration Upon Inflammatory Stimulation.”, *Cell Death & Disease*, 4, no. 4.

- Leblond, C. P., B. E. Walker, 1956, "Renewal of Cell Populations.", *Physiology*, 36, 255 – 276.
- Lenkowski, J. R., and P. A. Raymond, 2014, "Müller Glia: Stem Cells for Generation and Regeneration of Retinal Neurons in Teleost Fish.", *Progress in Retinal and Eye Research*, 40, pp. 94–123.
- Leung, C. T., P. A. Coulombe, and R. R. Reed, 2007, "Contribution of Olfactory Neural Stem Cells to Tissue Maintenance and Regeneration.", *Nature Neuroscience*, 10, no. 6, pp. 720–726.
- Levin, M., R. L. Johnson, C. D. Sterna, M. Kuehn, and C. Tabin, 1995, "A Molecular Pathway Determining Left-Right Asymmetry in Chick Embryogenesis.", *Cell*, 82, no. 5, pp. 803–814.
- Liberles, S. D., and L. B. Buck, 2006, "A Second Class of Chemosensory Receptors in the Olfactory Epithelium.", *Nature*, 442, no. 7103, pp. 645–650.
- Lim, D. A., and A. Alvarez-Buylla, 2016, "The Adult Ventricular–Subventricular Zone (V-SVZ) and Olfactory Bulb (OB) Neurogenesis.", *Cold Spring Harbor Perspectives in Biology*, 8, no. 5.
- Lim, S., and P. Kaldis, 2012, "Loss of Cdk2 and Cdk4 Induces a Switch from Proliferation to Differentiation in Neural Stem Cells.", *Stem Cells*, 30, no. 7, pp. 1509–1520.
- Lledo, P. M., and M. Valley, 2016, "Adult Olfactory Bulb Neurogenesis.", *Cold Spring Harbor Perspectives in Biology*, 8, no. 8.
- Lois, C., and A. Alvarez-Buylla, 1994, "Long-Distance Neuronal Migration in the Adult Mammalian Brain.", *Science*, 264, no. 5162, pp. 1145–1148.
- Love, M. I., W. Huber, and S. Anders, 2014, "Moderated Estimation of Fold Change and Dispersion for RNA-Seq Data with DESeq2.", *Genome Biology*, 15, no. 12.

- Lugert, S., O. Basak, P. Knuckles, U. Haussler, K. Fabel, M. Götz, C. A. Haas, G. Kempermann, V. Taylor, and C. Giachino, 2010, “Quiescent and Active Hippocampal Neural Stem Cells with Distinct Morphologies Respond Selectively to Physiological and Pathological Stimuli and Aging.”, *Stem Cell*, 6, no. 5, pp. 445–456.
- Luo, W., M. S. Friedman, K. Shedden, K. D. Hankenson, and P. J. Woolf, 2009, “Gage: Generally Applicable Gene Set Enrichment for Pathway Analysis.”, *BMC Bioinformatics*, 10, no. 1, p. 161.
- Lust, K., and J. Wittbrodt, 2017, “Activating the Regenerative Potential of Müller Glia Cells in a Regeneration-Deficient Retina.”, *eLife*, 7.
- Ma, M., X. Grosmaître, C. L. Iwema, H. Baker, C. A. Greer, and G. M. Shepherd, 2003, “Olfactory Signal Transduction in the Mouse Septal Organ.”, *The Journal of Neuroscience*, 23, no. 1, pp. 317–324.
- Mackay-Sim, A., and P. W. Kittel, 1991, “On the Life Span of Olfactory Receptor Neurons.”, *European Journal of Neuroscience*, 3, no. 3, pp. 209–215.
- Manglapus, G. L., S. L. Youngentob, and J. E. Schwob, 2004, “Expression Patterns of Basic Helix-Loop-Helix Transcription Factors Define Subsets of Olfactory Progenitor Cells.”, *The Journal of Comparative Neurology*, 479, no. 2, pp. 216–233.
- Matsunami, H., and L. B. Buck, 1997, “A Multigene Family Encoding a Diverse Array of Putative Pheromone Receptors in Mammals.”, *Cell*, 90, no. 4, pp. 775–784.
- Medzhitov, R., 2008, “Origin and Physiological Roles of Inflammation.”, *Nature*, 454, no. 7203, pp. 428–435.

- Mendoza, A. S., 1993, "Morphological Studies on the Rodent Main and Accessory Olfactory Systems: The Regio Olfactoria and Vomeronasal Organ.", *Annals of Anatomy - Anatomischer Anzeiger*, 175, no. 5, pp. 425–446.
- Mescher, A. L., A. W. Neff, and M.W. King, 2017, "Inflammation and Immunity in Organ Regeneration.", *Developmental & Comparative Immunology*, 66, pp. 98–110.
- Ming, G., and H. Song, 2011, "Adult Neurogenesis in the Mammalian Brain: Significant Answers and Significant Questions.", *Neuron*, 70, no. 4, pp. 687–702.
- Miragall, F., D. Krause, U. De Vries, and R. Dermietzel, 1994, "Expression of the Tight Junction Protein ZO-1 in the Olfactory System: Presence of ZO-1 on Olfactory Sensory Neurons and Glial Cells.", *The Journal of Comparative Neurology*, 341, no. 4, pp. 433–448.
- Mombaerts, P., 2001, "How Smell Develops.", *Nature Neuroscience*, 4, no.S11, pp. 1192–1198.
- Mombaerts, P., 2004, "Odorant Receptor Gene Choice in Olfactory Sensory Neurons: The One Receptor–One Neuron Hypothesis Revisited.", *Current Opinion in Neurobiology*, 14, no. 1, pp. 31–36.
- Mombaerts, P., F. Wang, C. Dulac, S. K. Chao, A. Nemes, M. Mendelsohn, J. Edmondson, and R. Axel, 1996, "Visualizing an Olfactory Sensory Map.", *Cell*, 87, no. 4, pp. 675–686.
- Monje, M. L., H. Toda, and T. D. Palmer, 2003, "Inflammatory Blockade Restores Adult Hippocampal Neurogenesis.", *Science*, 302, no. 5651, pp. 1760–1765.
- Morrison, E. E., and R. M. Costanzo, 1992, "Morphology of Olfactory Epithelium in Humans and Other Vertebrates.", *Microscopy Research and Technique*, 23, no. 1, pp. 49–61.

- Moulton, D. G., 1974, "Dynamics of Cell Populations in the Olfactory Epithelium.", *Annals of the New York Academy of Sciences*, 237, no. 1, pp. 52–61.
- Mucignat-Caretta, C., M. Redaelli, and A. Caretta, 2012, "One Nose, One Brain: Contribution of the Main and Accessory Olfactory System to Chemosensation.", *Frontiers in Neuroanatomy*, 6.
- Murray, R. C., D. Navi, J. Fesenko, A. D. Lander, and A. L. Calof, 2003, "Widespread Defects in the Primary Olfactory Pathway Caused by Loss of *mash1* function.", *The Journal of Neuroscience*, 23, no. 5, pp. 1769–1780.
- Neurath, M. F., 2013, "New Targets for Mucosal Healing and Therapy in Inflammatory Bowel Diseases.", *Mucosal Immunology*, 7, no. 1, pp. 6–19.
- Niimura, Y., 2009, "On the Origin and Evolution of Vertebrate Olfactory Receptor Genes: Comparative Genome Analysis among 23 Chordate Species.", *Genome Biology and Evolution*, 1, pp. 34–44.
- Niimura, Y., and M. Nei, 2005, "Evolutionary Dynamics of Olfactory Receptor Genes in Fishes and Tetrapods.", *Proceedings of the National Academy of Sciences*, 102, no. 17, pp. 6039–6044.
- Niimura, Y., and M. Nei, 2005, "Evolutionary Changes of the Number of Olfactory Receptor Genes in the Human and Mouse Lineages.", *Gene*, 346, pp. 23–28.
- O'Carroll, A., S. J. Lolait, L. E. Harris, and G. R. Pope, 2013, "The Apelin Receptor Apj: Journey from an Orphan to a Multifaceted Regulator of Homeostasis.", *Journal of Endocrinology*, 219, no. 1.
- Ogata, A., Y. Kato, S. Higa, and K. Yoshizaki, 2019, "IL-6 Inhibitor for the Treatment of Rheumatoid Arthritis: A Comprehensive Review.", *Modern Rheumatology*, 29, no. 2, pp. 258–267.

- Oka, Y., L. R. Saraiva, and S. I. Korsching, 2011, "Crypt Neurons Express a Single VIR-Related Ora Gene.", *Chemical Senses*, 37, no. 3, pp. 219–227.
- Packard, A., N. Schnittke, R. A. Romano, S. Sinha, and J. E. Schwob, 2011, "NP63 Regulates Stem Cell Dynamics in the Mammalian Olfactory Epithelium.", *Journal of Neuroscience*, 31, no. 24, pp. 8748–8759.
- Palmer, T. D., E. A. Markakis, A. R. Willhoite, F. Safar, and F. H. Gage, 1999, "Fibroblast Growth Factor-2 Activates a Latent Neurogenic Program in Neural Stem Cells from Diverse Regions of the Adult CNS.", *The Journal of Neuroscience*, 19, no. 19, pp. 8487–8497.
- Palmer, T.D., J. Ray, and F.H. Gage, 1995, "FGF-2-Responsive Neuronal Progenitors Reside in Proliferative and Quiescent Regions of the Adult Rodent Brain.", *Molecular and Cellular Neuroscience*, 6, no. 5, pp. 474–486.
- Palominos, M. F., and K. E. Whitlock, 2021, "The Olfactory Organ Is Populated BY Neutrophils and Macrophages during Early Development." *Frontiers in Cell and Developmental Biology*, 8.
- Parker, V. J, J. A. Morrison, and M. J. Yaeger, 2010, "Olfactory Neuroblastoma in a Cat.", *Journal of Feline Medicine and Surgery*, 12, no. 11, pp. 867–871.
- Quast, C., E. Pruesse, P. Yilmaz, J. Gerken, T. Schweer, P. Yarza, J. Peplies, and F. O. Glöckner, 2012, "The SILVA Ribosomal RNA Gene Database Project: Improved Data Processing and Web-Based Tools.", *Nucleic Acids Research*, 41, no. D1.
- Reiten, I., F. E. Uslu, S. Fore, R. Pelgrims, C. Ringers, C. D. Verdugo, M. Hoffman, P. Lal, K. Kawakami, K. Pekkan, E. Yaksi, and N. Jurisch-Yaksi, 2017, "Motile-Cilia-Mediated Flow Improves Sensitivity and Temporal Resolution of Olfactory Computations.", *Current Biology*, 27, no. 2, pp. 166–174.

- Reynolds, B., and S. Weiss, 1992, "Generation of Neurons and Astrocytes from Isolated Cells of the Adult Mammalian Central Nervous System.", *Science*, 255, no. 5052, pp. 1707–1710.
- Richards, L. J., T. J. Kilpatrick, and P. F. Bartlett, 1992, "De Novo Generation of Neuronal Cells from the Adult Mouse Brain.", *Proceedings of the National Academy of Sciences* 89, no. 18, pp. 8591–8595.
- Ring, G., R. C. Mezza, and J. E. Schwob, 1997, "Immunohistochemical Identification of Discrete Subsets of Rat Olfactory Neurons and the Glomeruli That They Innervate.", *The Journal of Comparative Neurology*, 388, no. 3, pp. 415–434.
- Roesch, K., A. P. Jadhav, J. M. Trimarchi, M. B. Stadler, B. Roska, B. B. Sun, and C. L. Cepko, 2008, "The Transcriptome of Retinal Müller Glial Cells.", *The Journal of Comparative Neurology*, 509, no. 2, pp. 225–238.
- Rusznák, Z., W. Henskens, E. Schofield, W. S. Kim, and Y. Fu, 2016, "Adult Neurogenesis and Gliogenesis: Possible Mechanisms for Neurorestoration.", *Experimental Neurobiology*, 25, no. 3, pp. 103–112.
- Sakızlı, U. "The Contribution of Purinergic Signaling to Olfactory Neurogenesis in Zebrafish.", M.Sc. Thesis, Boğaziçi University, 2018.
- Saraiva, L. R., and S. I. Korsching, 2007, "A Novel Olfactory Receptor Gene Family in Teleost Fish.", *Genome Research*, 17, no. 10, pp. 1448–1457.
- Sato, Y., N. Miyasaka, and Y. Yoshihara, 2005, "Mutually Exclusive Glomerular Innervation by Two Distinct Types of Olfactory Sensory Neurons Revealed in Transgenic Zebrafish.", *Journal of Neuroscience*, 25, no. 20, pp. 4889–4897.

- Schindelin, J., I. Arganda-Carreras, E. Frise, V. Kaynig, M. Longair, T. Pietzsch, S. Preibisch, C. Rueden, S. Saalfeld, B. Schmid, J. Y. Tinevez, D. J. White, V. Hartenstein, K. Eliceiri, P. Tomancak, and A. Cardona, 2012, “Fiji: An Open-Source Platform FOR Biological-Image Analysis.”, *Nature Methods*, 9, no. 7, pp. 676–682.
- Schmidt, R., U. Strähle, and S. Scholpp, 2013, “Neurogenesis in Zebrafish – from Embryo to Adult.”, *Neural Development*, 8, no. 1.
- Schnittke, N., D. B. Herrick, B. Lin, J. Peterson, J. H. Coleman, A. I. Packard, W. Jang, and J. E. Schwob, 2015, “Transcription Factor P63 Controls the Reserve Status but Not the Stemness of Horizontal Basal Cells in the Olfactory Epithelium.”, *Proceedings of the National Academy of Sciences*, 112, no. 36.
- Scholpp, S., A. Delogu, J. Gilthorpe, D. Peukert, S. Schindler, and A. Lumsden, 2009, “Her6 Regulates the Neurogenetic Gradient and Neuronal Identity in the Thalamus.”, *Proceedings of the National Academy of Sciences*, 106, no. 47, pp. 19895–19900.
- Schwartz Levey, M., D. M. Chikaraishi, and J. S. Kauer, 1991, “Characterization of Potential Precursor Populations in the Mouse Olfactory Epithelium Using Immunocytochemistry and Autoradiography.”, *The Journal of Neuroscience*, 11, no. 11, pp. 3556–3564.
- Schwob, J. E., 2002, “Neural Regeneration and the Peripheral Olfactory System.”, *The Anatomical Record*, 269, no. 1, pp. 33–49.
- Schwob, J. E., and W. Jang, 2006, “Stem Cells of the Adult Olfactory Epithelium.”, *Neural Development and Stem Cells*, pp. 219–233.
- Schwob, J. E., K. E. Szumowski, and A. A. Stasky, 1992, “Olfactory Sensory Neurons are Trophically Dependent on the Olfactory Bulb for Their Prolonged Survival.”, *The Journal of Neuroscience*, 12, no. 10, pp. 3896–3919.

- Schwob, J. E., S. L. Youngentob, and R. C. Mezza, 1995, "Reconstitution of the Rat Olfactory Epithelium after Methyl Bromide-Induced Lesion.", *The Journal of Comparative Neurology*, 359, no. 1, pp. 15–37.
- Schwob, J. E., W. Jang, E. H. Holbrook, B. Lin, D. B. Herrick, J. N. Peterson, and J. H. Coleman, 2016, "Stem and Progenitor Cells of the Mammalian Olfactory Epithelium: Taking Poietic License.", *Journal of Comparative Neurology*, 525, no. 4, pp. 1034–1054.
- Shaker, T., D. Dennis, D. M. Kurrasch, and C. Schuurmans, 2012, "Neurog1 and neurog2 Coordinately Regulate Development of the Olfactory System.", *Neural Development*, 7, no. 1, p. 28.
- Simons, B. D., and H. Clevers, 2011, "Strategies for Homeostatic Stem Cell Self-Renewal in Adult Tissues.", *Cell*, 145, no. 6, pp. 851–862.
- Skupien, P., B. Hesl, M. Coolen, J. C. Moore, R. Madelaine, E. Kremmer, T. Faus-Kessler, P. Blader, N. D. Lawson, and L. Bally-Cuif, 2010, "Notch Activity Levels Control the Balance Between Quiescence and Recruitment of Adult Neural Stem Cells.", *Journal of Neuroscience*, 30, no. 23, pp. 7961–7974.
- Smith, C. G., 1938, "Changes in the Olfactory Mucosa and the Olfactory Nerves Following Intranasal Treatment with One per Cent Zinc Sulphate.", *Canadian Medical Association Journal*, 2, no. 39, pp. 138–140.
- Song, C., and B. E. Leonard, 2005, "The Olfactory Bulbectomised Rat as a Model of Depression.", *Neuroscience & Biobehavioral Reviews*, 29, no. 4, 5, pp. 627–647.
- Sorrells, S. F., M. F. Paredes, A. Cebrian-Silla, K. Sandoval, D. Qi, K.W. Kelley, D. James, S. Mayer, J. Chang, K. I. Auguste, E. F. Chang, A. J. Gutierrez, A. R. Kriegstein, G. W. Mathern, M. C. Oldham, E. J. Huang, J. M. Garcia-Verdugo, Z. Yang, and A. Alvarez-Buylla, 2018, "Human Hippocampal Neurogenesis Drops Sharply in Children to Undetectable Levels in Adults.", *Nature*, 555, no. 7696, pp. 377–381.

- Spalding, K. L., O. Bergmann, K. Alkass, S. Bernard, M. Salehpour, H. B. Huttner, E. Boström, I. Westerlund, C. Vial, B. A. Bucholz, G. Possnert, D. C. Mash, H. Druid, and J. Frisén, 2013, “Dynamics of Hippocampal Neurogenesis in Adult Humans.”, *Cell*, 153, no. 6, pp. 1219–1227.
- Su, C., K. Menuz, and J. R. Carlson, 2009, “Olfactory Perception: Receptors, Cells, and Circuits.”, *Cell*, 139, no. 1, pp. 45–59.
- Suh, H., A. Consiglio, J. Ray, T. Sawai, K. A. D'Amour, and F. H. Gage, 2007, “In Vivo Fate Analysis Reveals the Multipotent and Self-Renewal Capacities of Sox2<sup>+</sup> Neural Stem Cells in the Adult Hippocampus.”, *Stem Cell*, 1, no. 5, pp. 515–528.
- Sunderman, F. W. Jr., 2001, “Nasal Toxicity, Carcinogenicity, and Olfactory Uptake of Metals.”, *Annals of Clinical Laboratory Science*, 1, no. 31, pp. 3–24.
- Surzenko, N., T. Crowl, A. Bachleda, L. Langer, and L. Pevny, 2013, “Sox2 Maintains the Quiescent Progenitor Cell State of Postnatal Retinal Müller Glia.”, *Development*, 140, no. 7, pp. 1445–1456.
- Suyama, S., T. Sunabori, H. Kanki, K. Sawamoto, C. Gachet, S. Koizumi, and H. Okano, 2012, “Purinergic Signaling Promotes Proliferation of Adult Mouse Subventricular Zone Cells.”, *Journal of Neuroscience*, 32, no. 27, pp. 9238–9247.
- Suzuki, Y., J. Schafer, and A. I. Farbman, 1995, “Phagocytic Cells in the Rat Olfactory Epithelium after Bulbectomy.”, *Experimental Neurology*, 136, no. 2, pp. 225–233.
- Takahashi, H., S. Yoshihara, and A. Tsuboi, 2018, “The Functional Role of Olfactory Bulb Granule Cell Subtypes Derived from Embryonic and Postnatal Neurogenesis.”, *Frontiers in Molecular Neuroscience*, 11.
- Tang, P., S. Ma, M. Dong, J. Wang, S. Chai, T. Liu, and J. Li, 2018, “Effect of Interleukin-6 on Myocardial Regeneration in Mice after Cardiac Injury.”, *Biomedicine & Pharmacotherapy*, 106, pp. 303–308.

- Taub, R., 2004, "Liver Regeneration: From Myth to Mechanism.", *Nature Reviews Molecular Cell Biology*, 5, no. 10, pp. 836–847.
- Tomita, K., S. Nakanishi, F. Guillemot, R. Kageyama, and S. Nishikawa, 1996, "Mash1 Promotes Neuronal Differentiation in the Retina.", *Genes to Cells*, 1, no. 8, pp. 765–774.
- Vallières, L., I. L. Campbell, F. H. Gage, and P. E. Sawchenko, 2002, "Reduced Hippocampal Neurogenesis in Adult Transgenic Mice with Chronic Astrocytic Production of Interleukin-6.", *The Journal of Neuroscience*, 22, no. 2, pp. 486–492.
- Vassar, R., S. K. Chao, R. Sitcheran, J. M. Nunez, L. B. Vosshall, and R. Axel, 1994, "Topographic Organization of Sensory Projections to the Olfactory Bulb.", *Cell*, 79, no. 6, pp. 981–991.
- Vogalis, F., C. C. Hegg, and M. T. Lucero, 2005, "Electrical Coupling in Sustentacular Cells of the Mouse Olfactory Epithelium.", *Journal of Neurophysiology*, 94, no. 2, pp. 1001–1012.
- Wagner, S., A. L. Gresser, A. T. Torello, and C. Dulac, 2006, "A Multireceptor Genetic Approach Uncovers an Ordered Integration of VNO Sensory Inputs in the Accessory Olfactory Bulb.", *Neuron*, 50, no. 5, pp. 697–709.
- Wakisaka, N., N. Miyasaka, T. Koide, M. Masuda, T. Hiraki-Kajiyama, and Y. Yoshihara, 2017, "An Adenosine Receptor for Olfaction in Fish.", *Current Biology*, 27, no. 10, pp. 1437–1447.
- Walton, E. M., M. R. Cronan, R. W. Beerman, and D. M. Tobin, 2015, "The Macrophage-Specific Promoter *Mfap4* Allows Live, Long-Term Analysis OF Macrophage Behavior during Mycobacterial Infection in Zebrafish.", *PLoS ONE*, 10, no. 10.

- Wan, J., R. Ramachandran, and D. Goldman, 2012, “HB-EGF Is Necessary and Sufficient for Müller Glia Dedifferentiation and Retina Regeneration.”, *Developmental Cell*, 22, no. 2, pp. 334–347.
- Wang, Y., T. Yamagami, Q. Gan, Y. Wang, T. Zhao, S. Hamad, P. Lott, N. Schnittke, J. E. Schwob, and C. J. Zhou, 2011, “Canonical Wnt Signaling Promotes the Proliferation and Neurogenesis of Peripheral Olfactory Stem Cells During Postnatal Development and Adult Regeneration.”, *Journal of Cell Science*, 124, no. 9, pp. 1553–1563.
- Ward, L. D., G. J. Howlett, G. Discolo, K. Yasukawa, A. Hammacher, R. L. Moritz, and R. J. Simpson, 1994, “High Affinity Interleukin-6 Receptor Is a Hexameric Complex Consisting of Two Molecules Each of Interleukin-6, Interleukin-6 Receptor, and GP-130.”, *Journal of Biological Chemistry*, 269, no. 37, pp. 23286–23289.
- Wei, J., L. Ma, Y. Lai, R. Zhang, H. Li, C. Li, and J. Lin, 2019, “Bazedoxifene as a Novel GP130 Inhibitor for Colon Cancer Therapy.”, *Journal of Experimental & Clinical Cancer Research*, 38, no. 1.
- Westerfield, M., 2007. *The Zebrafish Book: A Guide for the Laboratory Use of Zebrafish (Danio Rerio)*, University of Oregon, Eugene.
- Yee, K. K., Y. Li, K. M. Redding, K. Iwatsuki, R. F. Margolskee, and P. Jiang, 2013, “Lgr5-EGFP Marks Taste Bud Stem/Progenitor Cells in Posterior Tongue.”, *Stem Cells*, 31, no. 5, pp. 992–1000.
- Yu, D., S. Rao, L. M. Tsai, S. K. Lee, Y. He, E. L. Sutcliffe, M. Srivastava, M. Linterman, L. Zheng, N. Simpson, J. I. Ellyard, I. A. Parish, C. S. Ma, Q. Li, C. R. Parish, C. R. Mackay, and C. G. Vinuesa, 2009, “The Transcriptional Repressor Bcl-6 Directs T-Follicular Helper Cell Lineage Commitment.”, *Immunity*, 31, no. 3, pp. 457–468.

- Yu, T., J. C. McIntyre, S. C. Bose, D. Hardin, M.C. Owen, and T. S. McClintock, 2005, “Differentially Expressed Transcripts from Phenotypically Identified Olfactory Sensory Neurons.”, *The Journal of Comparative Neurology*, 483, no. 3, pp. 251–262.
- Zhang, X., and S. Firestein, 2002, “The Olfactory Receptor Gene Superfamily of the Mouse.”, *Nature Neuroscience*, 5, no. 2, pp. 124–133.
- Zhao, C., 2006, “Distinct Morphological Stages of Dentate Granule Neuron Maturation in the Adult Mouse Hippocampus.”, *Journal of Neuroscience*, 26, no. 1, pp. 3–11.
- Zhao, C., E. M. Teng, R. G. Summers, G. L. Ming, and F. H. Gage, 2006, “Distinct Morphological Stages of Dentate Granule Neuron Maturation in the Adult Mouse Hippocampus.”, *Journal of Neuroscience*, 26, no. 1, pp. 3–11.

## APPENDIX A: Chemicals and Reagents

Table A.1. List of chemicals and reagents used in this study.

Name	Manufacturer
Absolute Ethanol	Sigma-Aldrich, USA
Bovine Serum Albumin (BSA)	New England Biolabs, USA
Paraformaldehyde	Sigma-Aldrich, USA
BrdU	Alfa Caesar, Germany
Hydrochloric acid	Sigma-Aldrich, USA
4',6-Diamidino-2-Phenylindole, Dihydrochloride (DAPI)	ThermoFisher Scientific, USA
TO-PRO-3	ThermoFisher Scientific, USA
Calcium sulfate	Alfa Caesar, Germany
Phenol Red	AppliChem, USA
Potassium Chloride	Sigma-Aldrich, USA
EdU Click-iT™ Cell Proliferation Kit, Alexa Fluor 488	ThermoFisher Scientific, USA
Sodium Bicarbonate	Sigma-Aldrich, USA
Sodium Chloride	Sigma-Aldrich, USA
Sodium Phosphate Monobasic	Sigma-Aldrich, USA
Potassium Phosphate Dibasic	Sigma-Aldrich, USA
Sodium Hydroxide	Sigma-Aldrich, USA
D-Glucose	Sigma-Aldrich, USA

Table A.2. List of chemicals and reagents used in this study (cont.).

<b>Name</b>	<b>Manufacturer</b>
Potassium Phosphate monobasic	ThermoFisher Scientific, USA
Triton X-100	AppliChem, USA
HEPES	AppliChem, USA
L-cystein	Sigma-Aldrich, USA
Tween 20	VWR, USA
Recombinant human IL-6 (206-IL)	R&D Systems, USA
Magnesium Chloride	Sigma-Aldrich, USA
Adenosine Triphosphate	Sigma-Aldrich, USA
2-(Methylthio)adenosine 5'-triphosphate	Sigma-Aldrich, USA
Suramin	Sigma-Aldrich, USA
Fluo4-AM (F14201)	ThermoFisher Scientific, USA
Cell Trace™ Far Red	ThermoFisher Scientific, USA
Pluronic™ F-127	ThermoFisher Scientific, USA
MK571	ThermoFisher Scientific, USA
Dimethyl Sulfoxide	Sigma-Aldrich, USA
Ethylene Diamine Tetra Aceticacid	Sigma-Aldrich, USA
Agarose Low Melting	Mallinckrodt, UK
MS222	Sigma-Aldrich, USA
Magnesium Sulfate Heptahydrate	Sigma-Aldrich, USA
Calcium Chloride	Sigma-Aldrich, USA

## APPENDIX B: Disposable and Non-disposable Equipment

Table B.1. List of disposable and non-disposable equipment.

<b>Name</b>	<b>Manufacturer</b>
LSM780/Axio Examiner	Zeiss, Germany
Leica SP5-AOBS	Leica, Germany
Leica TCS SP8	Leica, Germany
Stereomicroscope	Zeiss, Germany
VT1200S Vibratome	Leica, Germany
Micromanipulator, Femtojet	Eppendorf, Germany
CM3050S Cryostat	Leica, Germany
Coplin Jars	Leica, Germany
Capillary tubes (1mm)	Warner Instruments, USA
Forceps	Dumont, Switzerland
Drying oven	Nüve, Turkey
-20°C Freezer	Uğur, Turkey
-80°C Freezer	Thermoforma, USA
Glassware	Isolab, Germany
U-100 insulin needle (30G)	Beckon Dickinson, USA
Micropipette tips (2-1000 µl)	CAPP, Germany
Micropipettes (2-1000 µl)	Eppendorf, Germany
Glass Slides - Superfrost® Plus	Thermo Scientific, USA
Petri Dish	Fıratpen, Turkey

## APPENDIX C: Transcriptome Sequencing Depth Before and After FastQC

Table C.1. Read numbers before and after rRNA sorting and adapter trimming.

<b>Replicate experiments</b>	<b>Raw reads</b>	<b>Sorted</b>	<b>Sorted &amp; trimmed</b>
<b>E1_ctrl</b>	37396552	33857687	33616474
<b>E1_t4h</b>	37270726	28942482	28721991
<b>E1_t12h</b>	36936774	34856609	34591366
<b>E1_t24h</b>	36633967	32781814	32539337
<b>E1_t72h</b>	38456279	35645003	35306655
<b>E1_t120h</b>	37792714	34732872	34405790
<b>E2_ctr</b>	45027610	44305168	43704902
<b>E2_t4h</b>	41364605	37846364	37482715
<b>E2_t12h</b>	37975421	35754403	35415606
<b>E2_t24h</b>	37537816	36012706	35619273
<b>E2_t72h</b>	36700192	35323219	34673759
<b>E2_t120h</b>	40471706	38629087	38248599
<b>Minimum Read Number</b>	<b>36633967</b>	<b>28942482</b>	<b>28721991</b>

## APPENDIX D: Transcriptome KEGG Pathway GO term Analysis

Table D.1. List of KEGG pathway GO terms significantly regulated at 4h post lesion.

Direction	GAGE analysis: 4 hpl vs ctrl	statistic	Genes	adj.pval
Up	Ribosome	5.9943	125	1.90E-07
	RNA transport	5.9859	152	1.90E-07
	Spliceosome	5.5164	133	6.40E-07
	Salmonella infection	4.6338	256	2.50E-05
	Protein processing in endoplasmic reticulum	4.1673	183	1.70E-04
	Cytokine-cytokine receptor interaction	3.7189	176	8.70E-04
	MAPK signaling pathway	3.601	349	9.70E-04
	Focal adhesion	3.5998	229	9.70E-04
	Regulation of actin cytoskeleton	3.409	237	1.70E-03
	AGE-RAGE signaling pathway in diabetic complications	3.2002	120	3.40E-03
	TGF-beta signaling pathway	3.0051	106	6.00E-03
	Apoptosis	2.9365	171	6.50E-03
	NOD-like receptor signaling pathway	2.6497	153	1.40E-02
	Endocytosis	2.6069	300	1.50E-02
	Tight junction	2.5057	194	1.90E-02
	C-type lectin receptor signaling pathway	2.4384	119	2.10E-02
	Adherens junction	1.8679	106	8.20E-02

Table D.2. List of KEGG pathway GO terms significantly regulated at 12h post lesion.

<b>Direction</b>	<b>GAGE analysis: 12 hpl vs ctrl</b>	<b>statistic</b>	<b>Genes</b>	<b>adj.pval</b>
Down	Neuroactive ligand-receptor interaction	-4.5644	303	1.40E-04
Up	Ribosome	5.8399	125	7.80E-07
	RNA transport	4.7927	152	3.30E-05
	Spliceosome	4.1232	133	3.40E-04
	Cell cycle	4.0816	137	3.40E-04
	Cytokine-cytokine receptor interaction	3.7696	176	8.40E-04
	Focal adhesion	3.3166	229	3.20E-03
	Regulation of actin cytoskeleton	3.3124	237	3.20E-03
	Protein processing in endoplasmic reticulum	3.1875	183	4.40E-03
	AGE-RAGE signaling pathway in diabetic complications	3.0836	120	5.60E-03
	Salmonella infection	2.9851	256	6.60E-03
	Cellular senescence	2.8373	176	9.60E-03
	TGF-beta signaling pathway	2.7155	107	1.30E-02
	NOD-like receptor signaling pathway	2.5043	153	2.20E-02
	Wnt signaling pathway	2.3973	185	2.70E-02
	Melanogenesis	2.3021	121	3.30E-02
Adherens junction	2.1951	106	4.00E-02	

Table D.3. List of KEGG pathway GO terms significantly regulated at 24h post lesion.

Direction	GAGE analysis: 24 hpl vs ctrl	statistic	Genes	adj.pval
Down	Neuroactive ligand-receptor interaction	-5.5325	304	1.10E-06
Up	Ribosome	6.9143	125	3.90E-09
	Cell cycle	4.9451	137	1.70E-05
	RNA transport	4.6096	152	5.00E-05
	Spliceosome	4.3485	133	1.30E-04
	Focal adhesion	3.4473	229	2.70E-03
	Regulation of actin cytoskeleton	3.3615	237	3.10E-03
	Salmonella infection	3.1476	256	5.50E-03
	Cellular senescence	3.0372	176	7.10E-03
	TGF-beta signaling pathway	3.0078	107	7.20E-03
	Protein processing in endoplasmic reticulum	2.9554	183	7.50E-03
	NOD-like receptor signaling pathway	2.877	153	8.00E-03
	Cytokine-cytokine receptor interaction	2.8769	176	8.00E-03
	AGE-RAGE signaling pathway in diabetic complications	2.745	120	1.10E-02
	Oocyte meiosis	2.4078	131	2.60E-02
	Wnt signaling pathway	2.3235	185	3.00E-02
	Carbon metabolism	2.1902	115	4.10E-02
	Adherens junction	2.1461	106	4.20E-02
	Melanogenesis	2.1238	121	4.20E-02
	Oxidative phosphorylation	1.9795	129	5.70E-02
	Apoptosis	1.9451	171	5.70E-02
	Ubiquitin mediated proteolysis	1.9354	152	5.70E-02
Tight junction	1.8048	194	7.20E-02	
MTOR signaling pathway	1.6944	178	8.70E-02	

## APPENDIX E: Transcriptome biological process GO term Analysis

Table E.1. List of biological process GO terms significantly regulated at 4h post lesion.

Direction	GAGE analysis: 4 hpl vs ctrl	statistic	Genes	adj.Pval
Down	Sensory perception of smell	-13.608	122	9.4E-29
	Detection of chemical stimulus involved in sensory perception	-13.196	117	1.1E-27
	Detection of chemical stimulus involved in sensory perception of smell	-13.115	116	2.1E-27
	Sensory perception of chemical stimulus	-12.977	132	9E-28
	Detection of chemical stimulus	-12.857	119	4.8E-27
	Detection of stimulus involved in sensory perception	-11.131	137	2.7E-22
	Sensory perception	-10.221	260	7.8E-21
	Nervous system process	-9.6697	350	2.9E-19
	Detection of stimulus	-8.9465	183	6.6E-16
	Microtubule-based movement	-7.0752	187	2.3E-10
	Cilium organization	-6.4708	225	6.6E-09
	Synaptic signaling	-6.386	281	8.3E-09
	Chemical synaptic transmission	-6.3646	278	8.3E-09
	Anterograde trans-synaptic signaling	-6.3646	278	8.3E-09
	Trans-synaptic signaling	-6.352	280	8.3E-09
	Cilium assembly	-6.0788	212	4.5E-08
Microtubule-based process	-6.0586	462	3.5E-08	

Table E.2. List of biological process GO terms significantly regulated at 4h post lesion  
(cont.).

<b>Direction</b>	<b>GAGE analysis: 4hpl vs ctrl</b>	<b>statistic</b>	<b>Genes</b>	<b>adj.Pval</b>
Up	Ribosome biogenesis	12.3342	198	1.4E-26
	Ribonucleoprotein complex biogenesis	11.9419	287	1.4E-26
	NcRNA metabolic process	11.6661	318	2.9E-26
	NcRNA processing	11.6063	245	2.6E-25
	RRNA processing	10.6693	130	9E-20
	RRNA metabolic process	10.5877	145	6E-20
	Amide biosynthetic process	8.0635	477	9.7E-14
	Translation	7.8539	413	4.9E-13
	Peptide biosynthetic process	7.8006	416	6.4E-13
	TRNA metabolic process	7.0259	148	7E-10
	Peptide metabolic process	6.5619	487	2.3E-09
	Cardiovascular system development	6.1207	426	3.3E-08
	Vasculature development	6.0824	420	3.9E-08

Table E.3. List of biological process GO terms significantly regulated at 12h post lesion.

Direction	GAGE analysis: 12 hpl vs ctrl	statistic	Genes	adj.Pval
Down	Sensory perception of smell	-21.68	122	1.3E-54
	Detection of chemical stimulus involved in sensory perception of smell	-21.26	116	3.1E-52
	Detection of chemical stimulus involved in sensory perception	-20.729	117	1.6E-51
	Detection of chemical stimulus	-20.283	119	4.3E-51
	Sensory perception of chemical stimulus	-19.627	132	2E-51
	Detection of stimulus involved in sensory perception	-14.734	137	2.2E-34
	Sensory perception	-13.164	260	4.6E-32
	Nervous system process	-12.644	349	4.4E-31
	Detection of stimulus	-12.382	183	2.1E-27
	Synaptic signaling	-8.1549	280	7.5E-14
	Trans-synaptic signaling	-8.0985	279	1E-13
	Chemical synaptic transmission	-8.0583	277	1.2E-13
	Anterograde trans-synaptic signaling	-8.0583	277	1.2E-13
	Potassium ion transport	-7.2712	157	6E-11
	Cilium organization	-7.0822	225	1.1E-10
	Metal ion transport	-6.8749	446	2.1E-10
	Monovalent inorganic cation transport	-6.7825	330	4.1E-10
	Inorganic cation transmembrane transport	-6.7671	472	3.8E-10
	Microtubule-based movement	-6.7062	187	1.2E-09
	Cilium assembly	-6.5868	212	1.9E-09

Table E.4. List of biological process GO terms significantly regulated at 12h post lesion  
(cont.).

<b>Direction</b>	<b>GAGE analysis: 12 hpl vs ctrl</b>	<b>statistic</b>	<b>Genes</b>	<b>adj.Pval</b>
Up	NcRNA metabolic process	9.5885	317	1.7E-17
	Ribosome biogenesis	9.4644	198	2E-16
	Ribonucleoprotein complex biogenesis	9.1251	287	2.7E-16
	NcRNA processing	9.1192	244	4.6E-16
	RRNA metabolic process	8.0988	145	2.2E-12
	RRNA processing	7.9495	130	5.5E-12
	Translation	7.7613	412	1.7E-12
	Peptide biosynthetic process	7.6465	415	2.7E-12
	Amide biosynthetic process	7.4984	476	5.5E-12
	Peptide metabolic process	6.9884	486	1.6E-10

Table E.5. List of biological process GO terms significantly regulated at 24h post lesion.

Direction	GAGE analysis: 24hpl vs ctrl	statistic	Genes	adj.Pval
Down	Sensory perception of smell	-21.296	122	1.40E-54
	Detection of chemical stimulus involved in sensory perception	-20.869	117	1.20E-52
	Detection of chemical stimulus involved in sensory perception of smell	-20.7835	116	2.20E-52
	Detection of chemical stimulus	-20.1201	119	3.60E-51
	Sensory perception of chemical stimulus	-19.1796	132	4.80E-50
	Detection of stimulus involved in sensory perception	-15.2169	137	7.00E-36
	Detection of stimulus	-12.1523	183	1.70E-26
	Sensory perception	-11.8129	260	1.60E-26
	Nervous system process	-11.4343	350	5.20E-26
	Cilium organization	-8.01	225	2.80E-13
	Cilium assembly	-7.5692	212	5.90E-12
	Microtubule-based movement	-7.5618	187	7.10E-12
	Synaptic signaling	-7.5168	281	5.90E-12
	Potassium ion transport	-7.4902	157	1.30E-11
	Trans-synaptic signaling	-7.4625	280	7.40E-12
	Chemical synaptic transmission	-7.4389	278	7.70E-12
	Anterograde trans-synaptic signaling	-7.4389	278	7.70E-12
	Metal ion transport	-7.2606	446	1.30E-11
	Plasma membrane bounded cell projection assembly	-7.005	257	1.20E-10
	Cellular potassium ion transport	-6.8995	147	4.60E-10
Potassium ion transmembrane transport	-6.8995	147	4.60E-10	
Up	NcRNA metabolic process	8.2182	318	8.10E-13
	Ribosome biogenesis	8.0379	198	3.40E-12
	Ribonucleoprotein complex biogenesis	7.8532	287	3.40E-12
	Translation	7.7033	413	3.40E-12
	NcRNA processing	7.6874	245	1.00E-11
	Peptide biosynthetic process	7.5994	416	5.50E-12
	Amide biosynthetic process	7.4289	477	1.10E-11
	Peptide metabolic process	7.3859	487	1.30E-11
	DNA metabolic process	6.869	450	4.20E-10

## APPENDIX F: Transcriptome molecular function GO term Analysis

Table F.1. List of molecular function GO terms significantly regulated at 4h post lesion.

Direction	GAGE analysis: 4hpl vs ctrl	statistic	Genes	adj.Pval
Down	Olfactory receptor activity	-13.114	116	1.90E-27
	G protein-coupled amine receptor activity	-8.7057	156	6.20E-15
	Ion gated channel activity	-5.0954	254	1.10E-05
	Cation channel activity	-4.7516	268	2.60E-05
	Voltage-gated ion channel activity	-4.7455	153	2.60E-05
	Potassium ion transmembrane transporter activity	-4.7451	146	2.60E-05
	Voltage-gated cation channel activity	-4.7421	125	2.60E-05
	Ion channel activity	-4.7069	330	2.60E-05
	Substrate-specific channel activity	-4.6704	333	2.60E-05
	Tubulin binding	-4.6595	233	2.70E-05
	Gated channel activity	-4.5458	270	3.90E-05
	Neurotransmitter receptor activity	-4.5344	109	4.60E-05
	Metal ion transmembrane transporter activity	-4.5219	347	3.90E-05
	Voltage-gated channel activity	-4.5054	158	4.60E-05
	Monovalent inorganic cation transmembrane transporter activity	-4.2996	324	8.50E-05
	Microtubule binding	-4.2379	202	1.10E-04
	Potassium channel activity	-4.1925	105	1.60E-04
	Channel activity	-4.0556	350	1.90E-04
	Passive transmembrane transporter activity	-4.0556	350	1.90E-04
	Ligand-gated ion channel activity	-3.5801	108	1.30E-03
Ligand-gated channel activity	-3.5801	108	1.30E-03	

Table F.2. List of molecular function GO terms significantly regulated at 4h post lesion  
(cont.).

<b>Direction</b>	<b>GAGE analysis: 4 hpl vs ctrl</b>	<b>statistic</b>	<b>Genes</b>	<b>adj.Pval</b>
Up	Catalytic activity, acting on RNA	7.3289	261	6.80E-11
	Structural constituent of ribosome	6.6053	154	1.40E-08
	Structural molecule activity	5.0249	428	1.30E-05
	Cytokine receptor binding	4.2164	118	5.60E-04
	Cytokine activity	4.1851	120	5.60E-04
	Receptor regulator activity	3.4857	273	5.80E-03
	Receptor ligand activity	3.41	265	6.60E-03
	Protein heterodimerization activity	3.2715	129	9.80E-03

Table F.3. List of molecular function GO terms significantly regulated at 12h post lesion.

<b>Direction</b>	<b>GAGE analysis: 12 hpl vs ctrl</b>	<b>statistic</b>	<b>Genes</b>	<b>adj.Pval</b>
Down	Olfactory receptor activity	-21.26	116	1.40E-52
	G protein-coupled amine receptor activity	-13.341	156	1.00E-30
	Neurotransmitter receptor activity	-6.3704	108	1.90E-08
	Voltage-gated ion channel activity	-6.2474	153	1.90E-08
	Ion gated channel activity	-6.2471	253	1.90E-08
	Cation channel activity	-6.1284	267	1.90E-08
	Voltage-gated cation channel activity	-6.0754	125	2.70E-08
	Voltage-gated channel activity	-6.0582	158	2.70E-08
	Ion channel activity	-6.0175	329	2.70E-08
	Substrate-specific channel activity	-5.9964	332	2.70E-08
	Gated channel activity	-5.9661	269	2.70E-08
	Potassium ion transmembrane transporter activity	-5.9204	146	4.60E-08
	Metal ion transmembrane transporter activity	-5.8638	347	3.80E-08
	Monovalent inorganic cation transmembrane transporter activity	-5.4683	324	3.00E-07
	Channel activity	-5.1299	349	1.50E-06
	Passive transmembrane transporter activity	-5.1299	349	1.50E-06
	Potassium channel activity	-5.0313	105	4.10E-06
	Tubulin binding	-4.1168	233	1.60E-04

Table F.4. List of molecular function GO terms significantly regulated at 12h post lesion  
(cont.).

<b>Direction</b>	<b>GAGE analysis: 12 hpl vs ctrl</b>	<b>statistic</b>	<b>Genes</b>	<b>adj.Pval</b>
Up	Calcium ion transmembrane transporter activity	-3.7283	107	8.40E-04
	Microtubule binding	-3.6505	202	9.60E-04
	Structural constituent of ribosome	6.6831	154	9.40E-09
	Catalytic activity, acting on RNA	6.4011	261	9.40E-09
	Structural molecule activity	6.3328	428	9.40E-09
	Transferase activity, transferring one-carbon groups	4.4083	191	2.30E-04
	Helicase activity	4.2878	106	3.70E-04
	Cytokine activity	4.2419	120	3.70E-04
	Methyltransferase activity	3.9114	182	1.00E-03
	Cytokine receptor binding	3.8937	118	1.10E-03
	Metallopeptidase activity	3.6543	154	2.20E-03
	Peptidase inhibitor activity	3.599	109	2.60E-03

Table F.5. List of molecular function GO terms significantly regulated at 24h post lesion.

<b>Direction</b>	<b>GAGE analysis: 24 hpl vs ctrl</b>	<b>statistic</b>	<b>Genes</b>	<b>adj.Pval</b>
Down	Olfactory receptor activity	-20.784	116	1.50E-52
	G protein-coupled amine receptor activity	-15.43	156	5.80E-38
	Metal ion transmembrane transporter activity	-6.7406	347	7.30E-10
	Cation channel activity	-6.5314	268	2.60E-09
	Ion channel activity	-6.3904	330	3.80E-09
	Substrate-specific channel activity	-6.3765	333	3.80E-09
	Potassium ion transmembrane transporter activity	-6.3011	146	9.40E-09
	Ion gated channel activity	-6.2897	254	6.50E-09
	Voltage-gated ion channel activity	-6.2216	153	1.20E-08
	Voltage-gated cation channel activity	-6.2211	125	1.40E-08
	Gated channel activity	-6.0538	270	1.60E-08
	Voltage-gated channel activity	-6.03	158	2.50E-08
	Channel activity	-5.59	350	1.50E-07
	Passive transmembrane transporter activity	-5.59	350	1.50E-07
	Neurotransmitter receptor activity	-5.5452	109	4.50E-07
	Potassium channel activity	-5.4312	105	6.70E-07
	Monovalent inorganic cation transmembrane transporter activity	-5.1747	324	1.20E-06
	Calcium ion transmembrane transporter activity	-4.3364	107	8.10E-05
Up	Structural constituent of ribosome	7.6365	154	1.10E-10
	Structural molecule activity	6.2263	428	2.40E-08
	Catalytic activity, acting on RNA	5.8922	261	1.90E-07
	Catalytic activity, acting on DNA	4.4873	148	1.90E-04
	Transferase activity, transferring one-carbon groups	4.3321	191	2.60E-04
	Helicase activity	4.3178	106	2.70E-04
	Protein-containing complex binding	4.2101	426	2.70E-04
	Metallopeptidase activity	4.1297	154	3.80E-04
	Endopeptidase regulator activity	3.9886	102	6.90E-04
	Peptidase inhibitor activity	3.8881	109	8.20E-04
	Methyltransferase activity	3.8625	182	8.20E-04
	Cytokine receptor binding	3.8448	118	8.40E-04